Lawrence Berkeley National Laboratory
Recent Work

Title
PLASMA-ASSISTED SYNTHESIS AND PHYSICAL CHEMICAL CHARACTERIZATION OF TITANIUM NITRIDE FILMS

Permalink
https://escholarship.org/uc/item/5g21g5j5

Author
Hilton, M.R. (Thesis)..

Publication Date
1987-12-01

eScholarship.org Powered by the California Digital Library
University of California

UC-404

LBL-24584

c1

RECEIVED
LAWRENCE
BERKELEY LABORATORY
APR 11 1988
LIBRARY AND
DOCUMENTS SECTION

Center for Advanced Materials

CAM

Plasma-Assisted Synthesis and Physical Chemical Characterization of Titanium Nitride Films

M.R. Hilton

(Ph.D. Thesis)

December 1987

For Reference

Not to be taken from this room

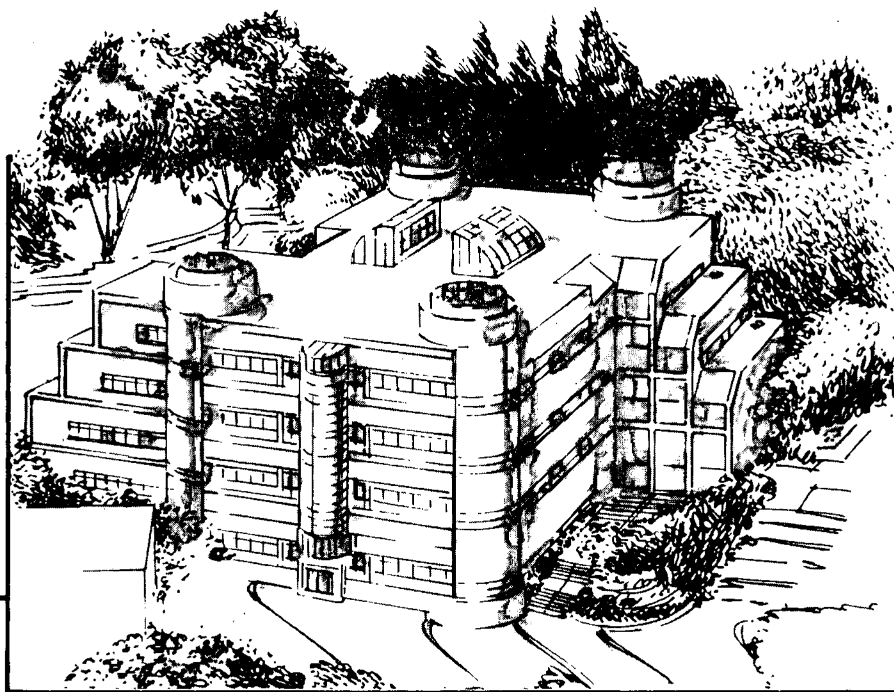

Materials and Chemical Sciences Division

Lawrence Berkeley Laboratory • University of California

ONE CYCLOTRON ROAD, BERKELEY, CA 94720 • (415) 486-4755

25

Prepared for the U.S. Department of Energy under Contract DE-AC03-76SF00098

LBL-24584 c.1

DISCLAIMER

This document was prepared as an account of work sponsored by the United States Government. While this document is believed to contain correct information, neither the United States Government nor any agency thereof, nor the Regents of the University of California, nor any of their employees, makes any warranty, express or implied, or assumes any legal responsibility for the accuracy, completeness, or usefulness of any information, apparatus, product, or process disclosed, or represents that its use would not infringe privately owned rights. Reference herein to any specific commercial product, process, or service by its trade name, trademark, manufacturer, or otherwise, does not necessarily constitute or imply its endorsement, recommendation, or favoring by the United States Government or any agency thereof, or the Regents of the University of California. The views and opinions of authors expressed herein do not necessarily state or reflect those of the United States Government or any agency thereof or the Regents of the University of California.

LBL-24584

PLASMA-ASSISTED SYNTHESIS AND PHYSICAL CHEMICAL CHARACTERIZATION OF TITANIUM NITRIDE FILMS

Michael Robert Hilton
Ph.D. Thesis

Department of Materials Science
and
Mining Engineering
University of California, Berkeley

and

Center for Advanced Materials
Materials and Chemical Sciences Division
University of California
Berkeley, California 94720 USA

December 1987

This work was supported by the Director, Office of Energy Research, Office of Basic Sciences, Materials Science Division of the U.S. Department of Energy under Contract Number DE-AC03-76SF00098.

Plasma-Assisted Synthesis and Physical Chemical Characterization of Titanium Nitride Films

Michael Robert Hilton

Department of Materials Science
and
Mining Engineering
University of California
and
Center for Advanced Materials
Materials and Chemical Sciences Division
Lawrence Berkeley Laboratory
Berkeley, California 94720

Abstract

The physical and mechanical properties of titanium nitride films synthesized by radio-frequency plasma-assisted chemical vapor deposition onto M2 tool steel were investigated. Titanium tetrachloride ($TiCl_4$) with ammonia (NH_3) or with hydrogen (H_2) and nitrogen (N_2) were the primary reactants used in the pressure range of 0.2 to 1.0 Torr. Auger electron spectroscopy, x-ray diffraction, and scanning electron microscopy revealed that film composition, structure, and mechanical properties were strongly influenced by chlorine concentration within the films and at the film-substrate interfaces. Chlorine concentration in the films de-

creased with increasing deposition temperature. A transition from an amorphous zone one morphology, to a fine-grained zone T morphology, to a highly crystalline zone two morphology with (200) preferred orientation was observed with increasing deposition temperature.

Films formed at temperatures lower than 400°C exhibited poor mechanical properties, demonstrated by their tendency to spontaneously disintegrate. At 400°C and above, film adhesion was influenced by initial deposition conditions. Films formed from $TiCl_4$ and NH_3 had low scratch adhesion test critical loads, with fracture occuring at the film-substrate interface. Auger analysis of scratch tracks created in vacuum revealed a high interfacial chlorine content. In contrast, films synthesized with hydrogen and nitrogen instead of ammonia exhibited higher scratch adhesion test critical loads, with fracture tending to occur within the film rather than at the interface. Auger depth profiling revealed no chlorine accumulation at the interfaces of H_2-N_2-based films. Early film growth was characterized by the nucleation and growth of TiN islands.

Other deposition parameters, such as power, gas flow ratio, and substrate bias primarily influenced film growth rates. The presence of a plasma enhanced TiN synthesis from $TiCl_4$ and NH_3; a plasma was essential for TiN synthesis from $TiCl_4$, H_2, and N_2. The chlorine concentrations of titanium carbonitride films, synthesized in a plasma with the addition of methane showed greater variation at fixed deposition temperature than those of pure nitride films. The use of an organometallic source, titanium tetrakis dimethylamide, $Ti(N(CH_3)_2)_4$, resulted in the formation of carbonitride powders.

Contents

Acknowledgements .... **vi**

List of Abbreviations .... **x**

1. Introduction **1**

1.1 Statement of the problem 1

1.2 Objective 2

1.3 Organization 3

1.4 Background 3

1.4.1 Coating Practice and Theory 3

1.4.2 Materials Properties 9

TiN, (TiC, and TiO) 9

M2 High Speed Steel 14

1.4.3 Studies of Sputtered TiN 19

1.4.4 PACVD 21

1.4.5 TiN Synthesis by PACVD 28

1.4.6 Studies of TiN-HSS Adhesion 31

1.4.7 Zone Models of Morphology 33

2. Technical Approach **36**

2.1 Research Strategy 36

2.2 Apparatus 36

2.3 Materials 40

2.4 Characterization 47

2.4.1 Physical Properties 47

Morphology and Thickness 48

Crystallinity 48

Film Composition 49

Interface Composition 52

2.4.2 Mechanical Properties 57

Adhesion Measurement 58

Background 58

Experirmental Procedure 70

Hardness Measurement 72

Background 72

Experimental Procedure 78

3 Experimental Studies and Results 80

3.1 $TiCl_4$, NH_3 studies 84

3.1.1 Deposition Conditions 84

3.1.2 Film Structure and Composition 84

3.1.3 Mechanical Properites 86

3.1.4 Effect of changing film deposition parameters 94

Deposition Temperature 94

Ammonia partial pressure and thickness variation 97

Effect of Argon Partial Pressure 97

R.f. power 100

Effect of d.c. biasing 100

3.1.5 Interface Composition 104

3.2 Organometallic CVD 112

3.2.1 Deposition Conditions 112

3.2.2 Results 112

3.3 Plasma Deposition using $TiCl_4$, N_2, and H_2 117

3.3.1 Deposition Conditions 117

3.3.2 Film structure and composition 118

3.3.3 Mechanical Properties 129

3.3.4 Effect of Deposition Parameters 135

Deposition Temperature 135

Effect of H_2/N_2 ratio 135

Effect of Argon partial pressure 139

Effect of Power 139

Effect of d.c. biasing 139

3.3.5 Thin Films-Interfacial Properties and Nucleation 144

3.3.6 Effect of Oxygen Pretreatment 147

3.4 $TiCl_4$, CH_4, N_2, and H_2 Studies 151

3.4.1 Deposition Conditions 151

3.4.2 Film Structure and Composition 151

3.4.3 Mechanical Properties 155

4 Discussion **163**

5 Conclusions **184**

6 Bibliography **187**

Dedicated

to my mother

and to the memory of

my late father.

"No man knows what he can do except he and even he does not unless he tries." -*Emerson*

"No, no. There is no try. Either do or do not do." -*Yoda*

Acknowledgments

I would like to extend my sincere gratitude to Professor Gabor A. Somorjai for his imaginative and enthusiastic support that he displayed throughout the project. Gabor is a dynamic leader, with a style that is best described in my opinion as a hybrid of those of two great American figures, the late General George S. Patton and President Ronald Wilson Reagan. The Somorjai organization is a unique enterprise with its own esprit de corps, which (like Patton's Third Army in World War II Europe) can cover more ground in its specialty in a shorter period of time than any other group in the world. Gabor's uncanny intuitive sense for defining imaginative research directions is truly impressive and is something that will influence me for the rest of my life.

I wish to thank Professor Didier de Fontaine for providing me a "home" within the bureacracy of UC Berkeley and LBL. It has been very valuable to observe how a theoretical group operates and solves its own set of difficult problems. I also wish to thank him for forcing me to maintain a full course load during my first semester while initiating my research. Completing these courses avoided problems that would have occured a year later when the Materials Science Department changed its program.

My work was invaluably assisted by Dr. Miquel Salmeron, who is one of a small number of people that is a member of the "paper bag" club–someone who could (almost) do surface science in a paper bag. Discussions with him have helped me greatly and it has also been exciting to watch the evolution of the STM at LBL. Those of us who have been able to work with Miquel have been truly fortunate.

Successful experimental surface science research requires first-rate mechanical and electrical technical support. I have to thank Mr. Keith Franck for educating

me in vacuum technology, and for designing and fabricating my early equipment. Working with Keith was quite an adventure, during the design and assembly of the plasma system, and especially during the rebuilding of the SAM system. Later it was a pleasure to work with Mr. Dan Colomb, who designed and fabricated the scratch removal device and modified the scratch adhesion tester, as well as executing a variety of jobs for me. I would also like to thank Mr. Weyland Wong, Mr. Glenn Baum, Mr. John Holtuis, Mr. Michael Kujala, Mr. Chip Flor, Mr. James Wu, and Mr. Herb Riebe for helping to solve problems that arose. Sincere thanks go to Mr. Jim Severns, for designing some of the unusual r.f./d.c. electronics and for keeping the standard electronics running. Credit also goes to Mr. Hank Brendel for keeping the interlocks and power systems in order. I also have to thank Ms. Sandra Stewart and Ms. Rebecca Hunt for always managing to expedite my purchase requests when I really needed them.

Most of this work was done with assistance from others, which included an outstanding group of undergraduates: L. Ravi Narasimhan, George Rodrigues, Ann Middlebrook-Carr, and Tim Levine. An enormous amount of labor was expended in this project, and results would have been far slower in developing without their help. Similar assistance from Dr. Shigeaki Nakamura and Gil Vandentop is also acknowledged.

The help and friendship of my colleagues within the Somorjai group and LBL is most appreciated. In the early days, Eddie Tysoe (especially late in the evening at the Albatross), Kurt Sieber, Andy Gellman, and Tom Gentle helped me greatly. Later support came from Marc Levin, Simon Bare, Mathew Mate (who made me aware of UHV friction experiments published in the literature), Greg Blackman, Ken Lewis, Jose Carrazza, Dave Godbey, Mark Logan, Tom Rucker, Gerard Vurens, Dan Strongin, Frank Olgetree, Mark Bussell, Gil Van-

dentop, Kevin Williams, Sabrina Fu, and Dave Zeglinski. I clearly remember the day when Dr. Andy Ninham poked his head in the office and asked if he "could buy your empty Coke bottles" (to be used to store his home-brewed beer). After settling that issue, he proceeded to refine my education in the topics of indentation hardness and deformation theory. For that and his friendship, I am truly thankful. Gratitude is also extended to Judy Glazer, Roseann Csencsits, Mike Kundman, Darrel Frear, Mike Strum (who brought Eberhart's work to my attention), Mike Rubin, Ellice Luh, Willie Miller, and Naomi Naito.

On the social side, the adventures of the "Four Horsemen" will be memorable. The friendship and support that I have received from the Venezuelans and Brazilians that I have met here has been vital. Marianella Ledezma and Rafael Pontes, Jose Carrazza, and Rita Sampaio are exceptionally fine people. I have to thank Rita for introducing me to Peggy Tong, who is now my wife. I thank Peggy for her love and support which has completely changed my life and which has made my final days here much easier. I thank her for doing the typing and all of the pasteup work on this thesis. The support of my mother and the rest of my family and friends in Chicago and elsewhere has been very important. The support of Carla Hilton and of Susan Prettyman deserve specific mention. The memories of my late father, Dr. J. Robert Hilton Jr., and of my late grandmother, Catherine Howard, have been inspirational.

Obtaining a Ph.D. requires a journey through the self. One of the issues to be solved is the apparent contradiction of the quotations on the previous few pages. However, one cannot dwell on any problem for too long. Quoting my uncle, James Clifford Hilton: "If something is easy then you are coasting, which can only mean that you are moving in one direction–downhill". Lately, the road seems to be fairly flat and it is time to find a new incline.

This work was supported by the Office of Energy Research, Office of Basic Energy Sciences, Material Science Division of the U.S. Department of Energy under contract number DE-AC03-76SF00098.

List of Abbreviations:

AES: Auger Electron Spectroscopy.

CMA: Cylindrical Mirror Analyzer; a type of spectrometer used in Auger electron spectroscopy.

CVD: Chemical Vapor Deposition (see section 1.4.4).

d.c.: Direct Current.

EDS: Energy Dispersive Spectroscopy.

EP: Elastic-Plastic.

HSS: High-Speed Steel.

Hv: Vickers hardness.

L_C: Critical load; applied load at which fracture initiates during a scratch adhesion test (see section 2.4.2).

M2: A particular type of tool steel (see section 1.4.2).

MS: Mass Spectroscopy.

OM: Optical Microscopy.

PACVD: Plasma-Assisted Chemical Vapor Deposition (see section 1.4.4).

PECVD: Plasma-Enhanced Chemical Vapor Deposition (see section 1.4.4).

P_C: Critical load; load at which fracture initiates under *static* impact using the Jindal test (see section 2.4.2).

R_C: Rockwell hardness test, 'C' scale, (see section 2.4.2).

r.f.: Radio-frequency.

SAM: Scanning Auger Microscopy.

SAT: Scratch Adhesion Test (see section 2.4.2).

SEM: Scanning Electron Microscopy.

SRT: Scratch Removal Technique (see section 2.4.1).

STEM: Scanning-Transmission Electron Microscopy.

STM: Scanning Tunneling Microscopy.

TEM: Transmission Electron Microscopy.

Ti-amide: $Ti[N[CH_3]_2]_4$.

UHV: Ultra High Vacuum.

XRD: X-Ray Diffraction.

zone (1,T,2,3): Grain morphology classifications; see section 1.4.7.

Chapter 1

INTRODUCTION

1.1 Statement of the problem:

Within the last decade, the use of hard, protective coatings of titanium nitride and titanium carbide on cutting tools to improve their wear resistance increased markedly (Hat:83). Thin films (1 to 10 microns) of these materials have been able to increase tool lifetime significantly, often by a factor of five to ten as compared to the lifetime of the uncoated tool. The coatings can be prepared by high temperature (>1000°C) Chemical Vapor Deposition (CVD) or by low temperature (<600°C) Physical Vapor Deposition (PVD). Chemical Vapor Deoposition refers to the thermally activated reaction of feed gases at the sample surface to form a solid product. PVD is a general term covering deposition by sputtering (d.c. or r.f.), evaporation processess such as ion plating (IP) or activated reactive evaporation (ARE), and plasma assisted chemical vapor deposition (PACVD). All these three processes utilize a partially ionized gas to create energetic species which promote reactions at lower temperatures, but differ primarily in the means used to introduce metal atoms into the gas phase. In sputtering, ion bombardment ejects metal atoms from a target surface. In evaporation processes, which includes ion plating and arc processes, metal atoms are thermally vaporized into the gas phase. In PACVD, the metal atoms are introduced in the form of a volatile compound, often a halogen or organometallic.

For coating tool steels, PVD processes are preferred over CVD because the latter usually operates above the austenite transition temperature (820°C-840°C) of these alloys (Wil:75). However, film adhesion is a problem for PVD processes relative to CVD because the higher operating temperature of the latter appears to preclean the substrate and to promote interdiffusion at the interface during deposition, which should create a stronger chemical bond. Thus, substrate preparation and initial deposition conditions are very important in determining the nature of the coating-substrate interface and the adhesive properties of the PVD films. Of the PVD processes, sputtering and ARE have been studied more extensively (Sun:83, Sun:832, Sun:833, Bun:83). The use of PACVD to form TiN coatings for tool applications has been bypassed until very recently (Arc:81, Kik:84, Shi:85, May:86, Wim:85). PACVD can produce more uniform deposits on substrates with complicated shapes than the other line-of-sight processes and thus it could be advantageous to employ in many circumstances. In addition, PACVD could be useful in the synthesis of diamond-like carbon and BN films, extremely hard materials which are relatively uncharacterized at present, but whose precursors are readily available in gas form, and thus are suitable for a vapor deposition process (Doi:83, Mat:82, Sav:81, Sun:86).

1.2 Objective:

The purpose of this research has been to investigate the applicability of the PACVD technique in forming protective coatings of TiN on tool steels. The relationship between the physical properties, including thickness, morphology, crystallinity, and composition of PACVD-produced TiN films and mechanical properties, including adhesion and hardness has been determined as a function of deposition conditions. Special emphasis has been placed upon understanding the relationship between coating-substrate adhesion and interfacial composition. These properties have been studied as a function of substrate pretreatment and initial

deposition conditions. The properties of PACVD TiN films are compared to literature data of coatings produced by other techniques.

1.3 Organization:

This dissertation has four major parts. Chapter one is the Introduction, containing a statement of the research problem, objectives, and general background of coating practice and theory, materials properties, deposition technologies, and film morphology. Chapter two describes the technical approach utilized in this research, reviewing the procedure of coating synthesis and characterization. Additional reviews have been included in the mechanical properties characterization sections because modern comprehensive reviews of these techniques are not available in the literature. Chapter three is a presentation of experimental studies and results. Chapter four places the results of this work into the context of deposition of coatings in general and discusses the applications potential of TiN coatings produced by PACVD.

1.4 Background:

1.4.1 Coating Practice and Theory:

Coated cutting tools first became commercially available in 1968, when cemented carbide (WC particles in a Co binder) substrates with a CVD-produced TiC layer 2-3μm thick were introduced (Sch:83). Improvements in lifetime ($> 2X$) and higher cutting and feed rates were obtained. In 1973, multilayer coatings consisting of TiC, Ti(CN), and TiN (on top) were introduced yielding further improvements in performance. Coatings with Al_2O_3 as one of the component layers between TiC and TiN became available in 1978, which yielded improved performance at higher temperatures. Al_2O_3 was found to be poorly adherent to Co(WC), but TiC adhered to both. Thin layers of TaC were also incorporated

between the Co(WC) substrate and the TiC layer to prevent carbon depletion from the WC to the TiC. This depletion embrittles the substrate, which degrades tool performance.

TiN-coated high speed steel (HSS) tools did not become commercially available until 1980 (Hat:83). Both CVD and PVD processes (sputtering, or evaporation– the latter known under the commercial names of ion plating or arc-deposition processes) are now available. Heat treatment of the steel substrate after deposition is required for the CVD process. This heating causes dimensional distortions, on the order of .001 in.(25μm), which are unacceptable for precision tools. For these types of tools, PVD is preferred to avoid this heat treatment. However, as stated earlier, the line-of sight nature of PVD processes and their relatively poorer adhesion make them less desirable when compared to CVD. TiN and TiC are the dominant coating materials utilized today, although (TiAl)N films were introduced in 1986 and are gaining in use (Jeh:86, Mun:86). This new material performs better than TiN at higher temperatures, apparently because the Al apparently segregates to the surface and forms Al_2O_3, which prevents oxidation TiN (Mun:86).

Although many types of tools and other components (such as jewelry) are now being commercially coated, there are two types of tools that are coated most often: cutting and forming. The performance of cutting tools, such as inexpensive inserts, expensive gear cutting and hobbing tools, and drills have been most successfully improved by coatings produced both by CVD or PVD. Coated forming tools, which include punches, broaches, and dies are a more recent phenomenon. If coating the tool improves performance, and this is not always the case, CVD processes appear to be more successful than PVD processes, with the latter having more adhesive-related failures (Swi:86). The tool used in forming operations is in a more dynamic stress environment, which may require better adhesion than in a cutting process. Forming tools are currently the subject of research and development efforts by many organizations.

The reason that protective coatings improve tool performance is not exactly known, because the process of tool wear is very complex and poorly understood.

It is important to realize that the coating seldom covers the entire active surface during cutting operations. Protective coatings are often 2 to 10 μm thick, but cutting tools are generally used until significant wear of the original tip or one side of the cutting surface has occured. This depth of this 'significant' wear is ultimately dictated by the adjustments that the machinist can conveniently execute with the tooling machine itself to compensate for the changing tool size. This depth can be as large as 250μm (Pet:83). However, other criteria, such as part surface finish, may be more severe than the machine compensation requirement and reduce the distance.

A more revealing example of the effect of partial coating coverage is the fact that worn coated cutting tools can be reground on one side to sharpen the cutting edge, which removes the coating on the ground side, and improved performance will still be seen relative to a completely uncoated tool, though not as good as a fully coated tool. If a particular form of wear dominates on one side of the tool, these regrinding results seem logical. However, studies by Ramalingam indicate that the phenomena can be more subtle (Ame:79). A cutting tool edge has a rake face, located above and behind the edge, where the cut metal chip contacts the tool, and a flank face, below and behind the cutting edge where the exposed new surface of the workpiece may touch and abrade the tool (Oak:83). Ramalingam studied rake and flank wear of cemented carbide (94% WC, 6% Co) inserts, either uncoated or coated with TiN only on either the flank or rake surfaces (Ame:79). His results showed that when the inserts were used to cut 1045 steel bars rake coating reduced both rake wear (also called crater wear because the hot metal chips adheres and bonds to the tool, and then breaks off leaving a crater where tool material was removed) and flank wear, but that flank coating only reduced flank wear. These results suggest that regrinding of the flank face, which removes the coating from this side, is appropriate for sharpening of metal cutting tools. However, when low cutting speeds are used, for example in gear shaping operations, flank wear generally dominates and rake/crater wear is seldom observed and therefore grinding of the rake face is recommended (Hat:83).

The explanations usually advanced for the reason that coatings improve tool wear resistance and general performance can be categorized as primarily chemical and mechanical (Kra:83, Oak:83, Sch:83). Chemical wear mechanisms take the form of substrate-workpiece interdiffusion, oxidation, and corrosion. A material that has a high melting temperature and relatively low chemical reactivity would reduce these forms of wear. Mechanical wear is being broadly defined in the present context to include any mechanism which ultimately requires the fracture of the original (ie. unoxidized, uncorroded) materials. High fracture strength, fracture toughness, and deformation resistance are required. The presence of a coating affects the stresses which ultimately develop in the substrate. Using a finite element approach, Van der Swang and Field have studied the effect of a thin hard coating on a model Hertzian (spherical indentor on a flat surface) contact stress field (Van:82, Van:83). The results indicate that tensile stresses developed during contact in the substrate are reduced by the coating and that this reduction increases with increasing coating elastic modulus and coating thickness. This reduction in substrate stress is accompanied by an increase in maximum tensile stresses in the coating itself.

Deformation of the tool during cutting can be elastic or plastic. It is desirable to keep deformation processes elastic to retain tool dimensions in subsequent operations which means that a low elastic modulus (E) and high yield strength (Y) are desirable. As pointed out by Halling, if stress levels during asperity contact remained elastic, (and below the fracture strength) the only mechanism of crack formation would be fatigue (Hal:83). Model asperity calculations suggest that for materials to remain elastic, the E/Y ratio should be less than 70 to 3.5; the maximum number decreased with increasing surface roughness. Interestingly, the values of this ratio for metals is generally between 500 to 3000, while the value for useful coating metal compound materials is typically 50 to 100, as shown in Table 1.1.

As deformation becomes plastic, high material hardness is an important requirement. Hardness is controlled by the strength of interatomic forces and by

Table 1.1: Values of the elastic modulus (E [GNm^{-2}])) and yield strength (Y [MNm^{-2}]) of selected materials (From Hal:83).

Material	E	Y	E/Y
Metals			
Cu	124	60	2070
Al	69	40	1720
Mild steel	196	220	890
Ti	116	180	650
Alloy steel En31	200	1700	120
Composites			
Wood along grain	12	45	270
Carbon-fibre-reinforced-plastic	135	670	200
Glass-fibre-reinforced plastic	30	200	150
Wood across grain	1	8	125
Concrete	50	400	125
Ceramics			
Tungsten carbide	600	6000	100
Titanium carbide	380	4000	95
Alumina	390	5000	78
Silicon nitride	400	8000	50
Glass	69	3600	20
Polymers			
Nylon	3	70	43
High density polyethylene	0.7	5	2
Rubber	0.01	30	0.3
Polyvinylchloride	0.01	45	0.2

the deformation mechanisms operative. It is very important to realize that on an atomic scale, a typical coating material's chemical properties, particularly the covalent-metallic bonding nature, leads to both chemical and mechanical wear resistance, as will be explained in the next section. Deformation mechanisms are influenced by microstructure, which will be further explored in chapter four. Finally, a coating would be of little value if it did not remain bound to the substrate. Adhesion is a critical property of the coating-substrate composite. Factors influencing adhesion will be further explored in section 1.4.6, 2.4.2, and chapters three and four. In the present study, the mechanical properties which were investigated were adhesion and hardness.

Table 1.2: Properties of titanium compounds (Tot:70, Oak:83).

Material	Tm(°C)	Hv(kg/mm^2)		Ther. Cond.	Ther. Exp. Coef.
		25°C	1000°C	cal/(s cm °C)	X 10^{-6} °C
TiN	2949	2000	> 200	0.07	9.95
TiC	3057	2900	200-300	0.08	7.6
TiO	~1800	1000			

1.4.2 Materials Properties:

TiN, TiC, and TiO

Although this research has primarily focused on the synthesis of TiN, some effort was directed towards the formation of Ti(CN), because of the high hardness of TiC. TiO is also interesting because angle-resolved photoelectron spectroscopy studies indicate that the near surface (~4 monolayers) of TiN films at room temperature is actually TiO (Ern:85). Fortunately, the structural and bonding properties of these materials are closely related. Therefore, for reasons of interest and similarity, the properties of all three compounds will be reviewed, when possible, with the understanding that the primary interest centers on TiN.

Table 1.2 lists selected values of physical and mechanical properties constants of the titanium compounds. Of particular importance for tool applications are the high hardnesses and melting temperatures of TiC and TiN. The thermal expansion coefficient of TiN (α=9.95x10^{-6}/°C) makes it the most suitable for coatings on steels (α=12.0x10^{-6}/°C). TiO has a lower hardness making it the least desirable of the three. However, the oxide is far more thermodynamically favored than the nitride or carbide in the temperature range of interest, as shown in table 1.3. For this reason, oxygen partial pressure must be minimized when TiC or TiN is synthesized. TiN oxidation by solid diffusion is negligible until temperatures of 600°C are exceeded (Mun:86). At room temperature, the surface of TiN is oxidized, presumably by a tunneling mechanism, to form TiO which changes continuously from

Table 1.3: Free energies of formation (JANAF).

Material	ΔG_f (kcal/mole)	
	298°K	800°K
TiN	-73.8	-62.5
TiC	-43.1	-41.8
TiO	-118.3	-108.8
TiO_2(rutile)	-212.6	-190.7

Ti(NO) to TiN within eleven Å from the surface (Ern:85).

The phase diagrams of the Ti-C, Ti-N, and Ti-O are shown in Figures 1.1-1.3 respectively. Studies of the interior of the phase tetrahedra are lacking. The TiC and TiN phases both have wide composition ranges, which means that they can have large populations of non-stoichiometric vacancies (Tot:70). One important distinction between the nitride and the carbide is that excess nitrogen is ejected as a gas in the former, while excess carbon is retained as a graphitic solid. Thus, synthesis of stoichiometric nitrides from the vapor phase can be accomplished by maintaining an overpressure of nitrogen.

The crystal structures of these three compounds are identical: the Bl NaCl fcc structure. The lattice parameters for TiN, TiC, and TiO are 4.24 Å, 4.32 Å, and 4.22 Å respectively. TiC and TiN follow the empirical rules formulated by Hägg determining the crystal structures of transition metal carbides, nitrides, borides, and hydrides. According to these rules, the crystal structure of these transition metal compounds will be determined by the radius ratio $r=r_x/r_{me}$, where r is the radius of the non-metal(x) or metal (me) species. If $r<0.59$, the metal atoms form simple cubic or hexagonal structures, while complicated structures are formed otherwise, because the metal lattice becomes too dilated and metal-metal interactions become too weak. Hägg noted that atomic volume occupied by the metal atom in the complex structure when $r>0.59$ was less than the volume occupied in the hypothetical simple structure.

The nature of bonding of TiC, TiN, and TiO is still controversial. Early theo-

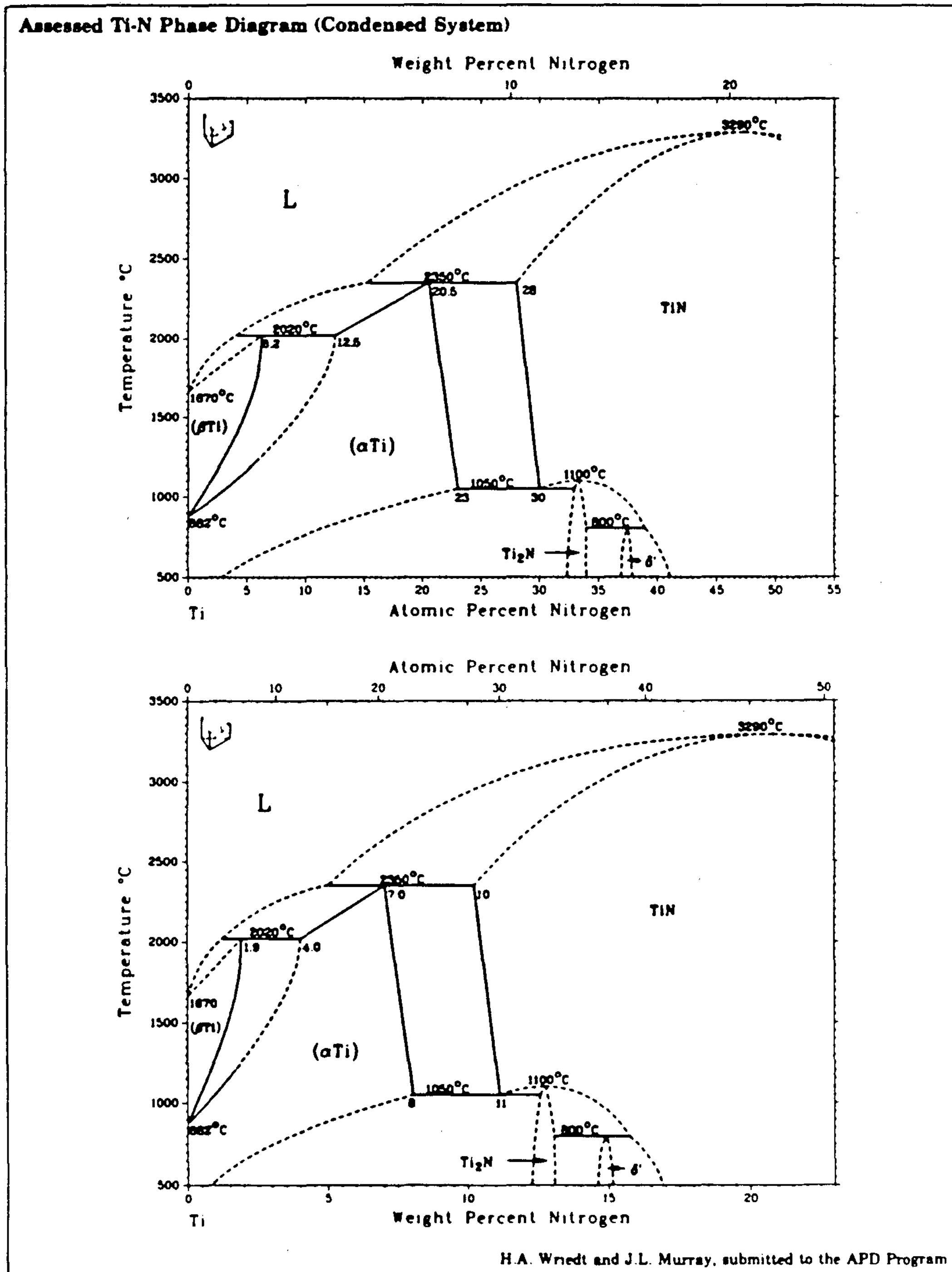

From Binary Alloy Phase Diagrams T.B. Massalski, Ed.
ASM 1986

XBL 876-2556

Figure 1.1: The TiN phase diagram.

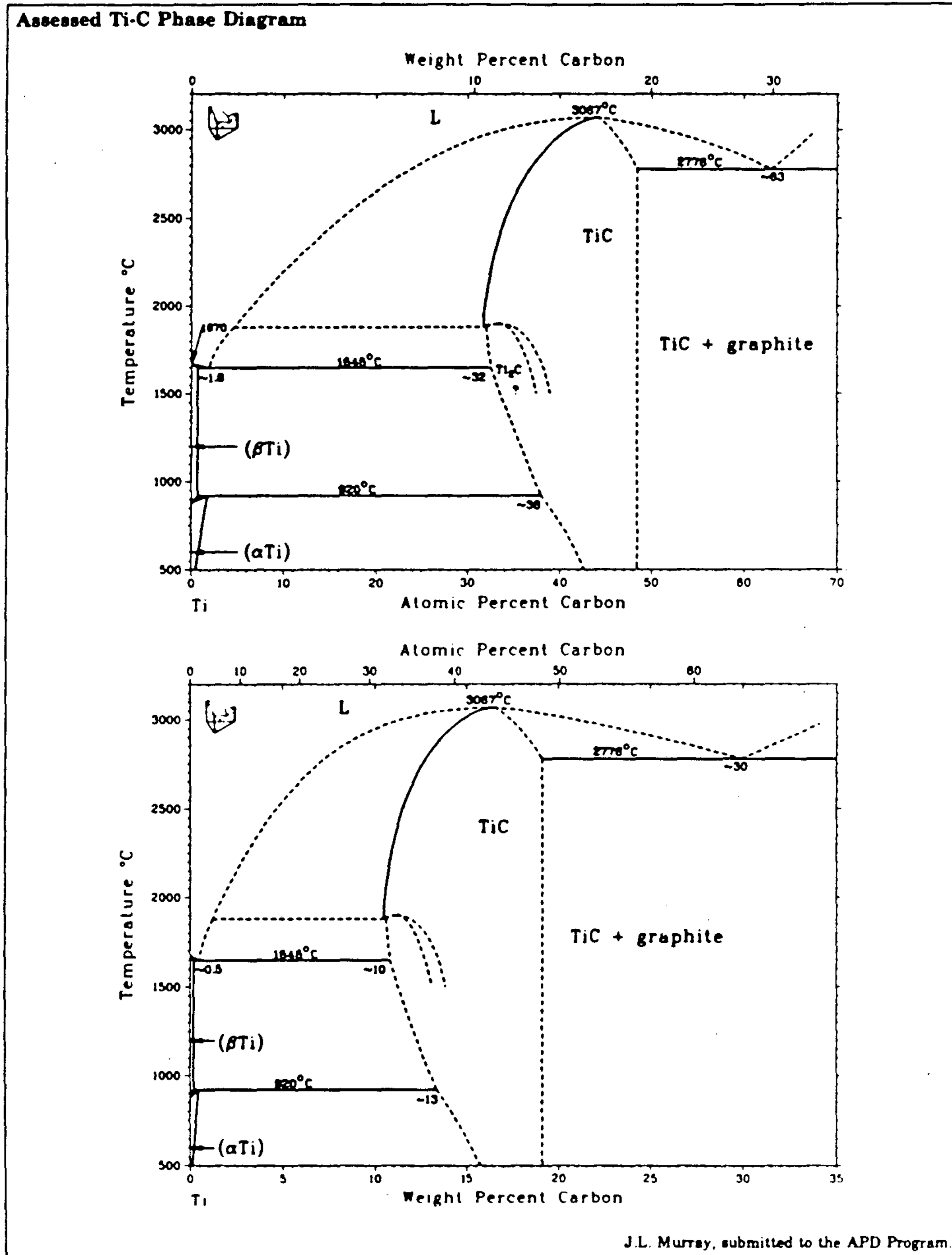

From Binary Alloy Phase Diagrams T.B. Massalski, Ed.
ASM 1986

XBL 876-2555

Figure 1.2: The TiC phase diagram.

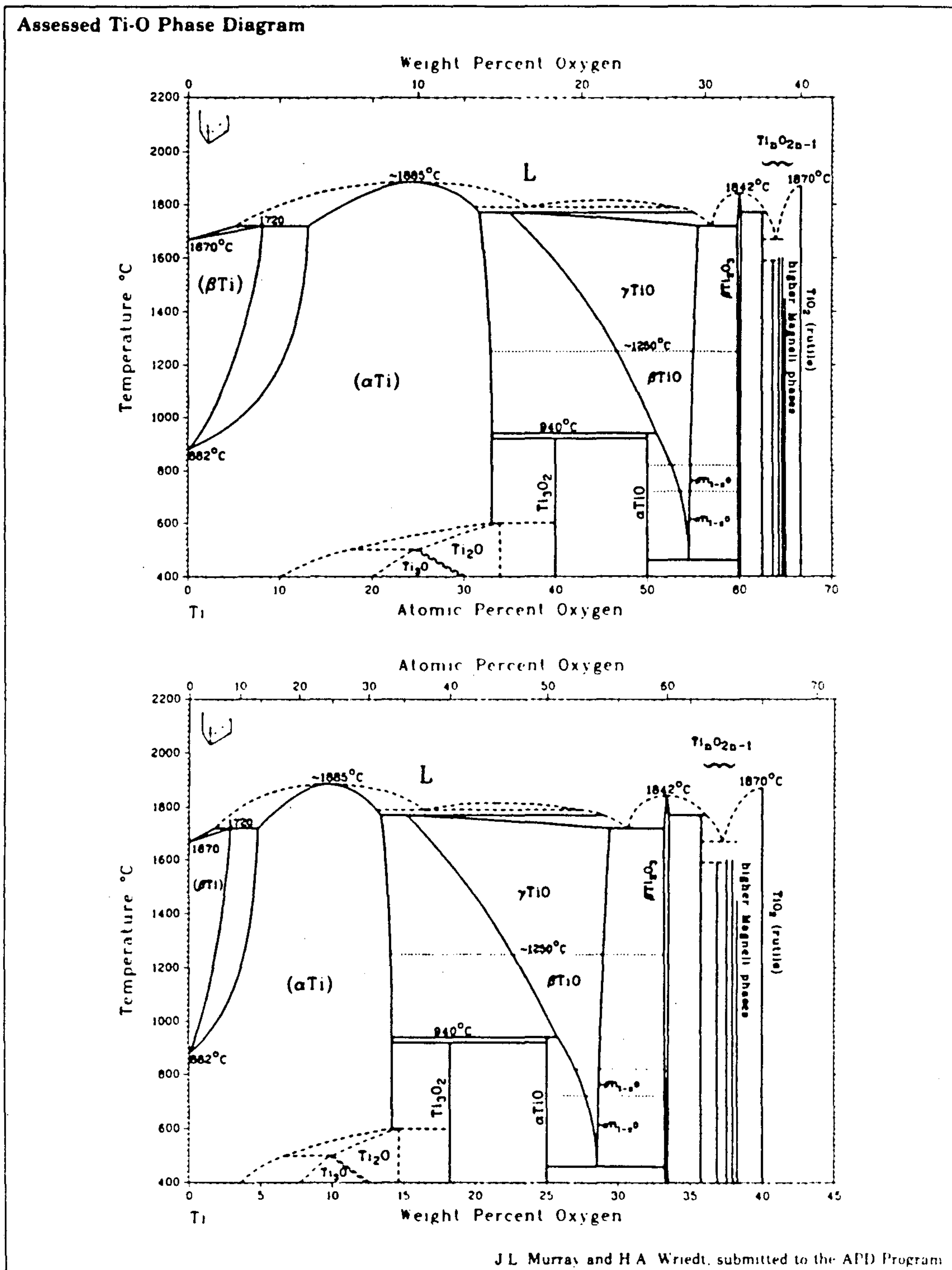

Figure 1.3: The TiO phase diagram.

ries emphasized either strong metal-metal or metal-nonmetal interactions. Recent approaches consider both important (Sun:86). A detailed evaluation of these approaches is beyond the scope of this text. Rather a qualitative summary is presented to relate some of the prominent physical properties, particularly hardness and melting temperature, with bonding characteristics. Figure 1.4 shows calculated band structures for the three compounds (Nec:76). A key point is that the d-bands are split into bonding and antibonding parts, separated by a low density of states between them. The Fermi level of TiC is at this minimum, while those of TiN and TiO are progressively located further up in the antibonding band. This increasing occupancy of the upper band correlates with a diminishing T_m, and contributes to the decrease in hardness observed. Another *atomic scale* contribution to hardness is the degree of covalent bonding. Figure 1.4 shows that the degree of titanium d-state and carbon p-state overlap is the highest for TiC, and decreases in order from TiN to TiO. Thus, the nature of bonding of these materials is related to their melting temperature and hardness, which in turn affects their chemical and mechanical wear resistance.

M2 High Speed Steel:

High speed steels (HSS) are used for machining at high speeds, with the M2 grade being a general "all-round" average representative (Wil:75). The important property of these steels is that they maintain high hardness, and toughness, at temperatures up to 550°C to 590°C, whereas most other steels soften at below 200°C. The key to the HSS hot or "red" hardness is that these steels contain complex alloy carbides, particularly of Mo, W, and V, which are hard and remain chemically stable up to the above mentioned temperatures. The alloy composition of M2 and the volume percent distribution of carbide phases are listed in Tables 1.4 and 1.5 for the annealed and oil-quenched (O.Q.) microstructures (Wil:75).

The carbon promotes the hardenability of the matrix, as well as being a con-

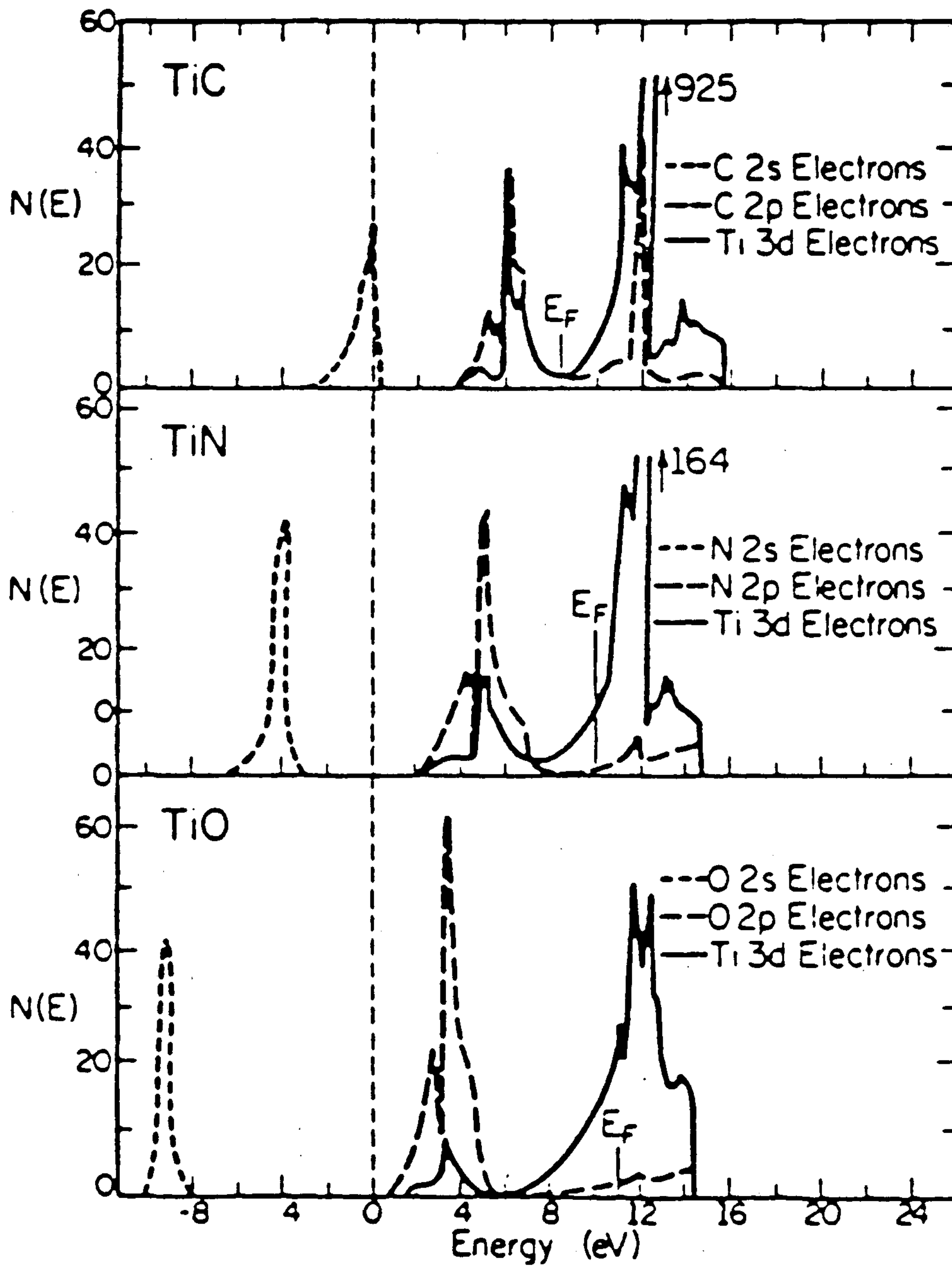

Figure 1.4: Calculated partial valence electron density of states for stoichometric TiC, TiN, and TiO. From Nec:76

Table 1.4: Elemental composition of M2 tool steel.

Elemental Composition of M2 Steel		
Element	Wt.%	At.%
C	0.85	4.1
Si	0.25	0.52
Mn	0.25	0.27
Cr	4.00	4.5
Mo	5.00	3.1
W	6.00	1.9
V	2.00	2.3
Fe	81.65	83.3

Table 1.5: Distribution of carbide phases in annealed and oil quenched M2 tool steel.

M2 Condition	Carbides (volume percent)			
	$M_{23}C_6$	M_6C	MC	Total
Annealed	9	16.0	3.0	28.0
1220°C O.Q.	0	7.5	1.5	9.0

stituent of the carbides. Chromium is added to promote depth hardenability, and exists as $Cr_{23}C_6$ in the annealed microstructure and it is dissolved in the austenitic and martensitic microstructures. W, Mo, and V as mentioned above, are present to form stable high temperature carbides. However, the W and Mo exist in an M_6C phase, either Fe_4W_2C or Fe_4Mo_2C, while vanadium exists as VC. The VC is also relatively insoluable at hardening temperatures and it retards austenite grain growth. It is worth noting that VC has the NaCl structure (a=4.18Å) like TiN (a=4.24Å).

The generic heat treatment cycle of M2 steel is shown in Figure 1.5, along with the hardness-tempering temperature curve and the Time- Temperature- Transformation (TTT) curve (Wil:75). Two features are worth further comment concerning tempering:1)retained austenite and 2)secondary hardening. Upon quenching to room temperature, the steel contains a significant amount of soft retained austenite often on the order of 20-25%. The retained austenite amount can be reduced by stabilization at liquid nitrogen temperature or by repeated tempering cycles or both. During tempering, several complex reactions occur. Tempered martensite forms accompanied by stress relief, which permits some retained austenite to transform to untempered martensite. In addition, if tempering is performed at around 500°C, fine transistory M_2C carbides of W and Mo form which transform to fine M_6C carbides upon cooling. An increase in hardness is observed after the temper, which is called secondary hardening. The fine carbides also remove carbon from the retained austenite. The martensite start temperature is therefore raised, which provides another driving force for the conversion of retained austenite to hard, but brittle, untempered martensite. A second temper is always required to temper the martensite formed from the first temper.

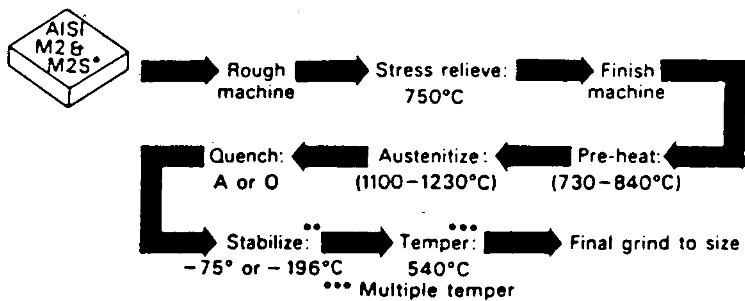

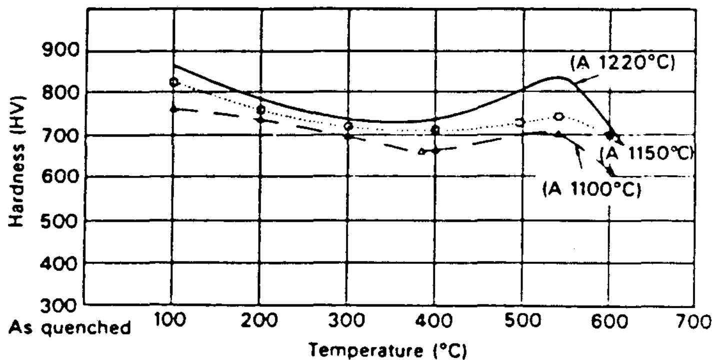

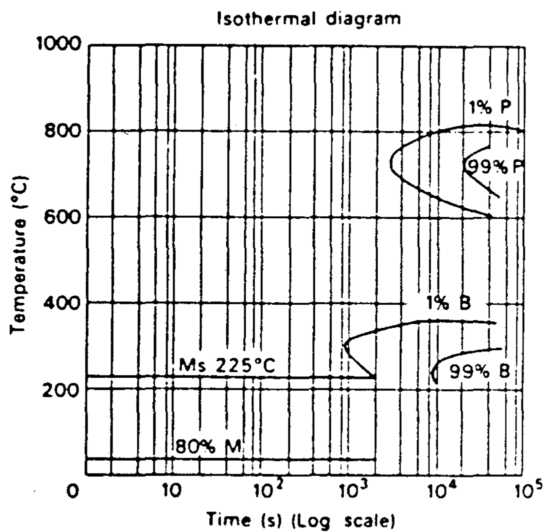

Figure 1.5: Data on M2 steel: generic heat treatment cycle, hardness-tempering temperature curve, and TTT curve. From Wil:75

XBL 8711-4599

1.4.3 Studies of Sputtered TiN:

At present, reactive sputtering is the technique with the highest deposition rate (85 Å/sec.) used in industry to form TiN coatings at temperatures below 550°C (Sun:83, Sun:832, Sun:833, Spr:83). Sproul has investigated the mechanical properties of sputtered TiN films. Using M2 tool steel (Rockwell C hardness of 65) as a substrate, TiN coatings of 9.5 micron thickness were found to have Vickers microhardnesses of 2359 (100gm load) and 2391 (200gm load) kg./mm.^{2} (Spr:83). Film adhesion was quantitatively assessed by the scratch adhesion test (SAT) in which the critical load for the onset of the loss of adhesion is measured (Per:83, Hin:84). Sproul found that the critical load increased from 2 to 8 kgf. linearly with thickness from 2 to 10 micron. TiN-coated end mill cutters, saw blades, and drills outlasted uncoated ones by factors of 3.5, 2.2, and 50 respectively in tests where 1035 steel was milled, cut, or drilled. The tools were tested until they failed catastropically.

The key to the high rate of deposition in Sproul's studies is a careful control of target surface composition during sputtering, accomplished by adjusting the N_2/Ar working gas ratio. If Ar alone is used, titanium films are formed. As the N_2/Ar gas ratio increases, films are formed with increasing nitrogen content, from α-Ti, to Ti_2N, to ultimately TiN. However, deposition rates drop dramatically as nitrogen is increased, quickly falling to 10% of the rates for pure titanium. This drop occurs because the Ti target becomes nitrided, and the sputtering rate of TiN is lower than that of Ti because of the stronger bond strength between Ti-N versus Ti-Ti. Chemisorption studies by Shih, and later Sundgren, of N_2 on Ti show that the sticking coefficient of N_2 drops as surface coverage becomess sufficient to achieve an underlayer structure which is essentially the TiN phase (Shih:76, Shih:762, Sun:83). During sputtering, if the nitrogen surface is kept at subsaturation levels, nitrogen will not be detected by residual gas analysis using mass spectroscopy (MS) because the nitrogen is gettered by the titanium. As

surface coverage is increased to form the underlayer structure, nitrogen will be detected by MS because it is no longer gettered by free titanium on the surface. The nitrogen signal determined by MS shows a sharp rise with nitrogen feed rate at this transition. At the onset of this rise, where the first two layers of the Ti target are essentially TiN, stoichiometric TiN will be sputtered off at very high rates, presumably because the third layer is still titanium. Sproul patented the process in which the nitrogen MS signal is used as a feedback control for the nitrogen gas feed rate to maintain high TiN sputtering rates (Spr:83). This process advance was of major significance in hard coating production.

Sundgren and his coworkers have done much to advance the fundamental scientific understanding of the TiN sputter deposition process and to investigate the properties of carefully prepared TiN films. Studies have included topics such as the effect of sputtering deposition parameters on coating properties (Sun:83), investigations of morphology and structure (Sun:832, Hib:83, Hib:84, Hib:85), the influence of substrate bias and shape on coating properties (Sun:833, Joh:84, Hak:87), adhesion of sputtered TiN to high speed steel (see section 1.4.6) (Hel:85), and single crystal TiN thin film growth (Joh:85). Results of the Sundgren studies will be reviewed in more detail in chapter four.

1.4.4 PACVD:

The process of plasma assisted chemical vapor deposition can be viewed as consisting of four steps, shown schematically in Figure 1.6 which depicts a parallel electrode geometry. Step one is the excitation of ground state atoms or molecules into excited states. The excited species adsorb onto the substrate in the second step. Adsorbate surface diffusion and reaction with coadsorbates and the substrate to form a solid condensate occurs in the third step. Desorption of reaction byproducts and etching (induced by the chemical environment or ion/electron bombardment) of surface material occurs in the fourth step. Ground state atoms/molecules can also undergo steps two through four, which is essentially chemical vapor deposition, a topic which has been recently reviewed in detail by Carlsson (Car:85). Excitation in step one is influenced primarily by plasma volume chemistry, while steps two through four involve plasma surface interactions (Tho:83, She:84).

Excitation occurs in a plasma, which is a partially ionized gas in which gas collisions are frequent enough to effect a long range electric coupling between ions. Gas pressures in the range of 50 mtorr to 5 torr will satisfy this condition, because of reduced gas mean free paths. The term glow discharge is often used to describe this plasma because of the characteristic luminescence that occurs in the visible range when excited states de-excite. The plasmas used in PACVD are weakly ionized, the ratio of the electron concentration to neutral species is of the order of 10^{-4} -10^{-6}. Electron (and positive ion) densities are between 10^9 and 10^{12} cm^{-3}, and average electron energies are in the range of 1 to 10eV (11600-116000 °K), while ion energies are approximately 0.04eV (464 °K) The energy for excitation is provided by an electric field, either d.c., r.f. (20 KHz - 40 MHz), or microwave. All commercial systems use r.f. The typical frequency is 13.560MHz because of the ready availability of r.f. sources designed for this wavelength, which was historically set aside by government regulators for industrial transmitters. Two electrode geometries are often used, either a parallel plate or

Plasma Assisted Chemical Vapor Deposition (PACVD)

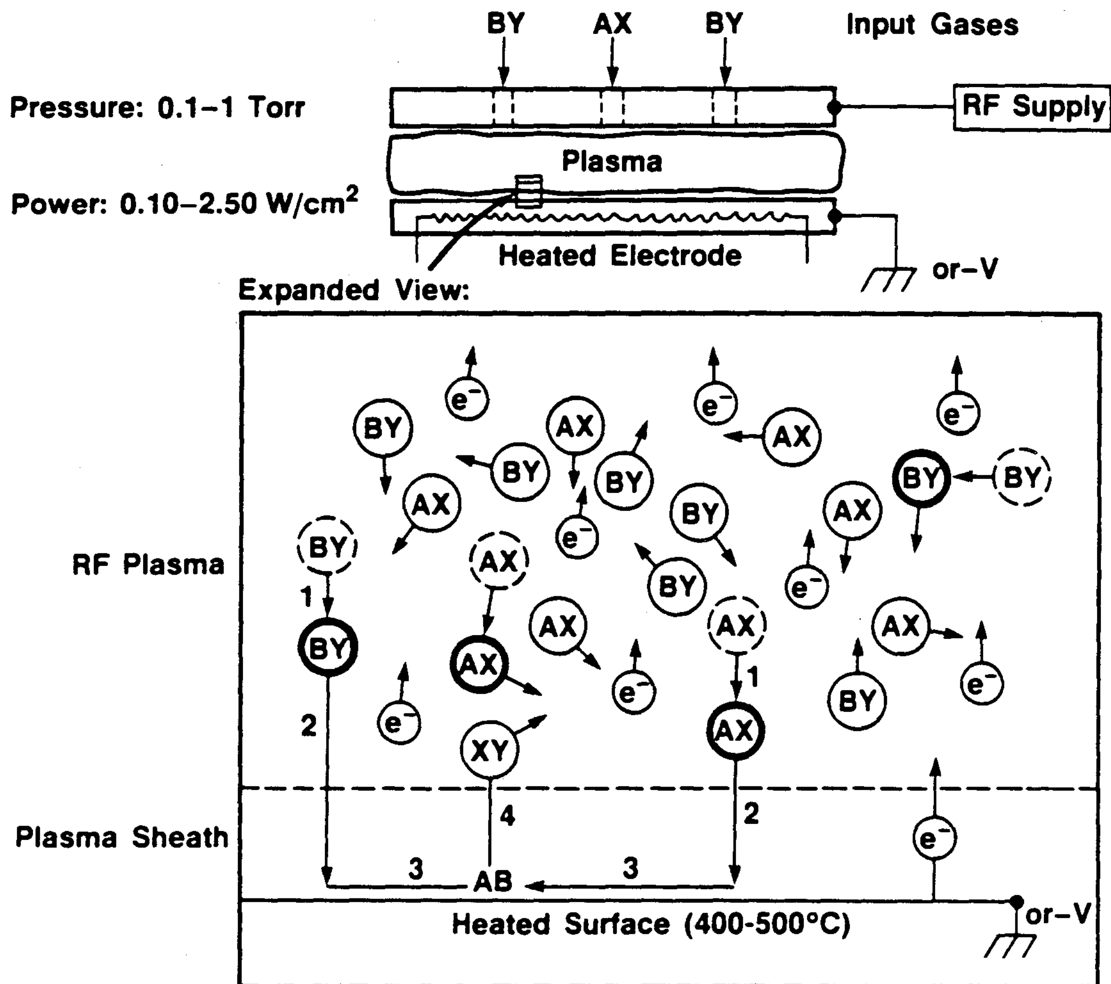

Film Deposition Sequence

1. **Excitation of ground state neutrals into ions, radicals, excited state neutrals.**
2. **Adsorption of excited species.**
3. **Surface diffusion of excited species and reaction to form a compound**
4. **Desorption of reaction by-products.**

XBL 869-89..

Figure 1.6: Schematic sequence of PACVD process.

a coil configuration. The parallel plate electrodes are typically inside the reactor, while the coils are usually external which removes electrode material influences in this case. The advantage of the former configuration is that electric field uniformity is maximized and plasma volume to electrode surface area ratio is minimized. The reverse is true of the coil arrangement, and the nature of the plasma has to be better understood in this configuration to obtain controlled, repeatable results for this approach (Ins:87). The parallel plate configuration was first developed by Reinberg and is extensively used in the semiconductor industry, where the materials to be processed are essentially planar (She:84). The coil geometry is useful for large batches, and for non-planar substrates. This configuration has been extensively studied by Inspektor and his collegues (Avn:84, Avn:85, Ron:83, Rav:83, Rav:832, Ins:80).

The low degree of ionization of these plasmas is maintained in a manner such that the rate of ion production owing to energy addition by the eletric field is balanced by the diffusion of charged particles to the walls where recombination occurs. As reviewed by Thornton, the process therefore involves the transfer of energy from an electric field of strength E and frequency f to the plasma electrons, the production of ionization in the working gas of density N and ionization potential U_i because of electron-gas particle collisions with a mean free path $\lambda=1/\sigma N$ (where σ is the collision cross section) and the diffusion of charged species to the walls in an apparatus geometry with characteristic diffusion length Λ (Tho:83). A detailed understanding of the physical chemical processes within a low pressure plasma requires a knowledge of the electron energy distribution with respect to E, f, and position; of collision cross sections; reaction rate constants; and of charged species diffusion rates. Most of these values are poorly understood.

Qualitatively, the reactions which occur in the plasma can be reviewed (Tho:83). Electron impact is believed to be the major source of charged species and radicals. Radicals are an important constituent in plasmas because of their high reactivity, which makes them a major contributor to solid materials synthesis from a plasma. Electron impact dissociation is believed to be an important source of free radicals

for two reasons. First, the threshold energy for dissociation will be in general considerably lower than the relevant ionization potential for the working gas, so that the dissociation rate will be several times the ionization rate. Second, excited electronic states in molecules greatly weaken the molecular bonds and often result in antibonding states and dissociation.

Atomic radical recombination surface reactions along with those involving other excited species such as molecular radicals and ionic species are of vital importance to PACVD materials synthesis because of their high reaction rates relative to ground state species. The transport of radicals and neutrals from the gas phase to the surface primarily involves the physics of diffusion and adsorption. The adsorption of ions and their subsequent surface reactions are more complicated because ionic species are accelerated towards surfaces by the electric field present in the plasma sheath at the surface, promoting adsorption and imparting energy for surface reactions and modifications. The sheath region forms because electron mobility is higher than ion mobility, and the electrons near a surface are quickly absorbed. The plasma developes a positive potential with respect to the electrode. The electric field at the surface retards the further flux of electrons from the plasma. The sheath region is characteristically dark because the low electron density prevents ion-electron recombination luminescence. Positive ions that diffuse into the sheath are then accelerated towards the surface by the electric field. Electrons ejected from the surface by the ion impact are accelerated into the plasma by the sheath field and they are the primary source of ion and radical generation in the plasma volume mentioned earlier. It is important to realize that all surfaces remain negative with respect to the plasma. The electrode connected to the r.f. supply oscillates in voltage (with respect to ground), over each frequency cycle, as shown in Figure 1.7. The opposing electrode, onto which the substrates are generally placed, also oscillates in voltage. However the magnitude of the substrate sheath field can be very different than that of the driven electrode. The substrate electrode can be either floated or grounded (Fig. 1.7a), or intentionally negatively biased (Fig. 1.7b). The average energy of bombarding species increases

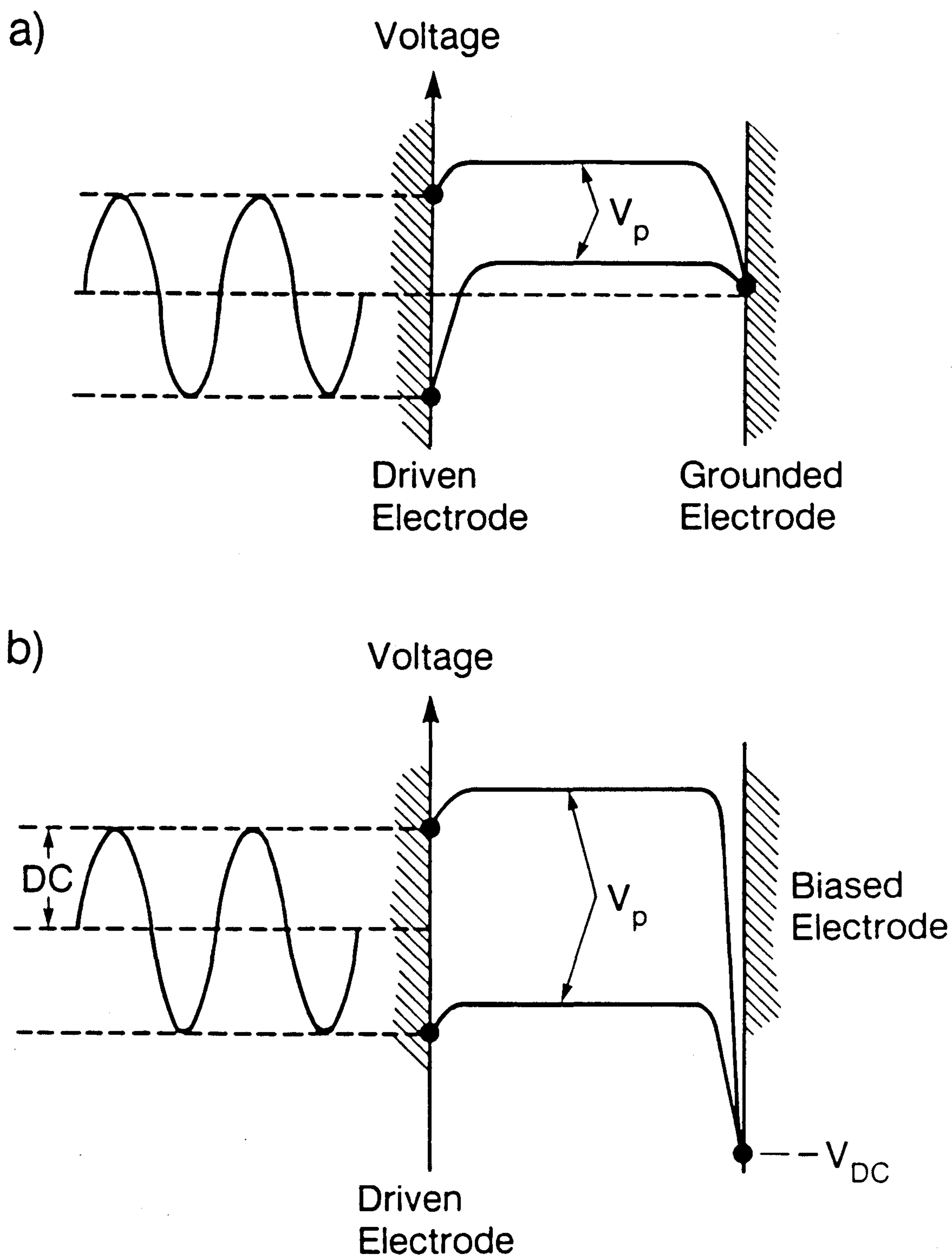

Figure 1.7: Voltage potentials between two plates in an rf plasma for a) grounded and b) biased electrodes.

with negative bias.

The energy of plasma generated species impacting a surface typically is in the range from a few eV to several hundred eV. Such energetic species do more than just provide reactive starting materials for low temperature synthesis. As noted by Thornton, these energies are equal to or exceed those which characterize a solid, such as surface atom binding/sublimation energies, U_s, of 3-10eV, sputtering thresholds of approximately $4U_s$, interstitial formation energies of about 5eV, and vacancy formation energies of about an eV. Ion bombardment can therefore induce sputtering of adsorbates or coating material, promote the formation of point or line defects within the bulk or at the surface, cause intermixing of underlying layers, increase adatom mobility or promote working gas incorporation. These processes can influence subsequent film properties, such as composition, morphology, structure, adhesion, density, and porosity.

Recounting briefly, step one of the PACVD process is the generation of excited state radicals and ions in the plasma volume, and step two is the adsorption of some of these species to the surface. The energetic adsorption of ions can induce structural and compositional modifications of the surface region. Step three is the diffusion, combination, and reaction of the energetic species with each other and surface sites to form a solid product. Additional energy from further ion bombardment and from thermal sources in the substrate (ie. intentional substrate heating) can affect both diffusion and chemical reactivity.

A variety of materials have been synthesized by PACVD, including elemental materials, semiconductors, oxides, carbides and nitrides (Vep:85, Hes:84. As classified by Veprek, a plasma can assist a CVD process in two ways: by a "kinetic effect" or by a "thermodynamic effect" (Vep:85). In the former, excited species created in the plasma accelerate reactions which are thermodynamically possible (using standard state thermodynamic values). High operating pressures, low power densities, and floating/grounded substrates favor this effect. The "thermodynamic effect" refers to situations where the plasma creates unique chemical equilibria which do not have conventional thermal counter parts. (In other words,

the electric field of the plasma is imparting energy to the system which is not accounted for in the conventional equation of state. The equation of state would have to be rederived with an energy term representing the electric field contribution in order for the system to be properly described thermodynamically. Thus, conventional thermodynamic values, either standard state [P = 1 atm.] or those adjusted for pressure, *can be* completely misleading in predicting chemical reaction favorability in a plasma environment.) Low operating pressures and high power densities favor this effect. High substrate bias also introduces unique states, particularly promoting the formation of high pressure metastable phases.

The final step of the PACVD process is the ejection of reaction byproducts–if any exist. The factors which influence this expulsion and the resulting properties of synthesized materials will be explored in Chapters 3 and 4.

1.4.5 TiN Synthesis by PACVD:

Archer was the first investigator to report the formation of TiN by PACVD with a d.c. plasma (Arc:81). Starting with N_2, H_2, and $TiCl_4$, TiN was claimed to have been formed at 400°C and above. Below this temperature the coatings flaked off, although they were still golden color (the color of TiN) down to 250°C. X-ray diffraction (XRD) was performed, but the results were not clearly stated. Film growth rates in the range of 3 to 10 Å/sec. were reported.

Kikuchi et.al. investigated TiN films formed by d.c. plasma of N_2, H_2, and $TiCl_4$, on M6 tool steel and cemented carbide inserts at 500°C and above (Kik:84). Although they did not explicitly prove that they had formed TiN, they obtained a material with an indentation hardness (Knoop test) of 2200 to 3000 kg./mm.^{2} with 100 gm. load (bulk TiN is 2000) that depended upon substrate bias. Film thickness was not mentioned. They found that film chlorine content increased with decreasing substrate temperature and increasing $TiCl_4$ flow rate, and adversely affected flank wear and crater wear in continuous cutting tests. Columnar grains and growth rates of 3 Å/sec. were reported. Wimber has also studied TiN produced by d.c. PACVD and has found that chlorine content was detrimental to mechanical properties (Wim:85).

Shizhi and coworkers also studied TiN formed by d.c. plasmas of N_2,H_2, and $TiCl_4$. Two conditions were investigated: 1) T=430°C, P=1 Torr, and d.c. voltage=1000V. 2) T=520°C, P=0.25T, and d.c. voltage=2250-2500V. A dense (zone 2, see section 1.4.7) structure was formed for condition one while the second condition yielded a more nodular structure, believed to be due to gas phase nucleation. Film thickness increased linearly with time, and with $TiCl_4$ partial pressure. Hydrogen was essential for film formation, but the highest hardnesses (20gm load, thickness unspecified) were obtained for low H_2/N_2 ratios (H_2/N_2=1). The films had a (200) preferred orientation. Chlorine content was about 10% for both pressure conditions.

Mayr and Stock have also reported results for TiN formed by d.c. PACVD (May:86). The reactive gases again were H_2, N_2, and $TiCl_4$. Substrate temperature was maintained at approximately 500°C, and deposition pressure was 5 mtorr. A (200) with some (220) oriented material formed consistently, with a composition that was stoichiometric over a wide range of N_2 and $TiCl_4$ partial pressures. Nitrogen deficient TiN was found at low P_{N2} and N-rich TiN (N/Ti=1.1) was found at low P_{TiCl_4}. However residual chlorine contents were not reported. High microhardnesses (2000-3000 Hv) were reported, but thickness was unspecified and the low indentation load (15gm) raises the possibility of indentation size effects and measurement error (see section 2.4.2) were present. The authors mention that homogeneous gas distribution is required in the cathode region to obtain films of uniform thickness and composition. Their film morphology was dense and columnar (Zone 2, see section 1.4.7); they did not encounter the nodular structures that Shizhi reported.

The difficulty with d.c. PACVD is that power density, voltage, and temperature (influenced by bombardment) are strongly interrelated. If an r.f. discharge is used, low power densities can sustain a plasma with relatively less bias and bombardment induced heating. Temperature and applied bias can be independently controlled by separate power supplies. Thus, plasma volume chemistry, sheath bias effects, and surface temperature can be more systematically investigated in an r.f. plasma system than in a d.c. system. Shizhi and Hongshun have reported forming TiN using an r.f. plasma (13.56 MHz) of N_2, H_2, and $TiCl_4$ at one Torr on glass, low carbon steel, and mica (Shi:85). Vickers microhardness values of 2000 kg./mm.^{2} were obtained with a 20 gram load (thickness unspecified) and film growth rates of 17 Å/sec. were determined. The Vickers magnitudes were determined by optical measurements, which are subject to error at these low loads and high hardness values (see section 2.4.2) (Shi:872). Columnar grained, golden films were found at 470°C and above. XRD showed that the material had a strong preferred orientation which could correspond to the (200) plane of TiN.

The important point to note in these studies is that the plasma allowed TiN to

form from N_2, H_2, and $TiCl_4$ at temperatures lower than are possible if the reaction was only thermally driven–the free energy of the reaction becomes negative at approximately 590°C (JANAF). The plasma also increased the growth rate. If ammonia, NH_3, is used instead of N_2 and H_2, the critical CVD temperature would be as low as 250°C. In conjunction with a plasma, an NH_3-$TiCl_4$ reaction should provide a fast, low temperature coating process.

Kurtz and Gordon have recently (their results being published simultaneously to results published and reported in this thesis (Hil:86, Hil:862)) reported the formation of TiN from $TiCl_4$ and NH_3 by CVD at atmospheric pressure between temperatures of 400°C to 700°C (Kur:86). Carrier gases of He and Ar were used. Chlorine content increased with decreasing temperature. Substrate materials were primarily glass or silicon, though stainless steel was investigated. Poor adhesion between the TiN and stainless steel substrates was qualitatively found. The authors speculated that Cl degraded the near surface region of the steel, because small amounts of iron would detach with the films. High growth rates (1000 Å/sec.) were obtained under some conditions, although growth rates of 5-70 Å/sec. were more typical. Chlorine contents were not specifically reported and indentation hardness was not measured.

An alternative approach for producing films at low temperatures by CVD is to use organometallic sources. Sugiyama et.al. reported the formation of TiN from titanium dialkylamides in the temperature range of 250°C to 700°C using CVD (Sug:75). The characterization indicates that a golden material formed with the NaCl lattice structure and it contained Ti, N, and some carbon. Oxygen content was not mentioned. Other groups have not been able to reproduce the Japanese results, which will be discussed further in Chapters 3 and 4 (Kur:86, Nie:86).

1.4.6 Studies of Titanium Nitride-High Speed Steel Interfacial Adhesion:

Two groups have published studies of the effect of interfacial composition and structure on coating-substrate adhesion in the context of high speed steel tool applications. Greene and his coworkers have studied sputtered TiC on steel (Pan:82, Gre:78, Gre:76,Muk:75). The substrates were cleaned prior to deposition by d.c. argon sputtering. Adhesion measurements determined by the Scratch Adhesion Test (SAT), a technique which will be discussed further in section 2.4.2, were correlated to interface composition, which was obtained by Auger Electron Spectroscopy (AES) while the coating was removed by argon sputtering to yield a depth profile. In addition, the interface was studied directly in cross-section by transmission electron microscopy (TEM). Specially prepared coatings having the interface composition through the entire coating were also analyzed by TEM. They found that adhesion was improved by substrate biasing and lower gas working pressures, which increased the energy of impinging atoms. This increased substrate bombardment resulted in the formation of wider interfacial zones, consisting of Ti, and Fe oxides. They concluded that the best adhesion was obtained by having a wide (1000-3000Å) interface region of TiC_XO_{1-X} rather than higher oxides of titanium.

Sundgren and his coworkers have published a study on the adhesion of sputtered TiN to high speed steel and the nature of this interface (Hel:85). The films were formed by reactive sputtering at temperatures between 150°C and 600°C. SAT experiments were performed as a function of temperature for three different pretreatments: degreased; degreased and sputter-etched; and degreased, sputter-etched, and deposition of an intermediate layer (1000Å) of pure titanium. Scratch adhesion test results were correlated to AES data. The authors propose that epitaxy plays a major role in the adhesion of this system. At high temperatures above 400°C, where higher critical loads were obtained, they reported that the

steel surface is FeO, which like TiN has the NaCl structure (a=4.31Å and 4.24 Å respectively). At lower temperatures, Fe_2O_3 and/or Fe_3O_4 are present, which have different crystal structures. Identification of the iron oxides was based on Auger depth profiling data. To date, they have not confirmed their assignment of FeO with cross-sectional studies using TEM. They suggest that the Ti layer pretreatment may reduce these oxides and improve adhesion, as was indicated by SAT results.

1.4.7 Zone Models of Morphology:

The film formation process influences ultimate coating structure. Cumulative research of metal films and more recently of metal compound films produced by evaporation, sputtering, and CVD show that there are similarities in structures for all these techniques. A zone classification scheme has emerged which uses the dominant operating diffusion mechanism as a criterion. The original model was developed by Movchan and Demchishin, based on their investigations of metal films formed by evaporation and condensation in vacuum. Homologous temperature (T/T_m) of deposition was the only measure of diffusion mechanism dominance. Thornton expanded the model to include the influence of gas molecule inpingement on surface adatom mobility during film formation in sputtering processes (Tho:77, Tho:86). Along with homologous temperature, deposition gas pressure was incorporated as an additional gauge of adatom mobility–with lower gas pressures promoting higher surface mobility because impinging gas molecules had undergone fewer collisions in the gas phase resulting in higher gas kinetic energies at the point of impact. Sketches of the structures are shown in figure 1.8.

Using Thornton's classification, the zone 1 structure is the result of limited or no adatom mobility, favored at low T/T_m (Movchan $T/T_m < 0.3$) and higher gas pressures. The morphology consists of large, dome-capped grain with poorly defined fibrous interior structure. Each impinging atom is essentially frozen at the point of impingement. Geometric effects dominate the process, so that surface roughness and the shadowing of impinging atoms influences structure. The films can be crystalline or amorphous, are often porous, and have generally poor mechanical properties. The zone T (Transition) structure is favored by lower gas pressures and higher T/T_m. The zone T structure has been described as "the limiting form of a zone 1 structure at zero T/T_m on infinitely smooth substrates" (Tho:77). It appears as a material with the zone 1 fibrous interior, but with a flat top. Porosity is not present in these films, and they often have good mechanical

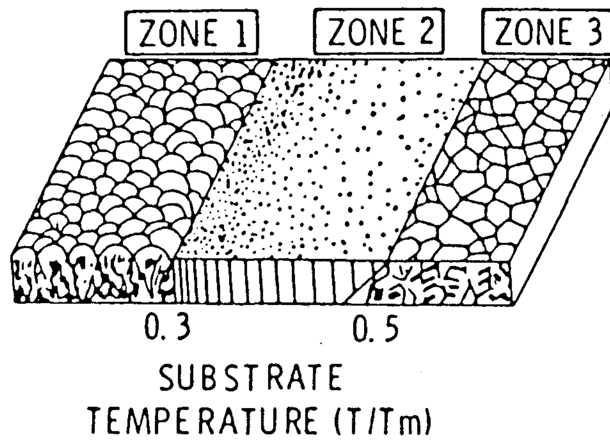

a) Movchan/Demchishin Model

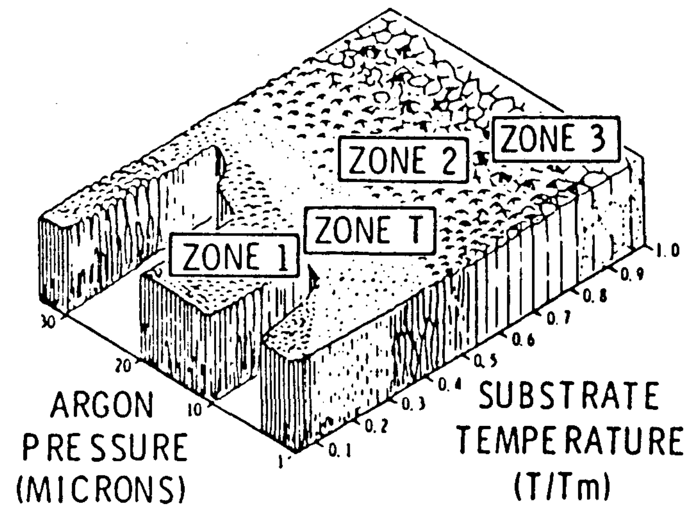

b) Thornton Model

J.A. Thornton

Ann. Rev. Mater. Sci. **7** (1977) 239.

XBL 8711-4598

Figure 1.8: Zone grain morphology models. From Tho:77

properties. The zone T structure was first defined and categorized by Thornton.

The zone 2 structure occurs when surface diffusion dominates. The morphology consists of well defined columnar grains with faceted or flat tops. Grain boundaries are dense and mechanical properties are good. Movchan defined it as occuring between 0.3 and 0.5 T/T_m. The zone 3 structures occurs when bulk lattice diffusion dominates. Grain growth or recrystallization can occur. The former will yield columnar grains of larger size while the latter will promote an equiaxed grain structure. The Movchan classification considered only the equiaxed possibility.

The Thornton classification has become a useful morphology labeling protocol in the literature. However, Sundgren has correctly stated that in the case of binary (or more) component films, chemical potentials can drive surface diffusion and increasing heats of compound formation can increase adatom mobility which leads to larger grain sizes (Sun:832). Sundgren's studies indicate that the homologous temperatures defined by Thornton as transition values between zones in unitary films are often lower for metal compound films (Sun:86). He attributes these variations to binary compound formation effects.

Chapter 2

TECHNICAL APPROACH

2.1 Research Strategy:

The operational strategy of this study has been to characterize the coating-substrate system as a function of deposition conditions. There have been two stages: 1) Design and construction of a deposition system. 2) Development of an understanding of the relationship between the physical properties including thickness, morphology, crystallinity, bulk and interface composition of the TiN and Ti(CN) coatings and the mechanical properties, including adhesion and hardness of the films. These properties, in turn, depended upon deposition conditions.

2.2 Apparatus:

A planar r.f. deposition system based on an earlier design (Wil:82, Wil:83) was built for these experiments. This apparatus is a smaller version of industrial models used for Si_3N_4 deposition and reactive ion etching (Tho:83, She:84, Hes:84). A chamber made of type 304 stainless steel (304 SS) served as the chemical reactor and a separate connecting chamber housed an EAI quadrupole mass spectrometer that monitored gas composition. A schematic diagram of the apparatus is shown in Figure 2.1 and a photograph is shown in Figure 2.2.

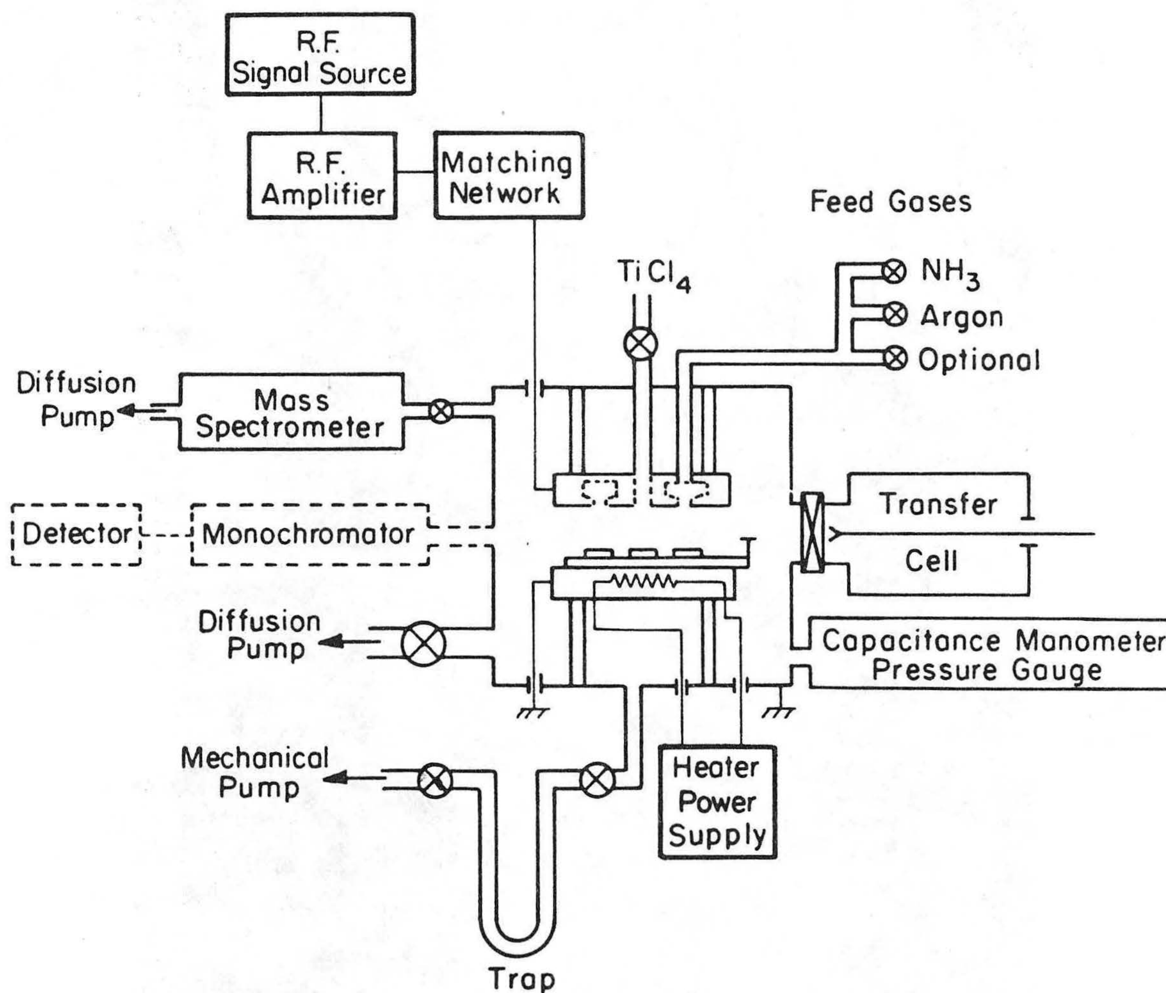

Figure 2.1: Schematic of plasma deposition chamber.

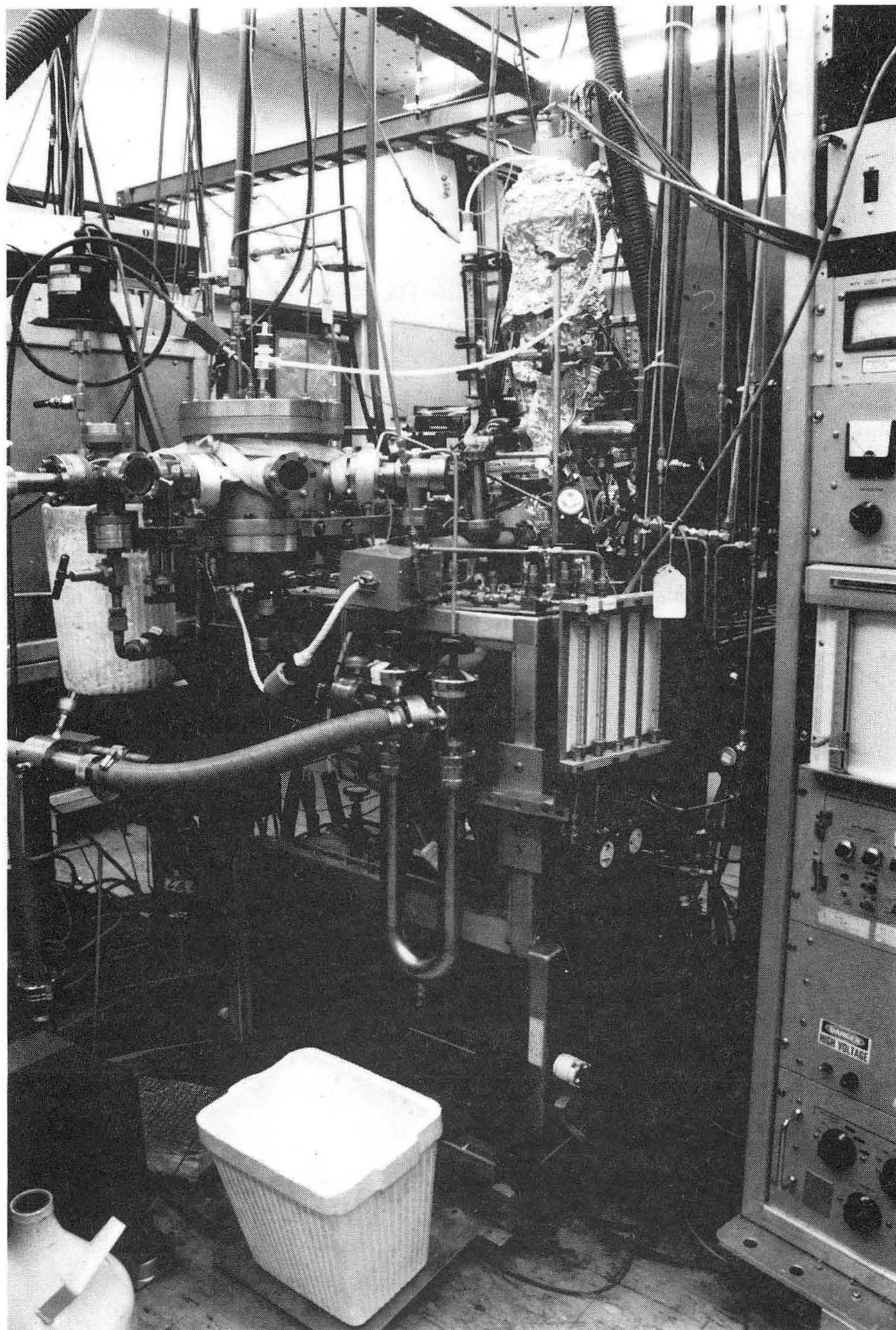

XBB 870-9579

Figure 2.2: Plasma deposition chamber.

Pressures in the range 0.1-1.0 torr were maintained during the reaction using a rotary mechanical pump (Sargent Welch 1397) with a trap cooled by liquid nitrogen employed in the foreline. During the deposition,the mechanical pump foreline pressure was maintained at 0.1 torr by flowing nitrogen gas to dilute the reactants (particularly NH_3) and to prevent oil backstreaming. The pressure in the reaction chamber was monitored with a capacitance manometer gauge (MKS Baratron 227A). The system pressure was adjusted by altering the input gas flow by needle valves and by throttling the pump. A mass flow controller (Porter Instruments model CM-4 monitor and model 200 F-S-V-C controllers [0-100 sccm]) was later installed for regulating hydrogen and nitrogen. This controller was used to prepare films discussed in Section 3.3.5 (biased films) and 3.4 (carbonitrides).

The electrodes were two parallel circular plates (of diameter 4 in) electrically isolated from the chamber. The isolation consisted of three ceramic r.f. standoff posts. Two rf sources were used. Initially, an r.f. oscillator set at 12 MHZ was amplified by an ENI model 2100L r.f. amplifier. Later, a more powerful amplifier (an International Plasma Corporation model RM-116) set at 13.600 MHz was used. A Heathkit model 5A-2060A antenna tuner matched the impedance of the rf amplifier to that of the plasma through the top plate. The matcher utilized a standard circuit consisting of two capacitors and an interposing coil. This plate had a hollow annulus, into which gases such as NH_3, H_2, N_2, CH_4, or Ar were injected from a connection at the upper side of the plate. The gases left the annulus through six centered holes on the lower side of the top plate, so that the gases flowed radially outward between the plates. $TiCl_4$ vapor drawn from a liquid flowed into the system through a quartz conduit passing through the center of the top plate. Externally, the $TiCl_4$ flowed through teflon lines and was stored in a glass Schlenk tube. The bottom electrode was a thin stainless steel plate secured over a heater, which in turn was resting on a macor ceramic spacer. The bottom ceramic was found to improve maximum sample temperature. This electrode was generally grounded, although it could be floated or biased. When biased, an isolation circuit (Figure 2.3) built at LBL was used to prevent the r.f.

signal from damaging the d.c. supply. The heater temperature was monitored with a thermocouple. An isolation circuit (Figure 2.4) designed at LBL was used to prevent the r.f. signal from damaging the thermocouple voltmeter. For the NH_3 and H_2/N_2 studies, a resistive ring heater (Chromalox model A-20) was used, which could provide a maximum temperature of 600°C. Later, a resistive flexible rod heater (ARi Industries model BXX-13B-33-4T, Addison, IL) was utilized in spiral form, which could provide a maximum temperature of 940°C.

Samples were clamped onto a holder (initially copper, later 304 stainless steel) which was placed onto the lower electrode through an interlock and transfer mechanism developed in our laboratory. (See Figure 2.5) The interlock chamber consisted of a UHV six-way cross with 2.75in conflat flanges. The interlock chamber was isolated from the plasma chamber with a hand-operated gate valve, as shown in Figure 2.6. The transfer chamber could be independently evacuated by a mechanical pump. The transfer device consisted of a claw mechanism which was mounted onto a hollow rod. The claw was opened by a push-rod located inside the hollow rod, activated by the hand of the operator, as shown in Figure 2.7. The rod could slide through an LRL vacuum fitting, which had a O-ring Parker seal assembly, as shown in figure 2.8. During deposition, the rod assembly was replaced on the transfer cell by a blank LRL plug. During deposition, the samples did not have thermocouples directly attached to them. Separate experiments were performed to calibrate the permanent thermocouple on the heater to the temperatures measured at the sample surfaces with thermocouples directly spot welded to them.

2.3 Materials:

Ammonia, hydrogen, nitrogen, argon, methane gases (Matheson) and $TiCl_4$ vapor (Roc-Ric Corporation, Sun Valley, CA) were the starting materials. Most of the deposition studies used M2 tool steel as the substrate, although coatings

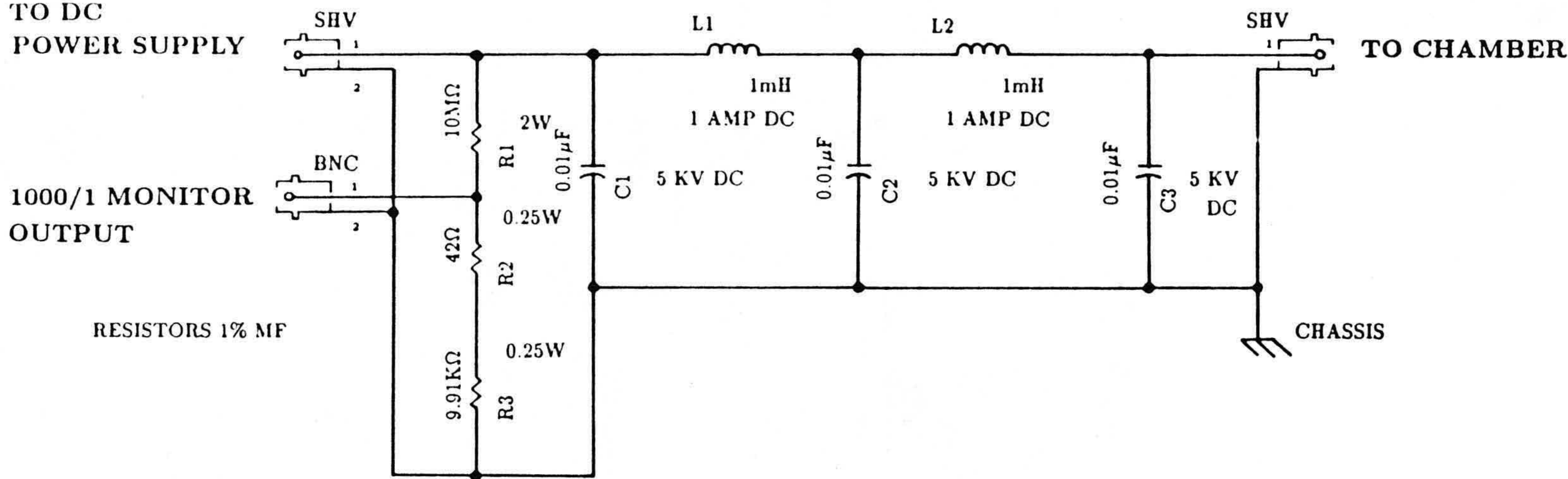

Figure 2.3: Schematic of the rf/dc isolation circuit.

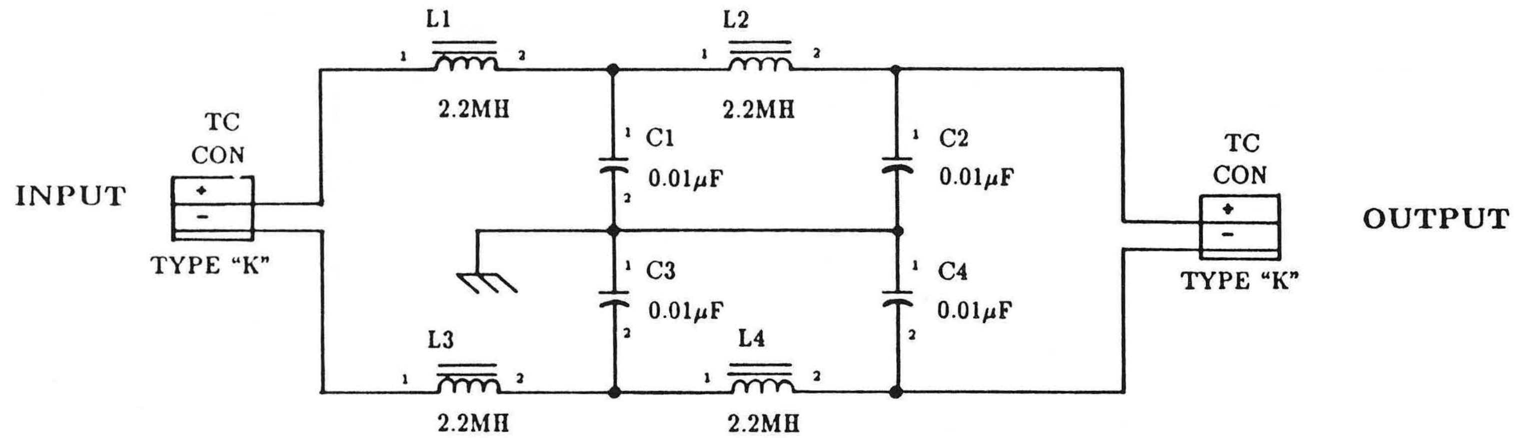

L1-L4: LBL STOCK ITEM 5950-43621

C1-C4: LBL STOCK ITEM 5910-57987

UCLBL-MCSD

10 MHz THERMOCOUPLE FILTER

XBL 8711-5010

Figure 2.4: Schematic of the thermocouple rf isolation circuit.

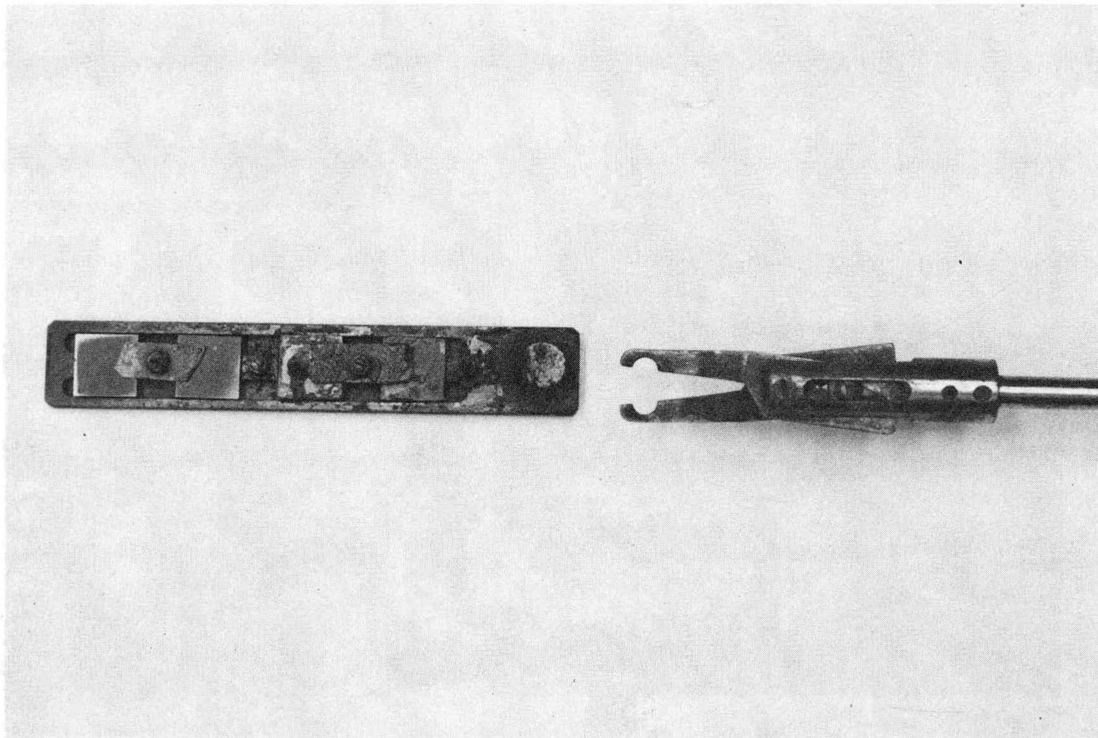

XBB 870-9588

Figure 2.5: Sample holder and the transfer claw. The M2 steel squares are 0.5in wide and long.

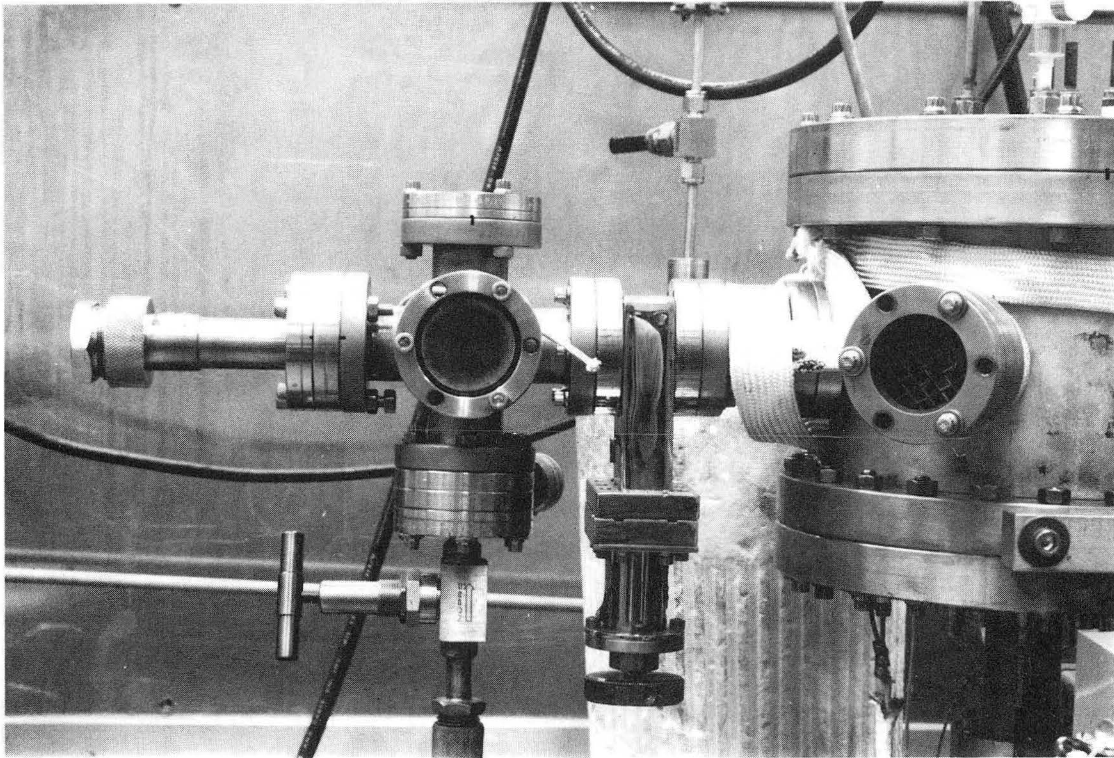

XBB 870-9582

Figure 2.6: The interlock chamber.

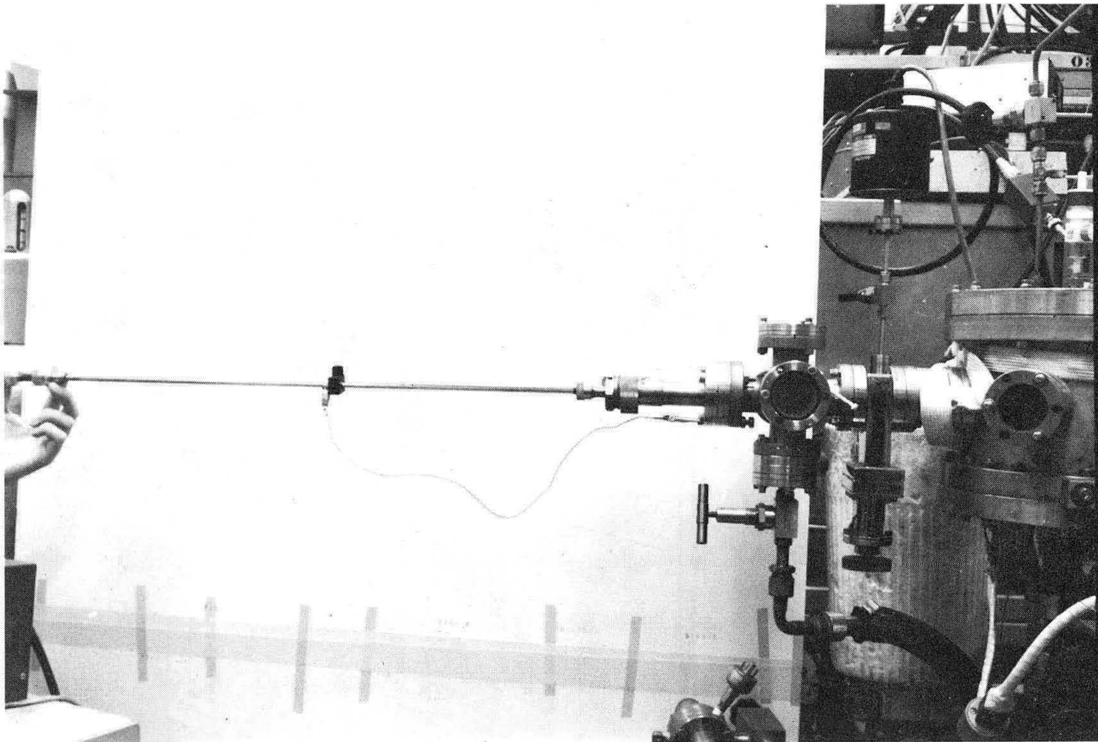

XBB 870-9584

Figure 2.7: The transfer rod and chamber assembly.

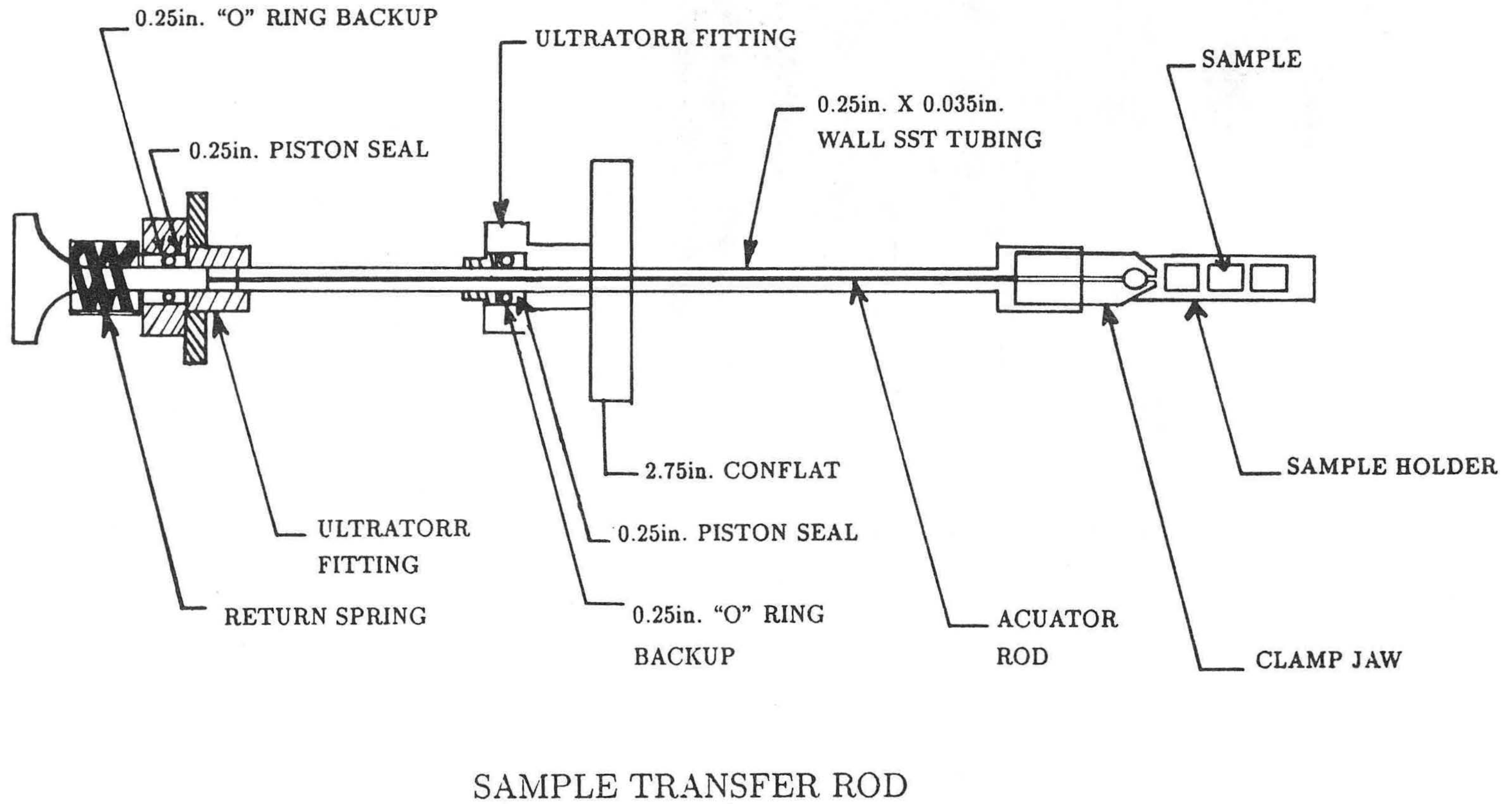

XBL 8711-5012

Figure 2.8: Schematic of the transfer rod seal assembly.

were also produced on glass and on 304 SS. The tool steel (Coulter Steel Co., Emeryville, CA) was rough cut into 1.27cm x 1.27cm x 0.48cm or 1.27cm x 0.64cm x 0.48cm rectangles, austenitized at 1225°C for one hour in argon and quenched in oil. The samples were tempered in air at 530°C for one hour and then at 510°C for one hour to achieve a Rockwell C hardness of 63-64. The thickness of the sample was reduced to 0.318 cm by grinding. The surface to be coated was subsequently polished with SiC paper and finally with 1μm diamond paste. The samples were then cleaned in acetone and then in ethanol. Metallographic investigation of the M2 steel revealed a mean grain size of 20μm, with a tempered martensitic microstructure having a fine carbide dispersion. Scanning electron microscopy (SEM) and energy -dispersive spectroscopy (EDS) analysis showed that the carbides either contain the alloying elements tungsten and molybdenum, or vanadium alone.

2.4 Characterization:

In this study, two groups of film properties were investigated: physical and mechanical. The former included morphology and thickness, crystallinity, and composition–both bulk and interfacial. The latter primarily centered on adhesion and hardness, although residual stress was also considered. Since excellent modern references exist for the techniques used to investigate physical properties (For SEM: Gol:75;for XRD: Sch:77, Cul:78; for AES and surface analytical techniques: Ert:74, Som:81, Bri:83). only the experimental conditions will be reviewed in this chapter. For adhesion and hardness measurement, the theory of the techniques will be presented followed by the experimental conditions.

2.4.1 Physical Properties:

Morphology and Thickness:

The morphologies of the M2 substrates and the TiN coatings were investigated by optical microscopy and scanning electron microscopy (SEM). In order to observe the coating cross section, the TiN-covered M2 substrate was impacted with a Rockwell C diamond indenter under a load of 150kgf. The coating was fractured around the indentation, often exposing the M2 substrate. By tilting the sample in an SEM (ISI model DS 130,ISI WB-6,AMR model 1000), the coating cross section morphology and thickness could be determined.The microscope beam voltage was generally either 20 or 30 KeV. Sample tilt for cross-sectional morphology studies was usually 45°. For studies of the early stages of film growth, the nucleation morphology was studied with lower tilt angles, of zero to 15°. For thickness determination, tilts of 45° and 80° were used.

Crystallinity:

The crystallinity of the films was investigated by X-ray diffraction (XRD) with a Siemens Kristallofflex diffractometer using Cu Kα radiation ($\lambda = 1.540$ $\AA$). The acceleration voltage was 40KV and the filament current was 30 mA. The angular width of the slits had openings of .05 to $.15^o$. Scan rates were either .01 or 0.1^o (2θ)/sec. XRD primarily yielded information on the crystalline orientation of the films. As will be shown in chapter three, the major feature of interest was the (200) peak of TiN. Table 2.1 lists the d-spacings and 2θ values for the various reflections of TiN, TiC, and TiO. Attempts were made to estimate coating grain size by measuring the peak full width at half maximum and by using Scherers equation: $D=0.9\lambda/B\cos\theta$ where λ is the x-ray wavelength, B is the FWHM (in radian), θ is the Bragg angle, and D is the average crystalline diameter increases. For a single crystal, the diffraction peak should be, in theory, a delta function. However,

Table 2.1: Crystallographic spacings and XRD angles (for Cu Kα radiation) of the simple titanium compounds.

Material	(hkl)	d (Å)	$^o 2\Theta$
TiN	111	2.4497	36.640
	200	2.1215	42.563
	220	1.5001	61.768
	222	1.2249	77.898
	400	1.0608	93.082
TiC	111	2.4994	35.887
	200	2.1645	41.678
	220	1.5305	60.411
	222	1.2497	76.071
	400	1.0584	93.357
TiO	111	2.4071	37.314
	200	2.0853	43.346
	220	1.4752	62.937
	222	1.2050	79.435
	400	1.0441	95.046

instrumental line broadening occurs, because, for among other reasons, that no diffractometer is perfect. The instrumental broadening of the diffractometer was measured by scanning a Pt(111) single crystal, which has a reflection at an angle ($2\theta = 40.1\ ^o$) close to that of TiN(200). Investigation of the crystal using a variety of slit aperatures revealed that line broadening is severe, in that the upper limit of measurable D was approximately 400Å. The source of the broadening was not resolved and the technique was not pursued further.

Film Composition:

The bulk chemical composition of the films was studied in a separate chamber by Auger electron spectroscopy (AES). This technique was selected because it could detect elements below atomic number eleven, a disadvantage of normal energy dispersive spectroscopy (EDS). The spectra were obtained with a cylindrical

mirror analyzer (CMA) system (Physical Electronics model 545 scanning Auger microprobe [SAM]) which was routinely maintained at 5x10^{-10} torr. The analyzer modulation was one volt and the electron beam energy was set at two keV. The sweep rate was three eV/sec and the time constant was 0.3 sec. Typical specimen currents were 75 nA. A channetron type detector was used (at voltages of 950 to 1200V).

Since AES is a surface sensitive technique, which detects only the first one to three monolayers, initial investigation revealed film surface composition. Bulk film composition was ascertained by AES analysis of films subjected to argon ion sputtering which progressively ejected film surface material. The sputtering was performed, (using a Varian gun, model 981-2043) under flowing conditions at a pressure of 5 X 10^{-5} torr using a 2KeV beam and an 880nA specimen current; under these conditions, the sputtering rate was approximately 8 $\AA$/min. The rate was calibrated by measuring the time to penetrate TiN samples of known thickness (the latter determined by SEM). The sample position for the CMA focal point was not coincident with the optimum sputtering condition. The two points were approximately 0.25 in. apart. Therefore, AES was not usually performed simultaneously with sputtering. When concurrent AES and sputtering were executed, the sample was positioned farther from the CMA, resulting in reduced signal and spectrum shifts (of approximately ten eV). Argon pressure was reduced to 2 X 10^{-5} torr, to conserve the electron gun filament, and the specimen current dropped to 380 nA. The sputtering rate was assumed to drop linearly with ion flux, yielding an estimated sputtering rate of approximately 3.4 $\AA$/sec.

The data obtained by AES was used to estimate film composition by employing a semi-quantitative calculation found in the literature (Dav:76). The elements of interest were chlorine ($L_2M_{23}M_{23}$ transition at 181 eV), carbon ($KL_{23}L_{23}$ transition at 273 eV), nitrogen ($KL_{23}L_{23}$ transition at 383 eV), titanium ($L_3M_{23}M_{23}$ transition at 387 eV and $L_3M_{45}M_{45}$ transition at 418 eV), and oxygen ($KL_{23}L_{23}$ transition at 510 eV). Analyzing the surface composition of the TiN films is made difficult by the overlap of the nitrogen peak and the titanium peaks at 383 eV and 387 eV

respectively. However, measurable changes occur in the intensity and shape of the 387 eV titanium peak as nitrogen is added. Specifically the $(Ti + N)_{387eV}$: Ti_{418eV} Auger peak ratio increases as nitrogen content increases. Schneider and Nold (Sch:81) found this ratio to increase from 0.74 to 2.03 in going from a pure metal to TiN, whereas Dawson and Tzatzov (Daw:85) using a retarding field analyzer (RFA) observed a change from 0.71 to 2.63. The value obtained by the latter researchers should be corrected to account for the varying resolution of CMA-type analyzers ($\Delta E \; \alpha \; E$). A first order correction converts the value of the ratio from 2.63 to 2.43. Although the reported values differ, the trends remain the same. This range of ratios from 2.03 to 2.43 probably stems from different spectrometer settings used by the investigators. Accurate determination of the stoichiometry of titanium nitride films requires the analysis of known standards using the same spectrometer under identical conditions. Such standards are not presently available. As a first order standardization, commercially prepared CVD TiN films (provided courtesy of Dr. Ron Peters, Fansteel VR Wesson) were examined by AES. The results will be discussed in chapter three.

In order to facilitate the calculation of impurity concentrations, an assumption was made that the N:Ti ratio was equal to one. For each element, the peak-to-peak amplitudes were measured on a plot of the derivative of the intensity with respect to energy during modulation (dN/dE) versus electron energy (E). The Ti_{418eV} peak was used to represent titanium. The amplitudes were scaled by sensitivity factors, determined by Levin (Lev:87) for a two keV incident electron beam. The values are: 1.01 for Cl, 0.157 for C, 0.511 for Ti, and 0.567 for O (the value for N would be 0.347). The atomic concentration for each element is given by the following equation:

$$C_X = (I_X/S_X)/\Sigma(I_i/S_i)$$

where C_X is the atomic concentration of element X, I_X is the peak-to-peak amplitude for a particular peak, and S_X is sensitivity factor for element X.

Interface Composition:

The ability of a coating to adhere to a substrate is an essential requirement for an effective protective film. Interface composition is an important factor influencing adhesion. In order to measure interface composition with AES, the entire coating must be removed to expose the interface. Argon ion sputtering has been traditionally utilized for this purpose. The sputtering technique is very time consuming when coatings of mechanically useful thickness (2-10μ) are studied. In addition, the intense forward momentum transfer from incident ions to surface atoms causes a substantial intermixing of surface and near-surface layers. Therefore, very sharp composition gradients within a thickness of a few monolayers at an interface cannot be adequately resolved. More importantly, the sputtering technique does not provide any information about the mechanical properties of the film. As will be discussed in section 2.4.2 the scratch adhesion test (SAT) is used to quantitatively evaluate the adhesive properties of protective coatings. A contacting diamond stylus causes film removal either in a cohesive mode (fracture occuring within the coating) or in an adhesive mode (detachment occuring at the interface) when a critical load (L_C) is exceeded. Auger analysis of scratches created in ultrahigh vacuum (UHV) provides information on the composition of the failed regions. If the adhesive mode is operative, interface composition can be assessed. This approach makes it possible to resolve sharp composition gradients and to quickly analyze coatings of mechanically useful thickness.

In order to test this approach, an UHV in-situ scratching device was designed and built in our laboratory, as shown in Figures 2.9-2.11. The device consists of a Rockwell C type diamond indenter (Wilson Instruments Co.) with a tip radius of 0.2mm identical to the type used in our SAT apparatus and similar to those used in commercial units (Per:83, Hin:84). A rod and bellows assembly transmits force and motion, applied manually by the operator. The device was positioned so that it could be sputter cleaned between scratches. Following analysis in the SAM

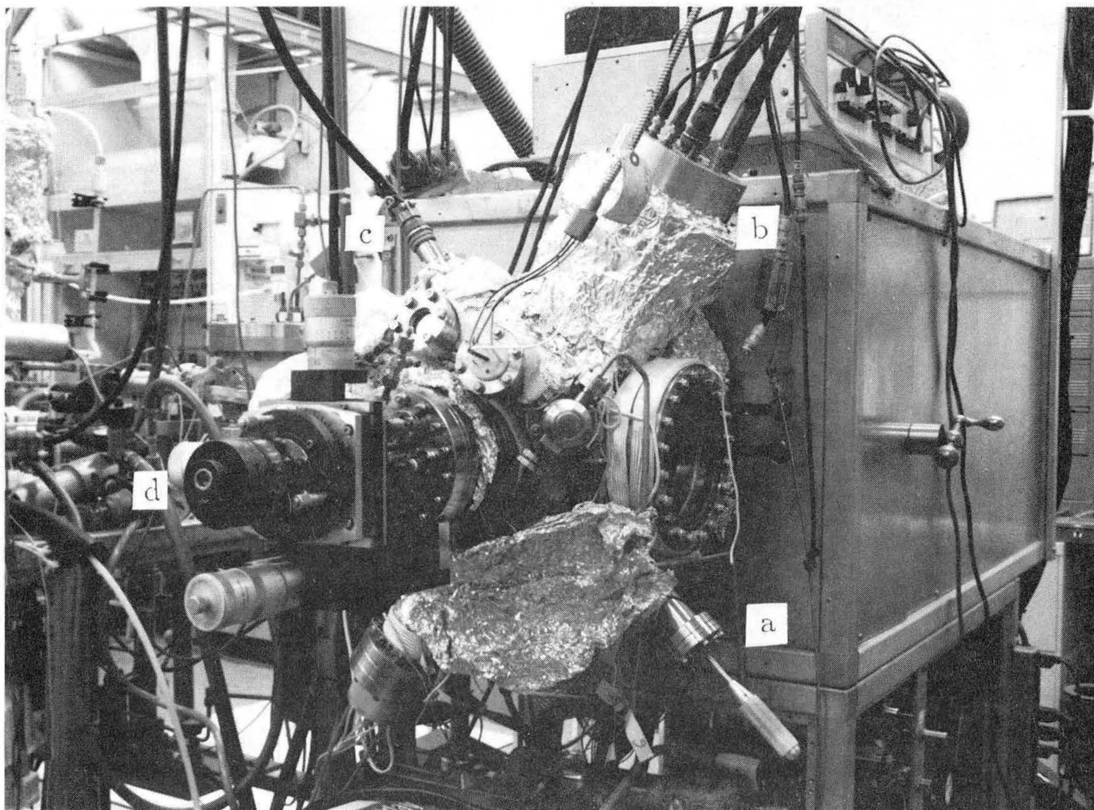

Figure 2.9: Photograph of the external SAM chamber, showing the a)scratcher, b)CMA, c)sputter gun and d)manipulator.

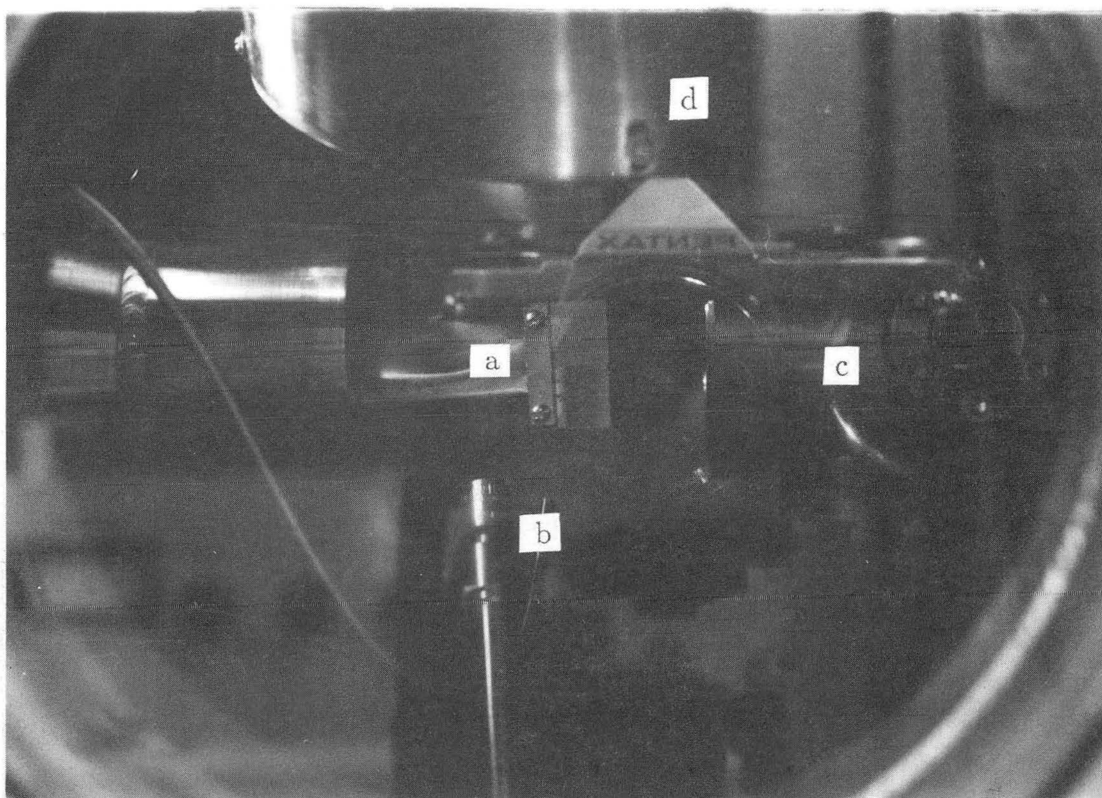

XBB 870-9594

Figure 2.10: Photograph of the internal SAM chamber, showing a)samples on manipulator, b)scratcher, c)CMA and d)high pressure cell (open position).

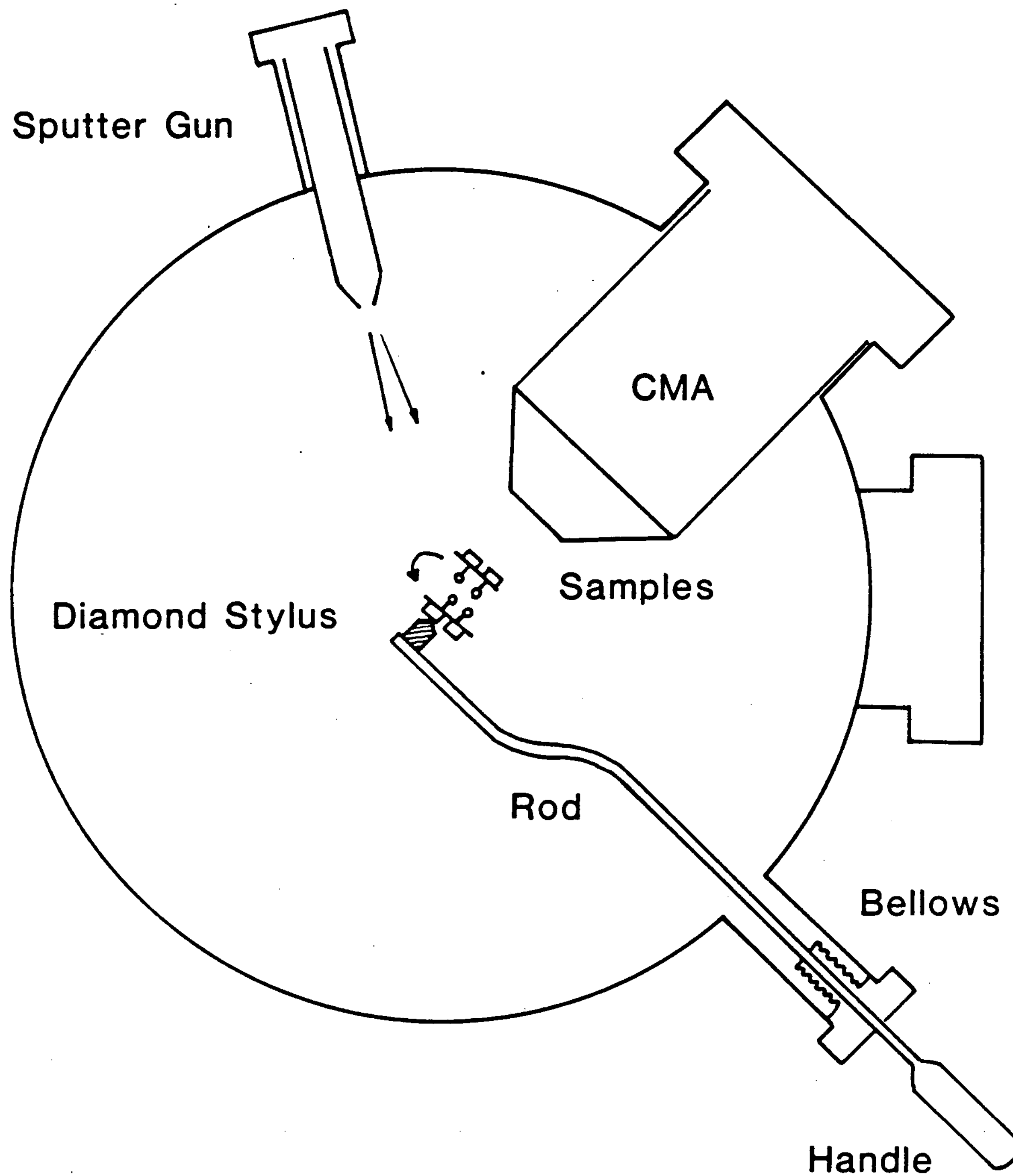

Figure 2.11: Schematic of the scratch removal device.

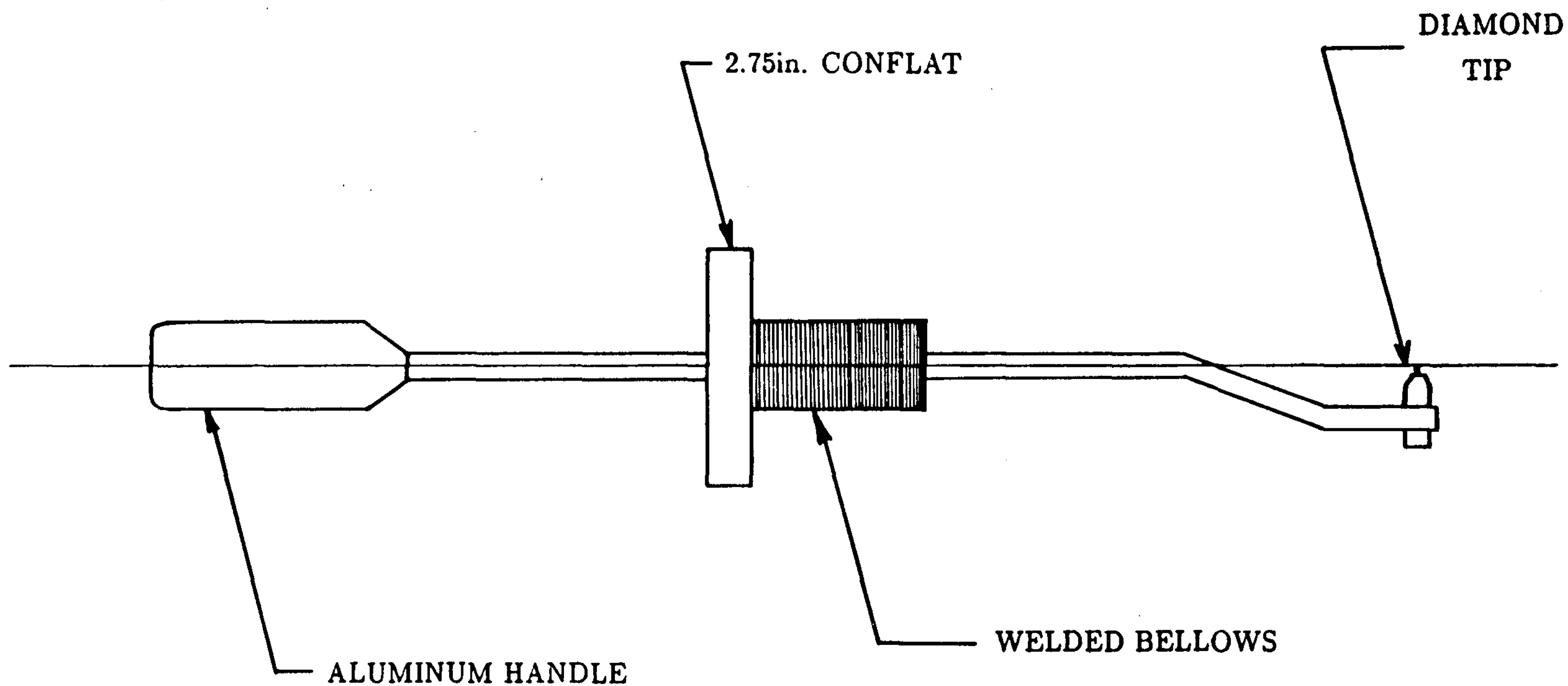

Figure 2.12: Design of the scratch removal device.

system, the morphology of the scratched regions was examined by SEM. EDS was also used to determine the bulk composition of various features.

2.4.2 Mechanical Properties:

At present, there is no set of laboratory mechanical tests which can accurately predict coating performance in tool applications. Field testing is still required for assessment of performance in particular situations. However, there are two coating properties which are important when comparing films made by different deposition conditions or techniques: adhesion and hardness.

Adhesion Measurement:

Background: Adhesion is often used in a broad sense to describe the sticking together of two materials with or without an intermediate layer. The situation can be quite complex since the average adhesive joint has two interfaces at which failure can occur and three regions of potential failure. Weaver suggests that the term adhesion should be strictly reserved for "the bonding between two different materials and carries the implication of intimate contact at the interface" (Wea:75). Attempts to measure adhesion defined in this manner face two difficulties, the first being to obtain perfect contact (or a known area of perfect contact) and the second to apply stress in a manner that allows the force (or energy) required to separate the two materials to be accurately determined. A corollary to the second point is that stresses intrinsic to the materials and energy dissipation processes other than separation, such as dislocation formation, surface reconstruction, and surface chemical reactions (i.e. adsorption, oxidation, or corrosion), must be eliminated or taken into account.

The problem of contact has proven to be formidable. One consideration is surface composition, which can be controlled with modern vacuum technology. When two clean metal, ie surface oxide and contaminant layers removed, surfaces are brought together in ultra-high vacuum, they join together and the forces required for separation can be very large. If well characterized dopants or adsorbates are placed onto the surfaces prior to contact, the force required for separation drops. Using surface analytical techniques and strain-gauged sample holders, Buckley and others have developed interesting correlations between the measured friction coefficient and prior surface chemistry (Buc:70, Buc:72, Miy:82, Miy:83). Attempts to extend this approach as an experimental model for solid-solid interfaces or grain boundaries have failed spectacularly, by yielding fracture strengths greater than the metal-metal cohesive strength (which should be the highest value measured since fracture will occur at the *weakest* link, either the metal-metal bond or the metal-dopant bond) and by suggesting that known grain boundary embrittling

Table 2.2: Estimates of the real area of contact of selected materials, utilizing the indentation hardness of the material and the Vickers relationship between load and hardness. The indenter material is assumed to be harder such that it is deforming elastically. Examples for two indentation loads are given.

Metal	Hardness	Area of Contact (mm^2)	
	(kg./mm^2)	1 g.	1000 g.
Al	15	6.7 X 10^{-5}	0.067
Au	20	5 X 10^{-5}	0.050
Cu	40	2.5 X 10^{-5}	0.025
Fe	120	8.3 X 10^{-6}	8.3 X 10^{-3}
Tool Steel	800	1.25 X 10^{-6}	1.25 X 10^{-3}

agents (such as P or S in steel) improve adhesion (Har:79).

The source of failure with this UHV approach stems from another issue of contact, the topography of real surfaces. Even well-polished surfaces are in fact rough on an atomic or near-atomic (10-1000Å)scale, which has long been known (Bow:60) and has recently been reemphasized by scanning tunneling microscopy (IBM:86, Sal:87). Table 2.2 shows estimates the real area of contact of selected materials, utilizing the indentation hardness of the material and the Vickers relationship between load and hardness (see the next section). The indenter material is assumed to be harder such that it is deforming elastically. Only under extreme pressure can reasonably high interfacial contact be developed between two materials. Release of this pressure produces partial separation due to the release of stored elastic energy. (This release does not happen in a friction experiment where the compressive load is applied throughout). The junctions of these separated surfaces are atomically sharp cracks, which can act as stress concentrators, amplifying applied stresses and promoting further separation. Though applied force can be accurately measured, the real area of contact, which is needed to compute adhesive energy per atom, is not easily measured. Resistivity measurements are subject to artifacts in the form of non-linear interactions between contact points when they are close (Bow:60) and the uncertainty of the effect of interfacial impurities

/dopants on resistivity. The relationship between the arrangement and concentration of previously placed dopants/adsorbates on surfaces prior to contact and within the junctions after contact is completely unknown. It is probable that the mechanical forces transmitted through the junctions and the chemical interaction of the surfaces joining heterogeneously induce redistribution and rearrangement of dopants. The chemical effect in this context, for example potential structural rearrangement of an adsorbate on a surface induced by the subsequent deposition of submonolayer to several monolayer coverages of additional *metal* atoms, has not been studied by surface analytical techniques, though studies of the interaction of CO and NO with organic adsorbates indicate that interactions can occur which affect adsorbate order (Lin:87).

There is a situation in which the problem of contact is minimized or often eliminated. When vapor atoms are condensed or reacted onto a surface, the resulting thin film or coating that forms generally has intimate conformal contact with the original surface. Since coating adhesion is of relevance to this text, this maximization would seem to be fortuitous. However, problems remain for quantitatively assessing true thin film-substrate adhesive strength (using Weaver's definition). The situation is more complicated than the ideal of measuring an applied force necessary to separate an interfacial area into two surfaces. Intrinsic stresses can be present which interact with applied stress, the summation constituting the actual stress that a material experiences. These intrinsic stresses will scale with film thickness. Another problem is that non-separation dissipation energy processes, mentioned earlier, must be eliminated or taken into account.

Before considering testing and measurement, it is prudent to consider the expected magnitudes of adhesion forces. If perfect contact is achieved, then the lower limit of adhesion should be van der Waals bonding. If lower adhesion values are reported, then the experiment is questionable and the artifacts of imperfect contact, intrinsic stresses, or defects which act as stress concentrators should be considered. As pointed by Weaver, a survey of the literature suggests that this lower limit is usually of the order of 10^9 dyne cm^{-2} ($10^8 Nm^{-2}$). He further notes

that:

> "Historically, there have been several approaches to measuring thin film adhesion. One is to stick, solder, or cement a solid object to a film, as a means of creating a mechanism for the transmission of force. A variation of this idea are peeling tests, one form of which is the 'Scotch-tape' test wherein a pressure sensitive tape is pressed on to a film and then stripped off rapidly. As a first approach, this test is a valuable qualitative tool. On a quantitative level, these tests generally give values below the van der Waals limit. Poor contact, force measurement difficulties, and the development of additional intrinsic stresses during the joining process are suspected sources of error. Film detachment during large acceleration in ultracentrifuges have been studied. However, the mass of the film is needed to calculate normal forces and in order to generate sufficient forces large masses are needed which increase the potential for intrinsic stress effects."

The most reliable method, to date, to *evaluate* film adhesion is the scratch adhesion test (SAT). As shown in Figure 2.13, the test consists of introducing stresses at the interface by deforming the surface by means of the indentation of a moving diamond tip (r=200μm, comical angle 120°). The applied load is increased until the deformation causes stresses which result in flaking or chipping of the coating. The smallest load at which fracture occurs, either adhesive failure at the interface or cohesive failure in the coating (or substrate), is termed the critical load (L_C).

The history of the scratch test can be divided into three eras. The first period consisted of the introduction of the test and its application to the study of thin metal films on glass (circa 1959-1970). The test was first proposed by Heavens and introduced by Benjamin and Weaver (Ben:60), who used a steel indenter instead of diamond. Failure was defined as the load sufficient to remove film which would allow light to pass through the exposed portions of glass. Their

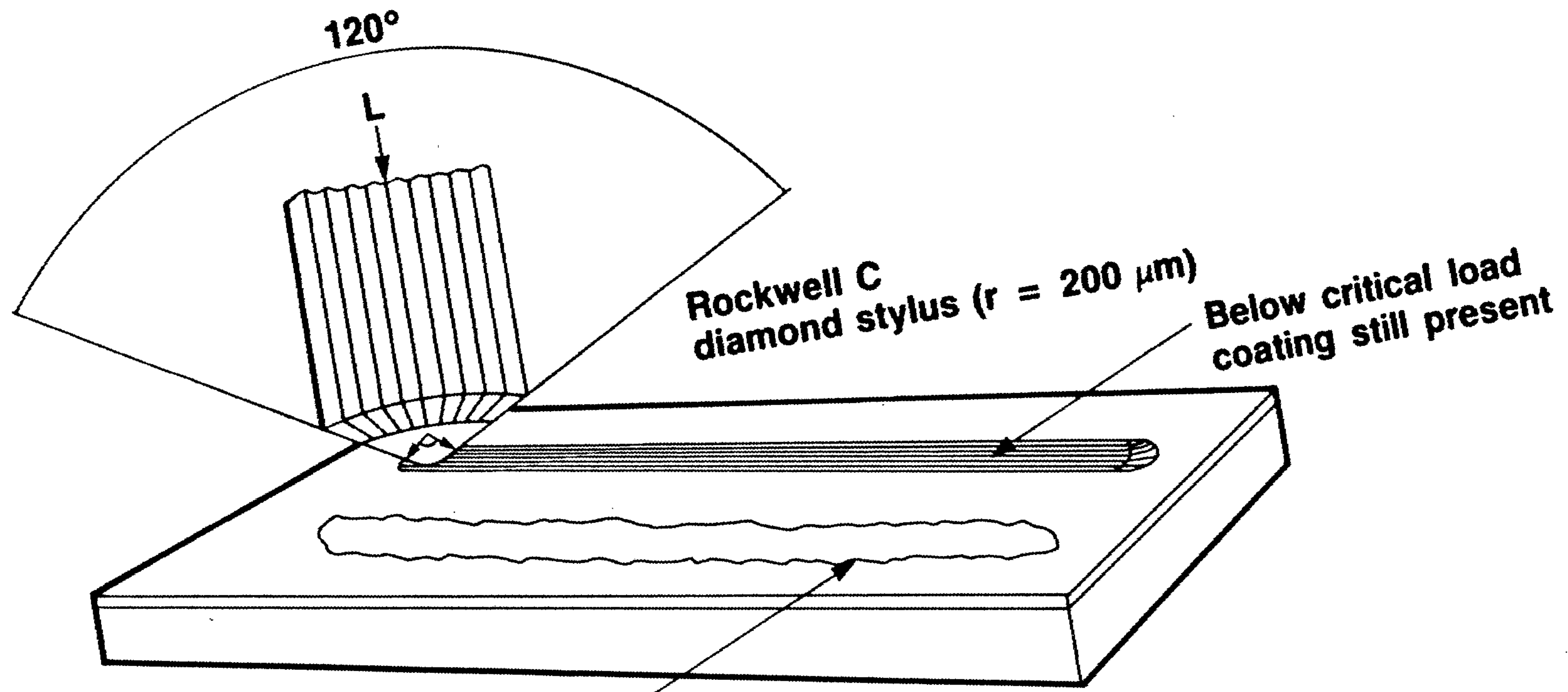

Figure 2.13: Schematic of the scratch adhesion test.

initial paper introduced the apparatus and presented an explanation as to how a compressive indentation could produce fracture. Their analysis showed that plastic deformation of the substrate introduced a shearing component or tensile hoop stress at the film substrate interface around the rim of the indentation. A simple relationship between the applied load and the shearing force was developed, so that adhesion could be calculated as a shearing force. They subsequently studied many metals evaporated on glass (deposition pressure: 10^{-5}Torr), including Ag, Al, Au, Cd, Cr, Cu, Fe, Mg, Mo, Ni, Pb, Sn, Ti, and Zn (Ben:602, Ben:61). They were able to correlate higher oxygen affinity of a particular metal and oxygen concentration with improved adhesion to glass. By depositing bilayers of Au and Al, the former adhering poorly and the latter adhering excellently to glass, they showed that adhesion improved as the aluminum diffused to the interface. Their studies showed that the L_C was determined by the properties of the film-substrate interface, varying with changes in one or the other material but showing no direct correlation to the mechanical properties of either. In subsequent years, SEM investigation of the scratches showed that the films detached ahead of the stylus, which was not predicted by the original deformation analysis. The discrepancy was attributed to the presence of intrinsic tensile stresses, which would tend to promote fracture beyond that created by the deformation stress, with the detached film curling in front of the stylus (Wea:75).

The second historical era of the scratch test began with Greene and his coworkers (circa 1974), who were the first to study a composite in which the coating was harder than the substrate, the first to present a means for determining L_C when an opaque substrate was used, and perhaps the first to routinely use a diamond tip (Gre:74). They investigated TiC films prepared by r.f. sputtering deposited (at a pressure of 1.7 X 10^{-3} torr) onto high speed steel squares. Their SAT apparatus consisted of an x-y-z micromanipulator upon which the sample was placed. The diamond tip (radius 35μm) was mounted on a modified triple beam balance which provided controlled loads. The scratches traverses were made either by a constant velocity motor or by hand. Failure was determined by Energy Disper-

sive Spectroscopy analysis of the scratches in an SEM. Significant detection of the substrate material was the criterion for failure. A 15 KeV, 2μm diameter electron beam was used, which was found to provide the best compromise between minimum penetration of electrons through the carbide coating (0.1-1.5μm thicknesses) to the steel substrate and the efficient excitation of the radiation of interest. In their initial study, they found that substrate preheating improved adhesion and that there was a room temperature aging effect, with SAT L_C improving for a period of time (20-50 hours) after deposition until the same constant value was obtained. The simple apparatus design used by Greene was refined in the late 70's and commercial instruments were available by the early 1980's (Per:83, Hin:84). The instrument has a diamond tip stylus (r=200μm 120°), which is motor driven. The load can be applied stepwise or continuously. L_C is determined by optical or electron microscopy and/or by acoustic emission (AE). There is a good correlation between the onset of AE signal and the observation of initial damage, though OM/SEM/EDS analysis is the most reliable. The repeatability of L_C determination for a particular specimen is generally within 10%.

The scratch adhesion test's most frequent use at present is as quality control monitor for industrial production of coatings. The test is repeatable, and results from different locations can be compared, provided that a variety of variables are kept constant. A great deal of empirical correlation exists between L_C values measured on various coating/substrate combinations and performance in actual application. Extensive studies by Hintermann and also by Perry empirically established credibility (Hin:84, Per:83). A major problem with the scratch test is that the relationship between the measured critical load and actual interfacial adhesion strength is not well understood. The third era of the scratch test, now underway, is the development of a better understanding of the test and sample parameters that influence fracture and a classification of the fracture modes. Apparatus parameters include stylus tip radius and stylus velocity. L_C has been found to increase with both, though velocity has less influence, and their values are generally standardized (r=200μm and dx/dt=10mm/min). The radius effect stems from the

fact that a smaller tip concentrates a given load into a larger deformation stress.

Materials related parameters that influence the value of L_C besides interfacial adhesive strength are tip-coating friction coefficient; coating thickness, modulus, and hardness; intrinsic stress; and substrate hardness and toughness. The critical load has been observed to drop with friction coefficient (Ste:85). The explanation is that the mechanical coupling between the tip and the coating improves with increasing friction, and the applied load is more efficiently transmitted into the film. Critical loads often rise with increasing coating thickness, but under some conditions no dependence or even a decrease is seen. When a solid is subjected to a localized force the magnitude of stress at an arbitrary point in solid decreases with the distance between the arbitrary point and the point of force application (the indentation at the sample surface in this case). Thus, in order to obtain a particular value of stress at an interface (which leads to a critical strain as will be explained), the load applied at the sample surface will have to be increased as the thickness increases. A flat dependence with thickness may indicate fracture initiation in the film. A decreasing L_C vs. thickness behavior is often attributed to severe intrinsic stresses, which would increase with thickness and could contribute, in conjunction with applied stress, to fracture.

The Young's modulus and indentation hardness characterize the elastic and plastic properties of a material, in particular relating stress to strain. By definition, adhesion of a coating to a substrate necessitates that the total strains of each material are equal at the interface. Unless their mechanical properties are identical, there will be a stress discontinuity at the interface when the system is subjected to external stresses. Interfacial failure will relieve the energy associated with this discontinuity as well as relieving stresses in the coating. The more dissimilar the mechanical properties are, the greater the stress discontinuity. As a general hypothesis, changes in the substrate or coating properties which increase this discontinuity should lower the critical load necessary to cause failure because the greater discontinuity amplifies the interfacial stress generated by a fixed applied load. Thus, for a hard coating on a softer substrate, a reduction in substrate

hardness should decrease critical load. This result has been observed for TiN and TiC on steels and cemented carbides, as noted by Steinmann (Ste:85) and by Perry (Per:87). Using the discontinuity argument, observed lower values of L_C for TiC relative to TiN on the same material substrate can be explained by the higher Young's modulus (and hardness) of the former compound.(E_{TiC}= 447 GPa, E_{TiN} = 250 GPa (Per:86)) Toughness, which is the resistance to crack propagation, is another important property. Though cemented carbides are harder than high speed steel, they have a lower toughness, and lower values of L_C for a given coating.

Mechanistically, there is an intrinsic relationship between the hardness test and the scratch adhesion test. Both use an indenter to cause an irreversible deformation of the coating and substrate. Benjamin's (Ben:60) and Weaver's (Wea:75) analysis utilized fully-plastic indentation theory, while Laugier used elastic Hertzian indentation theory (Lau:84, Lau:86). Burnett and Rickerby are the first to analyze the deformation beneath an indentation made on a coated substrate using the modern elastic/plastic (EP) indentation theory often found in the ceramics literature (Bur:87). A feature of their EP analysis is that plastic strain during indentation occurs only laterally, parallel to the surface. There is no vertical displacement or pile up around the indentation, which would occur with full plasticity, for example in the case of a soft metal.

A relationship between hardness and interfacial constant stems from this analysis as will be shown in the next section. As for the scratch test, using EP analysis, Burnett and Rickerby examined the effect of thickness, substrate and coating mechanical properties, friction, and coating internal stress on measured L_C. Two failure criterion were evaluated. One was the elastic energy balance criterion, initially proposed by Laugier, which states that the energy required to form the new surfaces generated by the detachment (spallation) of a coating must be balanced by the release of stored elastic energy. The other criterion is that of interfacial shear stress, whereby adhesion failure occurs when a critical shear stress is exceeded. Their analysis indicates that the critical shear stress criterion is better, correctly predicting the effect of various factors on L_C as compared to observed

data. The energy balance fails primarily because it predicts that L_C decreases with thickness. Given the number of factors which affect L_C, interpretation of SAT results is in the general case quite difficult. The only case where changes in L_C values qualitatively represent changes in interfacial adhesion is when all other factors (thickness, coating and substrate properties) remain constant. If adhesion is held constant, then other factors can be investigated.

Aside from the ambiguity of the relationship between L_C and adhesion, there has been a lack of common nomenclature in the literature to describe the exact nature of failure. Burnett and Rickerby's work will be landmark because they have provided such a classification system. They have defined five failure modes, shown in Figure 2.14 and defined as follows:

> "The spalling and buckling coating failure modes occur as a result of the compressive stress field preceding the moving stylus (Figs. 2.14 a, b). Spallation is the result of total delamination (adhesive failure) whilst partial delamination - at some characteristic distance ahead of the stylus - results in buckling and cracking in a roughly semi-circular arc in front of the scratch. When this buckling or spalling is close to the leading edge of the stylus the chip may be ridden over and embedded in the bottom of the track, whilst beyond the edges of the scratch such regions will still be free to spall resulting in a crack with regular chipping on either side. This is commonly found in scratch testing (e.g. Per:83, Ste:85 and Fig. 2.14 c). Je et al (Je:86) suggested similar mechanisms for coating failure modes.
>
> The remaining failures, conformal cracking and tensile cracking (Fig. 2.14 d and e) occur when the coating remains fully adherent. The conformal failure mode consists of cracking within the scratch only, the cracks following semi-circular trajectories parallel to the *leading* edge of the indenter. These form as the indenter deforms the coating and the underlying substrate resulting in tensile bending moments within the coating as it is pushed down underneath the indentor (see Fig. 2.14d).

> While the tensile cracking failure mode appears superficially similar to the conformal cracking described above, the semi-circular crack traces are now parallel to the *trailing* edge of the indenter, i.e. mirror images of the conformal cracking. (Fig. 2.14e) These cracks form as a result of the tensile frictional stresses present behind the trailing edge of the stylus, these balancing the compressive frictional stresses ahead."

The use of the Rockwell hardness indentor (C scale) as a tool for thin film adhesion assessment has been the subject of recent research by Jindal, Quinto and Wolfe (Jin:87). They have studied PVD-produced and CVD-produced TiN and TiC coatings on WC-Co substrates. Two parameters useful for adhesion quantification can be measured. First, the critical load (Pc) necessary for crack initiation along the interface around the indenter can be measured. In addition, a series of indentations above Pc can be made, which cause larger delamination beyond the indenter rim. A fracture toughness parameter can be derived from the shape of a load vs crack length plot. This procedure is very new and not yet employed on a wide scale. It is mentioned because some qualitative results that will be presented in Chapter 3 can be used to make comments on adhesion using Jindal et.al.'s quantitative study.

In summary, adhesion measurement between two solid bodies, in general, is a difficult problem. In the case of thin films or coatings prepared by vapor deposition techniques, the ambiguity of establishing perfect contact is minimized. Indentation contact processes are the most widely used means of applying forces in a controlled manner to quantitatively evaluate interfacial adhesion. The stress field under the indentation is quite complex, and the exact relationship between applied indentation force and interfacial adhesion is unknown. Deformation processes in the coating and the substrate, the discontinuity of material mechanical properties at the interface, and friction between the indentor and coating surfaces all obscure the relationship between indentation load and adhesive strength. If these factors are controlled, established tests like the scratch adhesion test can

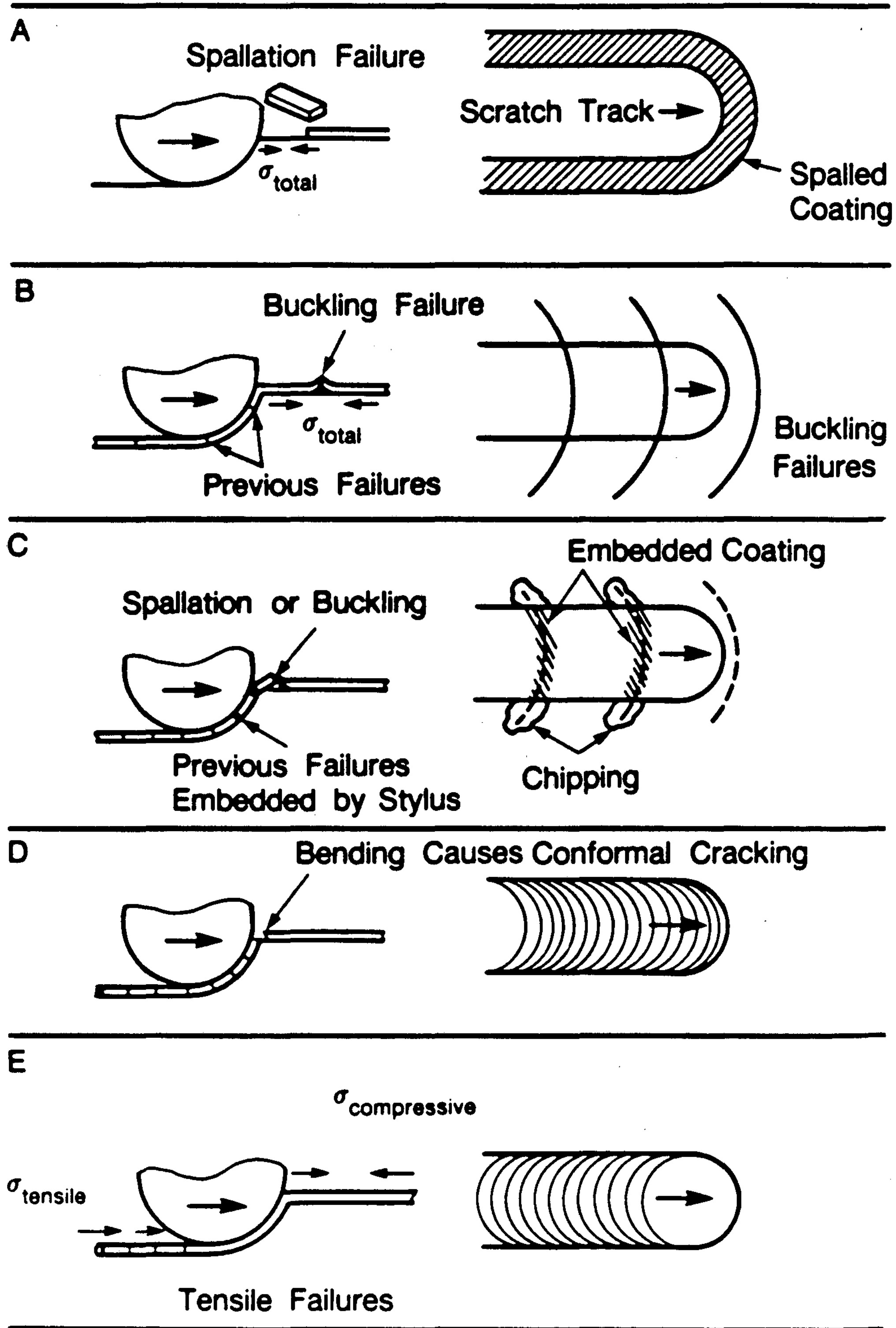

Figure 2.14: The Rickerby/Burnett SAT failure mode classification system. (Ric:87)

be used to evaluate the influence of deposition parameters on adhesion. There is a body of standardized data emerging into the literature which can be used, but only with caution.

Experimental Procedure: The TiN and Ti(CN) coatings produced by PACVD on M2 steel were quantitatively evaluated for adhesive properties with the scratch adhesion test. An instrument, based on the design of Greene was constructed in our laboratory. Shown in Figure 2.15, the device consists of an indenter, an x-y-z manipulator, and a loading balance. A Rockwell C 120° conical diamond indentor ($r=200\mu m$–checked with SEM) was mounted on the balance, pointing upward. Lead weights were placed on the balance, which has a 3:1 multiplication arm. The samples were glued onto a braced SS 304 block using a cyanoacrylate adhesive ('super glue'). The samples were mounted flush against the brace so that the shearing force of the diamond was absorbed primarily by the brace and not the adhesive. The diamond stylus, powered by the operator through manipulator screws, was traversed across the film surface towards the brace. Stylus velocity was of the order of ten mm/min. After each scratch, the sample holder was moved over to expose fresh surface to the diamond. Loads were adjusted after each scratch. After scratching, the films were examined by optical and often scanning electron microscopy to determine the onset of failure and the fracture mode.

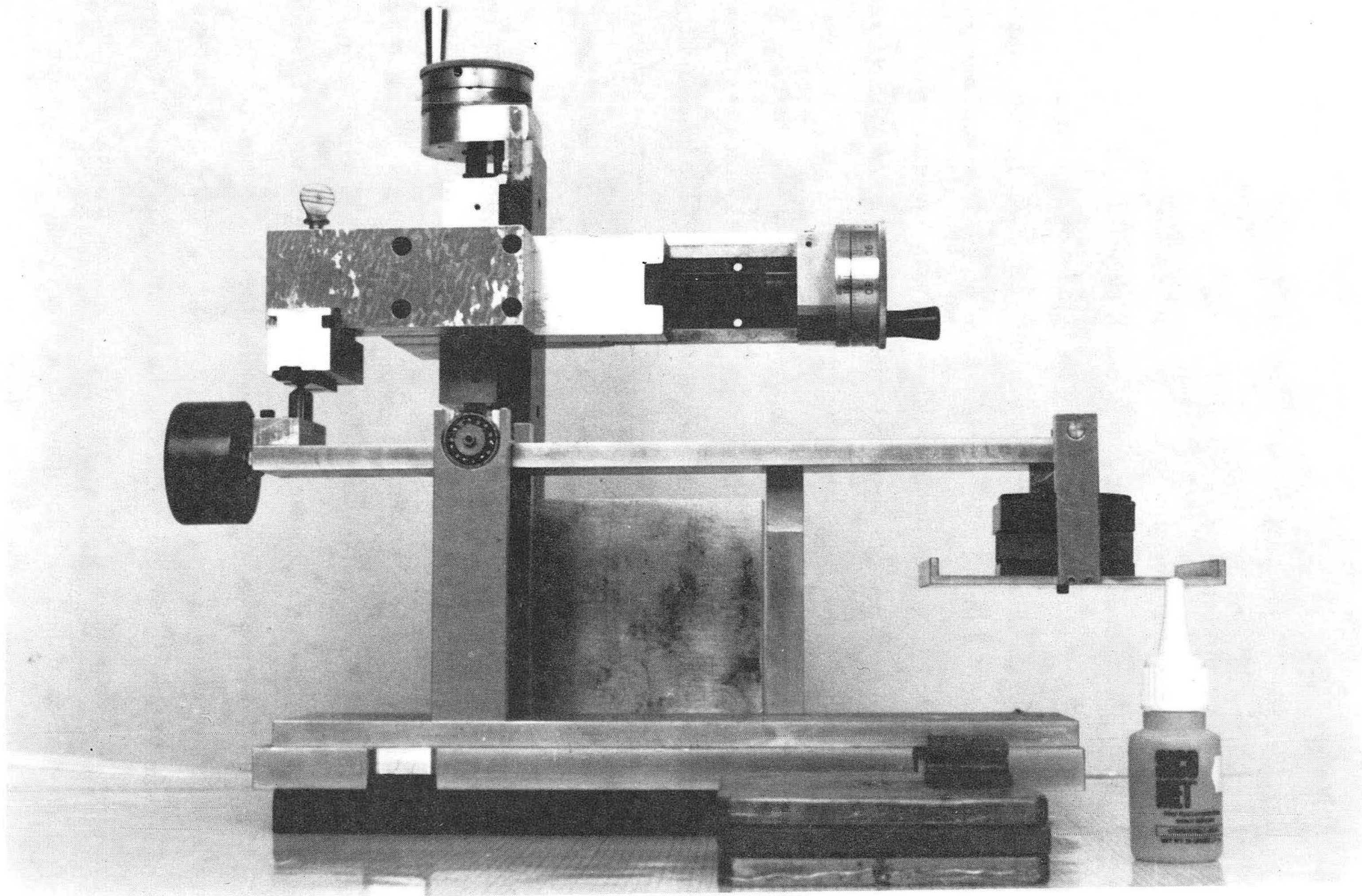

XBB 870-10206

Figure 2.15: Photograph of the scratch adhesion tester built at LBL used for this study.

Hardness Measurement:

Background:

The hardness of a material is a measure of its resistance to deformation. Although materials can deform elastically and plastically, the range of strain over which most crystalline metals and metal compounds elastically deform is small, so that their hardness is generally controlled by their plastic properties. As O'Neill wisely stated, "hardness, like the storminess of the seas is easily appreciated but not readily measured."(Tab:51). The oldest form of hardness measurement is scratch hardness, which depends upon the ability of one material to be sratched by another. This approach was put on a semi-quantitative basis by Mohs (Moh:22), who selected ten minerals as standards, ranging from talc (scratch hardness 1) to diamond (scratch hardness 10). Static indentation methods are the most widely used. These involve the formation of a permanent indentation in the surface of a material to be examined, the hardness being determined by the load and the size of the indentation formed. A third type of hardness measurement is that involving the dynamic deformation or indentation of a specimen. Elastic properties become more important with this approach.

Indentation hardness is the equivalent of the average pressure under the indentor, calculated as the applied load divided by the projected area of contact between the indentor and the sample. This average pressure is obviously related to the yield stress (Y) of a material. From plasticity theory, which is outside of the scope of this text, it can be shown that deformation begins under the indenter when the pressure exceeds 1.1 Y, and that the subindenter region is fully plastic when the pressure reaches 2.6 to 3Y. Thus, hardness test data can yield an estimate of Y. In addition, there often exist other correlations between hardness and other properties, such as ultimate tensile strength and wear resistance of materials. These correlations combined with the general ease and low cost of testing, explain why hardness measurement is popular for industrial bulk material characterization and quality control.

Every indentation hardness testing apparatus has three essential components: an indenter, a mechanism for applying the indenter with a controlled load against a surface, and a means of measuring the resulting indentation projected area. The Rockwell test (C scale) uses a circular diamond cone with an included angle of 120° and a spherical radius of 0.2mm ($200\mu m$). A load of 10kg is applied to establish contact and to provide a depth datum. An additional load of 150kg is then superimposed and the increased depth of penetration is measured by the instrument to give the hardness on the Rockwell C scale. In principle, knowledge of the penetration depth and geometry would yield projected area. However, the Rockwell value is defined as 100 - [depth of penetration (in hundredths of an inch)x100]. Thus the higher the Rc, the harder the material. A typical value of tempered tool steel is R_c=60. (For sake of completeness, it should be pointed out that there is an A and B scale to the Rockwell test, which uses steel ball indenters and lighter loads. These variations are used to provide quantitative information on softer materials.)

The Vickers test uses a polished sharp-pointed square pyramid of diamond having an included angle between opposite faces of 136°. Loads range from one g to one kg. The diagonals of the resulting impression are measured with an optical microscope. Using this diagonal displacement and the load, Vickers hardness (Hv-where F specifies the load in grams) is computed by the following relationship:

$$\begin{aligned} Hv_F &= \frac{TestLoad(Kgf)}{SurfaceAreaofIndentation(mm^2)} \\ &= \frac{2F sin(\theta/2)}{d^2} X 1000 \\ &= 1854 X \frac{F}{d^2} \end{aligned}$$

where F is the test load (g), d is the arithmetic mean of the two diagonals, and d_2 (μm), and θ is the angle between the opposite faces at the vertex of the pyramidal indenter (136°).

This equation indicates that the size of the diagonal and hence the indentation depth, diminishes as load decreases. Thus, the depth sensitivity of the hardness

test should decrease as load decreases which means that the Vickers test is more surface sensitive (and hence more relevant for studying thin films and coatings) than the Rockwell test. This, in fact, is true, but the depth sensitivity is governed by the regions beneath the indentation where plastic strains dominate or are comparable to elastic strains (referred to as plastic (P) and elastic-plastic (EP) deformation zones respectively), and is therefore greater than the indentation depth. Using slip-line analysis, Tabor using the geometry of a flat punch (Tab:51), and later Ninham using the geometry of a Vickers indenter (Nin:86), showed that the depth of the elastic plastic zone is on the order of the punch diameter or indentation diagonal. In the Vickers case, this can also be expressed as five times the indentation depth. Thus, to investigate coating hardness, the test load should be light enough to eliminate plastic deformation into the substrate. Experimentally, Jonson and Hogmark have found that elimination of the influence of the substrate on hardness measurement of film material requires that the ratio of indentation depth to film thickness should not exceed a critical value which generally varies between 0.07 and 0.2, where the most unfavorable case is that of a hard coating on a softer substrate (Jon:84). For TiN, Sundgren (Sun:83) and also Hummer and Perry (Hum:83) have observed that the minimum ratio of film thickness to indentation diagonal required to eliminate substrate effects is one. For TiC, which is harder than TiN on the same substrate, a ratio of 1.5 was required.

Even without substrate influences, other phenomena can occur at low loads. The previous equations can be rewritten as:

$$F = kH_o d^n$$

where k is a constant that accounts for indentation geometry, and H_o is the intrinsic hardness of the material. The exponent n is equal to two if measured hardness does not vary with indentation size. However, in some cases n has been found to be less than two, which implies that the measured hardness of a material should increase with decreasing d. Examples of three such cases are given in Figure 2.17. The origin of this 'indentation size effect' is not fully understood. If the near

Vickers Hardness Test (Hv)

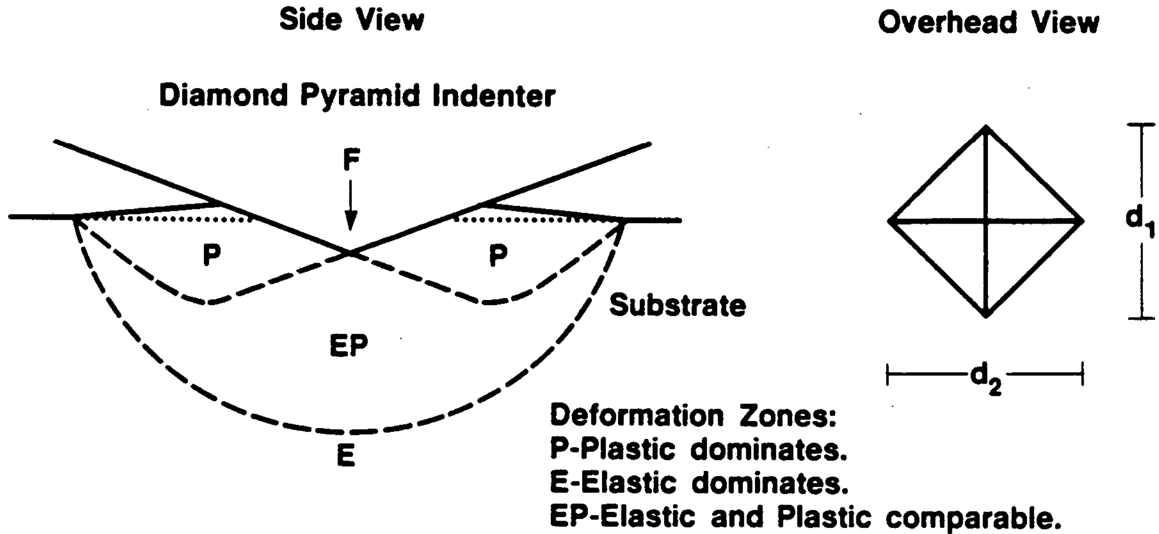

$$Hv = \frac{\text{Test Load (kgf.)}}{\text{Surface Area of Indentation (mm}^{2)}}$$

$$= \frac{2F \sin(\theta/2)}{d^2} \times 1000$$

$$= 1850 \times \frac{F}{d^2}$$

Hv = Vickers Hardness

F = Test load (gm)

d = Arithmetic mean of the two diagonals d_1 and d_2 (μm)

ρ = Angle between the opposite faces at the vertex of the pyramid indenter (136°)

D. Tabor
Hardness of Metals (1951)

XBL 869-8976

Figure 2.16: Schematic of the Vickers hardness test, showing the zones of deformation. (After Tab:51, Nin:86.)

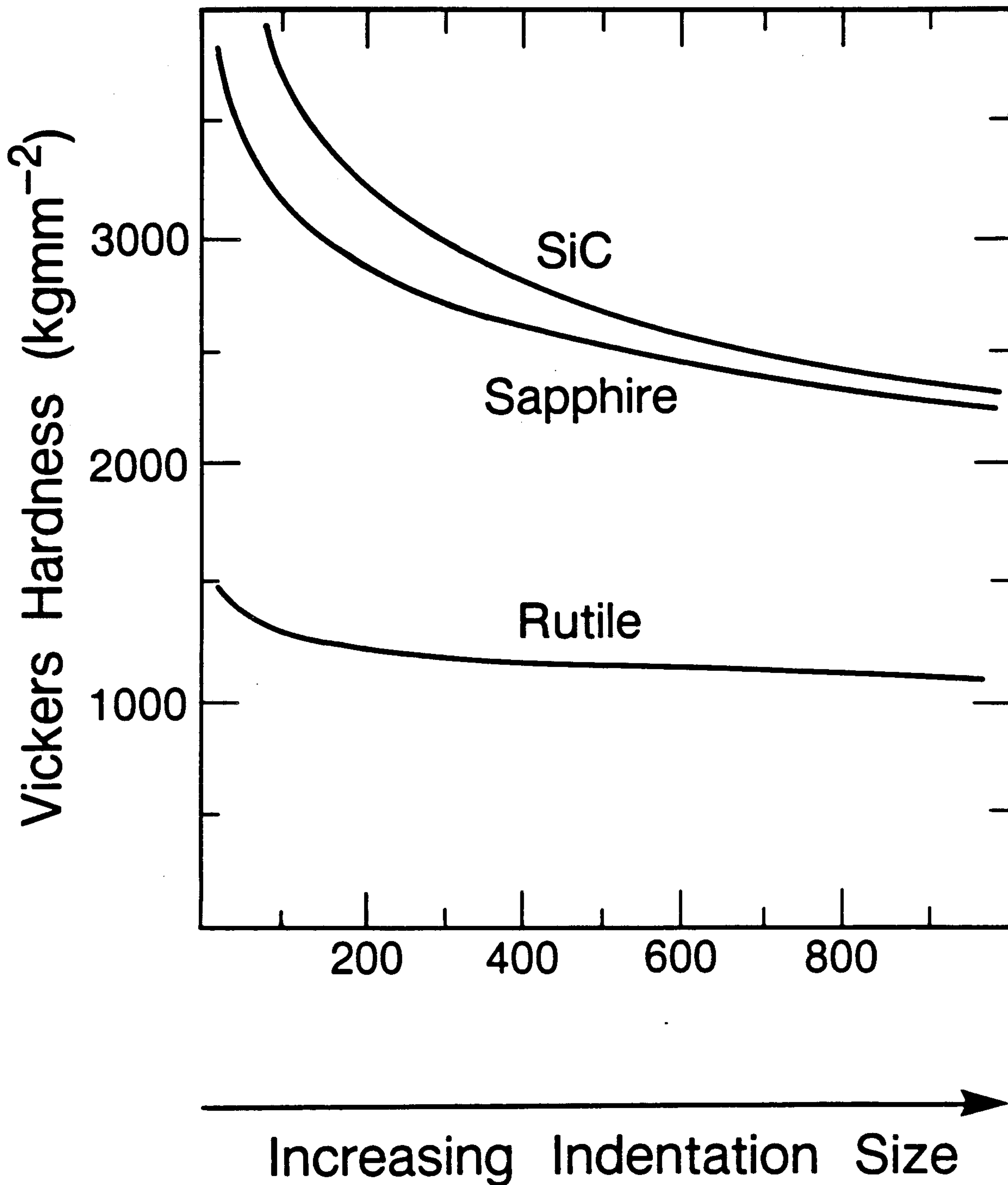

Figure 2.17: Hardness vs. load (or indentation size) for three bulk materials. (From Sar:78, Sun:86)

surface region due to a different atomic arrangement or defect structure is harder than the bulk, the results in Figure 2.17 can be qualitatively understood. Elastic recovery of the indentation may also be more dominant at light loads. Elastic recovery of the indentation has long been recognized to produce a greater *percent* contraction of the indentation depth length versus the diagonal length, making hardness estimation by the former more prone to error.

Given these considerations, there are three valid approaches for evaluating thin films in practice. The first approach is to use a standard Vickers tester in a range of reasonable moderate to high loads on thick films. This was done by Sproul in his study of TiN. Thicknesses of 9.5μm were used at 100 and 200 gm loads. Substrate influence was minimal under these conditions (given that the film hardness was ~2300kg/mm^2). The agreement between the results for the two loads suggests that indentation size effects were not operative. Finally, the large size of indentations reduced measurement error. The advantage to this approach is that commercial instrumentation is readily available. The disadvantage is that the films are often specially prepared, sometimes being thicker than these actually used in tools.

A second approach is to separate film and substrate contributions to measured hardness at low loads and thickness, obtained using conventional testing equipment, using a law-of-mixtures approach. The composite hardness H_{comp}, is defined as

$$H_{comp} = \frac{V_f}{V} H_f + \frac{V_s}{V} H_s X^2$$

where H_f,H_s are the coating and substrate hardness values, V_f,V_s are the deforming volumes of the coating, and X is an interface constraint parameter used to modify the size of the substrate deforming volume. This form was developed by Burnett and Rickerby (Bur:87) using elastic-plastic indentation theory; a variation has been used by Jonson and Hogmark (Jon:84). Values of V_f and V_s must be calculated and X experimentally determined. The higher the value of X, which means that interface adhesion is better, the more the substrate influences composite hardness. For TiN on tool steel, X≅1, while on stainless steel X≅0.67. The

technique allows standard equipment to be utilized at lower loads and thicknesses. Though good agreement has been obtained on a variety of film/substrate systems, the drawback of the technique is that the relative volumes are calculated.

The third approach is to miniaturize the indentation process, using low loads (10μN - 100mN) and sensitive depth sensing instrumentation. Ultramicrohardness testers using an inductive displacement transducer (Wie:84) or a capacitance bridge (New:82) are reported to have a resolution of depth measurement of 50Å. The most sensitive system is the nanoindenter (Doe:86, Doe:862) which can achieve a resolution of 20-30 Å with a capacitance gauge. However, in order to produce repeatable data and to minimize indentation size effects (which appear even with this instrument), the minimum displacement of the indenter is about 200Å and a film thickness of 2000Å is thus required. This instrument is just becoming commercially available. As stated earlier, measurement of indentation diagonals are less affected by elastic recovery as opposed to those of depth measurements. Therefore an instrument that can measure the diagonal is desirable. The scanning tunneling microscope (STM) seems to be a promising candidate for further developments in fine scale hardness measurement. This instrument can in principle make an indentation in a controlled manner and then image the deformation. Images of tip induced deformation have been reported (IBM:86). However, surface roughness will be the ultimate limit on hardness measurement. As an example, magnetic disks used in computer storage, which are manufactured in large volume, have stringent tolerance requirements. Yet the arithematic mean roughness (or average deviation from the centerline of the profile) of these devices often is of the order of 40-70Å (Tsa:87).

Experimental Procedure: A standard Vickers microhardness instrument was used (Buehler Micromet). Early studies of 2μm thick TiN films synthesized by PACVD using $TiCl_4$ and NH_4 were examined with loads of 15, 25, 50, and 100gm. Ten measurements were made for each load. Films synthesized using H_2 and N_2 instead of NH_3 were examined with loads of 100 and 200 g, though some

indentations at 25 and 50 g were performed. These films were 8 to 10 μm thick, and thus the measurements were along the approach taken by Sproul (Spr:83).

Chapter 3

Experimental Studies and Results

The results presented in this chapter are organized on the basis of the reactants used to synthesize TiN. This format is appropriate because the coating physical and mechanical properties are logically discussed within the context of deposition conditions. The initial priority of the project was to produce TiN at the lowest temperature possible by exciting the most reactive feedstocks in a plasma. Using $TiCl_4$ as a source of titanium, thermodynamic calculations of the standard state Gibb's free energy of formation, ΔG^o, shown in Figure 3.1 indicate that NH_3 would be a better coreactant than H_2 and N_2 because the former will form TiN without a plasma down to temperatures of 300°C. In contrast temperatures greater than 580°C are needed to form TiN from $TiCl_4$, H_2 and N_2, without a plasma; TiC synthesis requires temperatures in excess of 820°C when $TiCl_4$ and CH_4 are used without a plasma.

Based on these considerations, $TiCl_4$ and NH_3 were the first reactants investigated. However, HCl is not the only possible by-product of TiN synthesis. Using $TiCl_4$ and NH_3 vapor as starting materials, several reactions can occur that yield TiN and either solid NH_4Cl or gaseous HCl as the halogen byproducts. Figure 3.2 shows the Gibb's free energies of formation as a function of temperature for three representative reactions using data from the literature (JANAF). Reaction (1), forming solid NH_4Cl and TiN, becomes less favorable as temperature increases. Reaction (2), forming TiN and gaseous HCl, becomes more favorable with in-

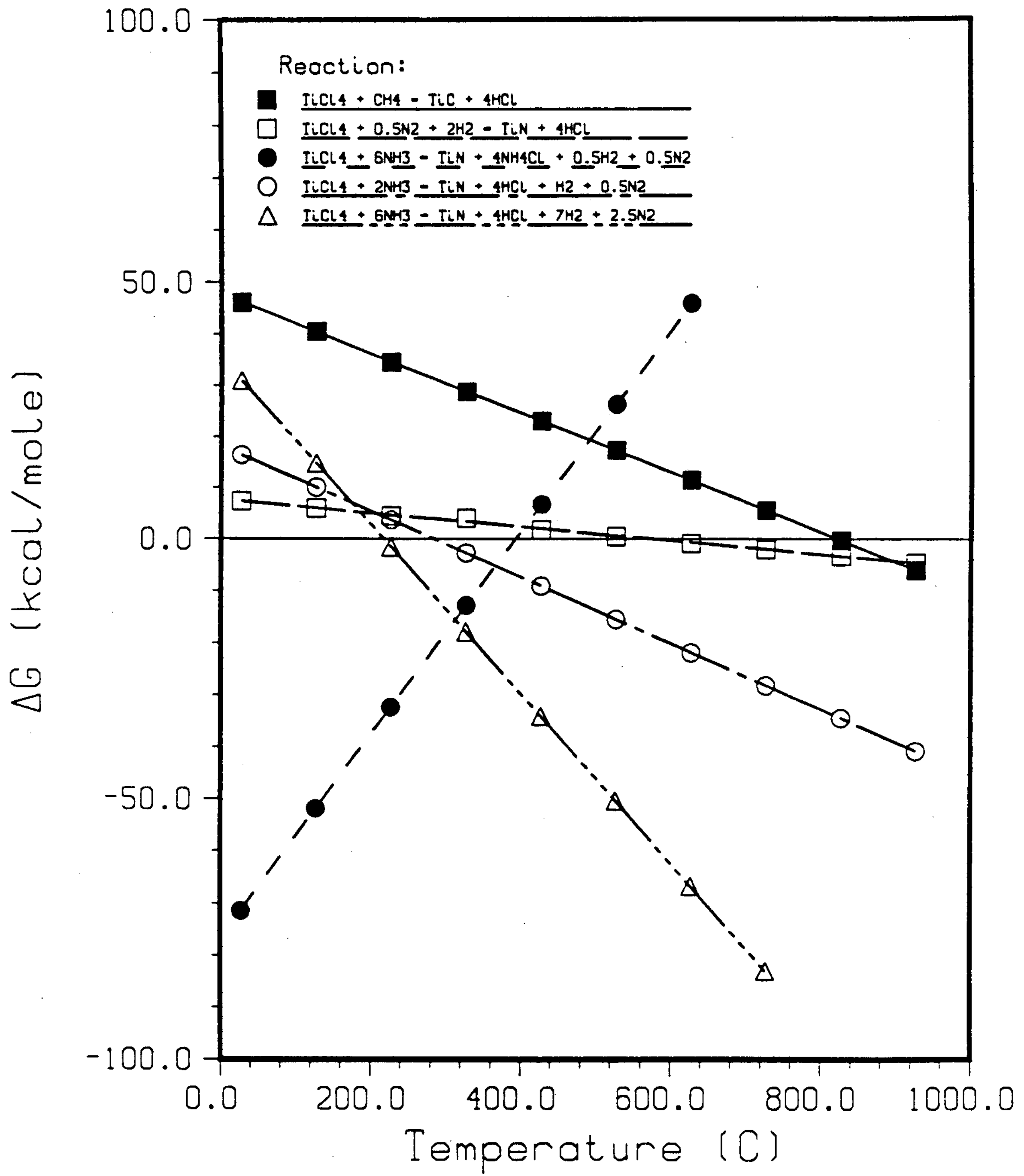

Figure 3.1: TiN and TiC formation reaction thermodynamics. (From JANAF.)

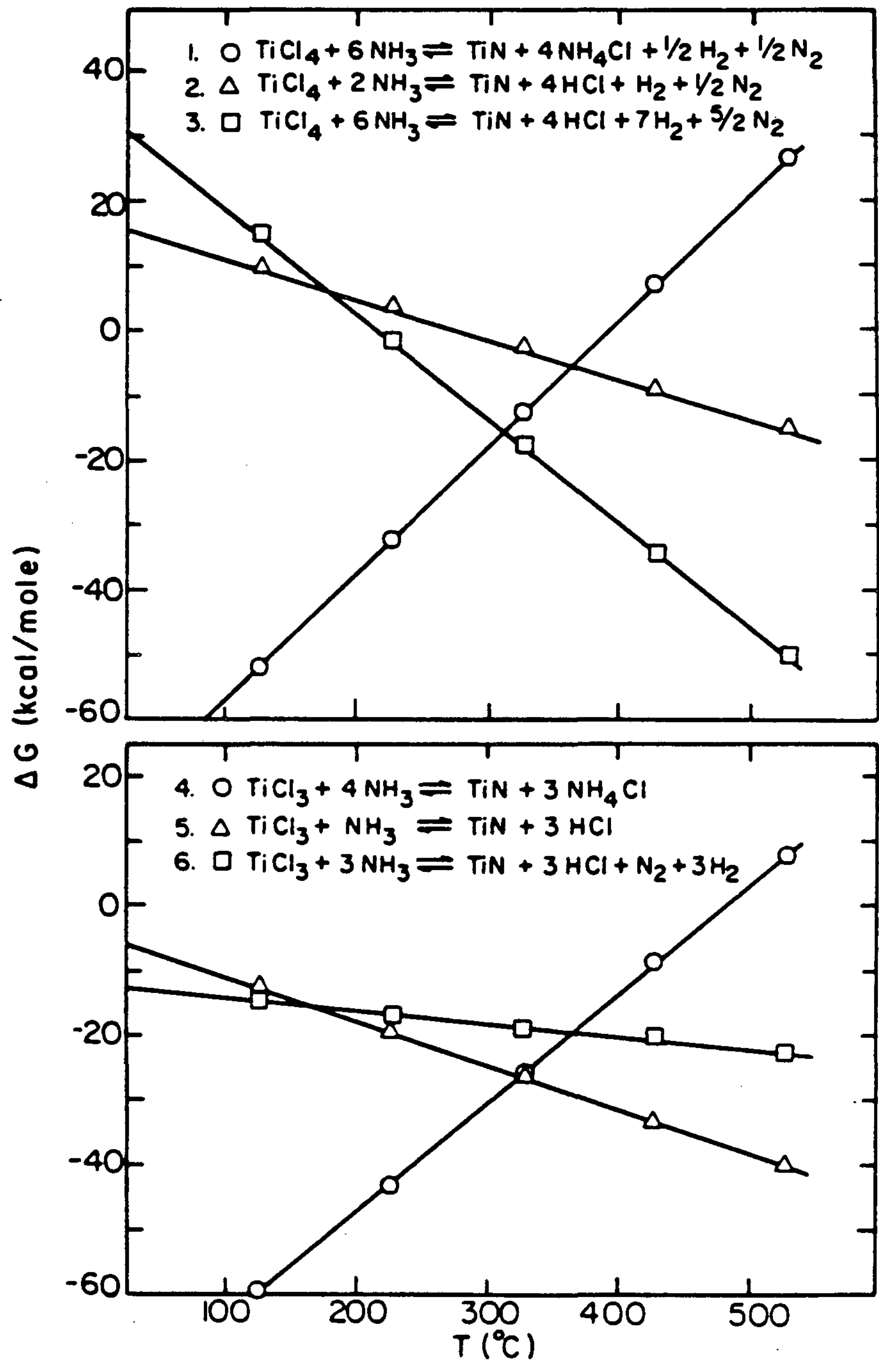

Figure 3.2: TiN formation reaction thermodynamics from $TiCl_4$ and $TiCl_3$. At higher temperatures, expulsion of HCl into the gas phase is favored over halogen incorporation into the growing film. (From JANAF.)

creasing temperature. Reaction (3), having more NH_3 and thus yielding more hydrogen and nitrogen molecules, is even more favorable than reaction (2) at the higher temperatures.

The intersection of curve (1) with curves (2) or (3) indicates the critical temperature separating HCl formation from NH_4Cl production. In principle, a very large excess of NH_3 could reduce the critical temperature to 180°C, but this is not a practicable option. If $TiCl_3$, which might be present in the plasma, is used instead of $TiCl_4$, the free energy curves are all shifted down, as shown in curves (4)-(6). However, the resulting critical temperature at which the reaction products change from NH_4Cl to HCl is similar to that with $TiCl_4$ because all of the free energy curves shift. These calculations indicate that in order to form TiN films without the presence of chlorine, using a pure CVD process, the deposition temperature must be above about 350°C.

An organometallic reactant, titanium tetrakis dimethyl amide, $Ti(N(CH_3)_2)_4$, was investigated because of reports by Sugiyama et.al. that TiN could be synthesized by CVD at temperatures as low as 200°C (Sug:75). As the research progressed, improvement of film mechanical properties became the highest priority, superceding reaction temperature suppression. $TiCl_4$ with N_2 and H_2 were utilized with the intent of improving film adhesion. Efforts were also directed towards the synthesis of titanium carbonitrides using $TiCl_4$, CH_4, N_2, and H_2. This work was motivated by the higher hardness of TiC versus TiN (2900 vs. 2000kg/mm^2). In addition, film hardness might also increase microstructurally, either through grain refinement if a two phase mixture was formed or if a single phase formed through induced modulation of C and N. Periodic composition modulations (of the order of 10-200Å) in films have been found to increase modulus in several bimetallic systems by Hilliard and his coworkers (see for example Hen:83) and to increase hardness in (TiV)N by Sundgren and Greene (Hel:87).

3.1 $TiCl_4$, NH_3 studies:

3.1.1 Deposition Conditions:

In this study, the substrate temperature, total pressure P_{TOT}, ammonia flow rate, r.f.power and deposition time were varied. The $TiCl_4$ flow was held constant at 0.21mmol min^{-1} during the experiment. The value of P_{TOT} ranged from 0.2 to 1 Torr by varying the ammonia flow 0.27 to 2.4mmol min^{-1}. In some studies, partial pressures of argon were present. The radio frequency was kept constant at 12.00MHz and the electrode spacing was one in. Substrate temperature varied from 175°C to 400°C and r.f. power was varied in the range 0-25W. The deposition time ranged from 5 to 90min. In all cases, the samples were initially placed on the heater, which was set for a sample temperature of 400°C. The samples were cleaned in a 0.3 Torr NH_3 plasma for 10 min. The system was then evacuated and the substrate temperature was readjusted to the desired deposition temperature. NH_3 was added to the desired level and the plasma was ignited. $TiCl_4$ was then allowed to flow into the plasma.

3.1.2 Film Structure and Composition:

The TiN coating properties over M2 steel were extensively investigated under fixed deposition conditions (which will be shown in Section 3.1.4 to be optimum in expediting coating production and characterization) of a film thickness of 2.00-2.30μm, a deposition temperature of 400°C, 200 W r.f.power, P_{tot} values in the range 0.2-1Torr, a $TiCl_4$ flow rate of 0.21 mmol min $^{-1}$ and NH_3 flow rates of 0.27-2.4mmol min^{-1}. Study by SEM showed that the TiN grew with columnar grains, as shown in Fig.3.3.

The columns appeared to be dense at the exposed grains and they extended from the substrate to the TiN surface. The external surface of the film followed the topography of the substrate. Using Thornton's classification system, the structure

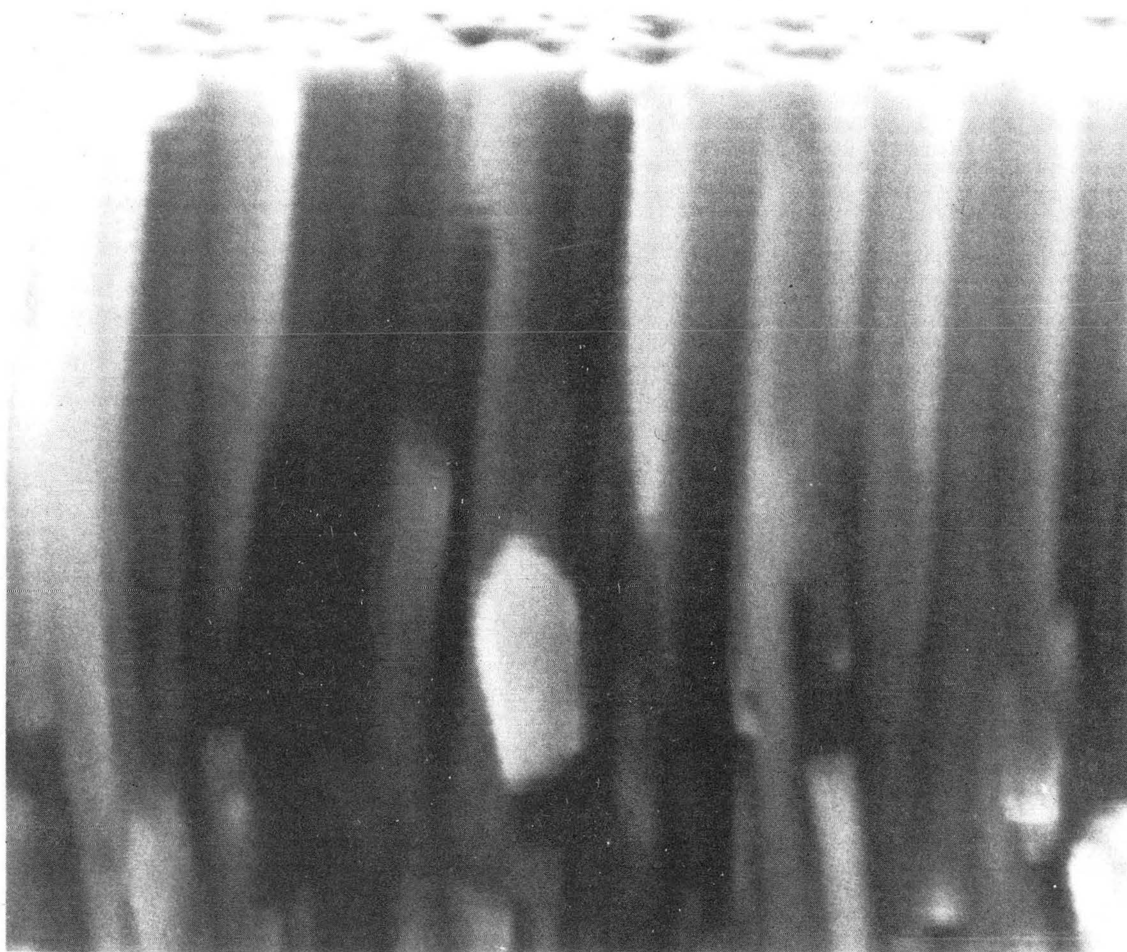

0.5 μm

XBB 856-5085

Figure 3.3: SEM micrograph of a TiN film cross section, created by the impact of a Rockwell C diamond indentor, showing the zone 2 type of columnar grain structure seen in the PACVD coatings of this study deposited 400°C.

appears to be a zone 2 type (Tho:77). The average grain diameter was approximately 2500Å, about two orders of magnitude less than the M2 steel grain size. Study by X-ray diffraction showed that the films had a strongly preferred orientation. (See Figure 3.4) The only peaks present in these films were the TiN(200) and TiN(400) reflections that correspond to the lowest energy plane of the TiN crystal lattice, which is of the NaCl type f.c.c. structure. This preferred orientation on the TiN deposits was also observed on glass and 304SS substrates. The formation of thin films of b.c.c., f.c.c. or h.c.p. structure having their most densely populated plane parallel to the substrate has been reported in the literature (Tho:77).

In these studies, AES and sputter profiling were used to estimate the bulk composition of the films. Figures 3.5 and 3.6 show the Auger spectra of a film before and after sputtering respectively. The $(Ti+N)_{387eV}:Ti_{418eV}$ values of sputtered films ranged from 2.1 to 2.3, which is within reported TiN ratios (Sch:81, Daw:85). AES analysis of commercially prepared CVD TiN films showed an identical range of $(Ti+N)_{387eV}$: Ti_{418eV} values. The film surfaces had large amounts of carbon and some oxygen that were removed by sputtering. After a short initial sputter treatment to remove the first few layers, the composition of the films did not vary until the M2 substrate was reached. The bulk oxygen, carbon and chlorine contents were less than 3 at.%, 8 at.% and 2 at.% respectively, as determined by evaluating the O(510eV):Ti(418eV), C(270eV):Ti(418eV) and Cl(180eV):Ti(418eV) Auger peak ratios and using the procedure described in the literature (Dav:76) and in section 2.4.1. The small amount of residual carbon inside the films appeared to be carbidic, as deduced from the shape of the AES peak (Haa:72, Hoo:77).

3.1.3 Mechanical properties:

Rockwell hardness tests indicated that the heating of the substrate during the depositions at 400°C or lower did not degrade the M2 microstructure. The hardness values did not change, within one point on the Rockwell C scale. Vicker's hardness testing of the coated and uncoated regions indicated higher values for

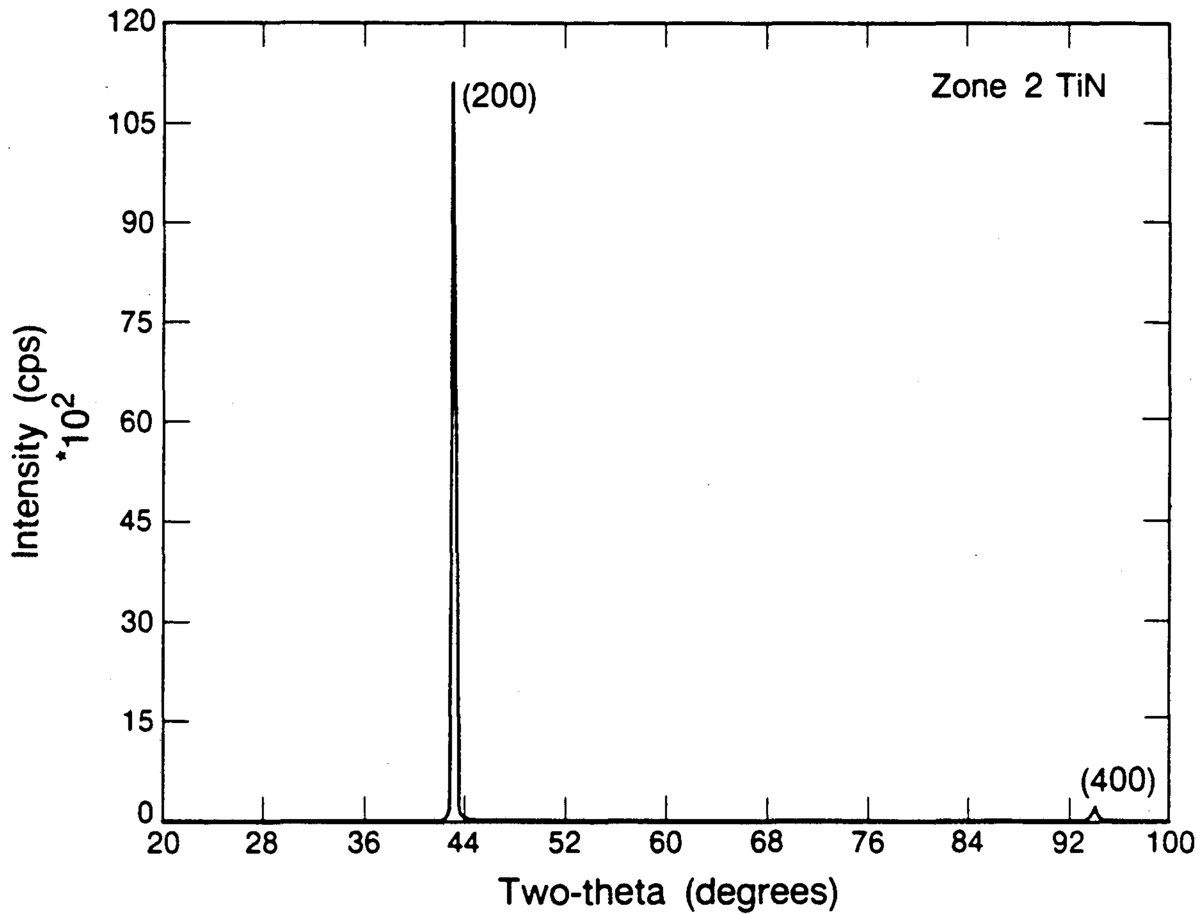

Figure 3.4: X-ray diffraction intensity vs 2θ for a TiN film deposited at 400°C. Strong (200) preferred orientation is evident.

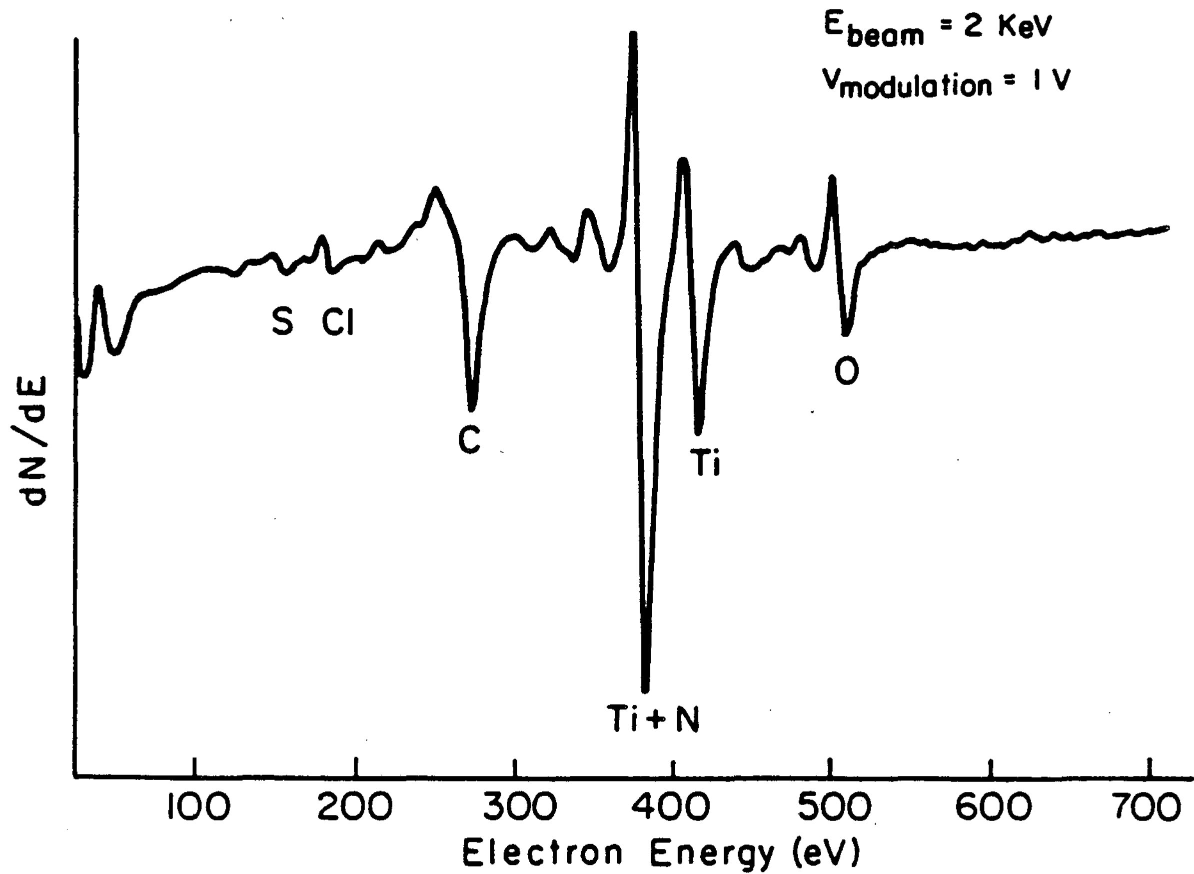

Figure 3.5: Representative AES spectra of a TiN film deposited at 400°C in the as-received condition.

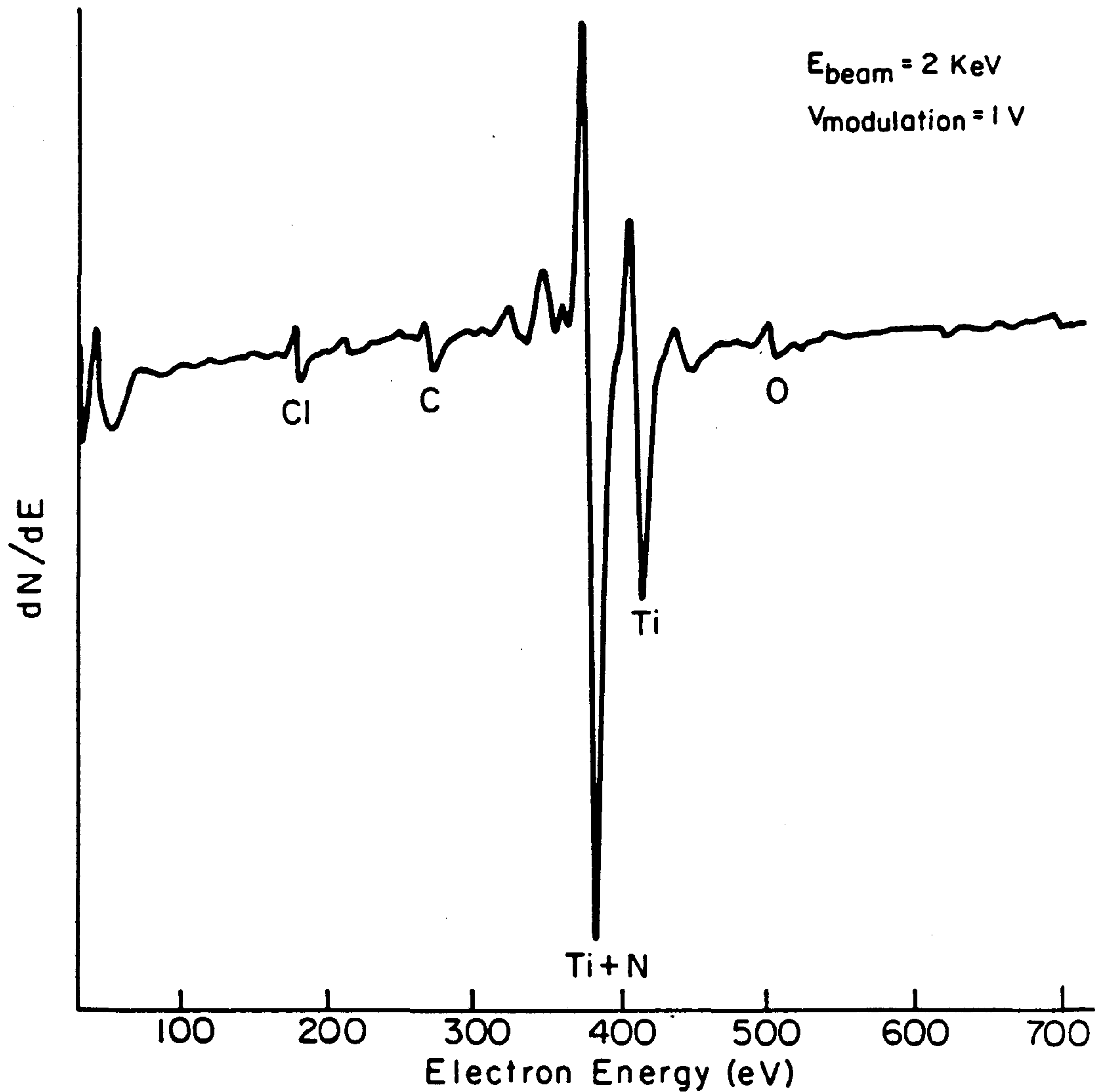

Figure 3.6: AES spectra of the film on the previous figure, after sputtering for 15 minutes. The film composition remained constant thereafter until sputtering penetrated to the substrate.

the former at the near surface as shown in Fig. 3.7. However, the bulk hardness value of TiN (2000 kgf mm^{-2}) was not obtained even at the lower loads(15gf) for a coating 2 μm thick. Sproul (Spr:83) obtained films with values of Vickers' hardness $H_v$of 2359-2391kgf mm^{-2} for coatings 9.5 μm thick (grown by r.f.reactive sputtering) at a 200gf load. Because of the differences in loads and thicknesses, the results cannot be directly compared. It is clear, however, that the PACVD hardness values are smaller than those of Sproul.

The SAT results of Sproul (Spr:83) using 2μm coatings and the present results can be directly compared. The PACVD films have inferior adhesive strength, failing at critical loads of 500-600gf while the r.f.-sputtered films fail at 2kgf. The low critical loads correspond to values reported by Helmersson et al (Hel:85) obtained on sputtered TiN films (5μm films) that were simply degreased with solvents (trichloroethylene, acetone and ethanol) prior to deposition. The PACVD films in the present study were degreased in acetone and cleaned in an NH_3 plasma. It is also important to note that Sproul's films had a very different morphology from the PACVD films, consisting of equiaxed grains 300-400Å in diameter. The morphology of Helmersson et al.'s films was not reported explicitly in that reference. However, in later references, they have reported zone T and zone 2 morphologies with grain sizes on the order of 600-6000Å (Sun:86).

SEM investigation of scratch adhesion wear tracks indicated that the coating appears to be removed from a region wider than the indentation, with failure at the coating-substrate interface, i.e. adhesive. Study by EDS confirms that the failure is by delamination near the interface, since titanium cannot be detected at the exposed surfaces. Using the Burnett/Rickerby classification, the films failed by a severe spallation (Type A, see Figure 3.8) or an extensive, extended chipping mode (Type C). The failure region around a Rockwell hardness indentation is similar, except that the TiN remains in the indentation with the coating absent from the undeformed perimeter as shown in Figure 3.9.

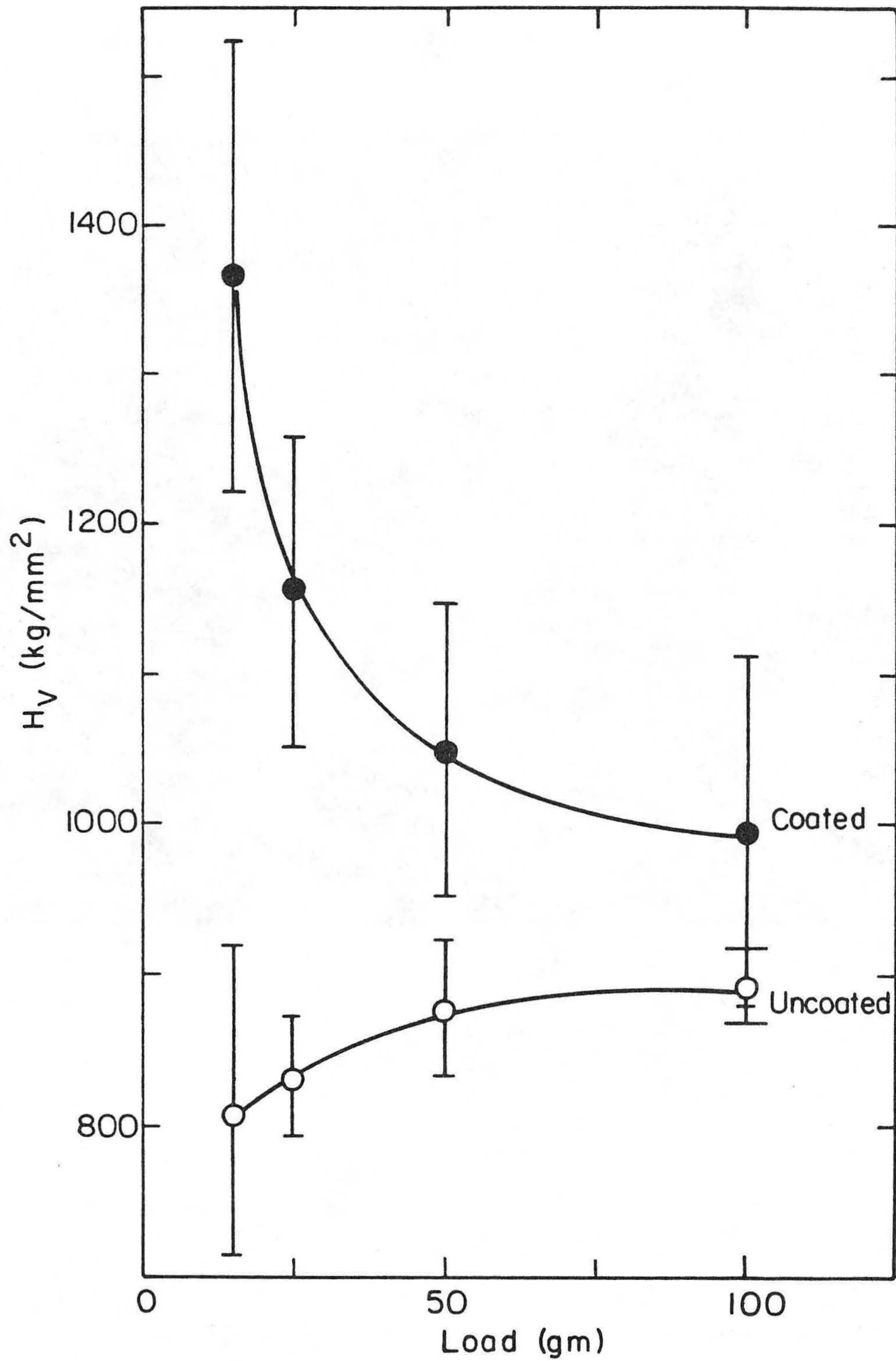

Figure 3.7: Vickers hardness as a function of test load for TiN coated (closed circle) and uncoated (open circle) regions on an M2 steel substrate (coating thickness, 2.25μm.

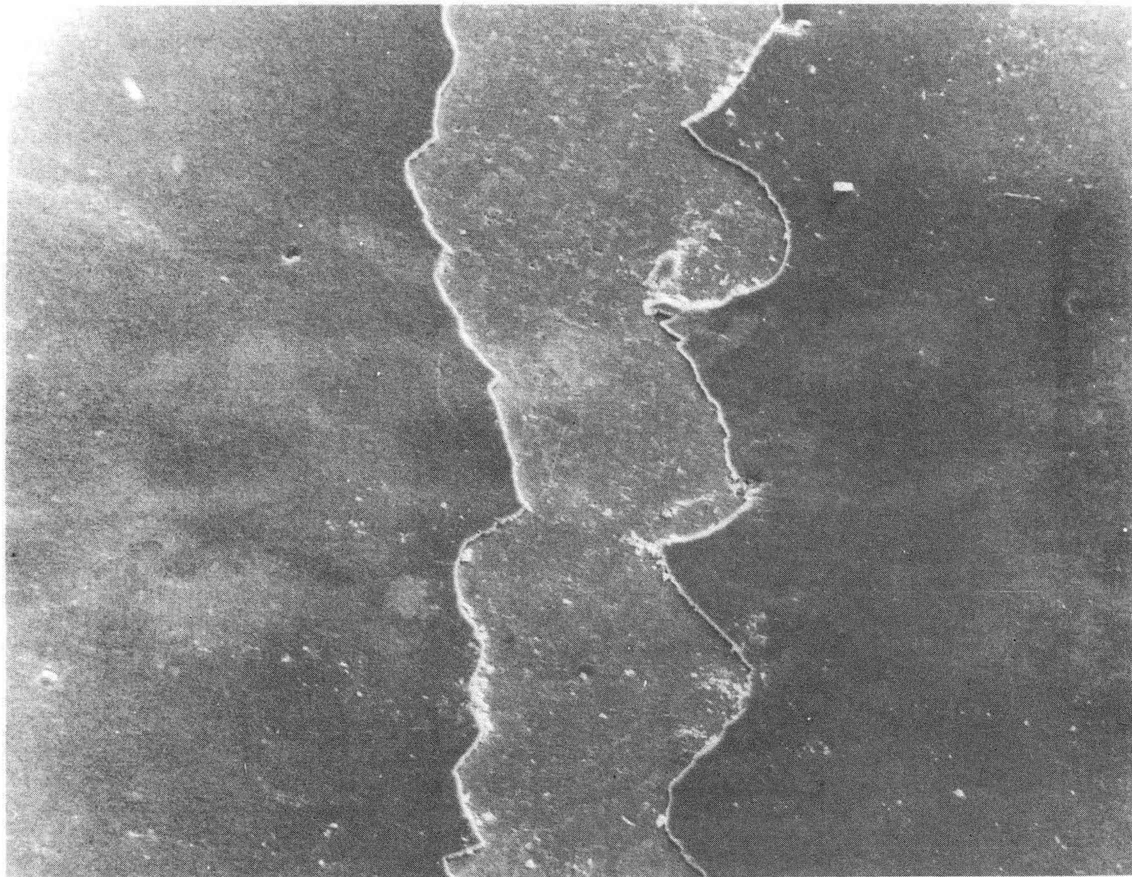

Figure 3.8: SEM micrograph of a SAT wear track of a $TiCl_4$-NH_3-based film. The mode failure is Rickerby/Burnett type A. L_C=600g. (Film thickness: 2μm.)

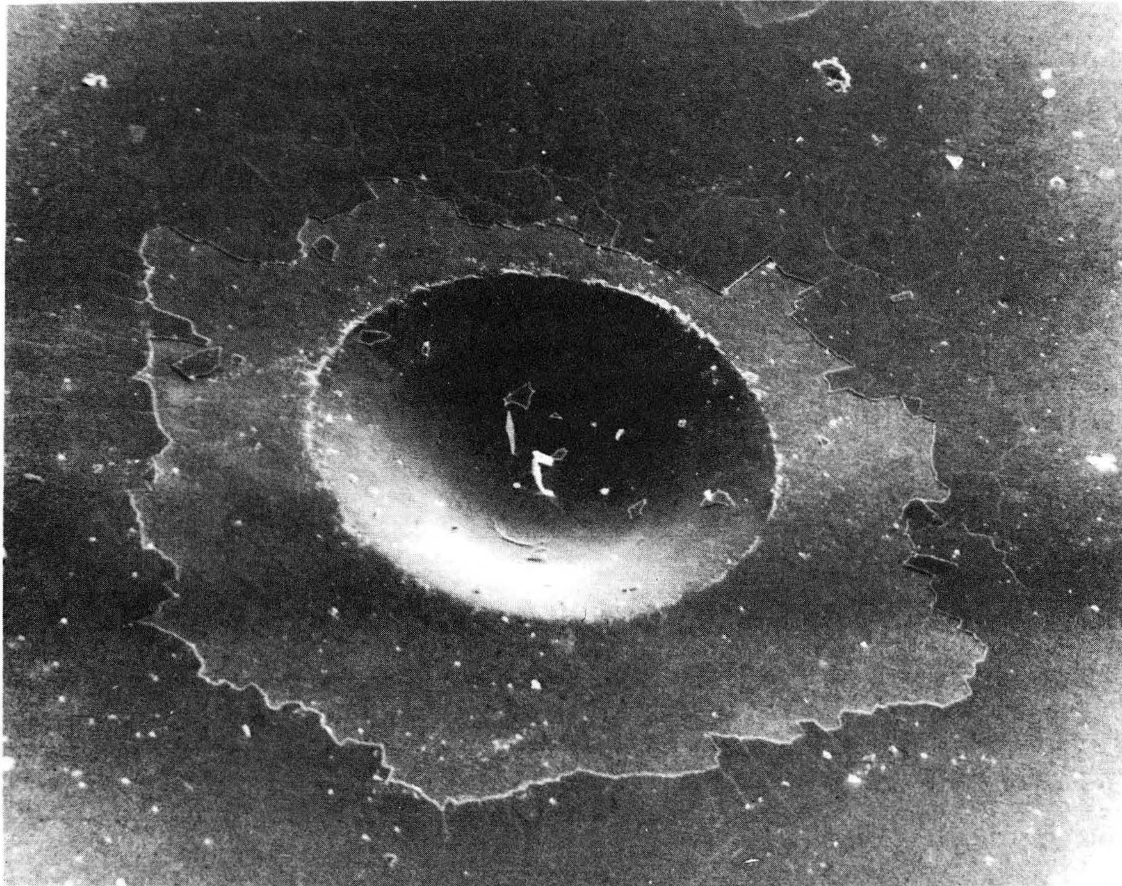

200 μm

XBB 870-8274

Figure 3.9: SEM micrograph of a Rockwell C indentation on an $TiCl_4$-NH_3-based film. Extensive film delamination is evident.

3.1.4 Effect of changing film deposition parameters:

This section describes the results of the influence of the various experimental parameters that can be varied in the deposition system on the physical and mechanical properties of the TiN films. The parameters include substrate temperature, reactant pressure, reactant composition, r.f. plasma power, and substrate bias.

Deposition temperature:

The sample temperature during deposition was varied in the range 170-400°C. As the temperature decreased, the color of the coatings would shift from gold-bronze through purple-blue to blue-black, independent of the film thickness. Black films appeared below 300°C. The film became amorphous and no traces of crystallinity were detected by XRD. The (200) and (400) lines in the XRD patterns were observed only at 300°C and above. Few studies were possible on the lower temperature(below 300°C) coatings because they tended to disintegrate spontaneously (flake off) after production. The low temperature coatings that were observed by SEM had a columnar appearance, as did all films deposited at 300°C and above. These low temperature grains appeared to be of a zone 1 type (hemispherical capped tops with a fibrous and porous interior, see Figure 3.10) of the Thornton classification system, instead of a zone 2 type. Figure 3.11 shows that chlorine content in the coatings decreased, as the temperature increased, to levels below 2 at.%. The temperature at which crystallinity appears and at which the chlorine content decreases significantly is close to the temperature at which the thermodynamically favored halogen byproduct changes from solid NH_4Cl to gaseous HCl. The ratio of mass spectrometry peak heights of HCl to NH_3 sampled during deposition increased with temperature as shown in Fig. 3.11.

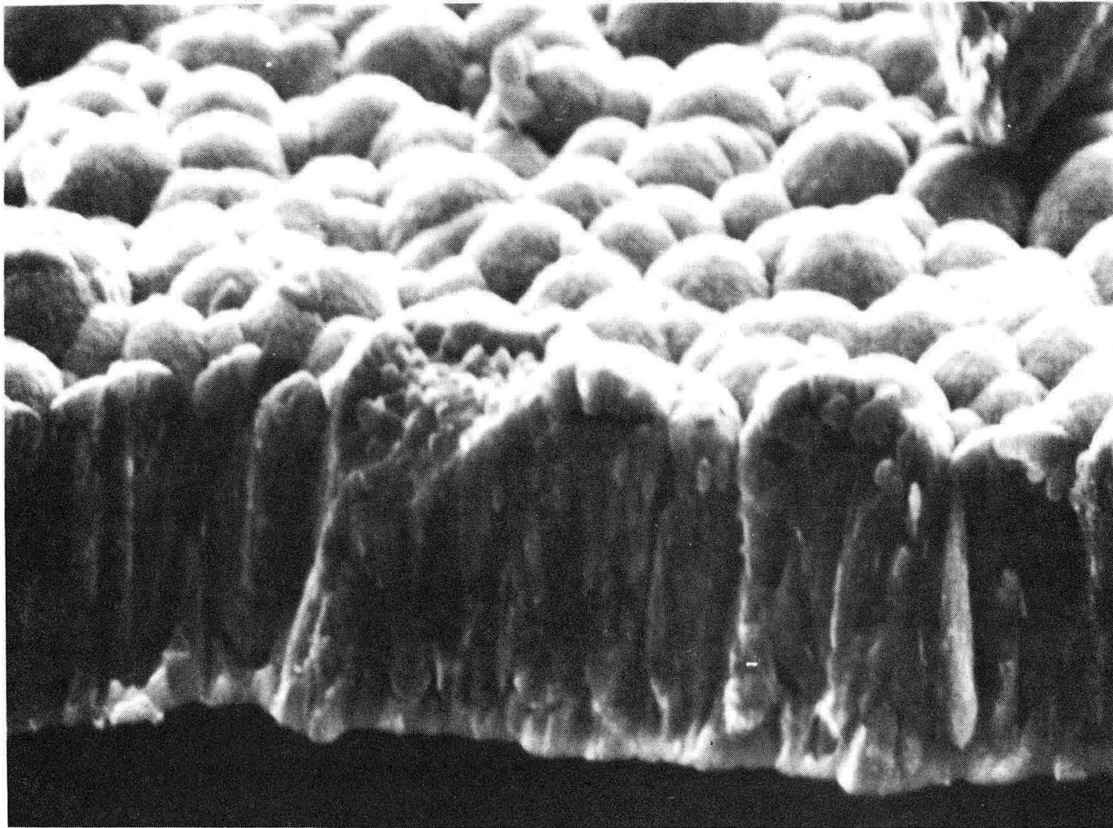

2 μm

XBB 870-8272

Figure 3.10: SEM micrograph of a TiN film cross section exposed by Rockwell impact, revealing a zone one morphology seen at deposition temperatures below 300°C. Film deposition temperature=230°C.

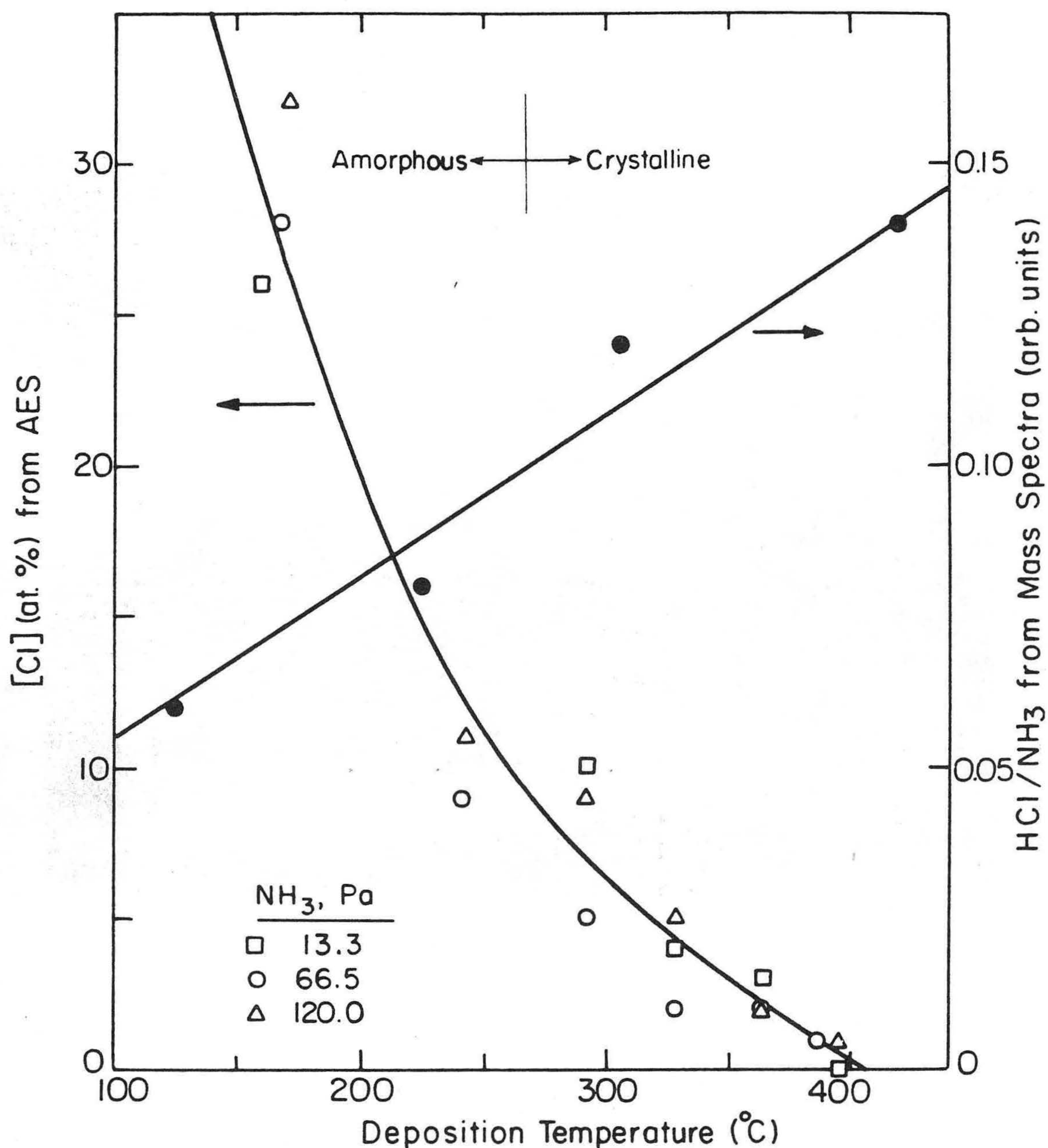

Figure 3.11: Chlorine content in the TiN film vs. deposition temperature at various NH_3 partial pressures, as determined by AES(left-hand ordinate). The temperature regime where TiN crystallites were detected by XRD is indicated. The ratio of the HCl to NH_3 mass spectrometry peak heights, determined by sampling gas from the plasma during deposition is also shown(right-hand ordinate). As the temperature increases, the deposition reaction favors the elimination of chlorine from the film into gas phase HCl.

Ammonia partial pressure and thickness variation:

The ammonia partial pressure was varied from 13.3 to 120Pa.(0.1 t0 0.9 torr) Figure 3.12 shows that P_{NH_3} did not significantly affect the film chlorine content or crystallinity as a function of temperature. The grain size of the films did not change as P_{NH_3} was varied at 400°C. The film growth rate was found to vary at a rate of approximately 2.6x10^{-2}nm $s^{-1}PA^{-1}$ as shown in Fig 3.12. Using various values of P_{NH_3}, coatings of thickness up to 8 μm were prepared. However, coatings that were greater than 5μm thick tended spontaneously to buckle away from the substrates in localized regions, suggesting that the coatings were under residual compression. TiN films deposited onto glass under identical conditions caused the substrate to bow upward, indicating residual tension. This change in residual stress state suggests that thermal expansion mismatch is an important factor for films deposited by the process. Sproul did not report any significant residual stress problems in his sputtered TiN films.

Effect of Argon Partial Pressure:

The effect of argon in the plasma was investigated, motivated by the results of Manory et al. (Man:85), who showed that silicon deposition from tetrachlorosilane and hydrogen was enhanced by argon in the plasma which promoted ion-molecule collisions with concurrent generation of H radicals. In the present PACVD study the deposition temperature was 400°C and total pressure was 0.4 Torr. Figure 3.13 shows that reaction rate generally increased as Ar increased. With 100% Ar (no NH_3), a substoichiometric oxide was formed. The lower growth rate coatings also show higher oxygen contents. Film thicknesses were in the range of 0.5-3.0μm and SAT L_C's ranged between 300 and 600g.These results clearly demonstrate that the population of *excited*-state species of reaction feedstocks is a more important rate-limiting factor than the actual feedstock population from which excited species

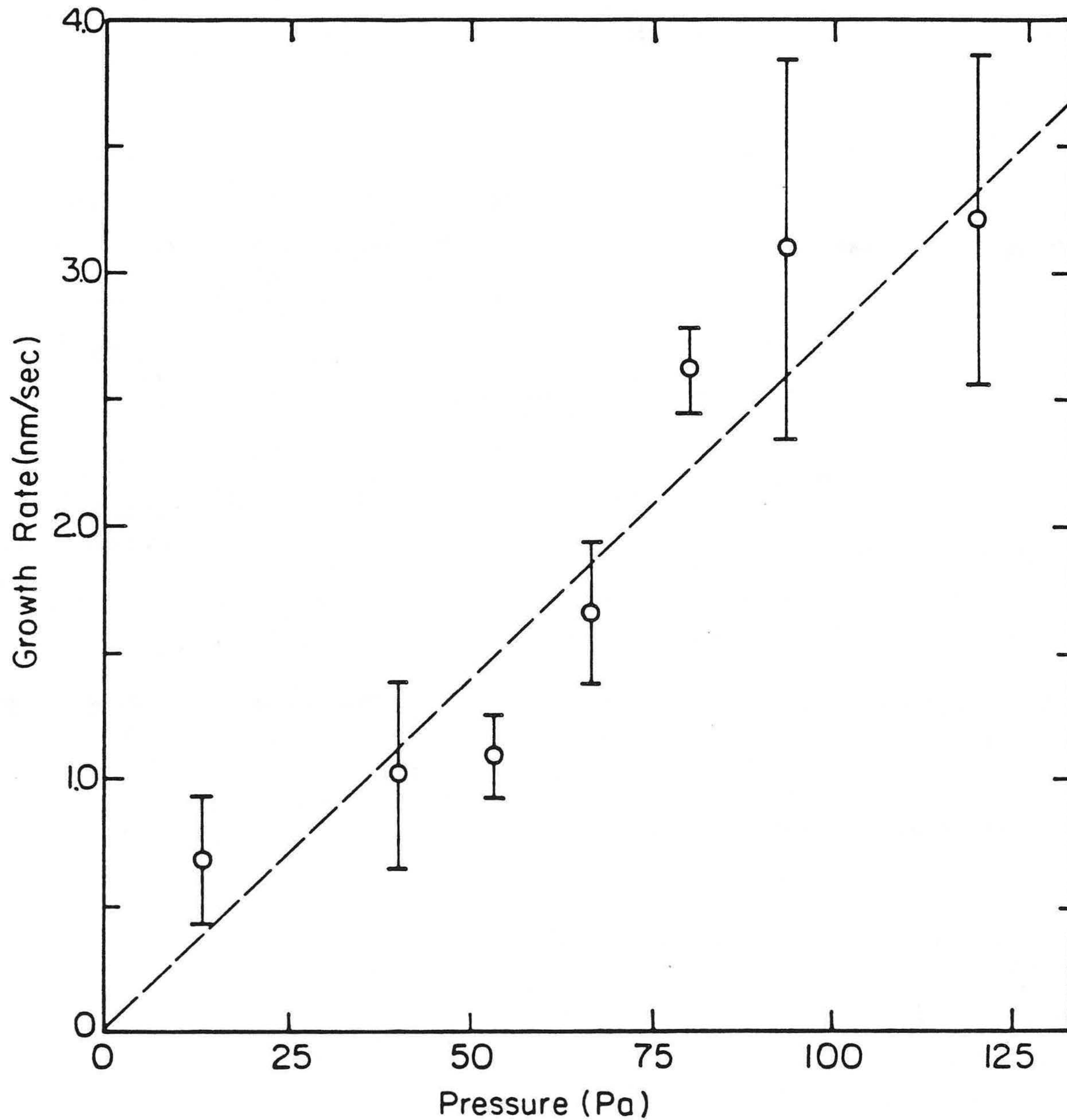

Figure 3.12: Relationship between the film growth rate and the ammonia partial pressure for a fixed $TiCl_4$ film rate of 0.21 mmol/min. (Deposition temperature: 400°C, r.f.power: 20W.)

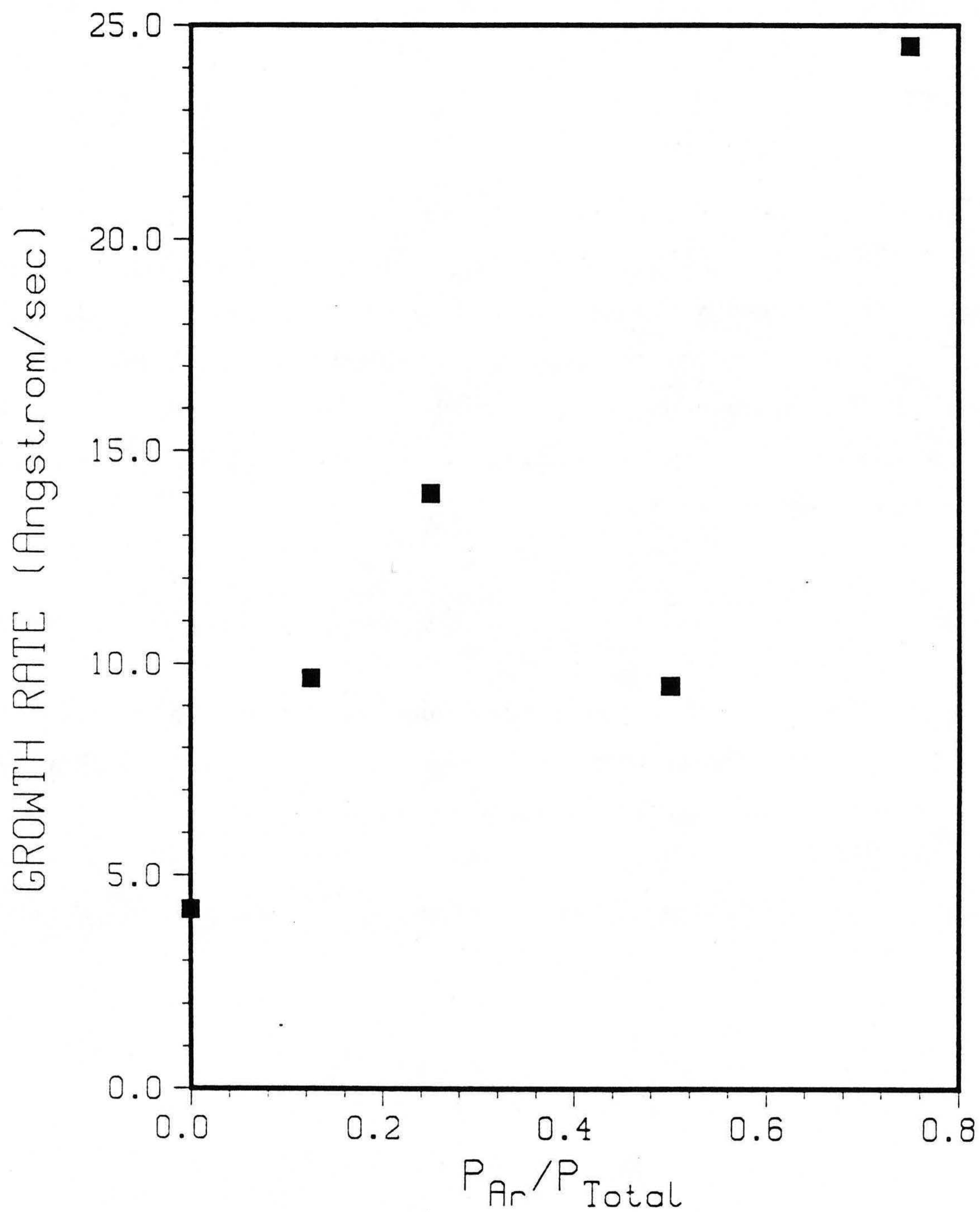

Figure 3.13: Growth rate vs. the partial of argon over total pressure for TiN films formed from $TiCl_4$, NH_3 and argon. The total pressure was 0.4 torr and the deposition temperature was 400°C.

originate.

R.f.power:

Figure 3.14 shows the film growth rate as a function of r.f. power at 400°C and three different values of P_{NH3}. Even with zero power(i.e. no plasma) a TiN formation reaction readily occurred. Increasing the plasma power increased the growth rate between five and ten times in the range studied, which was between zero and 25 W. These studies were performed with the ENI r.f. supply. Figure 3.15 shows results at higher powers using the IPC supply at 0.9T NH_3. The growth rates of samples are seen to optimize at 50W.

Effect of d.c. biasing

Figure 3.16 shows the film growth rate diminishes as a function of biasing at 400°C, 20W power. Composition, as determined by AES, did not vary significantly with biasing. The -100 and -200V film were too thin to evaluate by SAT. The grounded, -25V, and -50V films had thicknesses of 4.3, 3.3, and 1.6μm respectively and had L_C's of 300g, 400g, and 300gm respectively. They failed in a Type A mode.

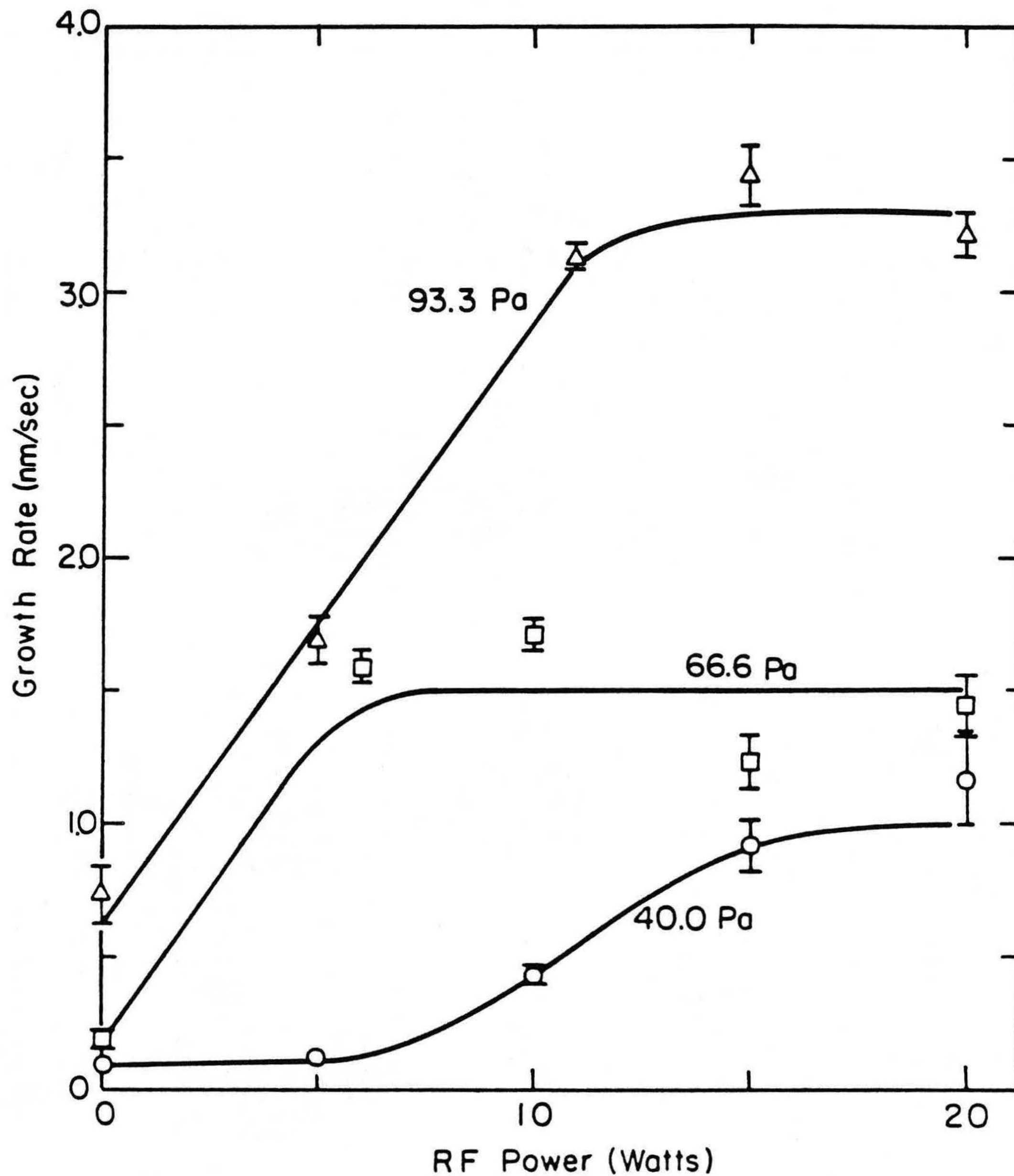

Figure 3.14: Film growth rate vs. r.f. power for three different ammonia partial pressures at 400°C, using the ENI supply.

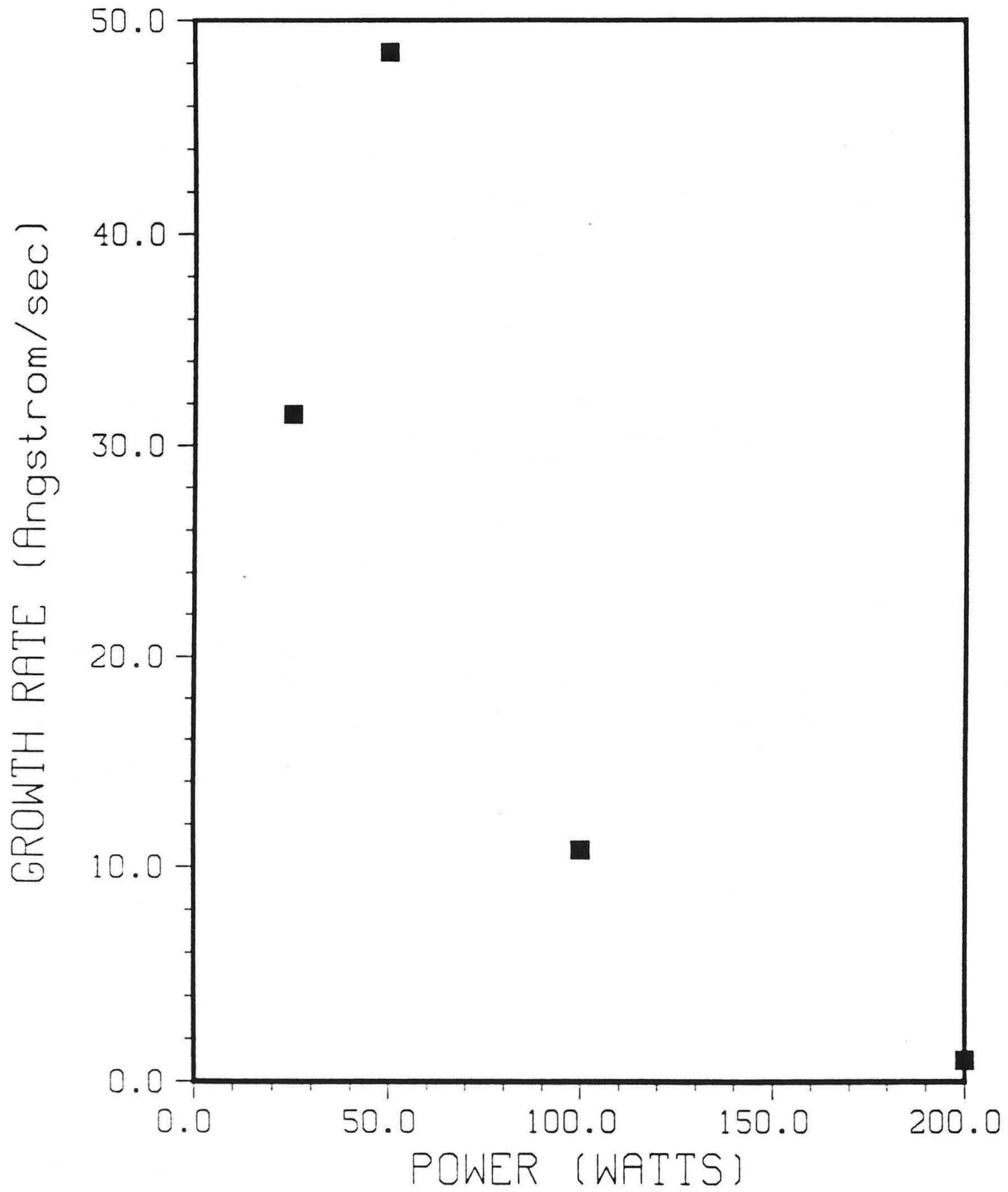

Figure 3.15: Film growth rate vs. r.f. power at 0.9 Torr (120 Pa) using the more powerful IPC supply.

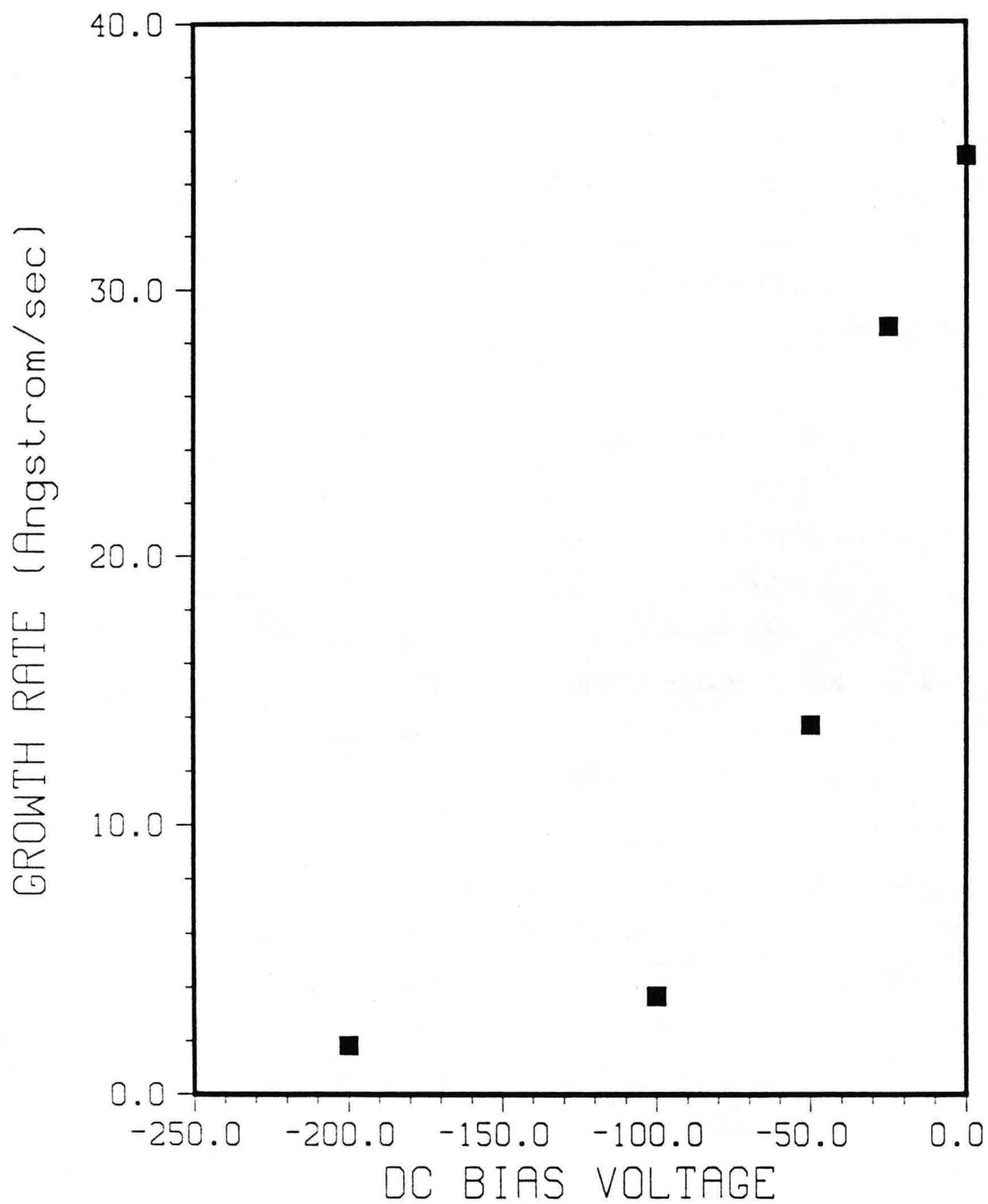

Figure 3.16: Film growth rate as a function of substrate d.c. bias for films formed from $TiCl_4$ and NH_3 at 400°C.

3.1.5 Interface Composition:

The interface composition of the $TiCl_4$-NH_3-based films was investigated with the scratch removal technique and with conventional depth profiling. For the scratch removal study, 0.6-2 micron thick coatings were used. All films examined were deposited at 400° C and the bulk chlorine content was less than 2 at.%. In the sputter Auger depth profiling experiments, Ar ions of 2 keV were used at a pressure of 1.05 X 10^{-2}Pa; under these conditions the sputter rate was approximately 8 Å/min.

Figure 3.17 shows a typical AES spectrum of a film after sputter cleaning of the surface, revealing a stoichiometric TiN film with low Cl, C, and O content. AES analysis of the scratched regions revealed a very high chlorine content as shown in Figure 3.18. Extensive investigation of scratches on the films showed that the chlorine content was higher near the edges of the track. This fact is illustrated in Figure 3.19, which shows the AES peak intensities of Cl_{181eV}, $(Ti{+}N)_{387eV}$, Ti_{418eV}, and Fe_{703eV}, as a function of distance across a scratched region. Iron is concentrated at the center with chlorine bimodally distributed on each side. Carbon and oxygen intensities decreased slightly in the track and have been omitted for clarity. This figure is representative of many profiles though several asymmetric Cl distributions were found. The ratio Cl_{181}/Ti_{418} generally was in the range of 0.5-1.0 at the distribution maximum. AES argon depth profiling of these high chlorine regions indicated that the chlorine is highly concentrated at the newly exposed surface, the majority within the first one to three monolayers (see Fig.3.20). The sputtering rate was 3 Å/min.

Figure 3.21 shows a typical depth profile through a 0.6 micron film. Only the Auger peak intensities (uncorrected for sensitivity differences) are shown. Chlorine and Ti concentrations decrease together. In contrast with the results of the scratch removal described above, no sharp increases of chlorine in the transistion region were observed. Oxygen content (not shown) follows behavior similar to

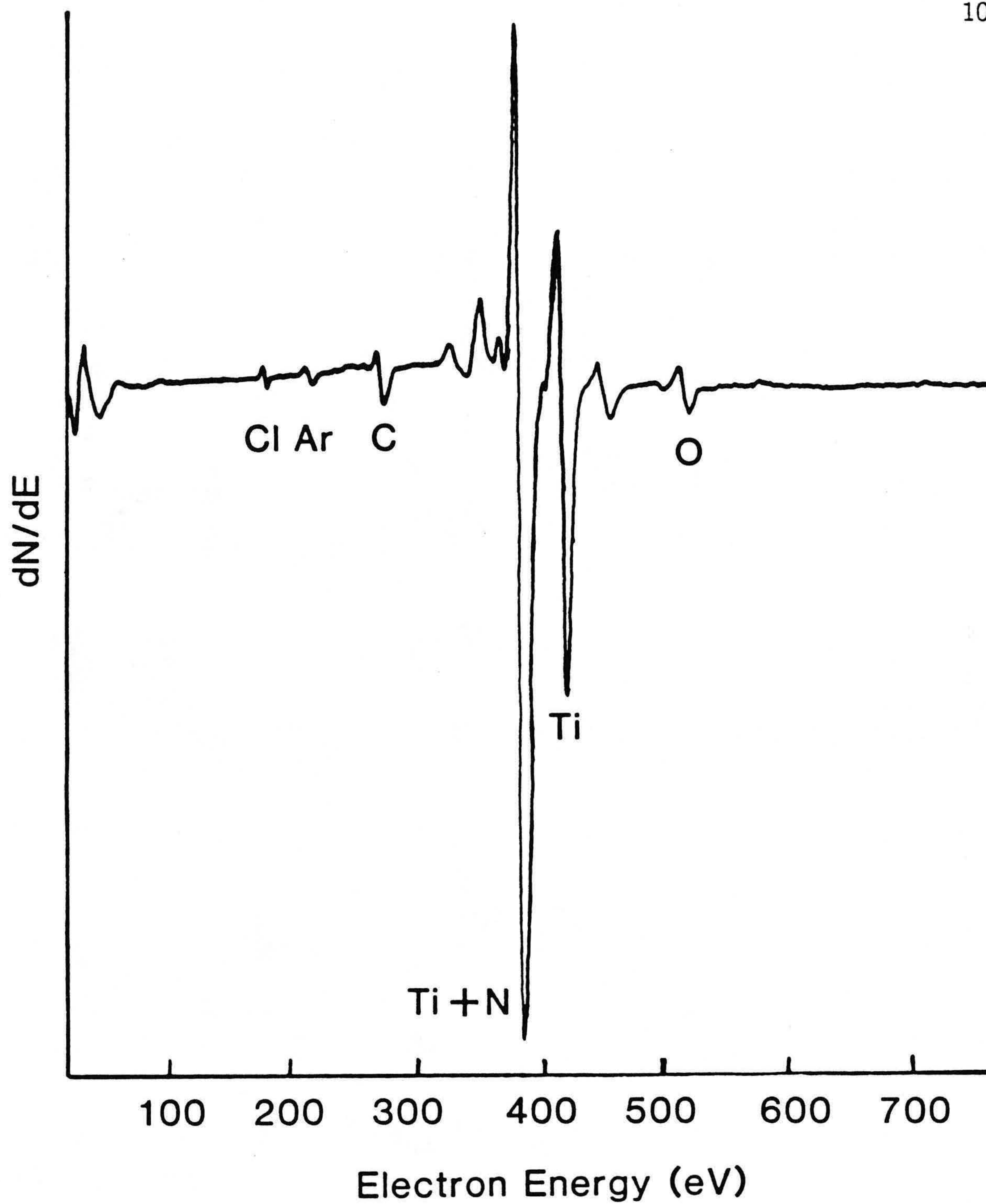

Figure 3.17: AES of a TiN film after sputtering prior to in-situ scratching.

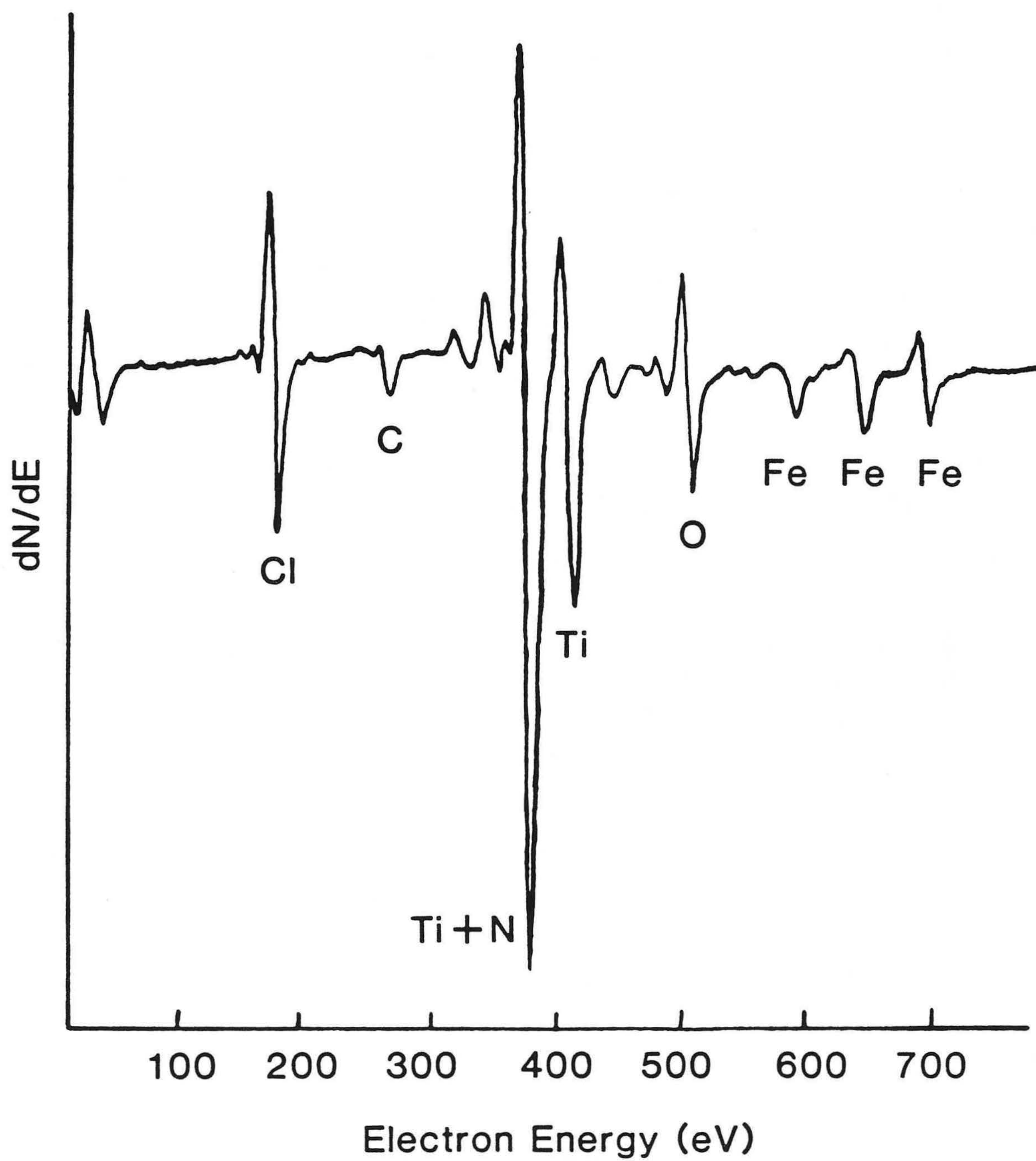

Figure 3.18: AES of the scratched region of the film after in-situ scratching.

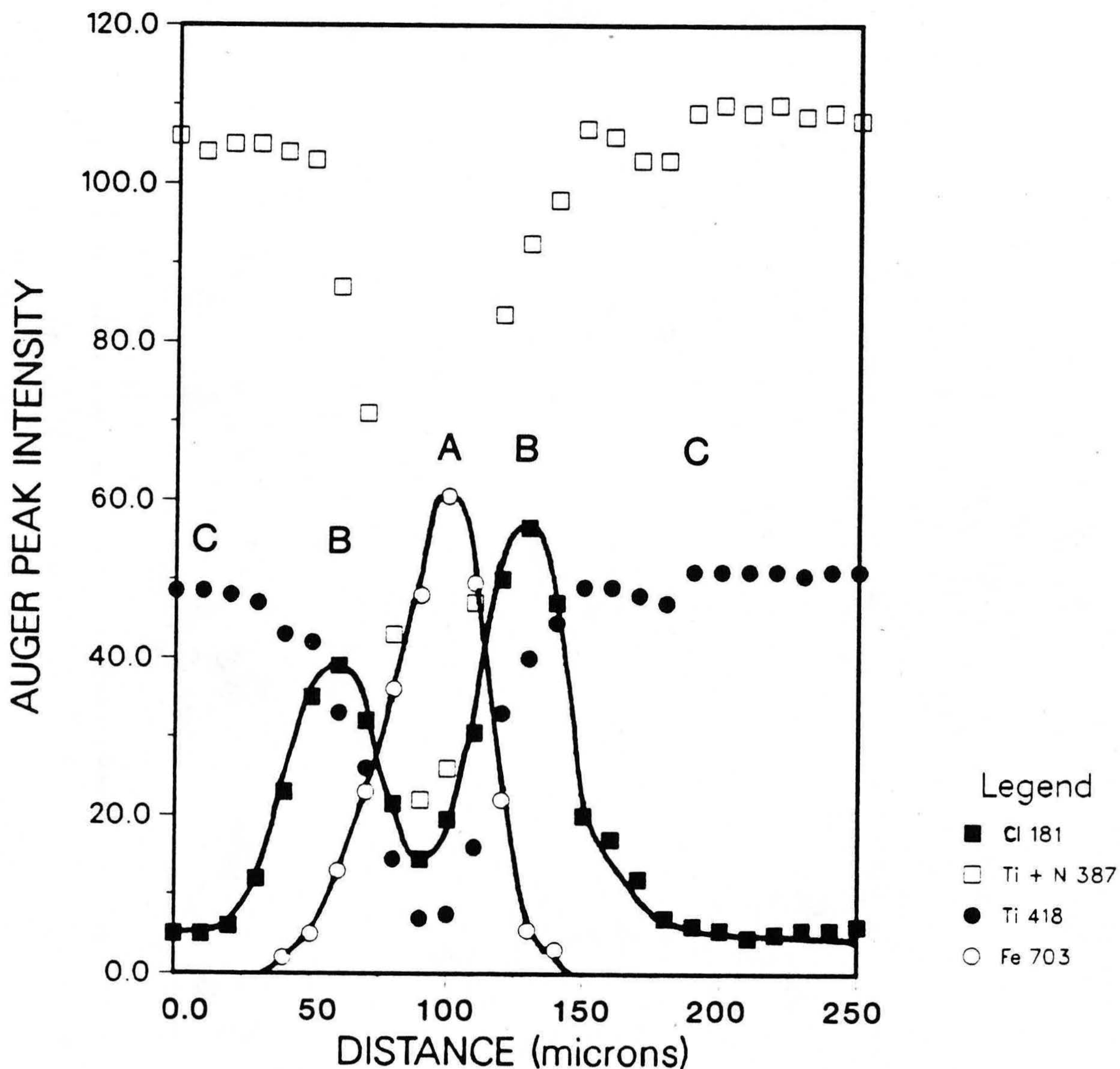

Figure 3.19: Auger peak intensity of Cl_{181eV}, $(Ti+N)_{387eV}$, Ti_{418eV}, and Fe_{703eV} as a function for distance along a traverse across a scratch produced in UHV. Fe content peaks at the center of the scratch (A). The chlorine content is bimodally distributed (B), with a maximum on each side of the Fe peak. The Cl content at the exposed surface representing the prior interface is higher than the bulk. Region C represents the undisturbed TiN film. See Fig. 3.22 for a physical interpretation of regions A and B.

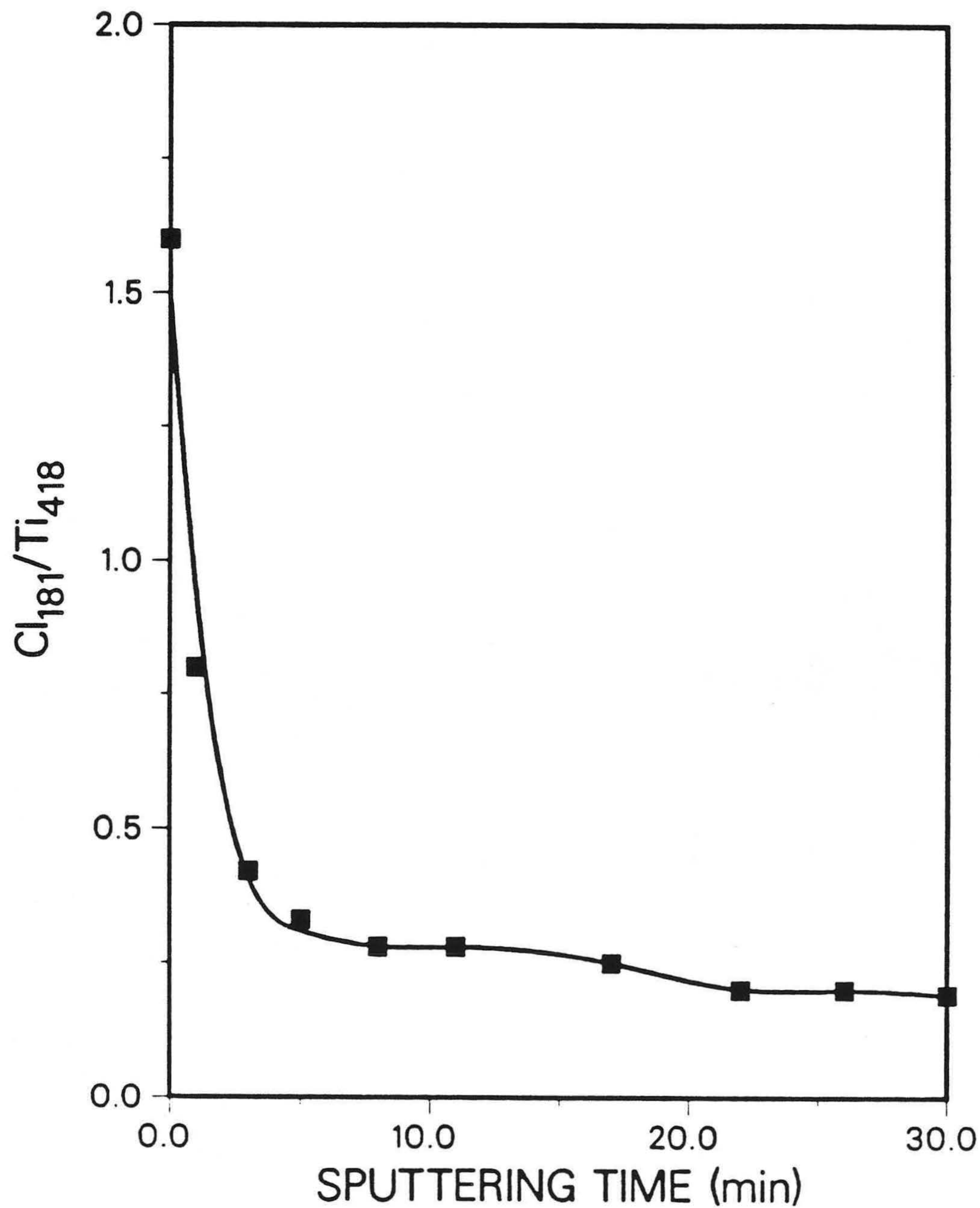

XBL 863-1190

Figure 3.20: Chlorine content as a function of sputtering time for a chlorine-rich region in a scratch (corresponding to a B area in Figs. 3.19 and 3.22). The sputtering rate was 3 Å/min. The sharp drop in the first 3 min. indicates that Cl is highly concentrated at the exposed surface representing the prior interface.

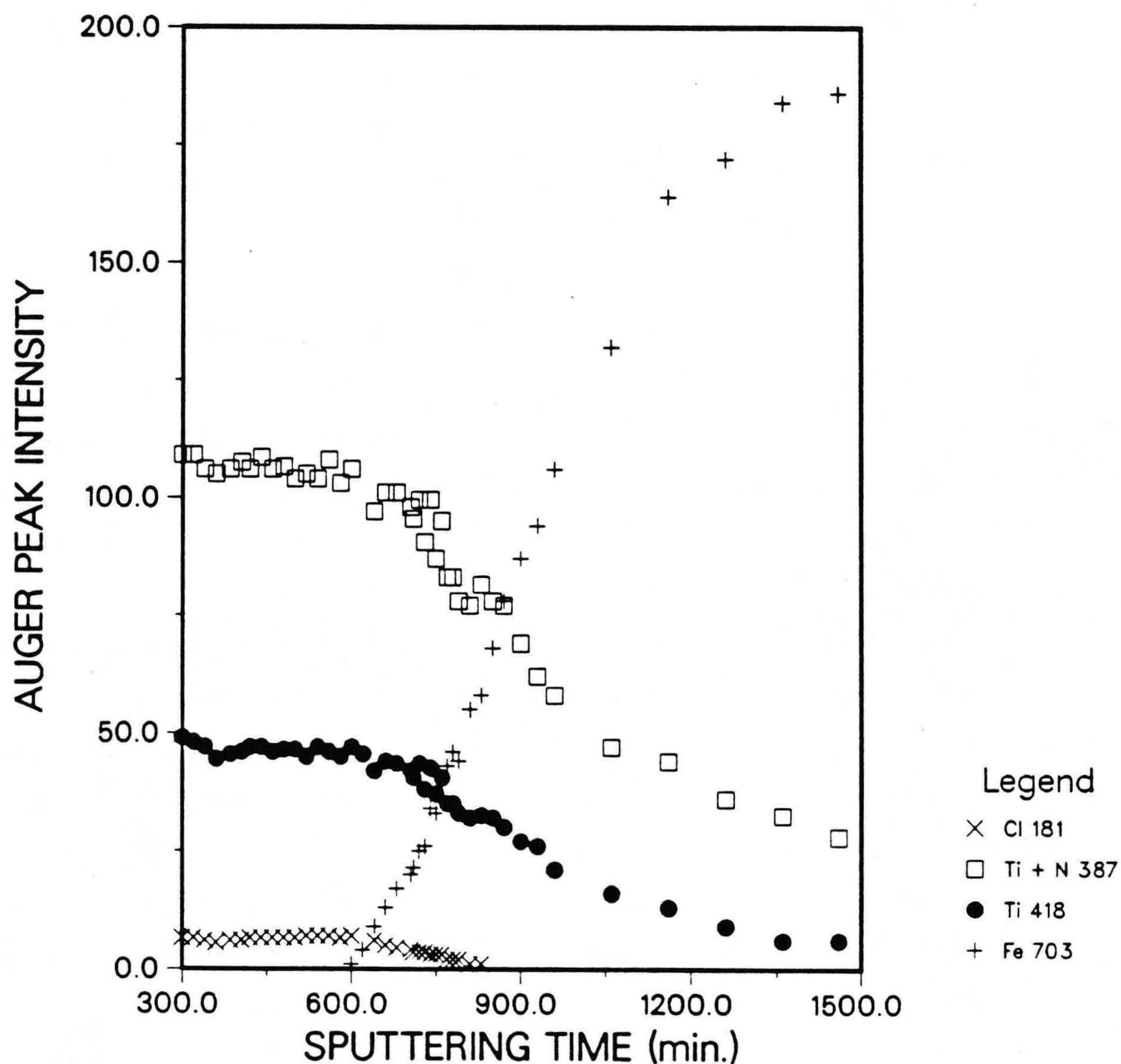

Figure 3.21: Auger peak intensity as a function of sputtering time for a PACVD-produced TiN coating on M2 tool steel. The sputtering rate was estimated to be 8 Å /min. No high chlorine content is seen at the interface. The ion bombardment process would disrupt any sharp interface concentration gradient like that shown in Fig. 3.20.

chlorine content, though there is a small amount of oxygen present in the M2 steel. The steel also contains nitrogen which presumably arises from the NH_3 plasma pretreatment prior to TiN deposition.

SEM of the scratched regions after UHV studies revealed that the track contained two regions, as shown in Figure 3.22. The center, labeled A, appears to be a region of worn or stylus-contacted substrate. On each side there are regions of exposed substrate and TiN film debris (confirmed by EDS), labeled B. The outer exposed regions were created by the stress field of the impacting stylus. Region C are adjacent TiN films that remain intact. The high chlorine content seen in Figure 3.19 appears to correspond to the B regions. The chlorine is associated either with the exposed substrate side of the interface or with the newly created surfaces of TiN particles that were originally part of the interface and were subsequently overturned or grain boundaries exposed by the scratch process.

One sample revealed copper in conjunction with chlorine. Review of the deposition history indicated that this particular sample was produced in the first deposition sequence after chamber repair and cleaning. The chamber had exposed copper components (wires) for electrical connections. It is believed that residual HCl reacted with the Co and vapor transported it to the steel prior to deposition. After one deposition, all components were covered with TiN (or a TiN-NH_4Cl compound) which passivated the surfaces. The copper wires components were not used after this point in time and were replaced with stainless steel.

Unfortunately, the spatial resolution (beam size of the order of 50 μm) of the SAM system prevented the direct examination of the exposed substrate. High-resolution scanning Auger microscopy studies are need to determine the exact distribution of chlorine exposed by the scratch removal process.

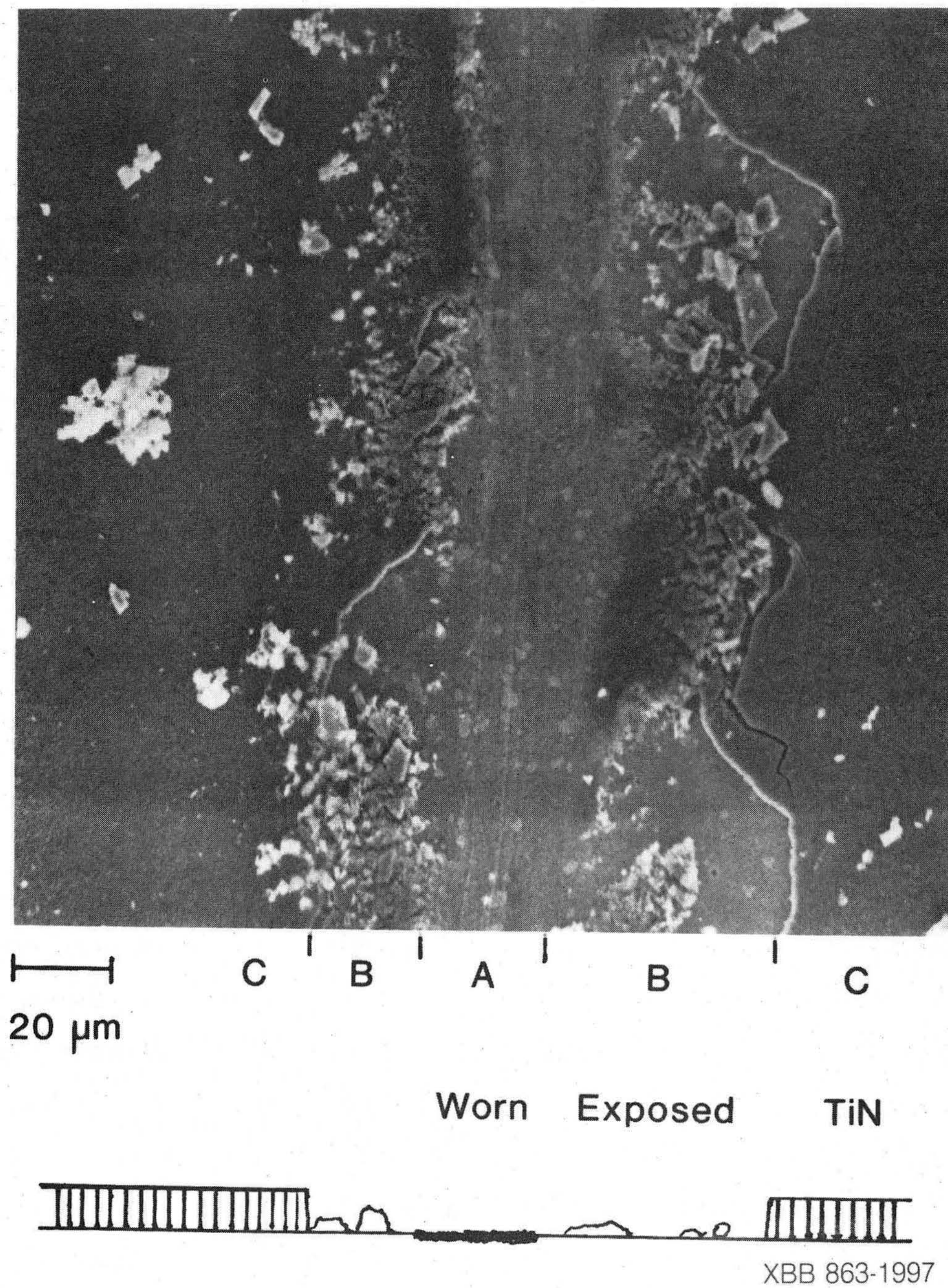

Figure 3.22: (Upper)SEM micrograph of a scratch created in UHV. The track has three distinct regions, shown cross sectionally in the sketch (lower). The center (region A) is a slightly worn or stylus-contacted area. Region B consists of film debris (some overturned) and exposed steel substrate, created by the stress field of the impacting stylus. Region C is the unaffected coating. The three regions correspond to the composition regimes indicated in Fig. 3.19.

3.2 Organometallic CVD

3.2.1 Deposition Conditions:

Experiments were performed to determine the suitability of titanium tetrakis (dimethylamide) [hereafter Ti amide] as a precursor for TiN formation by PACVD. The compound was synthesized from $TiCl_4$ (And:85). Early studies utilized the plasma apparatus (with no plasma) as a deposition chamber. Later studies utilized a glass chemical vapor transport (CVT) apparatus patterned after the design used by Sugiyama et. al. who reported success in making golden TiN films at temperatures as low as 200°C (Sug:75). A stainless steel version, evacuated by a turbomolecular pump, was later used. A variety of conditions were explored: deposition temperature, 200 to 800°C; Ti amide bath temperature, 40°C to 80°C; carrier gases, Ar, He, and N_2; chamber pressure, 0.1 to 760 torr.

3.2.2 Results:

The material produced from titanium dimethylamide decomposition was one of two forms: dense oxides or carbonitride powders. The oxides were produced in studies with the plasma deposition chamber under pressure conditions at which $TiCl_4$ and NH_3 produced TiN. The typical microstructure is shown in Figure 3.23 and the representative AES spectrum is shown in Figure 3.24. Oxides were also formed in the CVT chambers if either air leaks or residual water were present.

If the CVT chambers were properly baked, an agglomerated powder (or porous nodular coating) was formed indicating that gas phase nucleation had occurred, as shown in Figure 3.25. The AES spectrum both carbidic and graphitic carbon, with titanium, nitrogen, and oxygen as shown in Figure 3.21. Because of the porous microstructure, it was impossible to determine if the graphitic carbon and the oxygen were inherent to the film or absorbed surface species. These results highlight the general difficulty with titanium organometallics: 1) They are extremely

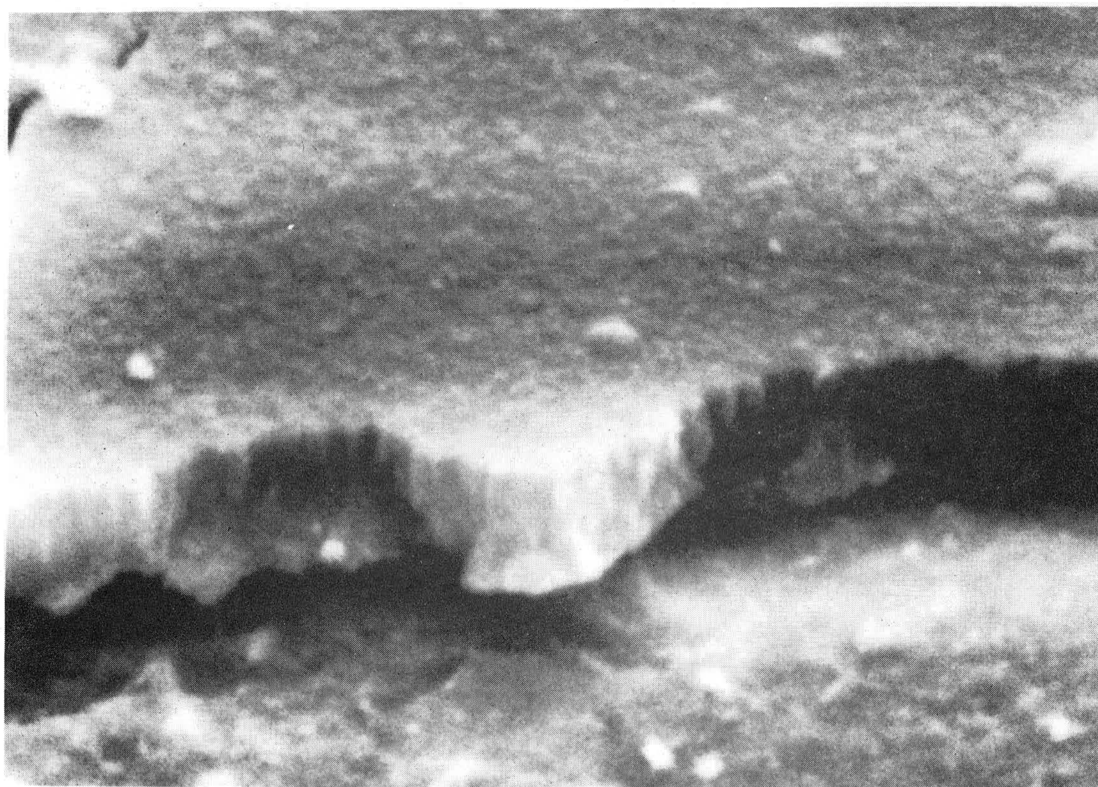

2 μm.

XBB 870-9261

Figure 3.23: SEM micrograph of a film formed by Ti-amide decomposition in the plasma deposition chamber.

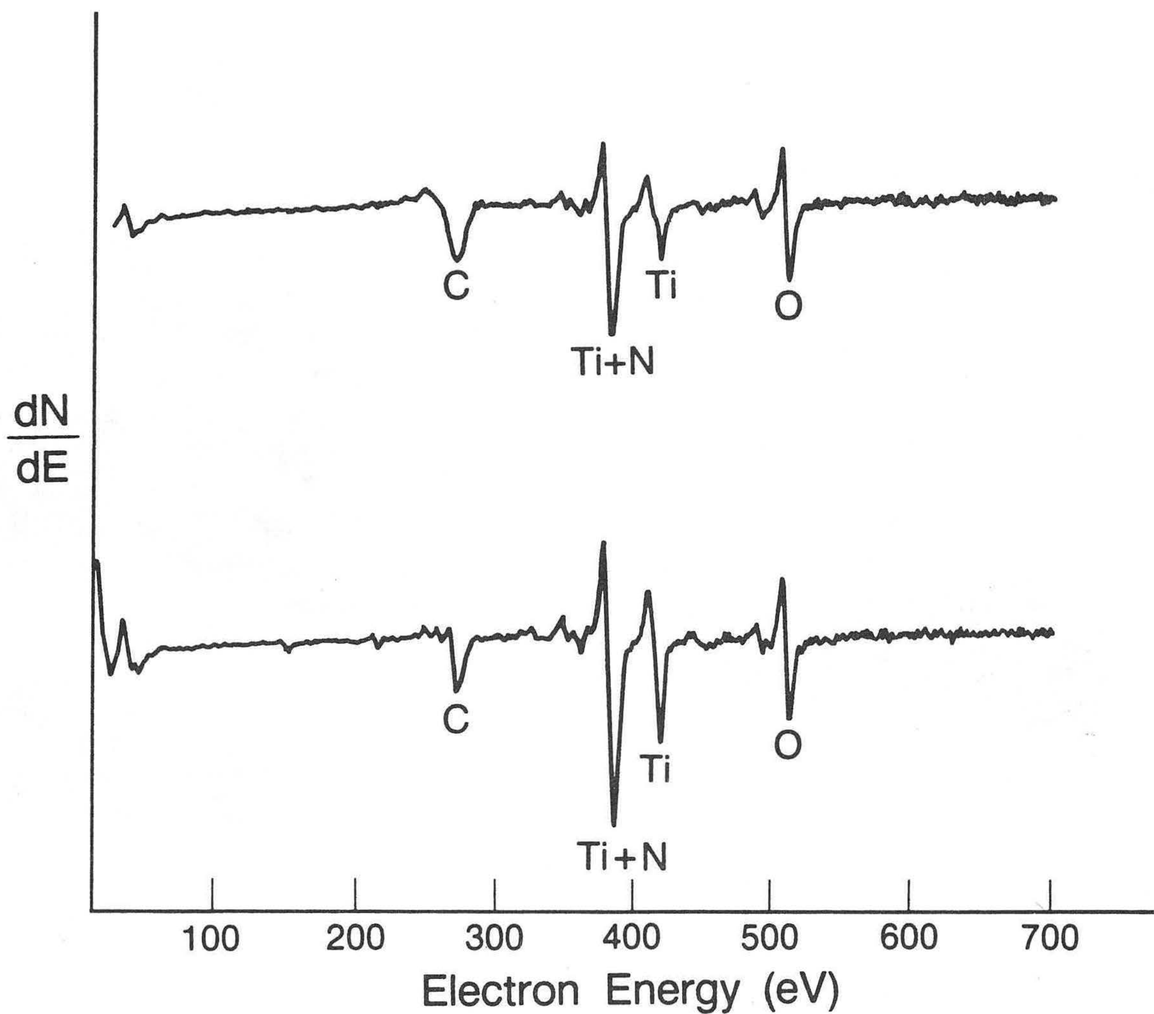

Figure 3.24: AES spectra of the film shown in the previous figure before (top) and after (bottom) a five minute sputter. Significant oxygen and graphitic carbon contents are observed.

XBB 860-8277

Figure 3.25: SEM micrograph of a film formed by Ti-amide decomposition in the turbomolecular-backed CVT chamber. The microstructure is indicative of gas phase nucleation.

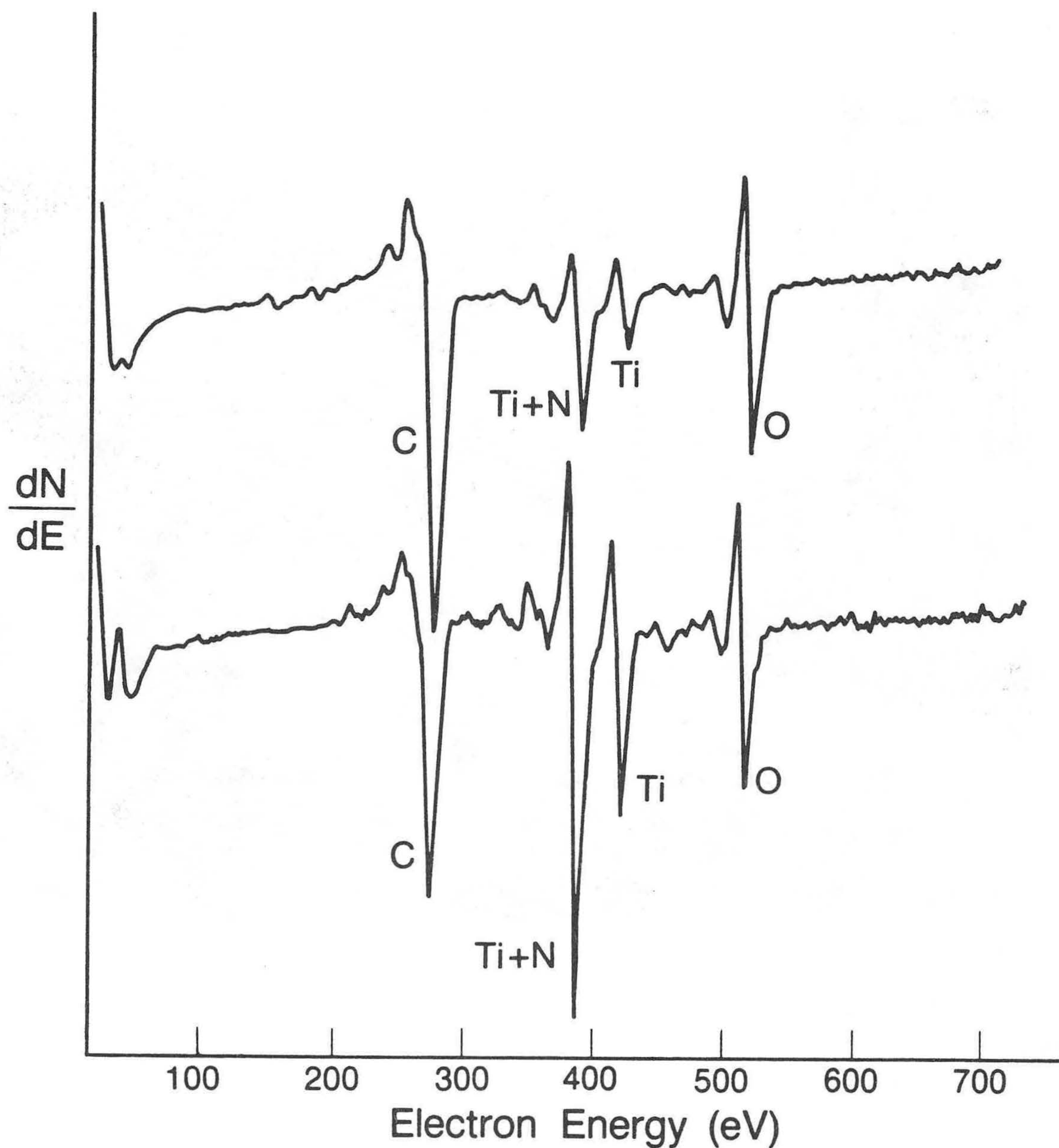

Figure 3.26: AES spectra of the nodular film before (top) and after (bottom) a fifteen minute sputter. Significant amounts of graphitic carbon and oxygen are present. However it is impossible to separate the signal from the sputtered surface from that of the shadowed pores of the powder.

sensitive to water and oxygen; 2) The compound vapor pressures are low which necessitates heating of the feed line; 3) The compounds are very reactive and can easily decompose during transport.

3.3 Plasma Deposition using $TiCl_4$, N_2, and H_2.

3.3.1 Deposition Conditions:

The PACVD TiN films produced on M2 steel were prepared with the IPC apparatus. In this study, the substrate temperature, H_2/N_2 gas ratio, argon use r.f. power, and substrate bias and substrate pretreatment were varied. The $TiCl_4$ flow rate was held constant at 0.21 mmol min^{-1} during the experiment. Total pressure was one Torr. Substrate temperature ranged from 340°C to 500°C, H_2/N_2 ratio varied from 0.7 to 4.5, power ranged from zero to 200 W, and applied bias from -250 V to 0 V (both grounded and floating conditions were tried). Two classes of films were prepared: 1) thick coatings (2-10μm), used to correlate bulk physical and mechanical properties, 2) thin films (deposition times: 5, 15, 30, 60, 120, 300, and 600 seconds), used to elucidate interface composition and film nucleation. In almost all cases, the M2 substrates, previously cleaned in acetone and ethanol ultrasonic baths, were placed on the lower electrode and heated to the desired temperature. N_2 gas was allowed to flow for five minutes, followed by H_2 (bringing P_{TOT} to 1 torr) for five more minutes. An r.f. plasma was then ignited and $TiCl_4$ was added after five minutes. In some cases, the plasma pretreatment was extended to 15 minutes. Alternatively, the entire pretreatment was shortened to less than two minutes. It was not possible to start the gas flow (in a stable condition) and ignite the plasma instantly to avoid this pretreatment. Some studies of oxygen pretreatment were also performed.

3.3.2 Film structure and composition

The properties of TiN coatings deposited on M2 steel were extensively investigated at substrate temperatures of 500°C and 400°C without an applied bias. SEM indicated that the films grown at 500°C grew in a columnar Zone 2 structure as shown in Figure 3.27 while the films deposited at 400°C grew in a fibrous Zone T structure (large 'grains' with partially curved tops having a poorly defined, fibrous internal morphology), shown in Figure 3.28. In contrast to the poorly adherent NH_3-based TiN coatings reported previously (Hil:86), film delamination did not readily occur around the Rockwell indentation in the Zone 2 films (Figure 3.29), though some film delamination occurred with the Zone T films. Closer investigation of the Zone 2 films shows that fracture occured within the coating and not at the interface. (Figures 3.30-3.31). The average grain diameter of the Zone 2 structure was 2500Å. The diameter of the zone T structures was 2 to 7μm while the internal fiber diameters were 600 to 3000 Å. In addition, XRD showed that the films had strong (200) preferred orientation, as shown in Figure 3.32. For Zone 2 films only the (200) and (400) peaks were observed, these peaks were sharp and in contrast to the broader (200) peaks observed in the zone T films. The zone T films sometimes had a small, broad (111) peak present, as shown in Figure 3.33. In some instances, the Zone 2 structures had nodules (Figure 3.34), which appeared related to the Zone T structures. These structures have been reported in the literature and are attributed to an energetic nucleation site (Tho:77). The source of these nodules was not isolated due to infrequent occurence. These nodules appear to be detrimental because they detach when a crack runs along them (Figure 3.35). Their elevation makes them bright in an SEM. Around a Rockwell indentation, these nodular highlight cracks running along the directions of maximum substrate shear, as shown in Figure 3.35 (Nim:862).

AES revealed that the $(Ti+N)_{387eV}$:Ti_{418eV} ratio of the films following sputtering ranged between 2.1 and 2.3 under all unbiased deposition conditions at 400°C

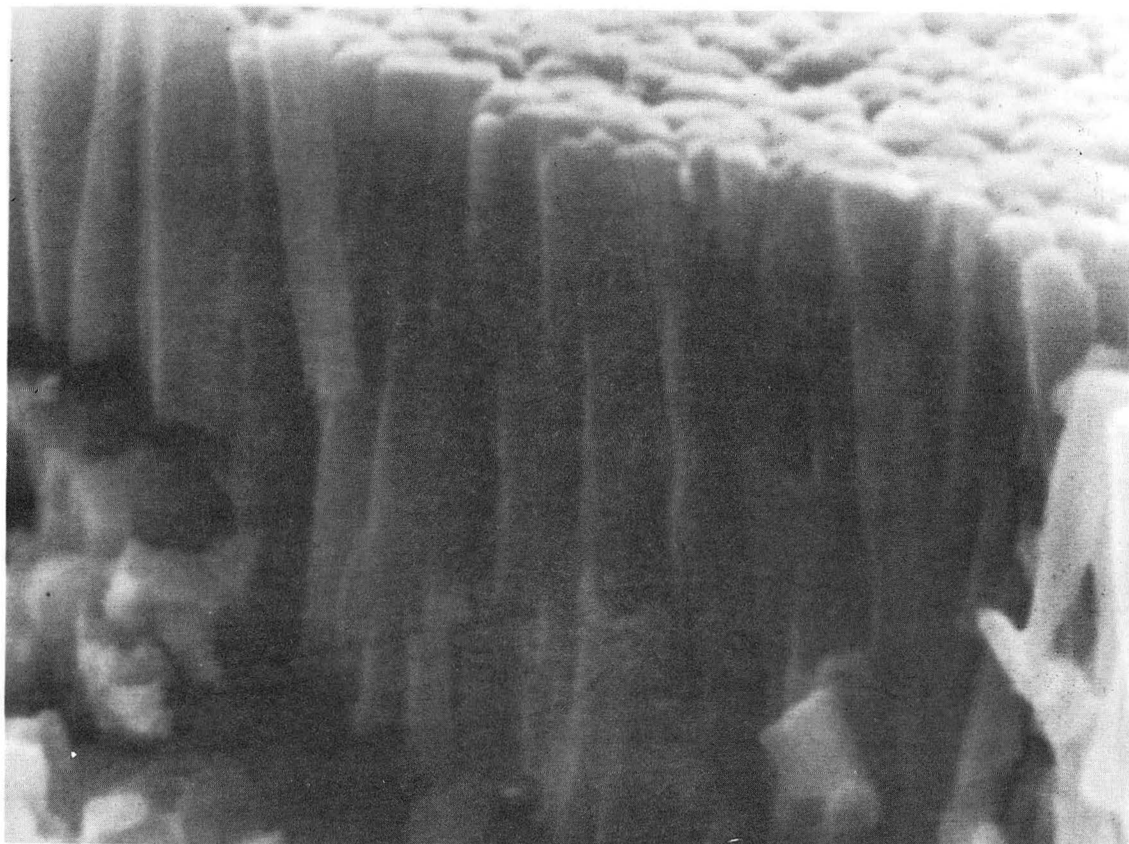

2 μm.

XBB 870-9269

Figure 3.27: SEM micrograph showing the zone 2 morphology found in TiN films formed from $TiCl_4$, H_2 and N_2 at 500°C.

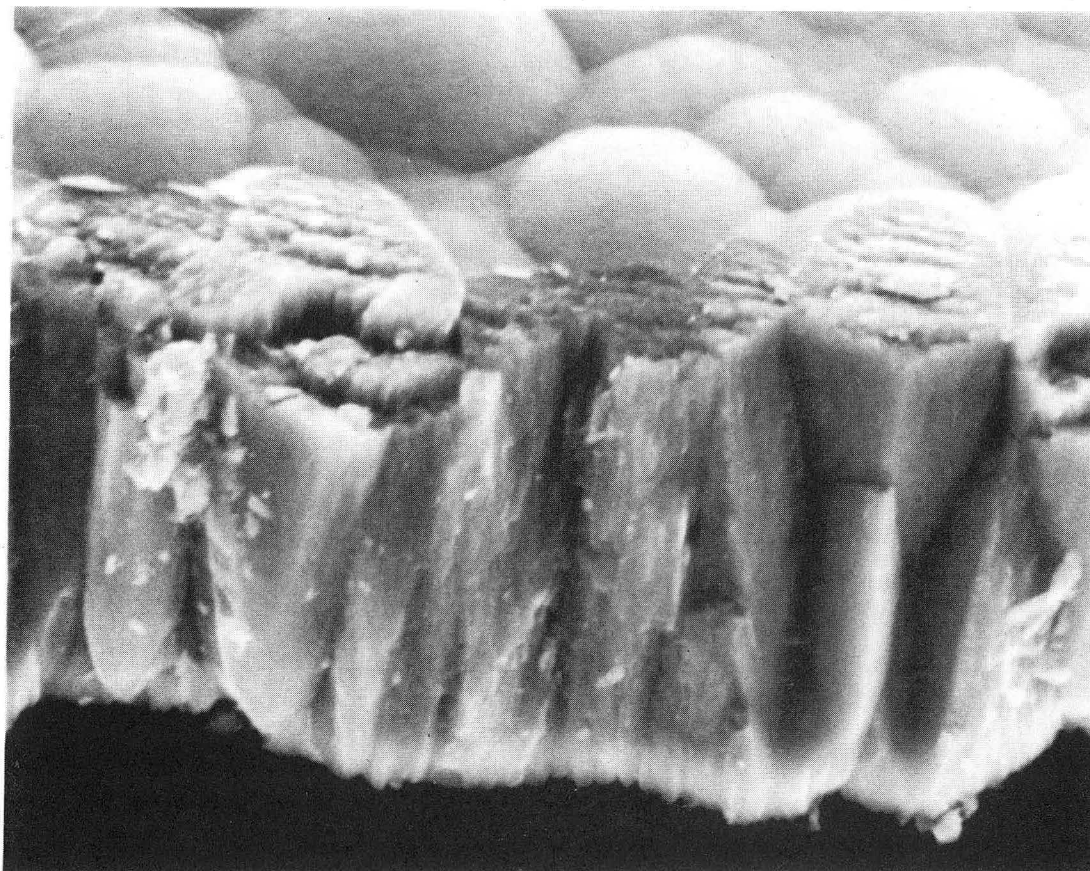

5 μm.

XBB 874-3277

Figure 3.28: SEM micrograph showing the zone T morphology found in TiN films formed from $TiCl_4$, H_2 and N_2 at 400°C.

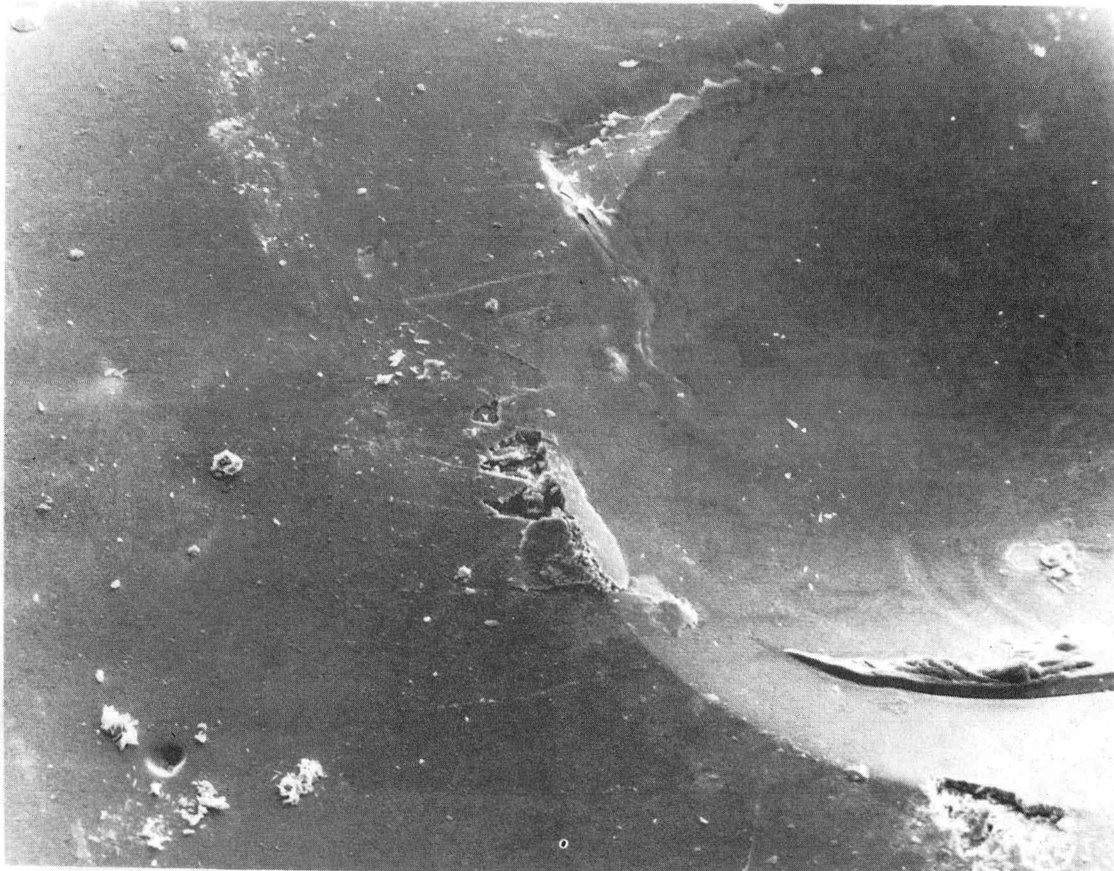

60 μm

XBB 860-8281

Figure 3.29: SEM micrograph of a Rockwell C hardness indentation on a $TiCl_4$-H_2-N_2 based film. Unlike the ammonia based film with zone 2 morphology, extensive delamination is not seen.

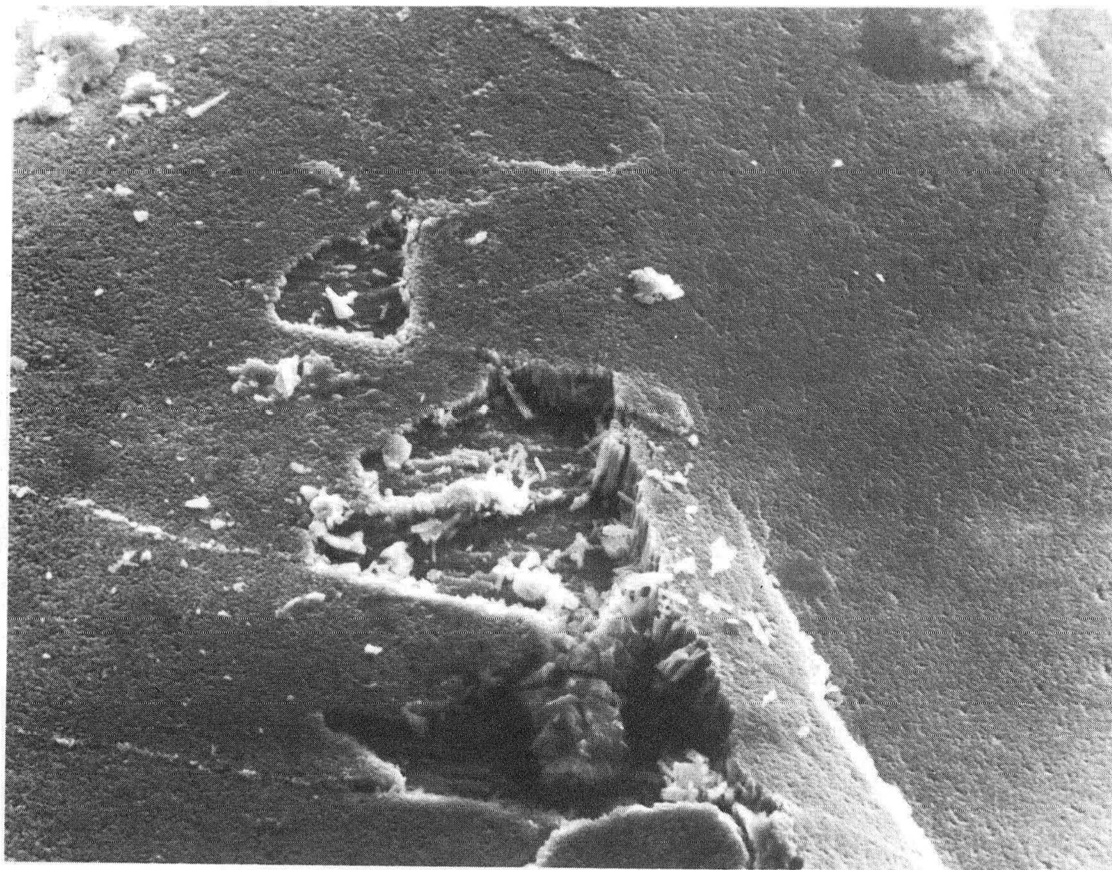

20 μm

XBB 860-8271

Figure 3.30: Close up of the previous micrograph.

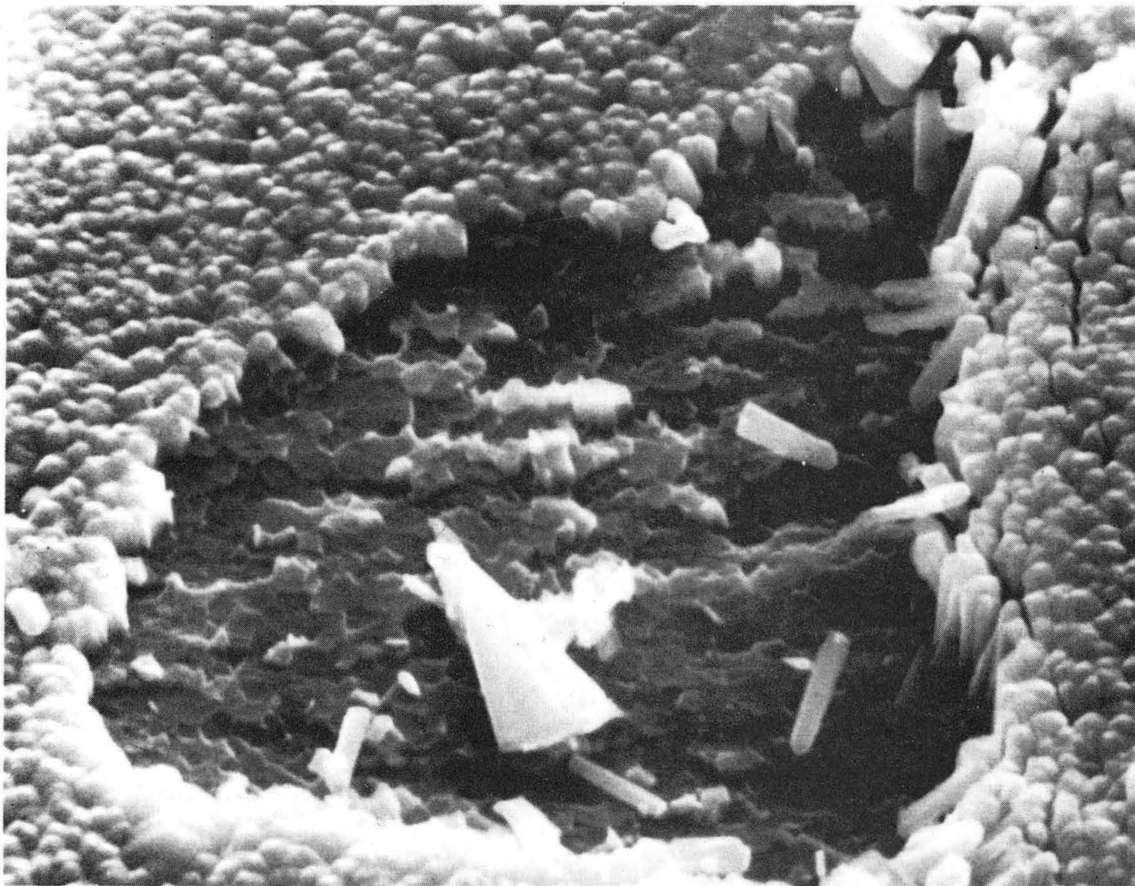

Figure 3.31: Closeup of the previous two micrographs, showing that fracture induced by Rockwell-impact is in the coating and not at the interface, unlike ammonia-based films or zone T H_2-N_2 based films formed at 400°C.

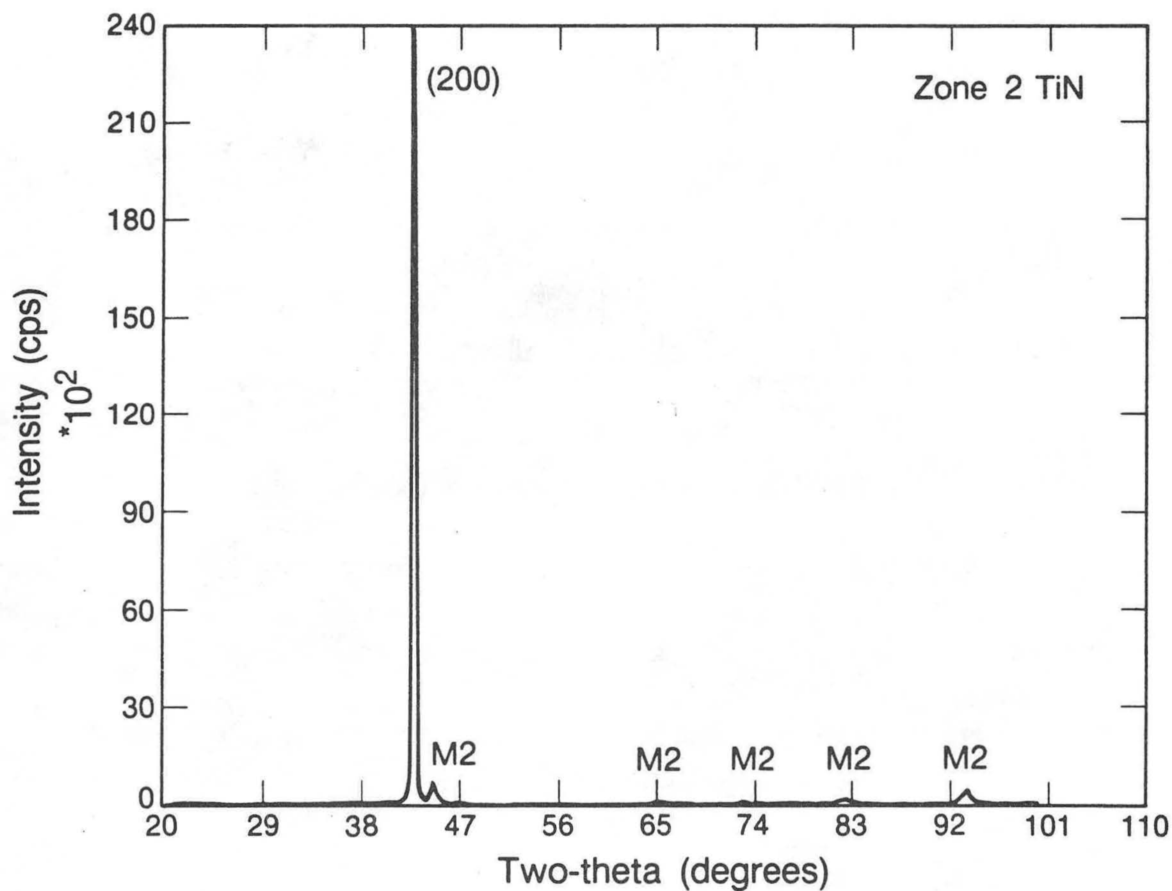

Figure 3.32: XRD intensity vs. 2θ for a TiN film deposited at 500°C from H_2, N_2, and $TiCl_4$. The film had a zone 2 morphology. A strong (200) preferred orientation is seen. The M2 steel stems from SAT wear tracks surfaces.

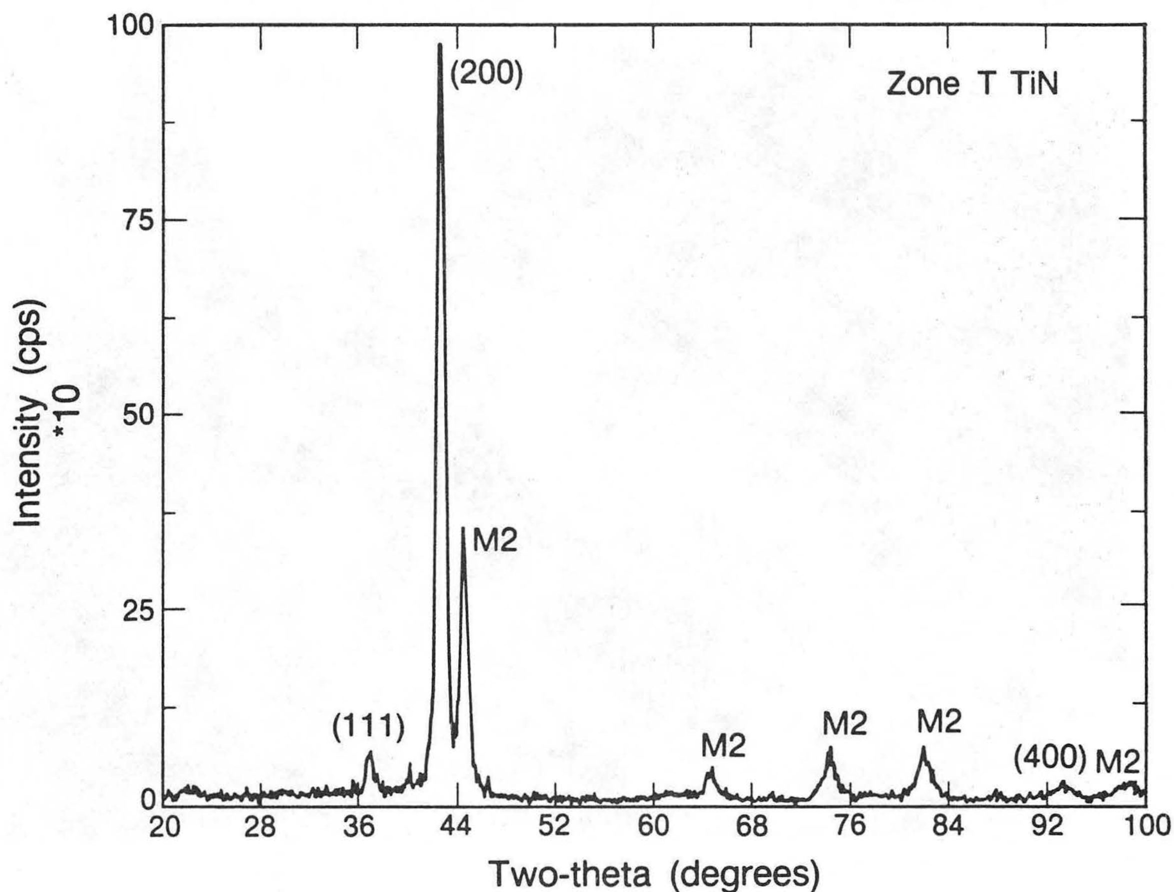

Figure 3.33: XRD intensity vs. 2θ for a TiN film deposited at 400°C from H_2, N_2 and $TiCl_4$. The film has a zone T morphology. A strong (200) preferred orientation is present, though there is a small (111) component. The M2 steel stems from SAT wear track surfaces.

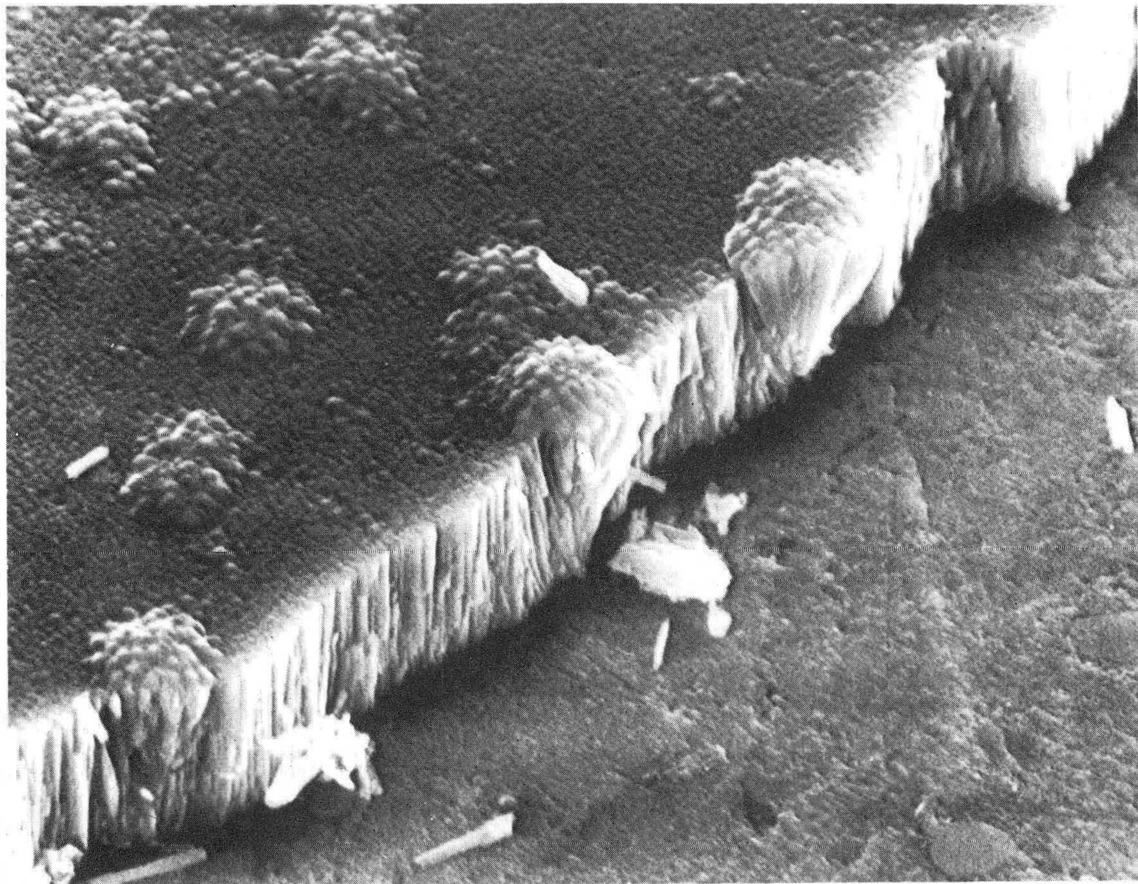

Figure 3.34: SEM micrograph of a nodular growth defect which occurred in some zone 2 films.

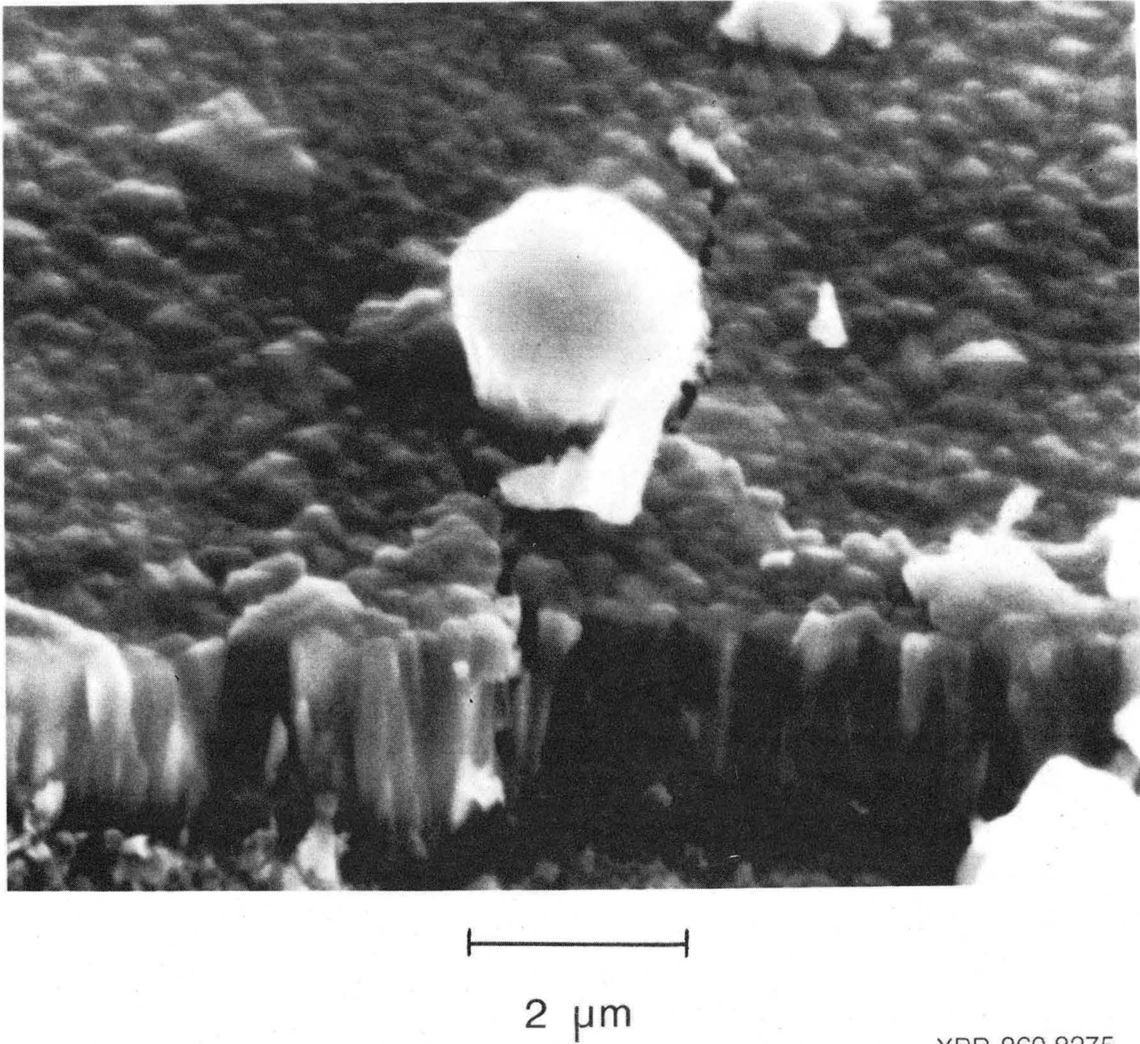

Figure 3.35: SEM micrograph of a nodular growth defect detached along an in-film grain boundary fracture, suggesting that these defects are a preferred weak point that would be detrimental in a protective film. The elevation of the detached defect makes it bright in the SEM.

Figure 3.36: SEM micrograph the Rockwell C hardness indentation of a film containing growth nodular defects. The elevated nodules highlight fracture that occurs along the directions of maximum shear stress that develop around the indentation during deformation.

and 500°C, suggesting that these films are stoichiometric or nearly stoichiometric. The Zone 2 films contained less than 2%Cl, while the Zone T films generally had 3 to 5%Cl. Carbon content in the films was less than 10 % and oxygen content was less than 3 %.

3.3.3 Mechanical Properties

Figure 3.37 shows the SAT critical load (L_C) values as a function of thickness for TiN films prepared at 400°C and 500°C with no applied substrate bias. Several different deposition conditions are plotted together. Also plotted, for comparison, is a linear summary of values obtained by Sproul (Spr:83) for sputtered TiN on M2 steel and the L_C values found from the earlier study of PACVD-produced TiN formed from NH_3 and $TiCl_4$ (Section 3.1). The data indicates that PACVD-produced TiN from $TiCl_4$, N_2 and H_2 can be made as adherent as sputtered TiN. Critical load values were repeatable within 200 gm for a given sample. There was a significant amount of scatter as a function of thickness, which could not be correlated with deposition conditions or by changing the duration of H_2/N_2 plasma pretreatment. Failure in the Zone 2 films took the form of cracks emanating adjacent to the stylus track or by occasional chipping within the coating (Figures 3.38,3.39). Since the cracking was inclined along the *trailing* edge of the diamond, the failure mode appears to be a Burnett/Rickerby Type E (Tensile failure). The Zone T films failed by similar cracking or by periodic chipping, both within the coating and at the interface (Figures 3.40, 3.41). However, in this case cracking was inclined along the *leading* edge of the stylus, like that of a Burnett/Rickerby type B (Buckling failure). The appearance of chipping (Figure 3.41) is a Type C failure. These modes were unsuitable for interface composition analysis by the scratch removal technique (The resolution of our SAM system prevented the study of the chip failure mode). These failure modes indicate better substrate-film adhesion than the continuous delamination observed in NH_3-based films.

Rockwell C hardness tests indicated that the heating of the substrate during

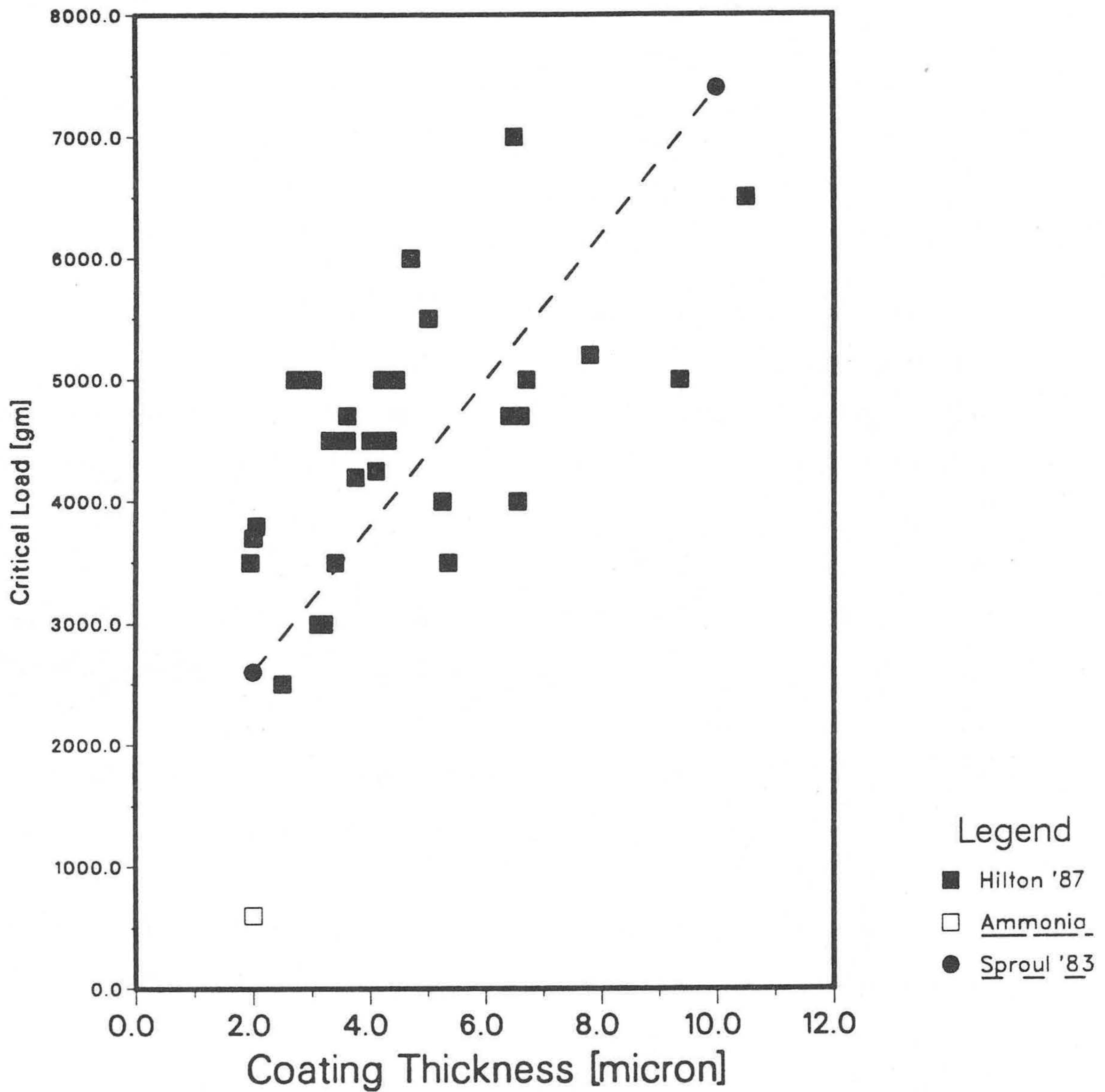

Figure 3.37: Scratch Adhesion Test Critical Loads (L_c) of TiN films on M2 steel as a function of film thickness produced by PACVD from $TiCl_4$, N_2, and H_2. A linear representation of data for sputtered TiN (Spr:83) and the value for NH_3-based PACVD TiN are also plotted for comparison. The data shows that PACVD-produced TiN can be as adherent as sputtered TiN.

Stylus Motion

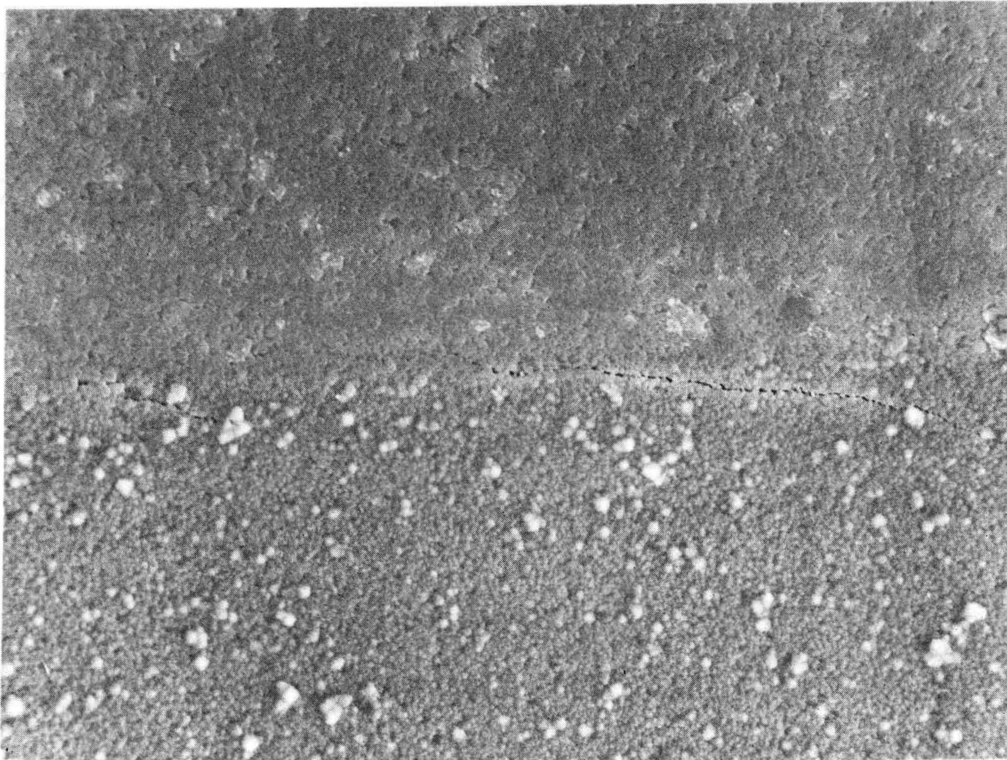

20 μm.

XBB 870-9257

Figure 3.38: SEM micrograph of cracking mode of SAT failure often observed in zone 2 films formed from H_2, N_2 and $TiCl_4$. The cracks oriented with the trailing edge of the diamond stylus, suggesting a Rickerby/Burnett type E tensile failure.

Stylus Motion

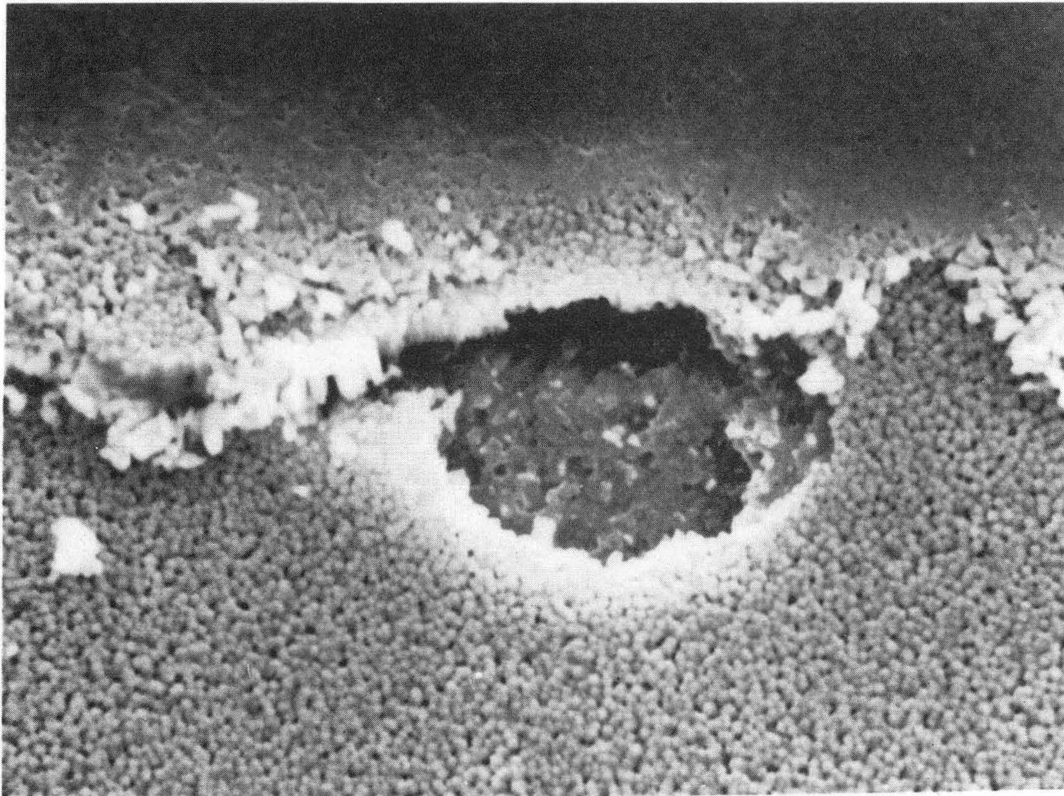

5 μm.

XBB 870-9258

Figure 3.39: SEM micrograph of a chipping mode of SAT failure occasionally observed in zone 2 films, formed from H_2, N_2 and $TiCl_4$, in addition to the cracking mode of the previous figures. The chipping occurs within the coating.

Stylus Motion

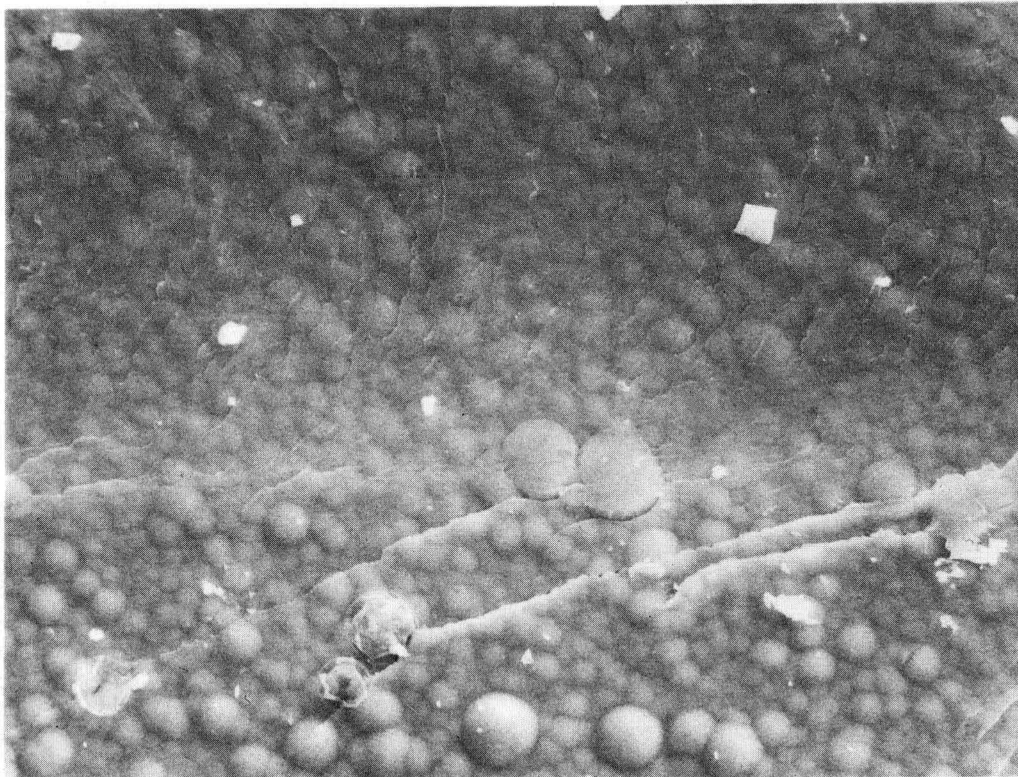

40 μm.

XBB 870-9255

Figure 3.40: SEM micrograph of a cracking mode of failure often observed in the zone T films formed from H_2, N_2, and $TiCl_4$. The crack orientation suggests a Rickerby/Burnett Type B buckling failure.

Stylus Motion

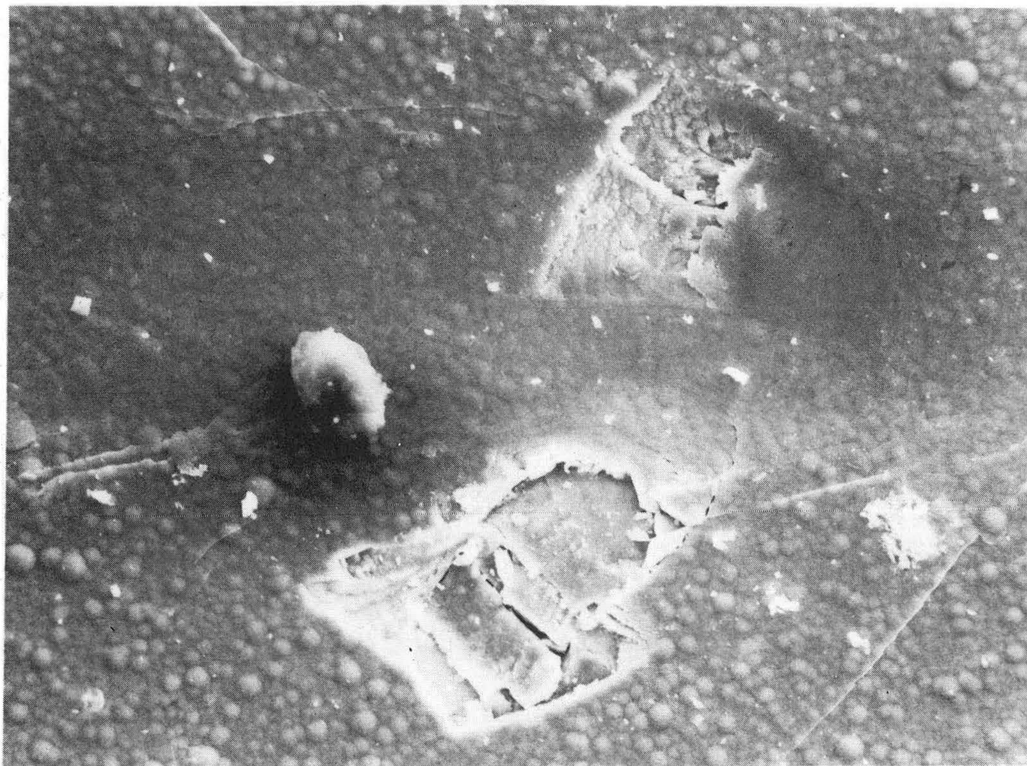

50 μm.

XBB 870-9256

Figure 3.41: SEM micrograph of a chipping mode of failure sometimes observed in zone T films formed from H_2, N_2 and $TiCl_4$. Chipping occurs with the coating and at the interface. The mode is a Rickerby/Burnett Type C buckling/spallation failure.

deposition did not degrade the M2 microstructure. The highest intended operating temperature was 500°C. Since the minimum temperature for softening of M2 steel is around 560°C to 590°C (Wil:75), the results indicate that the r.f. plasma did not impart substantial thermal energy to the substrate. Vickers microhardness (Hv) increased with film thickness. For a 10μm film, the Hv_{200} was 1520 kg/mm^2. This is lower than the bulk value (2000 kg/mm^2) and lower than that obtained for this thickness (2300 kg/mm^2) by Sproul (Spr:83).

3.3.4 Effect of Deposition Parameters

Deposition Temperature:

As in the ammonia study, film deposition temperature influenced chlorine incorporation into the films, with chlorine content increasing as temperature decreased, as shown in Figure 3.42. At 400°C and above, a constant $(Ti+N)_{387eV}:Ti_{418eV}$ ratio was observed. The morphology, as stated earlier, changed from zone 2 at 500°C to zone T at 400°C. Deposition temperatures below 340°C were not investigated.

Effect of H/N ratio:

Figure 3.43 shows that film growth rates decreased as H/N gas input ratio increased. Concurrently, resultant film chlorine content is seen to rise slightly with increasing H_2/N_2 ratio, as shown in Figure 3.44, though there is some scatter in the data. With no hydrogen, a thin titanium oxide was obtained. The O/Ti ratio determined from AES suggested that the material was the monoxide phase.

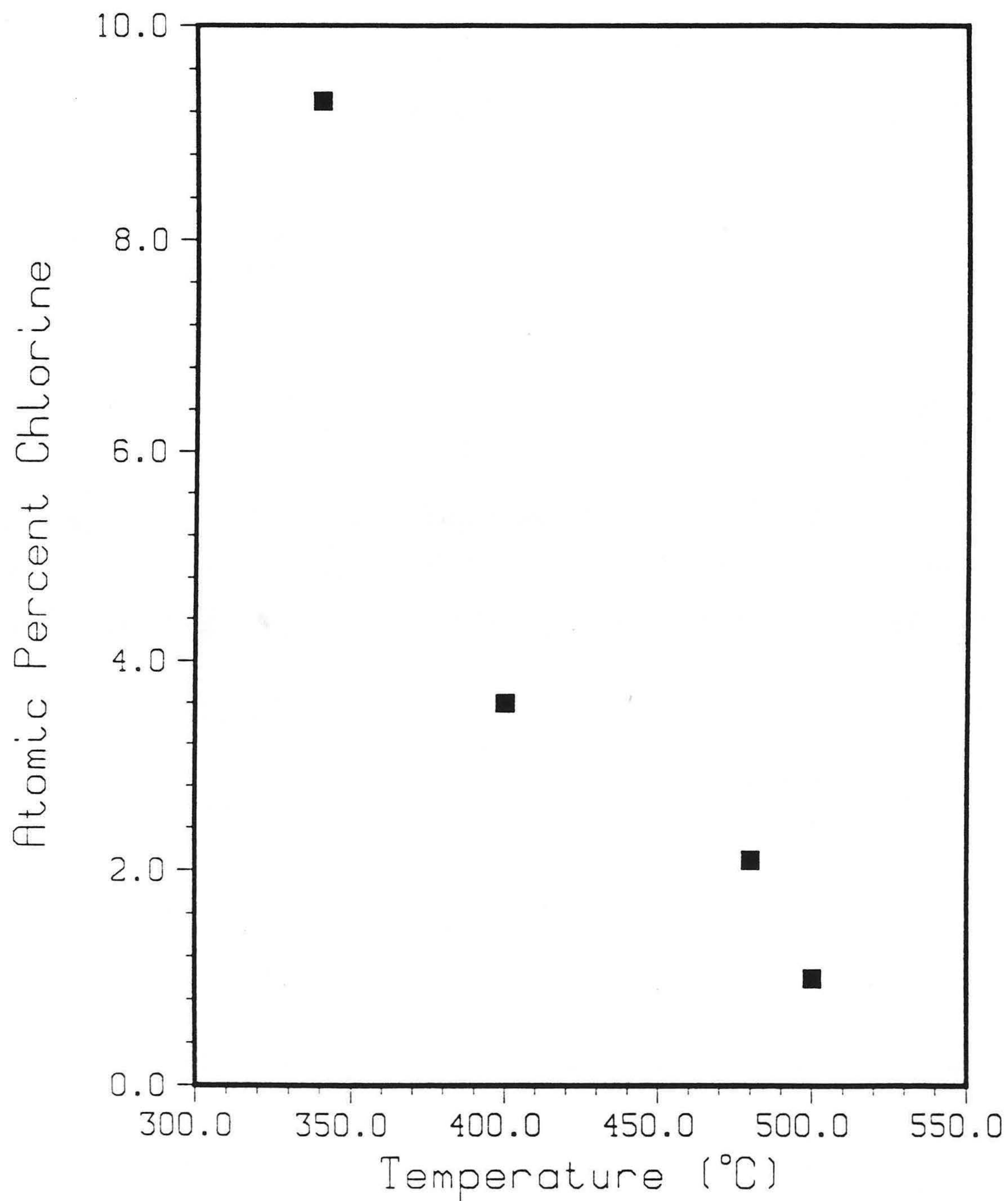

Figure 3.42: Film chlorine content determined by AES as a function of deposition temperature.

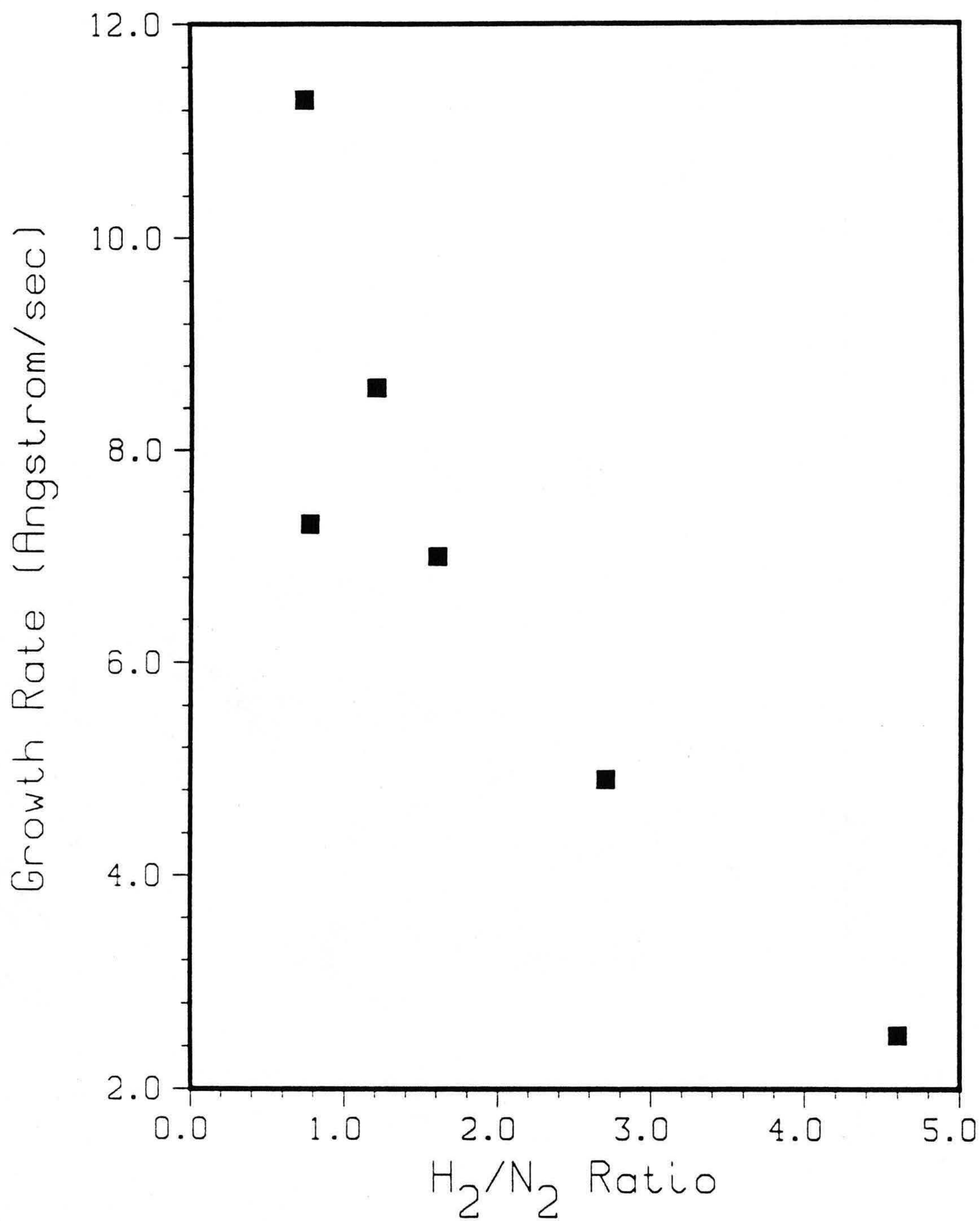

Figure 3.43: Film growth rate as a function of H_2/N_2 gas ratio.

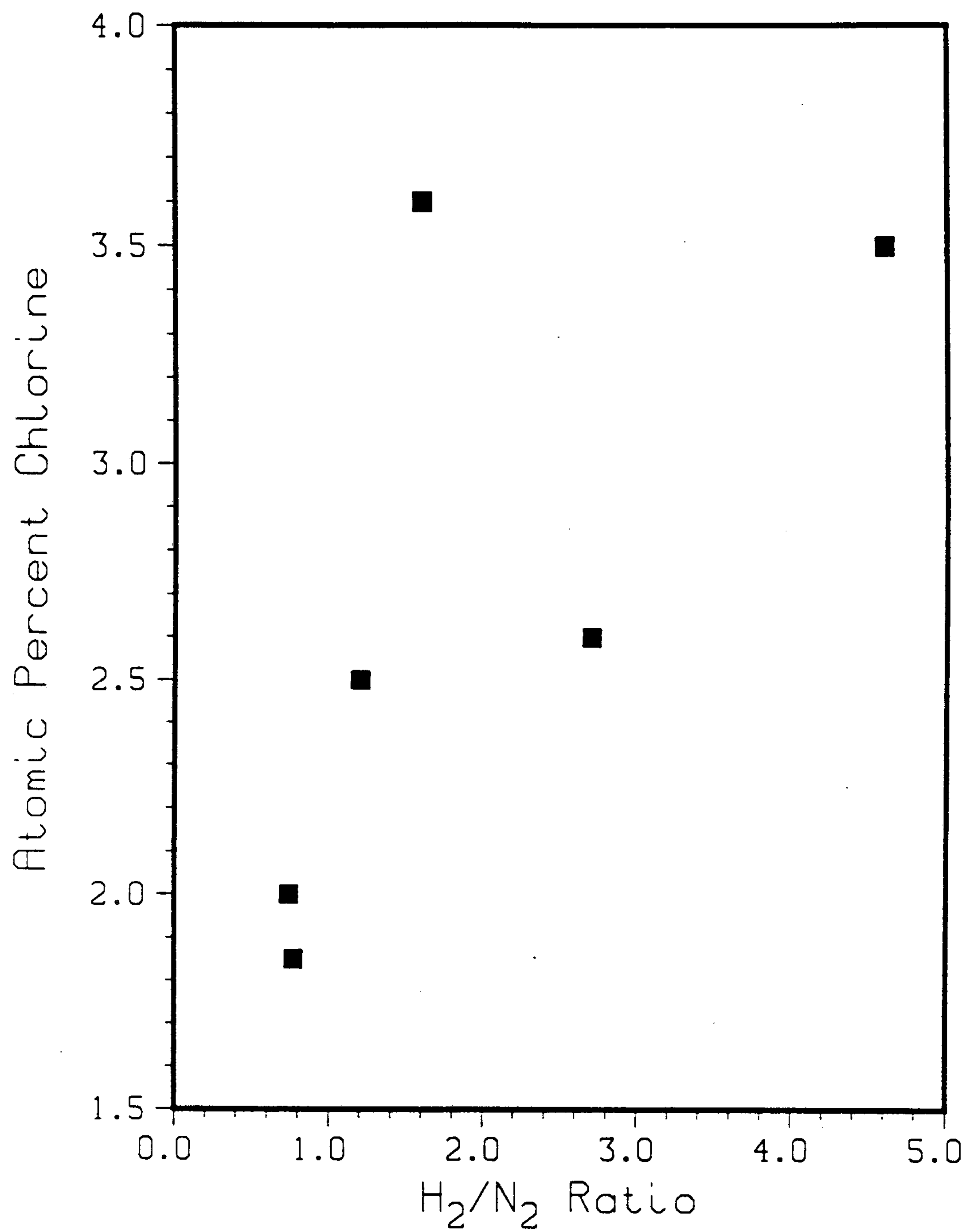

Figure 3.44: Film chlorine content determined by AES as a function of H_2/N_2 ratio.

Effect of Argon partial pressure:

Figure 3.45 shows that the presence of argon steadily diminished film growth rates. The argon acted as an inert dilutent, behavior which is in contrast to the NH_3-argon experiments, in which the latter gas enhanced growth rates. The argon had no systematic effect on bulk film composition.

Effect of Power:

In contrast to the ammonia studies, a plasma was essential for TiN film synthesis when hydrogen, nitrogen, and titanium tetrachloride were mixed at temperatures of 500°C (the highest temperature studied) and below. As shown in Figure 3.46, power could show an optimum an optimum behavior (growth rate would increase with power up to some value and then decline). The floating or grounded substrate did not differ, except at 200 watts, where the floating condition had a growth rate twice that of the grounded. AES did not reveal differences with changes in power.

Effect of dc biasing:

Growth rates decreased with increasing negative substrate biasing, as shown in Figure 3.47. Placing a negative bias on the opposite electrode had no effect. Studies of biasing above the magnitude of 250 volts were not successful because of arcing to the walls. Studies of thick films were limited to magnitudes upto -100 volts because the growth rates became exceptionally low. The morphology of the films did not change with biasing, though there appears to be some grain refinement (Figure 3.48) in the zone 2 films. The grain size in the zone T films could not be adequately resolved. Composition relative to unbiased films was not affected by biasing. Vickers hardness testing of a ten micron zone T film

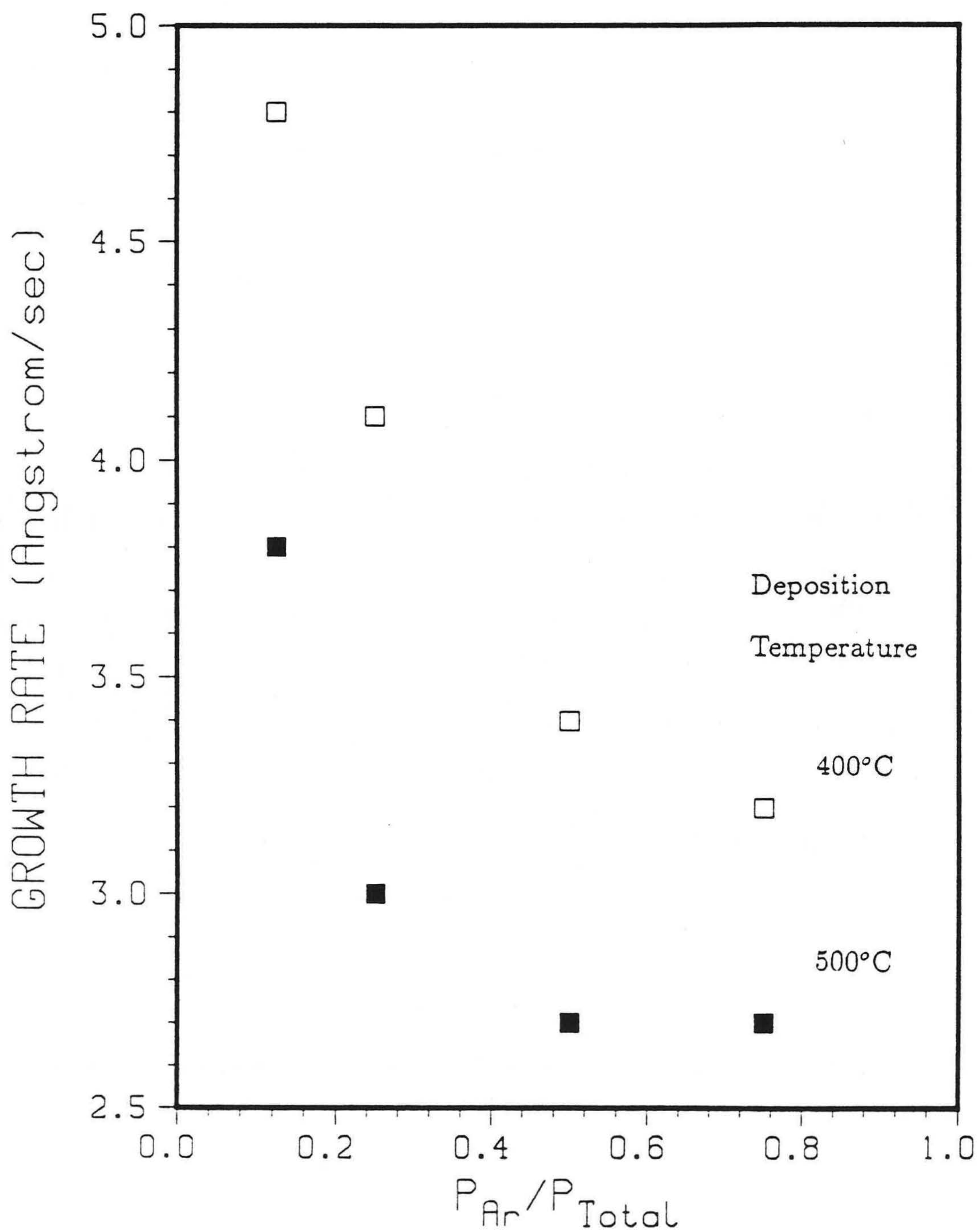

Figure 3.45: Film growth rate vs. partial pressure of argon vs. P_{Total} (1 Torr) for films formed from $TiCl_4$, H_2, N_2 and Ar. Unlike the Ar-NH_3 experiments, Argon did not enhance film growth.

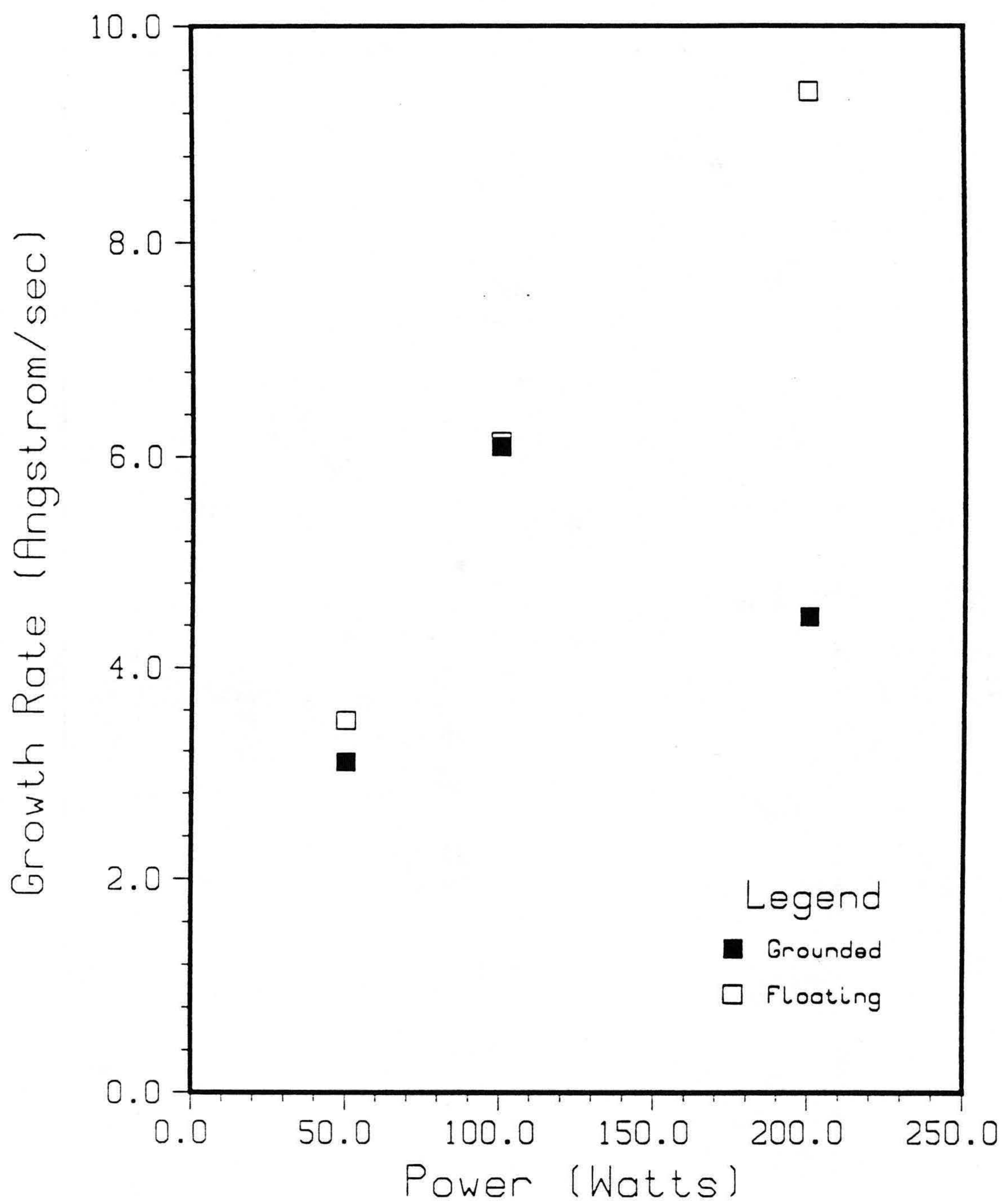

Figure 3.46: Growth rate as a function of power for TiN films formed from H_2, N_2, and $TiCl_4$, on grounded or floating substrates.

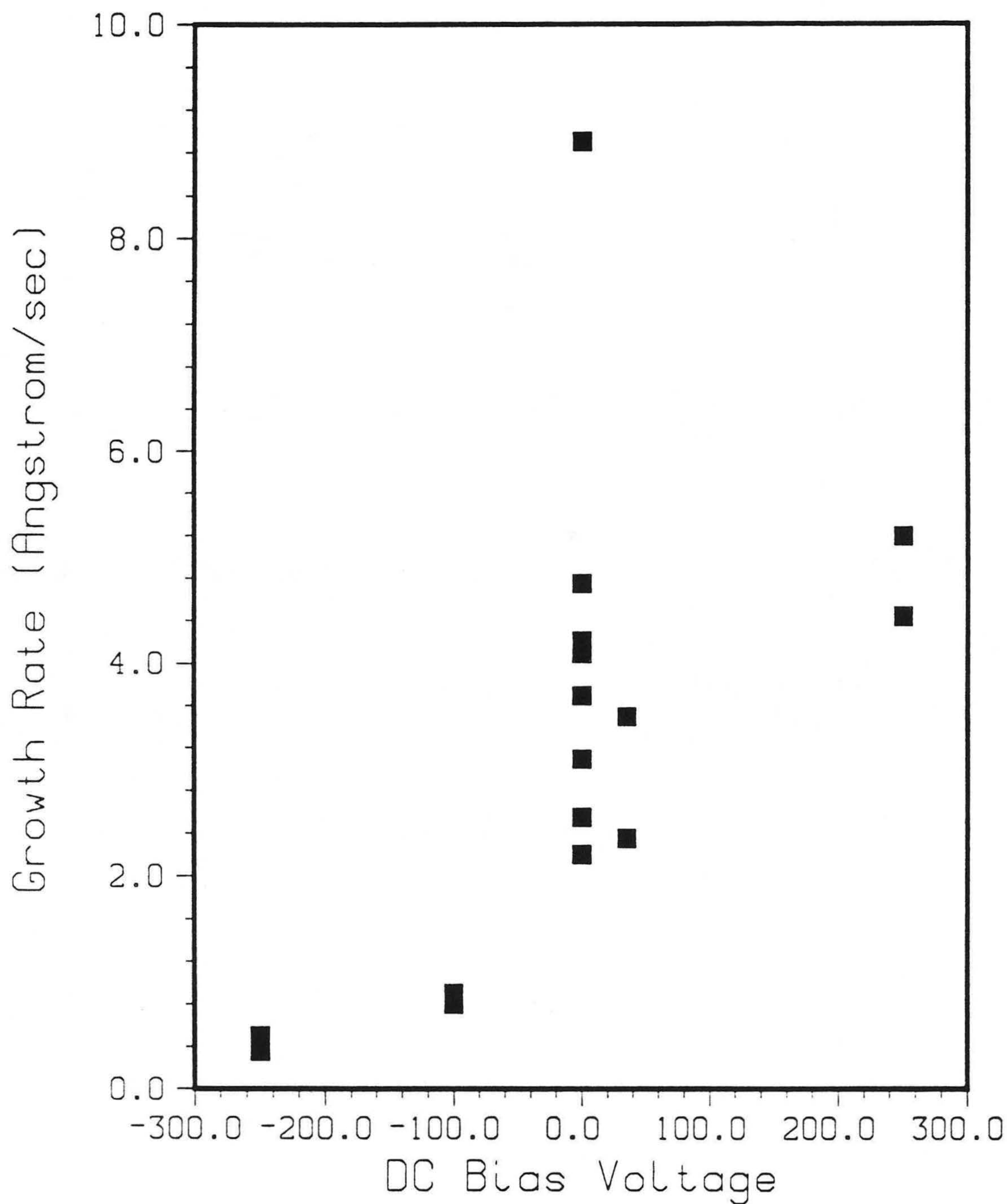

Figure 3.47: Growth rate as a function of biasing for films formed from H_2, N_2, and $TiCl_4$. The positive value of voltage represents a negative voltage on the r.f. electrode.

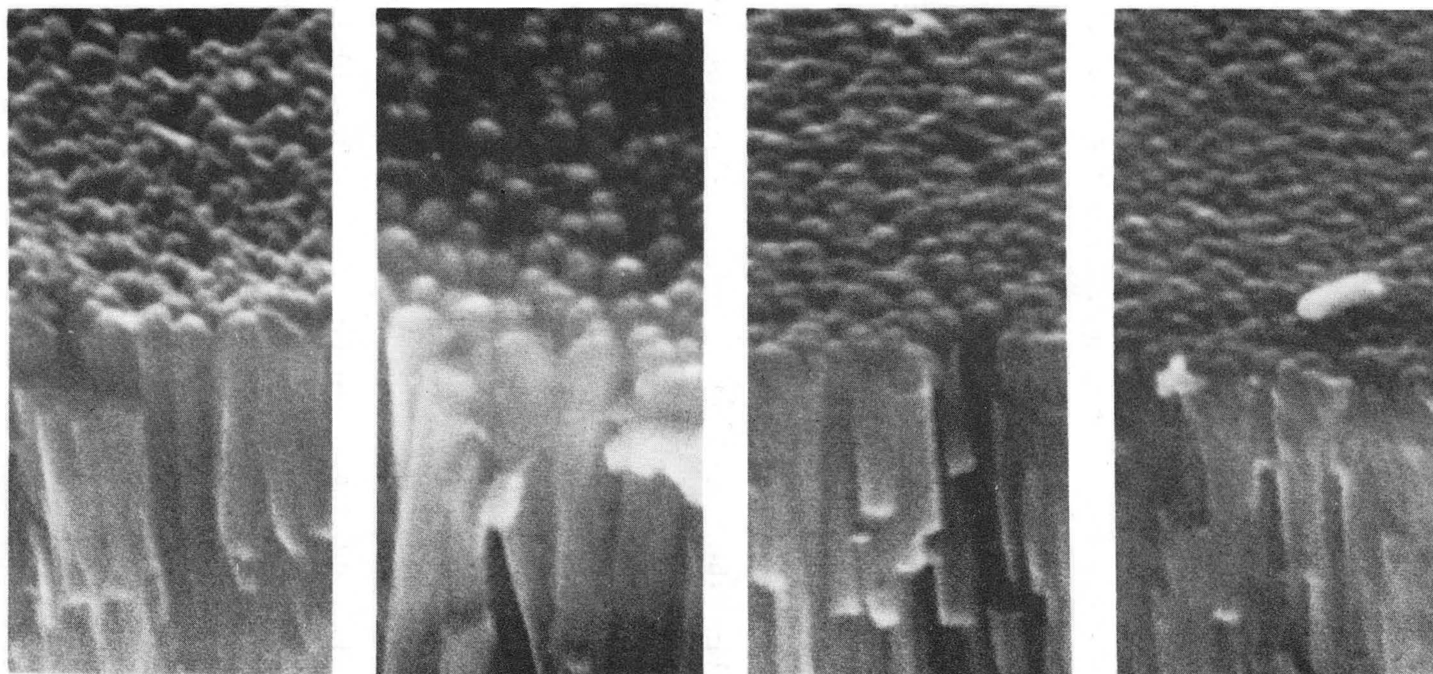

Grounded NH_3 | Grounded H_2-N_2 | -50 Volts H_2-N_2 | -100 Volts H_2-N_2

2 μm.

XBB 870-9271

Figure 3.48: SEM micrographs of TiN film formed with grounded substrates or negative d.c. bias. The micrographs were taken under identical microscope conditions.

grown during -100 volt biasing revealed a H_{V100} of 1623 kg/mm^2 and a H_{V200} of 1322 kg/mm^2. An eight micron zone 2 film had values of 1182 and 1164 kg/mm^2 respectively. These values are well below the bulk hardness of TiN (2000 kg/mm^2) or reported values of sputtered TiN (2400 kg/mm^2).

3.3.5 Thin Films–Interfacial Properties and Nucleation

The films prepared in this study had an average growth rate (based on measurements of thick films prepared with the same deposition conditions) of 3-4 $\AA$ sec^{-1}. All samples had surface contamination from transport in air in the form of carbon and excess oxygen which could be removed by 60 to 90 sec of sputtering. Figure 3.49 shows two representative spectra of samples with deposition times of (a) 30 seconds and (b) 300 seconds. Both spectra indicate that the TiN-M2 interface is fairly sharp (<60 Åwide); Chlorine accumulation was not seen. There is evidence of nitrogen penetration into the steel. A small nitrogen peak was also seen in a separate investigation of M2 samples heated in the plasma chamber for five minutes, (therefore tracing normal predeposition sequence.) The N_{383eV}:Fe_{703eV} ratio was of the order of .05 to 0.1. However significantly larger amounts of chlorine and oxygen were present. Making quantitative estimates is difficult, since the latter impurity probably was a result of sample transport in air. The chlorine surface concentration clearly diminishes in an active H_2/N_2 plasma, as the thin film sputtering results do not show chlorine accumulation at the film-substrate interface. The constant presence of iron in the initial stages of sputtering of the 30 second sample suggests that TiN islands or nuclei on M2 steel are present in the early stages of growth. Investigation of the films with SEM, prior to sputtering, supports this idea. Distinct island-like structures are observed at short deposition times (Figure 3.50, 30 sec), while these nuclei have coalesced at longer deposition times (Figure 3.51, 300 sec). These nuclei have a center to center distance on the order of the grain size of the Zone 2 films.

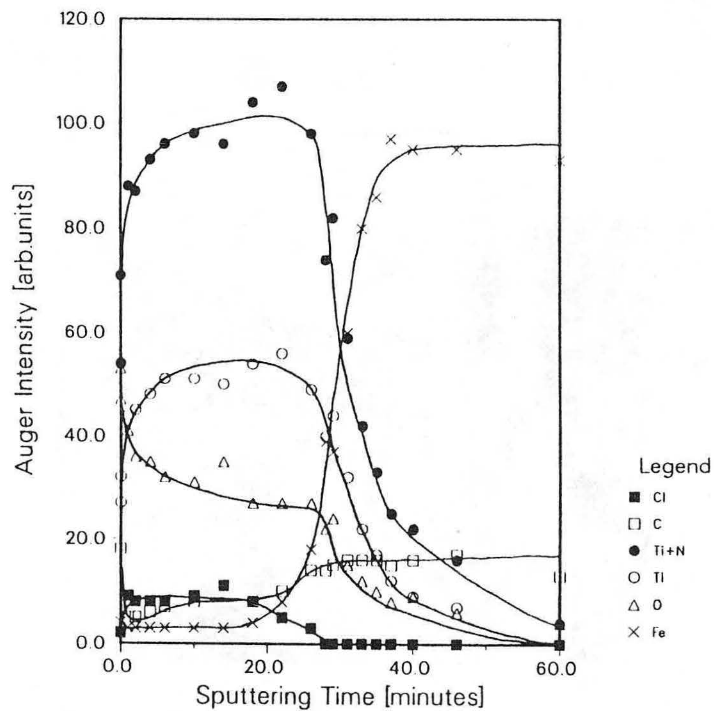

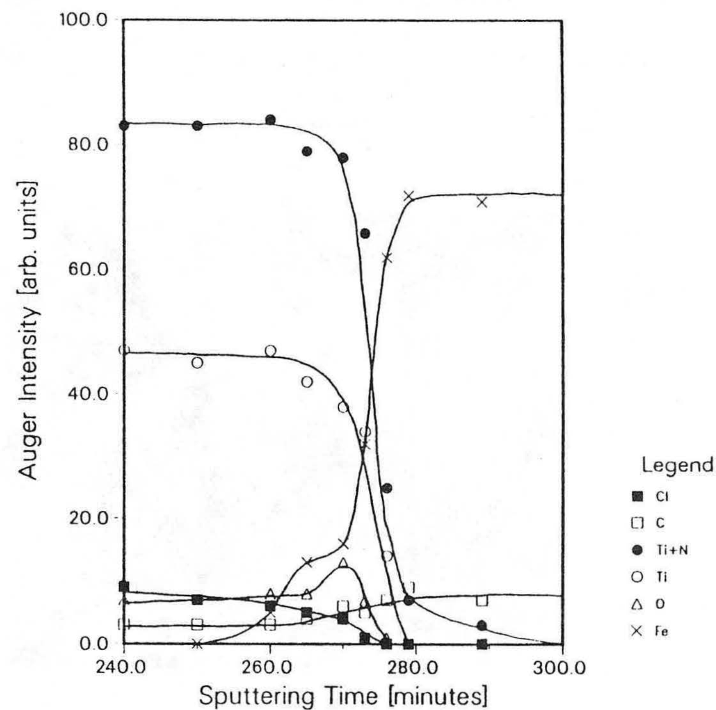

Figure 3.49: Typical AES sputter depth profiles for TiN films with deposition times of: a) 30 seconds and b) 300 seconds. The sputter rate was 3 Åmin−1. The initial and constant presence of iron in the early stages of sputtering of the 30 second sample suggests that film deposition starts by the nucleation of TiN islands on the steel surface.

Deposition Time:

30 Seconds

300 Seconds

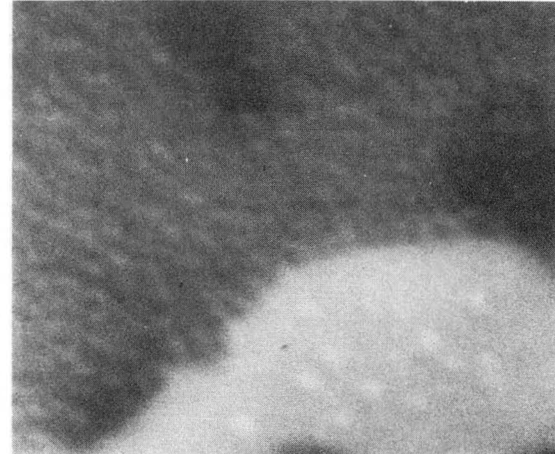

0.8 μm.

0.8 μm.

XBB 870-9270

Figure 3.50: SEM Micrographs of the surface of TiN films on M2 steel formed with deposition times of: a) 30 seconds and b) 300 seconds. The micrographs were taken prior to the sputter depth profiling represented in the previous figure. Distinct island-like features are observed at the early stages of growth which fuse as deposition time progresses.

3.3.6 Effect of Oxygen Pretreatment:

Studies were undertaken to actively influence the interface composition by substrate pretreatment to elucidate if elemental doping (with O, C, or B) would affect adhesion. Oxygen was the first dopant studied. Three conditions were executed: A) One torr exposure to an oxygen plasma for ten minutes, followed by a five minute evacuation, and then a five minute H_2/N_2 plasma; B) a two minute oxygen plasma followed by a five minute evacuation and a five minute H_2/N_2 plasma; C) a ten minute oxygen plasma, followed by a five minute nitrogen plasma, and a five minute H_2/N_2 plasma. In the third case, the plasma was never extinguished– the new gases were introduced concurrently with the decrease of the previous gas. The films were then grown under otherwise standard conditions.

These films had extremely poor adhesion, tending to disintegrate easily after synthesis. Examination by SEM revealed a morphology change relative to unpretreated films. The films with long oxygen exposure had nodular morphologies typical of gas phase nucleation (similar to the organometallic results in section 3.2), while the shorter oxygen exposure film had a hybrid zone 1-nodular morphology, as shown in Figures 3.51-3.53.

The results suggest that oxygen was present in the gas phase after pretreatment, which promoted gas phase nucleation. Oxygen may have been adsorbed by the walls during pretreatment and then subsequently desorbed during the initial stages of film formation. The films did not survive long enough to be examined by AES. This result highlights the fact that composition control during film growth can be complex. Experiments with methane will be discussed in section 3.4. Experiments with boron were not attempted because it was learned that BCl_3 (which forms readily when B is in the presence of HCl) is an excellent plasma-assisted etchant of TiN (Hom:87).

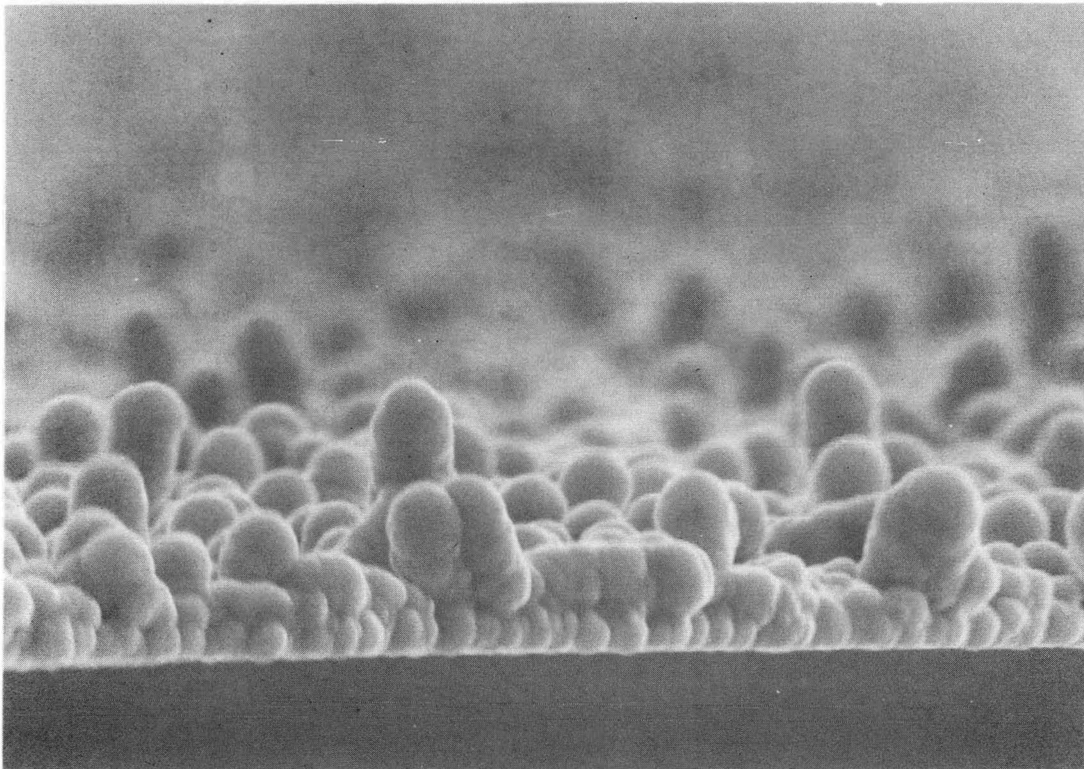

20 μm.

XBB 870-9263

Figure 3.51: SEM micrograph showing the nodular morphology, indicative of gas phase nucleation, that developed when a film had the following substrate pretreatment: 0_2 plasma exposure (1 torr) for 10 minutes; 5 minute evacuation; 5 minute H_2/N_2 plasma (1 torr).

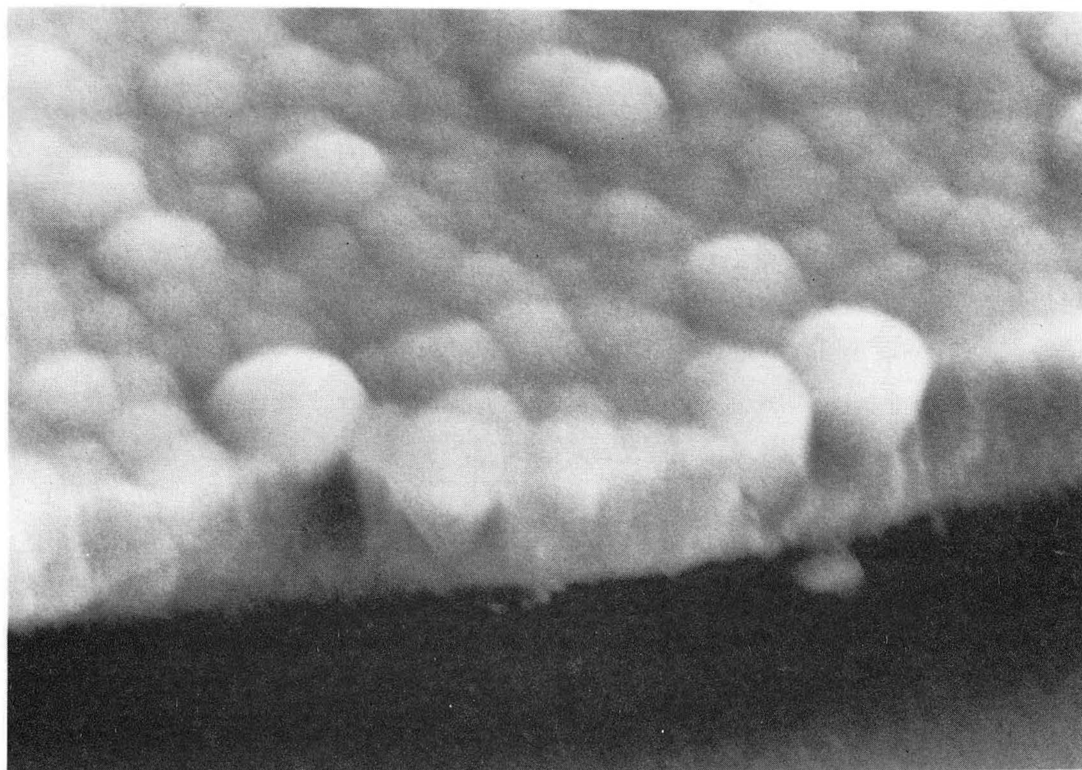

4 μm.

XBB 870-9262

Figure 3.52: SEM micrograph showing a zone one morphology, that developed when the film had the following pretreatment: 0_2 plasma exposure (1 torr) for two minutes; 5 minute evacuation; 5 minute H_2/N_2 plasma (1 torr).

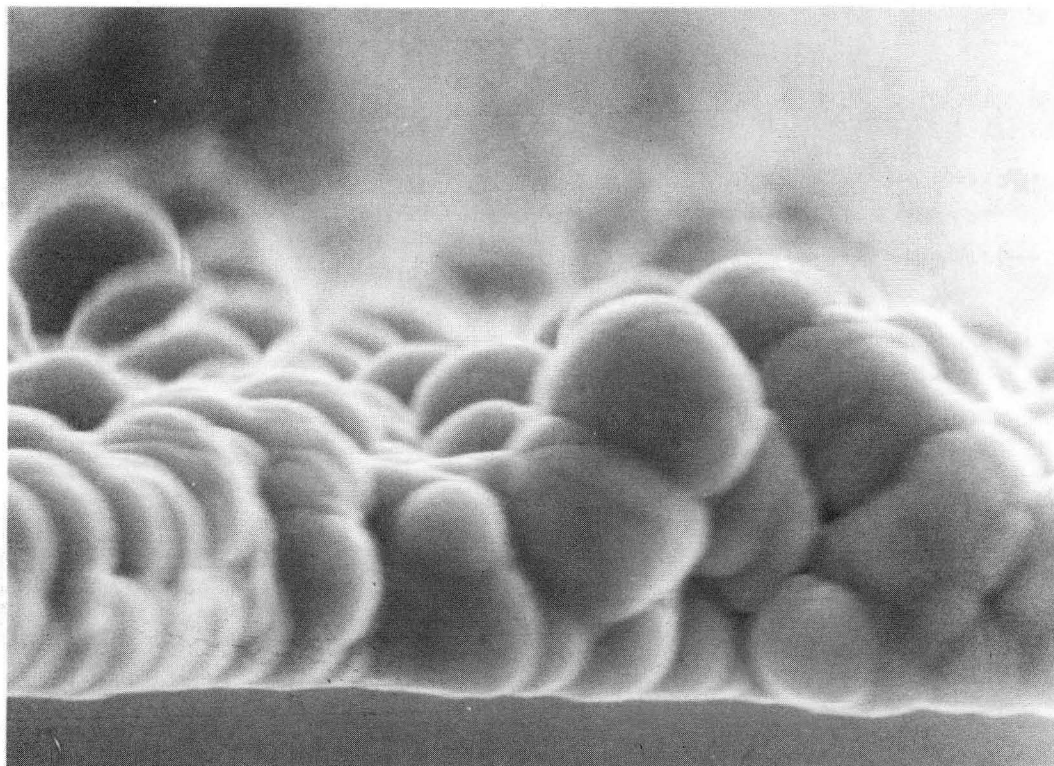

10 μm.

XBB 870-9265

Figure 3.53: SEM micrograph showing a nodular morphology, indicative of gas phase nucleation, that developed when the film had the following pretreatment: 0_2 plasma exposure (1 torr) for ten minutes; followed by a five minute nitrogen plasma (1 torr); followed by a five minute H_2/N_2 plasma (1 torr). The plasma was never extinguished during pretreatment or films growth–the new gases were introduced concurrently with the decrease of the previous gas.

3.4 $TiCl_4$, CH_4, N_2, and H_2 Studies:

3.4.1 Deposition Conditions:

In this study, the CH_4/N_2 ratio (with H_2/N_2=2), the H_2/N_2 ratio (with P_{CH_4}=0.2 torr), initial gas introduction, and deposition time were varied. The $TiCl_4$ flow rate was held constant at 0.21mmol/min. Total pressure was one torr, r.f. power was 50W, r.f. frequency was 13.56MHz, (IPC supply), and substrate temperature was 500°C. The samples previously cleaned in acetone and ethanol ultrasonic baths were initially placed on the heater, which was set for 300°C. The heater temperature was then adjusted to raise the sample temperature to 500°C. After fifteen minutes, hydrogen and nitrogen gases (H_2/N_2=2) were added to bring total pressure to one torr. These gases flowed for ten minutes, after which a plasma was ignited for five minutes. Gas flow was then reduced to a level such that CH_4 subsequently added would resume total pressure to one torr. In some experiments methane was added prior to $TiCl_4$ introduction, otherwise, $TiCl_4$ was added first. In each case the second gas was added within one minute of the first.

3.4.2 Film Structure and Composition:

SEM indicated that the films grew in a zone T morphology, consisting of fibrous grains within an apparently large aggregate. The fibrous interiors were difficult to resolve with SEM but appeared to have a diameter on the order of 1000Å; the diameter of the aggregate or cluster was on the order of 1μm. Film delamination was readily found around the Rockwell indentations, unlike films formed from H_2 and N_2 at these temperatures. XRD revealed various types of preferred orientation, ranging from a sharp (200) structure, to a mixed poorly crystalline (200) and (111) structure, to a nearly amorphous structure, as shown in Figures 3.54-3.56. This transition was concommitant with increasing Cl and C contents. No evidence of distinct TiN and TiC phase separation was observed–however, the peak broadening

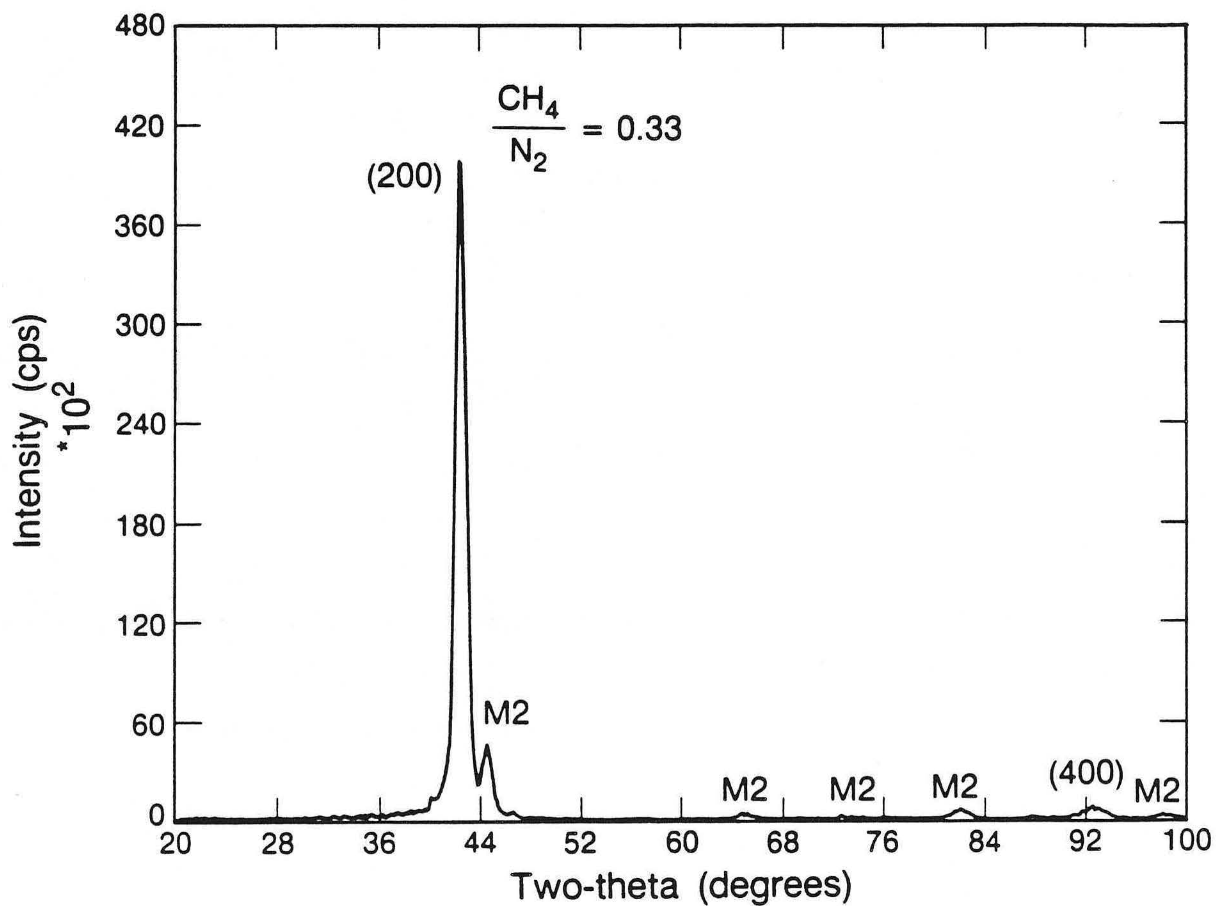

Figure 3.54: X-ray diffraction intensity vs. 2θ for a titanium carbonitride film formed with CH_4/N_2 gas flow ratio of 0.33.

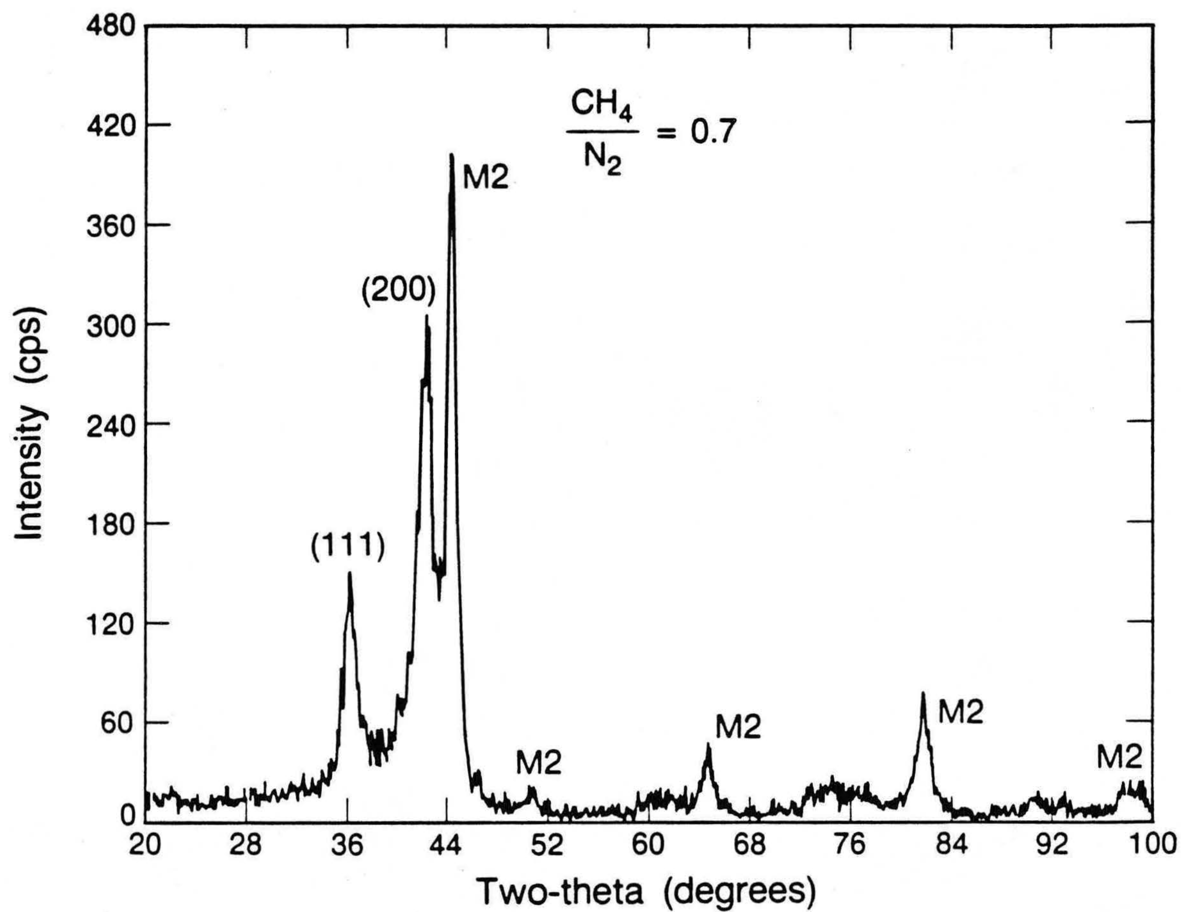

Figure 3.55: X-ray diffraction intensity vs. 2θ for a titanium carbonitride film formed with with CH_4/N_2 gas flow ratio of 0.7.

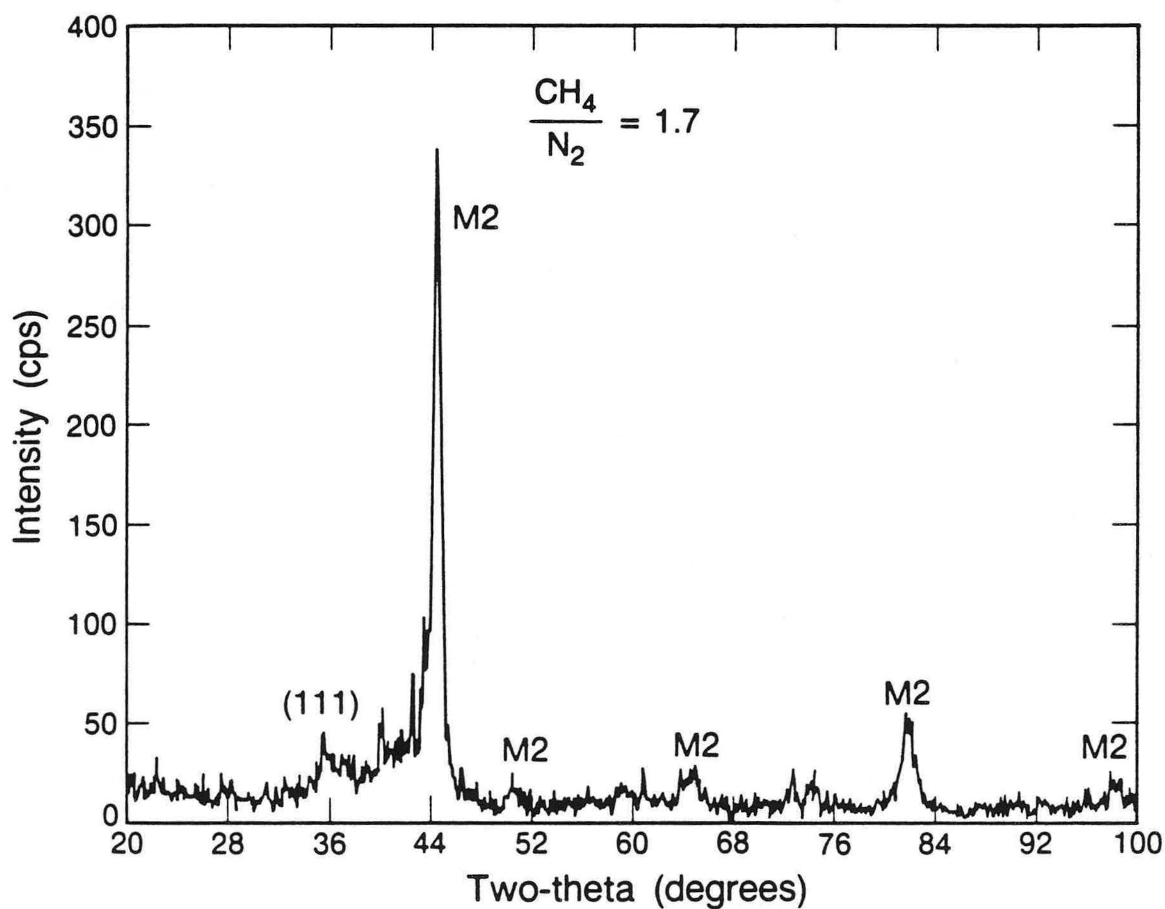

Figure 3.56: X-ray diffraction intensity vs. 2θ for a titanium carbonitride film formed with with CH_4/N_2 gas flow ratio of 1.7.

observed could mask TiN and TiC phases.

AES revealed that the films contained a significant amount of Cl. The amount of Cl increased with the CH_4/N_2 flow ratio, as shown in Figure 3.57. However, the amount of scatter in the data also increased, which suggests that the process control of the plasma volume is becoming more difficult. Variation of the H_2/N_2 flow ratio has relatively negligible effect on film Cl content (Fig 3.58). Carbon content in the film increases with CH_4/N_2 flow ratio, and the $(Ti+N)_{387ev}$: Ti_{418ev} ratio concurrently decreases. The exact nitrogen content is difficult to access, due to the overlap of the N_{383ev} peak and Ti_{387ev} peak, and the unknown influence of carbon and chlorine on the peak shape of the Ti_{387ev} $L_3M_{23}M_{23}$ transition. Analysis of the films containing large amounts of carbon with varying amounts of Cl indicates that the increased chlorine content more strongly correlated with the decreasing (200)/(111) orientation ratio and decreasing overall film diffraction peak intensity than did the carbon content. Film growth ratio increases somewhat with CH_4/N_2 ratio (Figure 3.60), though a comparison with the Cl content of the same films shows a far better correlation (Figure 3.61).

3.4.3 Mechanical Properties:

Initially, films were prepared in which CH_4 was introduced prior to $TiCl_4$. Some of these films delaminated spontaneously after synthesis. Considering that CH_4 without $TiCl_4$ in a plasma might yield carbon polymers, subsequent films were synthesized using the procedure of $TiCl_4$ introduction prior to methane. The SAT critical load values, L_C, of some of these films as a function of thickness is shown in Figure 3.62. Values of ion plated titanium carbide on tool steel reported by Perry (Per:83)is shown for comparison. The Perry data shows two trends: 1)The linear increase in Lc with thickness is attributed to an increasing critical load required at the surface to generate a critical fracture stress at the interface as that region is moved further from the surface. 2)Increasing the difference in mechanical properties between the coating and the substrate, in this case the

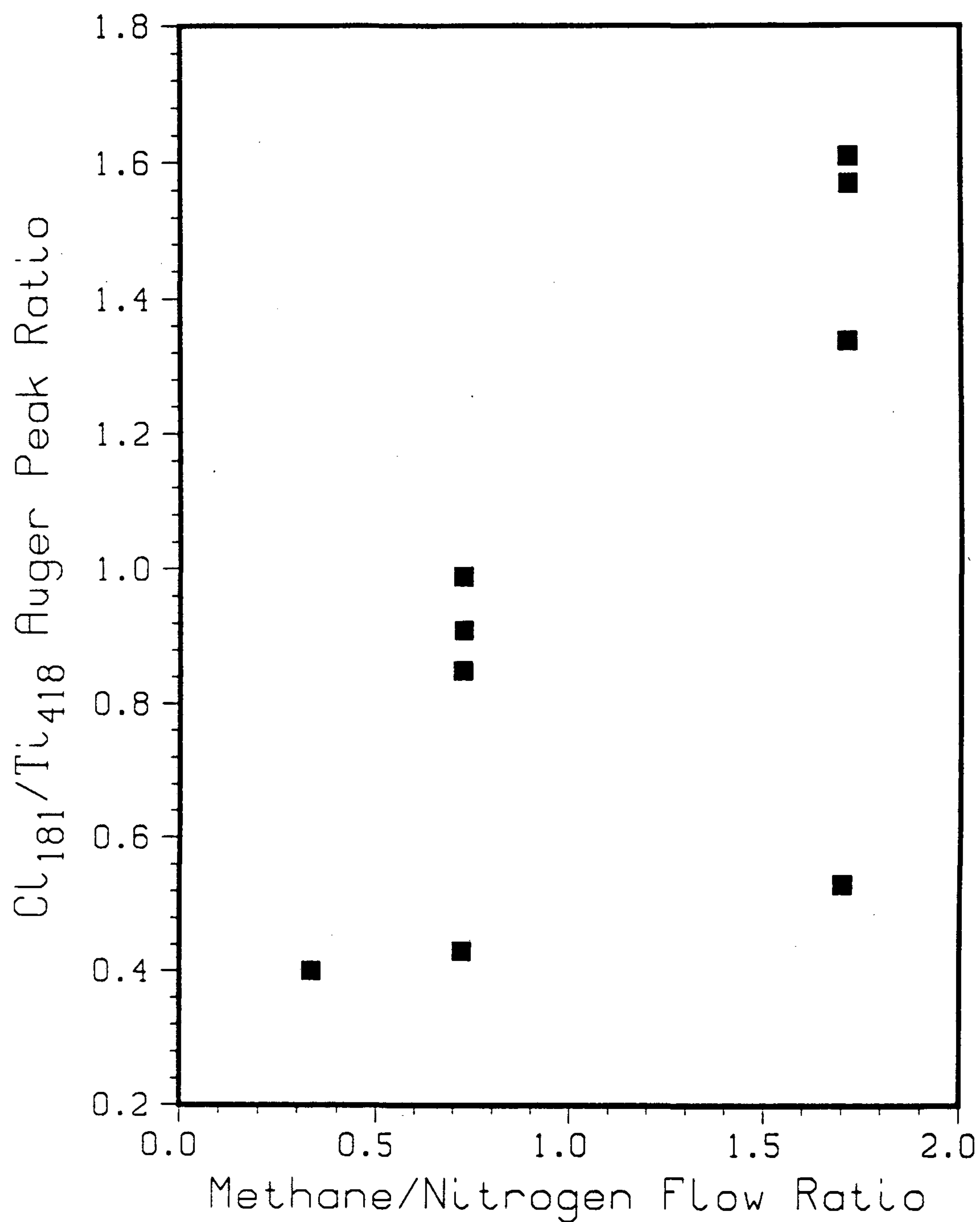

Figure 3.57: Chlorine content determined by AES in the titanium carbonitride films as a function of CH_4/N_2 gas ratio during deposition (H_2/N_2=2).

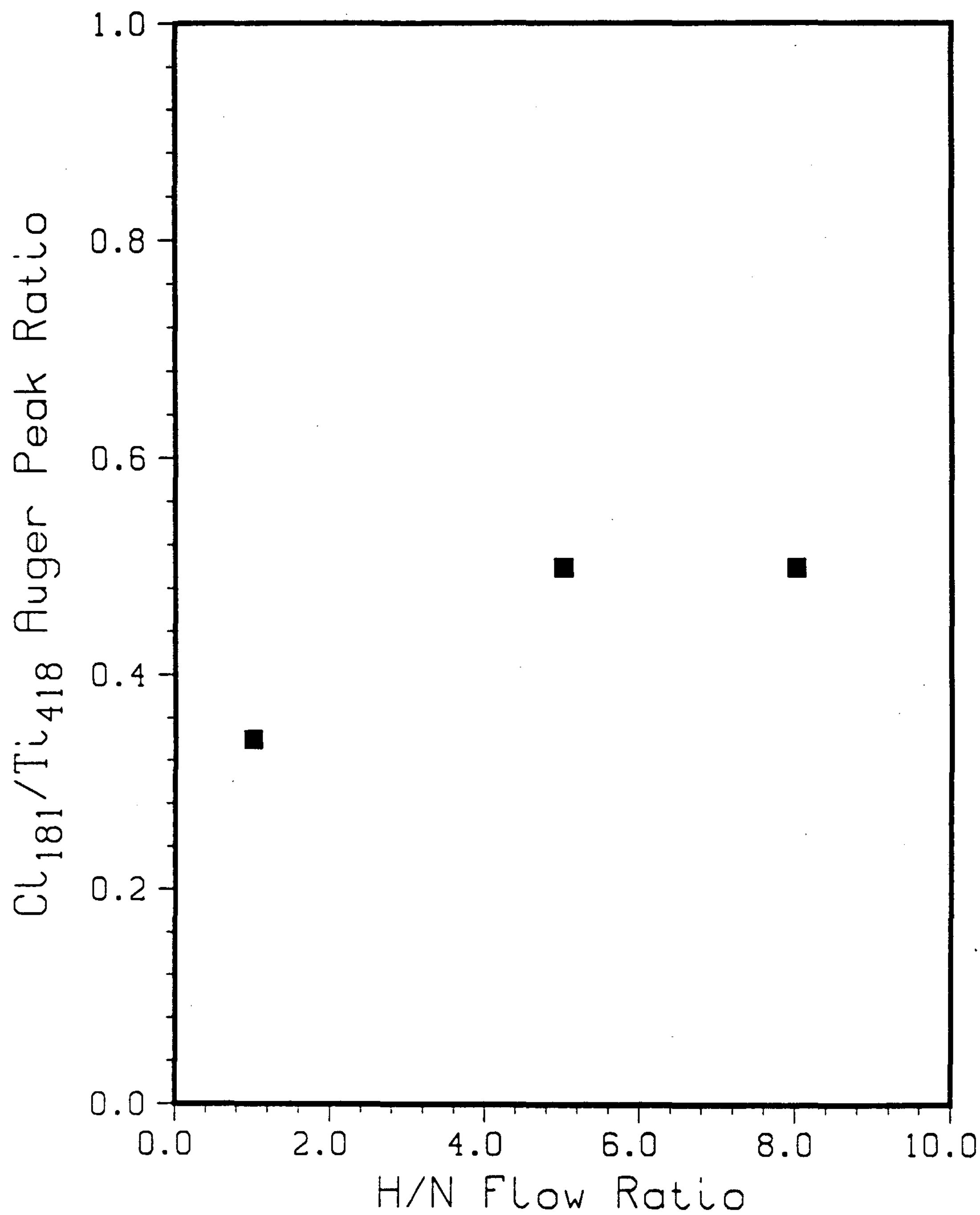

Figure 3.58: Chlorine content determined by AES in the titanium carbonitride films as a function of H_2/N_2 ratio.

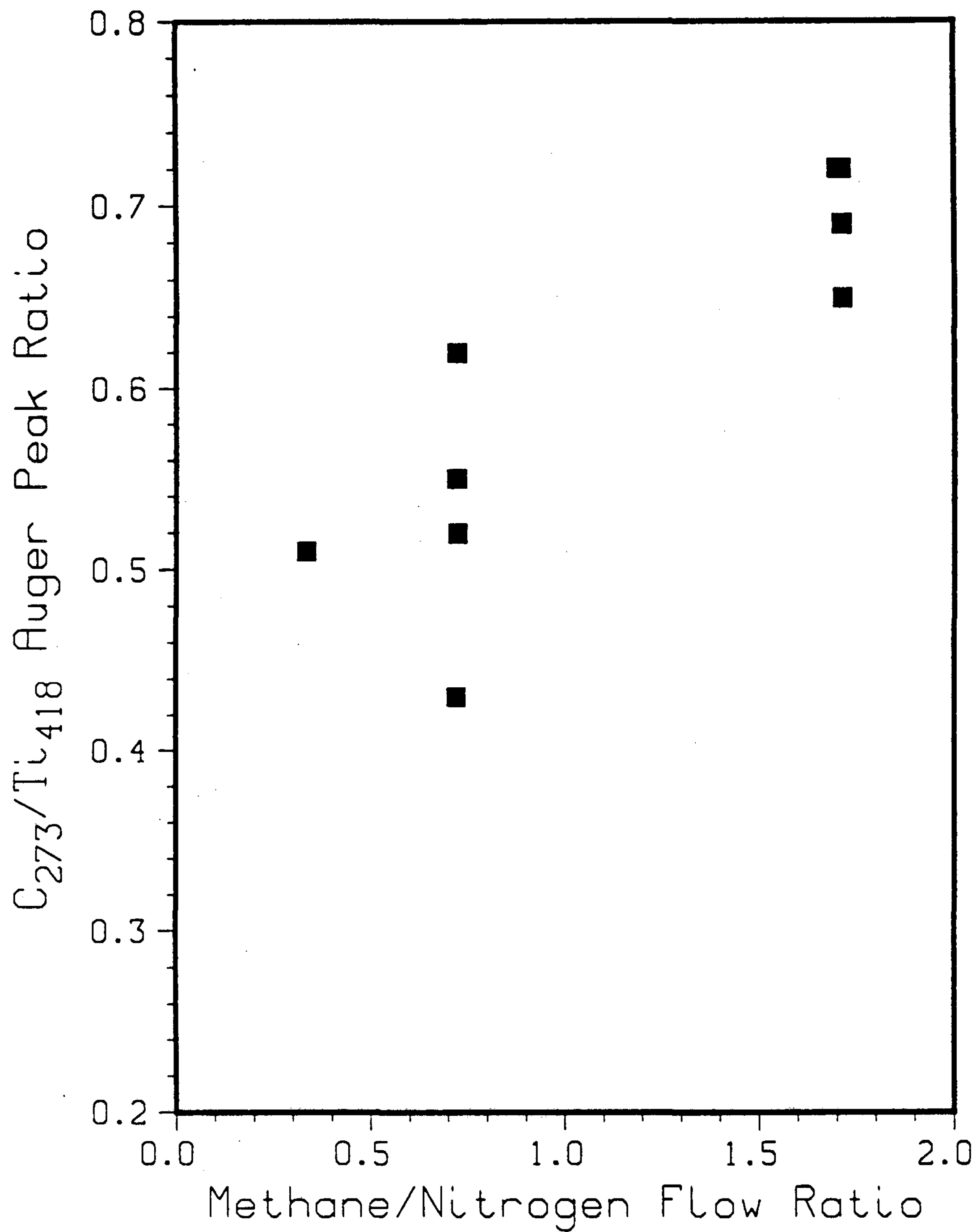

Figure 3.59: Carbon content as determined by AES in the titanium carbonitride films as a function of CH_4/N_2 gas ratio during deposition. (H_2/N_2=2.)

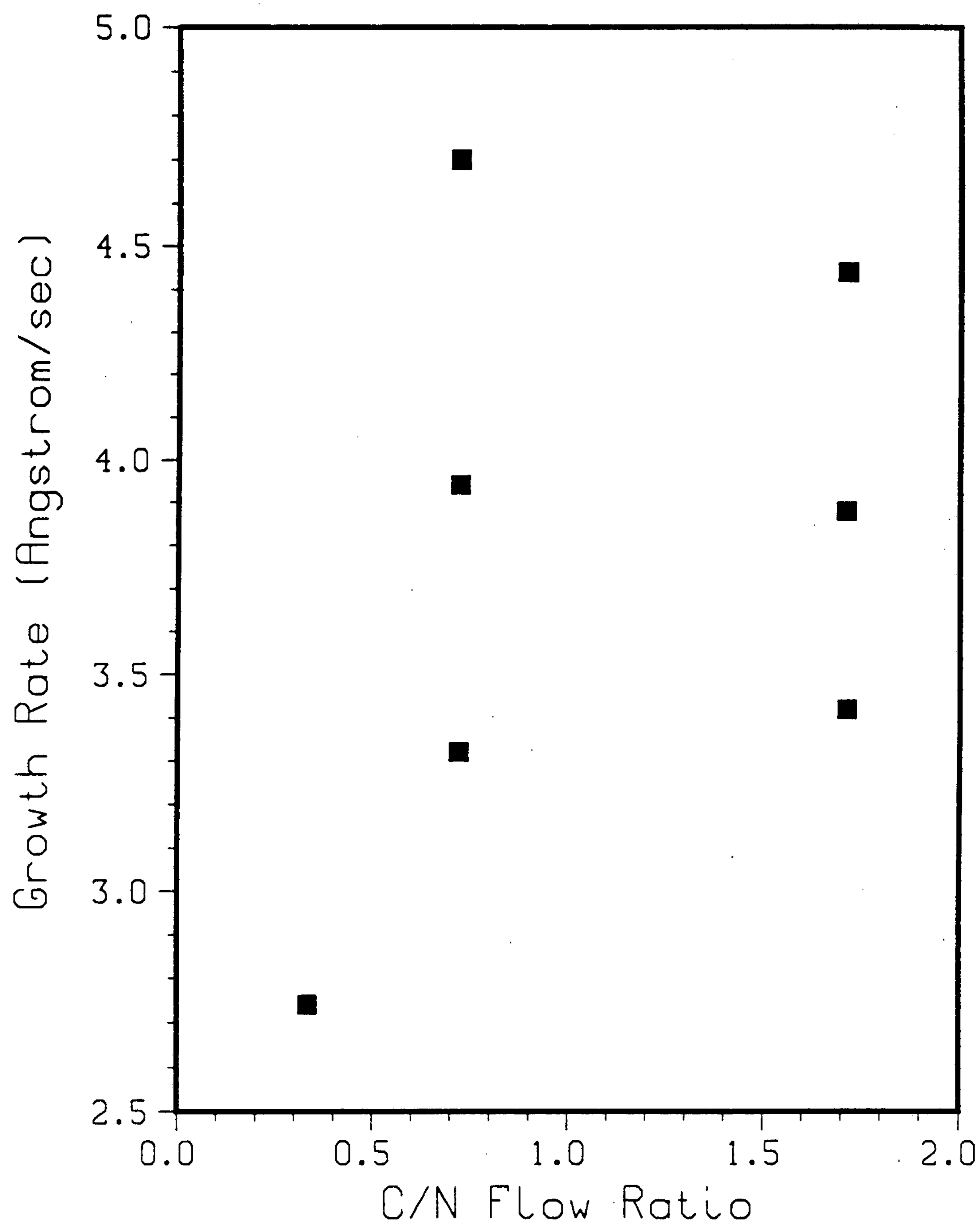

Figure 3.60: Carbonitride film growth rate as a function of CH_4/N_2 (H_2/N_2=2).

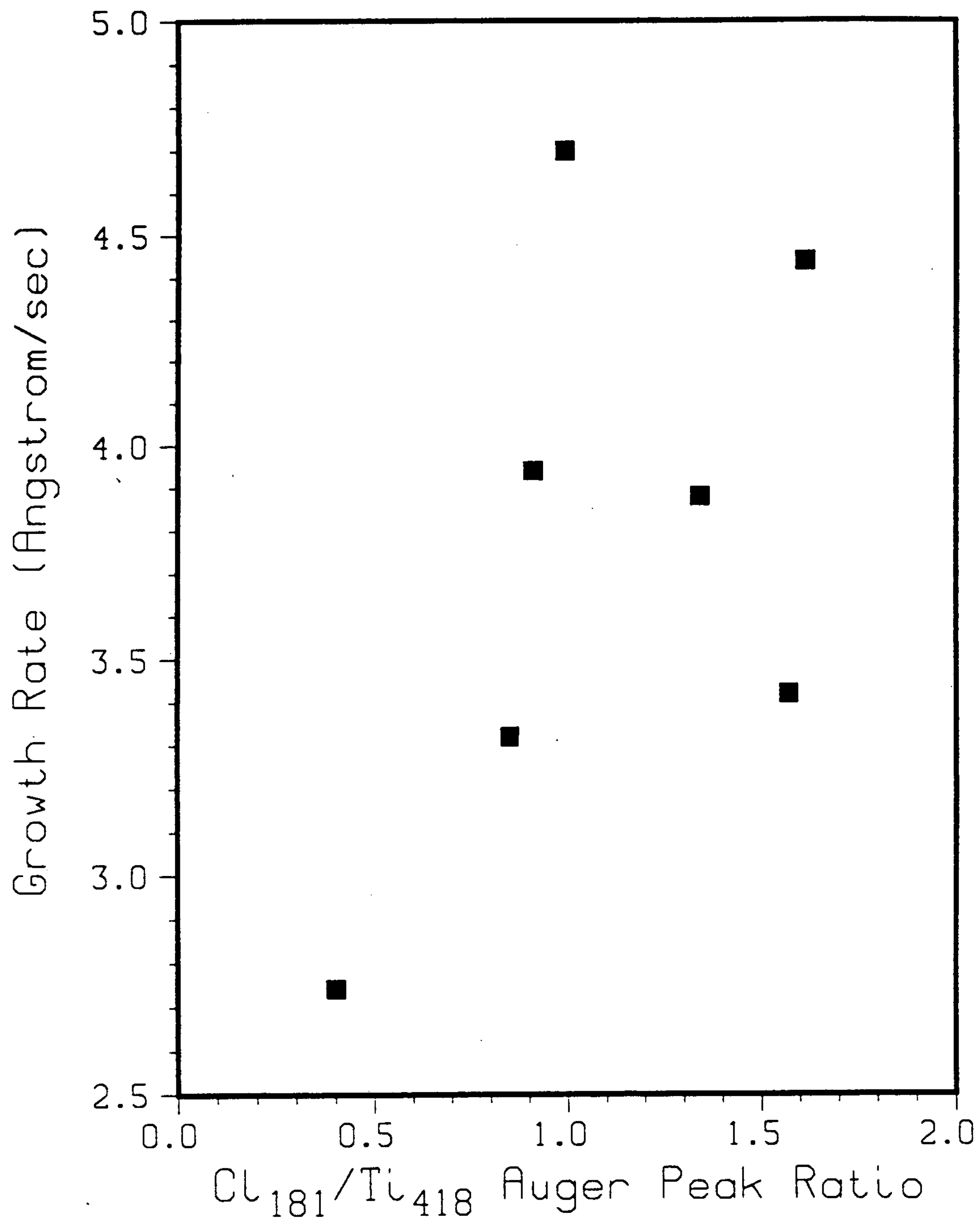

Figure 3.61: Carbonitride film growth rate as a function of chlorine content for the films shown in the previous figure.

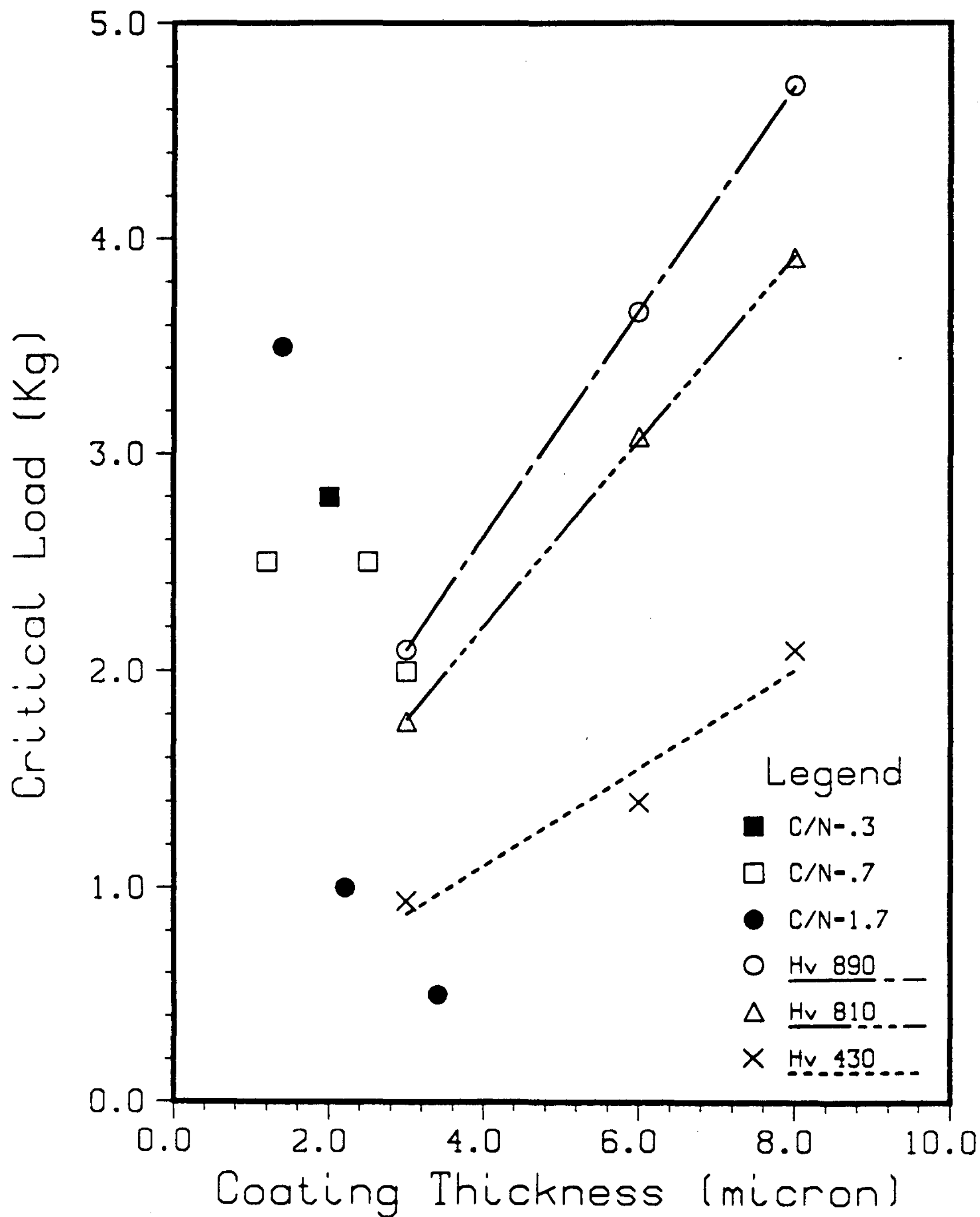

Figure 3.62: SAT critical load (L_C) for the carbonitride films as a function of film thickness. The trend (negative slope) suggests poor adhesion, with films delamination due to residual stress which increases with thickness. Also plotted for comparison is data from Perry (Per:83) for TiC on high speed steel with three different substrate hardnesses.

difference in material hardness by decreasing the substrate hardness, lowers the critical load necessary for failure because the differential in mechanical response of the two solids at the interface is increased. The PACVD data shows a general decrease in L_C with increasing thickness for a given deposition condition. This result is interpreted to indicate that a buildup of residual stress which occurs with increasing film thickness is decreasing critical load and that interfacial adhesion strength fairly is low. It is important to remember that the PACVD films are not TiC, but rather a carbonitride with significant amounts of Cl.

The film hardness is also low. Vickers hardness of a 4.4 μm film was 1037 kg/mm^2 for 100g load and 940 kg/mm^2 for 200gm load (substrate hardness was 940 and 900gm respectively). Though the elastic plastic zone of the indenter clearly sampled the substrate in both measurements, the 100gm value still seems very low. The high chlorine content of the film is a probable cause. The low film hardness may contribute to the relatively high L_C's observed at low film thickness, by lowering the differential between substrate and film hardness.

Chapter 4

Discussion

The experimental evidence indicates that the structural and thus the mechanical properties of TiN films, synthesized by PACVD using $TiCl_4$ as a starting reagent, are controlled by the removal of chlorine at the growing TiN-gas interface. At low temperature, where thermodynamic equilibrium favors the formation of solid NH_4Cl, the film quality is poor. As soon as HCl formation becomes thermodynamically favorable (above 350°C), higher quality (in terms of composition and crystallinity) TiN films are produced. The fact that the composition of the film is controlled by the substrate temperature indicates that surface reactions, as opposed to gas phase reactions, are determining this coating property. This effect has been modeled by the reactions shown in Figure 3.2. The important point is that the change in slope in all cases from positive to negative occurs at temperatures in the range 300-350°C and is determined by the change in the sign in ΔG^o for NH_4Cl decomposition either to NH_3 and HCl or to N_2, H_2, and HCl. Whether the starting material is $TiCl_4$, $TiCl_3$ or a lower chlorine is not important in this model. Since chlorine is detrimental to mechanical properties, this change in by-product places a lower limit on the deposition temperature of the PACVD process for TiN formation from $TiCl_4$.

The scratch removal studies in UHV indicate that chlorine concentration at the film-substrate interface can be higher than that within TiN film at temperatures above 350°C. As pointed out by Carlsson (Car:85), the substrate can participate in

Table 4.1: Morphologies observed in the PACVD-produced TiN films as a function of deposition temperature and nitrogen reagent. (NI- not investigated.)

Temperature(°C)	T/Tm	Morphology	
		NH_3	H_2-N_2
200	0.146	1	NI
300	0.179	1-T	NI
400	0.209	2	T
500	0.239	NI	2

the overall film formation reaction during the initial stages of growth. Therefore, the reaction thermodynamics are more complicated and it is not surprising that chlorine composition could change. The higher interfacial chlorine content in the NH_3-$TiCl_4$ studies could stem from: 1)retention of Cl from $TiCl_4$ by the steel (primarily Fe) surface, during the initial film formation reaction, 2)residual HCl present in the chamber as a background gas that absorbs onto the substrate prior to deposition and which is trapped by the nucleating TiN, or 3)both 1 and 2. A H_2-N_2 plasma seems to be more efficient at removing this chlorine than an NH_3-based plasma. Both add nitrogen to the steel. The NH_3 may be more prone to forming NH_4Cl on the substrate surface.

The morphology of the TiN films formed by PACVD from $TiCl_4$ are well categorized by the Thornton model. The change in morphology from an amorphous zone 1 structure, to a partly crystalline zone T, and finally to a highly crystalline zone 2 structure with increasing temperature occurs because surface mobility increases. The homologous temperatures of the operating deposition temperatures with respect to the melting temperature of TiN (3222°K) are listed below:

The zone 2 and T structures occur in the PACVD TiN films at temperatures below the range suggested by Movchan (T< 0.3 Tm) for the zone 2 structure (Tho:77) in metal films. This result agrees with data reported by Sundgren, who has found that the higher mobility morphologies are present at lower homologous temperatures in binary films formed by PVD (Sun:86). As stated in section 1.4.7,

he suggests that chemical potential effects and compound heats of formation can increase surface adatom mobility, which can lead to a reduction in the surface temperature needed to facilitate diffusion. It is important to remember that chlorine incorporation increases with decreasing deposition temperature in the present PACVD process, which may inhibit surface adatom mobility. Film growth rate also increases with decreasing deposition temperature. Increasing growth rates should in principle lower adatom mobility. However, the NH_3-based films had higher growth rates at lower temperatures than the H_2-N_2-based films with identical morphology. Therefore film growth rate within the range observed does not appear to be a dominant factor in determining morphology in the present context.

Carbonitride films were deposited only at one temperature. A zone T structure was observed, while a zone 2 structure was observed at the same temperature in the TiN films. Chlorine content was also higher in the former films along with scatter in this data. The melting temperature of TiC is only slightly higher than that of TiN (3330°K vs 3222°K), and the homologous temperature difference is small (.232 vs. .239 at 500°C). In addition, the exact T_m of the Ti(CN) films formed is unknown. Thus, differences in T_m do not account for the change in morphology. The lower mobility morphology of the Ti(CN) films probably stems from a lower chemical driving force for diffusion or the higher chlorine contents or both. The more unfavorable thermodynamics of TiC vs. TiN formation (Figure 3.1) and the relative free energies of formation (Table 1.3) correlate with the lower mobility in the carbon-containing films.

The carbonitroxide films formed from Ti amide decomposition clearly show a morphology associated with gas phase nucleation. Curiously, the nitride films formed after oxygen pretreatment show this type of morphology. This result indicates that the oxygen is present in the gas phase during later stages of growth. The degree of the modular morphology seems to correlate with the time of oxygen exposure. A possible explanation is that the pretreatment may saturate the chamber wall, and the porous debris on them, which provide a source of desorbing oxygen during subsequent deposition.

The zone 2 films have a high degree of crystallinity, with a strong, exclusive (200) preferred orientation. (In fact, the data is a textbook-quality example of it). The zone T films have broader (200) peaks, occasionally with a small (111) peak and an amorphous component. The zone 1 films are amorphous. Thus, crystallinity decreases with decreasing surface adatom mobility during deposition. The increasing chlorine content with decreasing substrate temperature may also contribute to the decrease in crystallinity by disrupting the NaCl structure. The (200) preferred orientation observed in the zone 2 films has been observed by other investigators of PACVD (Shi:84, Shi:85, May:85). Higher temperature CVD films have a more random orientation (Per:86). Films formed by PVD (sputtering, ARE) techniques at similar temperatures to the present study tend to have a (111) preferred orientation (Per:86). Thus, the type and degree of preferred orientation seems to depend on the specific nature of condensation and compound formation that occurs with each technique.

Thornton has observed that the preferred orientation in vapor deposited films generally occurs along the close packed plane of fcc, bcc, and hcp materials (Tho:77). For fcc, this is the (111) plane, which is observed as mentioned before. This orientation consists of alternating planes of Ti and N parallel to the growing surface. The (200) orientation consists of an equal exposure of Ti and N within a single plane. An atom located along a (111) surface has nine nearest-neighbor-bonds, while an atom along a (200) surface has five nearest-neighbors with several close second-and third-nearest neighbors. The situation is complicated by the fact that adjacent atoms are different.

The nature of the adsorbate may influence the type of preferred orientation, ie. whether the adsorbate is atomic or molecular. In the sputtering or evaporation case, the adsorbates are probably primarily atomic. The PACVD process uses molecular feedstocks, which are excited by the r.f. or d.c., field utilized. Although molecular dissociation to atoms does occur, partially dissociated molecules or molecular ions still exist and dominate. In particular, the $TiCl_x$ complex is probably not completely dissociated. Organometallic chemistry studies indicate that

the last Cl ligand is difficult to remove (And:85). This author suspects that the (100) surface stabilizes the titanium atom in a adsorbed TiCl complex, weakening the Ti-Cl bond, which fascillitates Cl removal with the assistance of hydrogen.

A model involving the breaking of Ti-Cl bonds at the surface requiring nitrogen to promote the weakening of the TiCl bond would favor the formation of stoichiometric TiN. (Of course, if oxygen or carbon are present, oxides or carbides can form). The Auger data indicates that the TiN films formed at 400°C and above have a consistent NiTi ratio independent of plasma conditions as long as oxygen and carbon are not present. Within the error of AES (~5%), these films appear to be stoichiometric. The α-Ti and Ti_2N phases have never been observed. As stated in chapter 3, a thin titanium oxide would form if N_2 were not present with $TiCl_4$ and H_2. Background CO may have been the source of the oxygen. The fact that the layer was relatively thin suggests that the oxygen was required to break the TiCl bond, otherwise a thicker layer of Ti should have formed with a thin oxidized surface. Hydrogen is also essential for the final removal of Cl, since a highly chlorinated film is formed when $TiCl_4$ and N_2 are used.

The above argument explains why nitrogen-deficient TiN is not formed. A review of the Ti-N phase diagram can provide a reason why overstoichiometric TiN is not synthesized. Quite simply, above 51-52% N, solid TiN and N_2 gas are the thermodynamically favored phases. Excess nitrogen present on the surface during deposition is ejected or awaits the arrival of more Ti before being incorporated into the lattice. Thus, at a sufficiently high temperature, the PACVD process is self-regulating towards the formation of stoichiometric TiN. Substoichiometric TiN does not form because hydrogen and nitrogen are needed to promote chlorine removal. Overstoichiometric TiN is not formed because excess nitrogen is ejected. This self-regulating feature of PACVD makes the process appealing for industrial applications, provided that TiN is the desired material. For research on the properties of the entire Ti-N system, sputtering or activated evaporation processes appear to be a better synthesis route, since the entire phase diagram can be accessed in a controlled manner.

The fact that high temperatures and hydrogen plasmas promote Cl removal complicates surface science studies of the TiN surface as deposited or of the interfacial region as deposited in the initial stages of growth, since chlorine will deposit as soon as the plasma is extinguished and/or as the sample is removed from the hot deposition system. Thus, an in-situ transfer capability from the PACVD chamber to a UHV analytical system is inappropriate in this case, since the surface is altered immediately upon cessation of the plasma and heating. Transfer in air will only add oxygen to the already altered surface. Such capability would be useful in studies of sputtered or evaporated films, where operating pressures are lower (10^{-2} -10^{-7}torr) and where temperature-dependent surface reactions are minimal when the source or iomized gas is extinguished. The ability to study surface composition during growth of PACVD films will require the development of non-linear optical spectroscopies, such as sum-frequency harmonic generation (She:86).

The present study has shown that the interface composition of the PACVD TiN-steel system can be investigated after deposition with present surface science techniques. The study of weak interfaces has been particularly successful and is of immediate importance towards the improvement of adhesion. A new procedure, the UHV scratch removal technique (SRT) was developed in this study. SRT can be quite useful in identifying elements that promote failure. One advantage of the method is that films with thicknesses of 2 to 10 μm can be analysed quickly. While these dimensions are necessary for useful mechanical properties, they make conventional sputter depth profiling very time consuming. Of particular importance is the fact that specific batches of films can be examined that have anolomously poor mechanical properties relative to other batches with ostensibly identical deposition conditions. SRT can also resolve very sharp concentration gradients at interfaces that would be destroyed by ion bombardment during sputtering. The quantitative composition data generated by SRT is dependent upon the exact area examined. This fact necessitates the use of microscopy to study the structure of the scratched regions. Further development of SRT will require the use of a high-resolution SAM that has better capability than the older system used in this study.

The design of the apparatus utilized in the present investigation was deliberately kept simple to determine if the exposed scratch area could provide useful information. The evidence indicates that such studies are beneficial. In a future SRT design, knowledge of the load applied and precise control of the stylus velocity would be useful, so that *in situ* SAT could be performed and the surface composition of the fracture regions investigated. UHV-compatible friction and adhesion testing devices incorporating strain gauges and motor drives have already been successfully built and employed by Buckley and his co-workers (Miy:83).

While studying weak interfaces is of prime importance, the study of strong interfaces in of interest because of the desire to know what impurities or dopants improve adhesion. The study of a strong interface provides a challenge to the surface scientist, because, by definition, such a boundary will not be exposed by fracture. In this investigation, strong interfaces were analyzed by sputtering through specially prepared thin films of TiN. This traditional approach yields information but suffers two conceptual drawbacks: 1) The sputtering process potentially can broaden and distort sharp interfacial composition gradients. 2) The interfaces of the thicker films used for mechanical testing are not evaluated. Further improvements of the study of strong interfaces of PACVD films during deposition will require the in-situ optical techniques mentioned earlier. However, in the case of sputtered or evaporated films, in-situ transfer to a UHV analytical system is a viable approach worth exploring. Interface and subsequent film surface composition could be studied during the progressive stages of deposition and the mechanical properties of the film could be investigated after final formation.

The scratch adhesion test results, both critical load data and failure modes observed, indicate that the H_2-N_2-based PACVD TiN films had better adhesive properties than the NH_3-based films or the carbonitride films. The critical load data of the H_2-N_2 based TiN films compares well with the results of Sproul for sputtered TiN on M2 steel. In contrast, the L_C magnitudes for the NH_3-based TiN or the carbonitrides are low, comparable to values observed by Helmersson et.al (Hel:85) for sputtered TiN on high speed steel (ASP 23 not M2 steel, though comparable)

in which the substrate had only been only solvent degreased. However, the presence of chlorine appears to be the detrimental feature in the inferior PACVD films. The failure mode transition from massive spallation (Burnett-Rickerby type A), for the NH_3-based TiN and carbonitride films, to a buckling/chipping (Burnett-Rickerby Type B,C) or tensile cracking (Rickerby Type E) for the zone T and 2 H_2-N_2-based TiN films also indicates relative improvement in adhesion for the latter films. The failure mechanisms present in Sproul or Helmersson's studies were not explicitly reported. The critical load data for the H_2-N_2-based zone T and 2 TiN films was identical within scatter. Yet, the tensile failure mode of the zone 2 coatings indicates better adhesion than the zone T films, which had the partial chipping or buckling failures. The fact that the zone 2 films had better resistance to delamination during Rockwell (or Hertzian) impact than the zone T films also suggests that the former would be better for tool applications. Since the Rockwell impact load was fixed, the results of Jindal et als.'s (Jin:87) investigation of film adhesion using static Rockwell stylus indentation suggest that the zone 2 films have better interfacial fracture toughness than the zone T films. The difference in SAT and Rc fracture mode with morphology may actually stem from the difference in bulk chlorine contents and not the morphology itself.

The adhesion test data in conjunction with the interface studies indicate that the presence of excessive chlorine in the steel-film interface is detrimental to adhesion when bulk chlorine content is low. When bulk chlorine content is high (low temperature TiN for the carbonitride films) the films are of very poor quality, tending to spontaneously disintegrate or easily delaminate. Thus, chlorine removal is essential. The role of oxygen and nitrogen in affecting adhesion has been obscured by chlorine. Another issue is contamination. Helmersson et.al's study indicates that contaminant (primarily hydrocarbon) removal is essential and partial iron oxide reduction is desirable (Hel:85). Conventional CVD accomplishes these goals by the high operating temperature of the deposition, which expels chlorine and other impurities. In addition, the high temperature promotes diffusion across the interface between coating and substrate during the entire deposition.

In order to obtain adherent TiN films by PVD, investigators have reported that substrate bombardment with argon at a kilowatt or more potential is required prior to deposition (Spr:83, Hel:85, Sun:86). In the present work, the samples were generally grounded and the sheath potential was of the order of tens of volts which means that these bombardment cleaning effects, by H_2 and N_2 as opposed to Ar, were minimized. Instead, it is proposed that the excited state hydrogen from the plasma facilitates sample cleaning, as well as promoting removal of chlorine from the Fe surface. In other words, a plasma assisting reaction or etching is occuring which can suitably prepare substrates instead of a momentum process. Thus, within the PACVD process, there is an inherent capability for substrate preparation using chemical means which avoids the structurally disrupting aspects of the sputtering process. This investigation has shown that in terms of final film-substrate adhesion, the plasma pretreatment can yield an equivalent result when compared to presputtering.

Poor adhesion means that cohesive strength of the interface is lower than those of either the coating or substrate and that interfacial fracture initiates and propagates prior to deformations processes in either material. There are several possible mechanisms by which chlorine could degrade adhesion. As pointed out by Carlsson (Car:85), a reactant like chlorine could combine with the iron substrate and form gaseous by-products, yielding corrosion and subsequent porosity which disrupts complete contact and acts as a stress concentrator. This would be expected at elevated temperatures. At lower temperatures, Cl could form a brittle salt-like layer. The presence of chlorine as an impurity, without forming a distinct phase, could weaken the TiN-steel interface, analogous to the role of segregants promoting grain-boundary fracture in alloys or ceramics. Experimentally, the correlation between interfacial segregants and brittle intergranular fracture has been well known and documented for quite some time (Mar:69, Mar:72, Mar:722, Pal:69). There is also evidence that boron can do the opposite, that is promote grain boundary cohesion, in Fe-Mn alloys and in Ni_3Al superalloys (Hwa:80, Liu:85).

The embrittlement phenomenon has only recently been investigated by theo-

retical chemists. These studies are worthy of a short digression. In the ground-breaking work of Briant and Messmer (Bri:80, Bri:82) the influence of sulfur on the electronic properties of Nickel was investigated using the self-consistent-field Xα scattered wave technique. The segregating impurity was placed in a four atom polyhedron, believed to be representative of a grain boundary structure. Embrittling agents, such as S or P, were found to withdraw charge density from the Ni metal-metal bonds. They argued that such weakening correlated to a reduction in cohesive strength. The degree of charge withdraw correlated with tendency to embrittle, and was greatest for S, reducing in the order S>P>>C>B, with boron being a "cohesive enhancer" and not withdrawing charge from the metal-metal bonds. The effect of carbon was relatively neutral.

Eberhart et.al. pointed out that the Briant and Messmer model was valid only for dilute sulphur concentrations, ignoring sulphur-sulphur interactions. They investigated this issue with a larger cluster modeling grain boundaries of up to 20% sulfur concentration. As sulphur atoms interacted, charge transferred to the coordinating nickel atoms, making the material more covalent and directional than a dilute sulphur system. They have incorporated this information into a qualitative model describing the fracture process, which includes bond and orbital polarizability as factors, viewed in terms of the response of a crystal structure to an applied stress field, in this case the region nearby an atomically sharp crack being pulled in tension (following the crack tip stress field model of Rice and Thompson (Ric:74)).

The model is summarized as follows. When a material with a crack is subjected to tension in the arrangement of Figure 4.1, the system will lower its energy due to strain by deformation along the planes $\frac{\pi}{8}$ away from the tensile direction (the planes of resolved shear stress) or by fracture and extension of the crack. The particular response will be determined by the relative shear and cohesive strengths of regions in the stress field. Of particular importance to the fracture process are the atoms ahead of the crack tip along the cleavage plane. During elastic tension, the positions of the nuclei perpendicular to the cleavage plane (along the

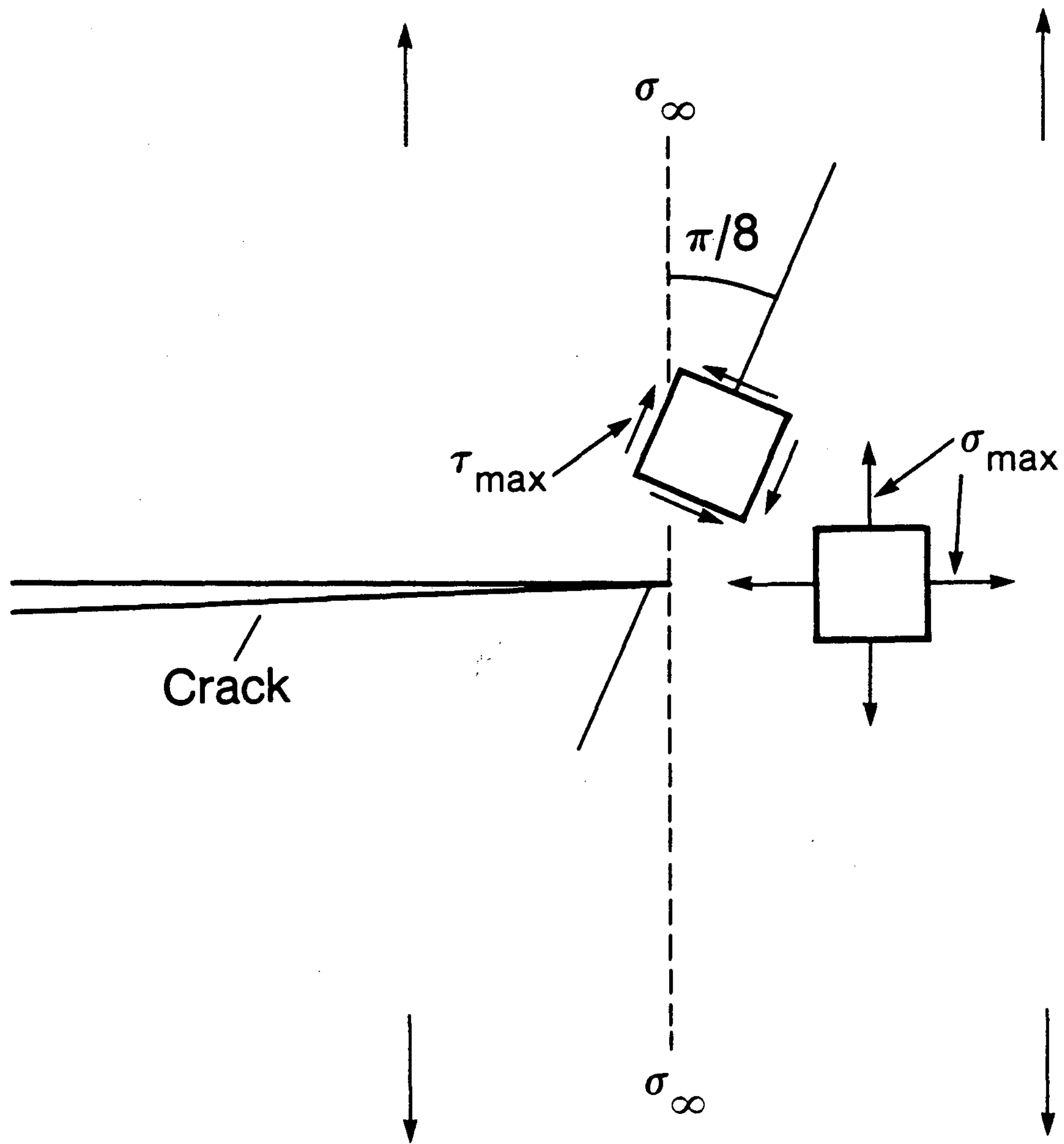

XBL 8710-7935

Figure 4.1: The nature of a stress field near an atomically sharp crack, following the model of Rice and Thompson (Ric:75, Ebe:86).

applied stress direction) are being dilated, ie. they are moving further apart. The electrostatic potential energy along this direction thereby increases because the nuclei are no longer in their equilibrium position at the minimum of the potential well. The electron density between the atoms can lower its potential energy by flowing into the unperturbed bonds perpendicular to the applied stress, if these orbitals are partially filled. This charge redistribution results in a contraction of the bonds parallel to the cleavage plane.

This configuration, of weakening bonds along the tensile stress axis and strengthening bonds along the perpendicular cleavage plane, is the perfect condition for further fracture. Eberhart et.al. are saying nothing more than that the cohesive strength is related to charge polarizability. (They also show how polarizability at the atomic level directly correlates with Poisson's ratio.) They further assert "that an impurity will facilitate brittle fracture if it increases the charge polarizability of the atoms across the cleavage plane" (Ebe:85). Such an impurity would also lower shear strength, and in terms of the Rice and Thompson geometry, should therefore equally promote deformation and fracture. However, the impurity concentration in the grain boundaries (or interfaces) of a material can differ from that of the bulk. While the tensile stress field ahead of a crack tip is applied across all planes, both bulk and interfacial, probing for a weak link between any two planes, the shear stress field (in this mode I loading arrangement) generally effects deformation via dislocation slip, which occurs in the bulk and not in the grain boundary (or in an interface).

In the S-Ni situation, the sulphur-nickel interaction in the dilute sulphur case is ionic, with electron density being drawn off the nickel atoms (as predicted originally by Messner and Briant) (Bri:80, Bri:82)). When sulphur atoms interact with each other, the coordinating Ni-S sulphur bonds become more covalent. When a tensile stress is applied, perpendicular to a grain boundary, the sulphur atoms across the boundary move further apart, becoming less interacting, making the S-Ni bonds across the boundary more ionic. Concurrently, sulphur (and nickel) atoms along each side of the boundary are moving closer, becoming more interact-

ing, and the metal-sulphur bonds along the boundary are becoming more covalent. This configuration will assist the flow of electrons in a direction that will promote bond breaking and fracture. Eberhart et al contend that "it is not the presence of sulphur-sulphur bonds per se that causes embrittlement, but rather the way in which sulphur facillitates electron transfer that promotes fracture" (Ebe:85). They are suggesting that "sulphur atoms 'catalyze' cleavage in nickel" (Ebe:85). Using similar arguments, the authors explain in detail the role of hydrogen in embrittlement and the phenomenon of environmentally assisted cracking.

This author is of the opinion that concepts in the Eberhart et al. fracture model are a useful theoretical framework for discussing adhesion in thin films, and perhaps some aspects of boundary lubrication. Although the stress fields in these situations are more complicated than the simple tensile case, fracture still occurs across a plane of atoms. The interesting plane in the thin film situation is the coating-substrate interface. As pointed out in section 2.4.2, adhesion by definition means that strain in coating and the substrate equal at the interface. Since the two materials have in general different mechanical properties, a stress gradient can be present at the interface, arising from intrinsic stresses as well as externally applied stress fields. For good adhesion, the bonds across the interfacial plane need to be resistant against charge redistribution into bonds along the interfacial plane. Dopants which decrease this polarizability should improve adhesion. Those having the opposite effect promote fracture. In the case of localized interfaces formed by asperity contact between two solids (the situation that occurs during boundary lubrication), polarization promoting impurities should act as atomic lubricants when the system is loaded in shear. Since the loading is in shear, these impurities promote a mode II shearing or sliding fracture. The shear strengths of planes along the direction of shear are increased by such charge redistribution. Buckley and his coworkers have observed dramatic decreases in friction coefficients determined in UHV environments after clean metal surfaces are covered with atomic adsorbates (S,P,O,C) of levels as low as 0.1-0.2 monolayers (Buc:70, Buc:72, Miy:82, Miy:83). These concentrations are curiously equivalent to the 1-20% impurity lev-

els observed on the grain boundaries exposed by fracture in UHV of ceramics and embrittled alloys (Mar:69, Mar:72, Mar:722, Pal:69).

As a final note, it is important to realize that the theoretical models of Eberhart et.al., and especially those of Messner, do not incorporate the effect of stress fields on the structure and thus the bonding of crystals. This development is needed. In fact, although the concepts introduced by Eberhart are an excellent framework for discussion, the state of the modelling is such that they can only explain phenomenon that have been observed. They have not predicted events. Advancements in such dopant-induced cohesion (de)stabilization theory will be of major importance in the area of composite material interfaces, thin film or otherwise. However, improvements in modeling predictive capability will require experimental verification. Thin film synthesis should provide a very controlled experimental environment to corroborate or reject theoretical predictions. Precise depositions methods, such as molecular beam epitaxy, or high vacuum evaporation or sputtering will probably be the techniques which offer the most compositional control. As this study has shown, the PACVD process is more complicated because surface chemical reaction equilibria, which can be indirectly influenced, ultimately control film composition. Thus, the PACVD technique is less suitable for experiments requiring precise and variable interfacial composition control.

The hardness values of the TiN films produced by PACVD on M2 steel are not as good as films produced by sputtering or even that of bulk TiN. The higher load (100-200gm) data of thicker films (8-10μ) clearly indicates this conclusion. The best value of Vickers hardness obtained was about 1500kg/mm^2. This is contrasted to bulk TiN (2000kg/mm^2) or reported values of sputtered TiN on high speed steel ($\sim$2400 kg/mm^2). The low load data is more inconclusive, showing no consistent rise or fall. An indentation size effect was not evident. Rather, it appears that measurement error effects (the large variation in calculated hardness for small changes in diagonal size when the latter length is small) present are the source of the scatter. The two microstructures observed, zone 2 and zone T, do not show significant differences. Biasing (up to -100V) does not show an effect. Grain size

decreased slightly with increasing bias while morphology and bulk composition did not change. Thus, grain size or morphology does not appear to be a dominant microstructural feature controlling microhardness in the present context.

The previous observations need to be reviewed in the context of knowledge in the literature. The factors controlling hardness in thin compound films are not well understood. As described in section 2.4.2, hardness is controlled by the strength of interatomic forces and by the deformation mechanism operative. Microstructural features influence hardness through the latter factor. The high hardness of TiN is often explained by its band structure, as in section 1.4.2, in that the material has a high degree of covalent bonding and that the antibonding orbitals are fairly unoccupied. This study, as well as others, (Kik:84, Wim:85), indicate that chlorine is detrimental to mechanical properties. Chlorine could be detrimental in two ways: 1)if incorporated into the lattice by disrupting or altering the band structure. 2)by forming regions of a separate, brittle chlorine-rich phase.

Though the effect of impurities on the bonding component of hardness is relatively easy to explain, there is a real lack of knowledge concerning the deformation mechanisms operative in compound films and the role of microstructure in controlling these mechanisms. Sproul and Sundgren have reported hardnesses in thin films higher than bulk TiN (2400 kg/mm^2 vs. 2000 kg/mm^2). These higher hardnesses can only stem from microstructural influences on the deformation mechanisms. This subject is a topic of active research by Sundgren. There are two general mechanisms of deformation that are often invoked: dislocation glide and grain boundary sliding/cracking. Recent TEM studies by Hakansson et.al. indicate that sputtered TiN films have a highly dislocated structure when deposited on a grounded substrate (Hak:87). A negative substrate bias actually decreases dislocation density up to about -100V, and then the dislocation density rises with further magnitudes of bias. They propose that the grounded films have a high dislocation density because of low adatom mobility during growth, which promotes the incorporation of defects. Increasing bombardment energy by biasing increases surface adatom mobility, which decreases defect density. However, above some

critical voltage, the bombardment process itself induces defects in the crystalline structure, of a greater magnitude than the dislocation annealed out of existence.

The dislocation density and structure of the TiN films produced by PACVD is not known. The relationship between dislocation density deposition conditions, and film mechanical properties requires further study, and needs to be compared to sputtered film data. Of particular interest is the effect of biasing on dislocation density and structure. The fact that biasing does not strongly affect the hardness of PACVD films suggests that the situation is more complex than the sputtered case. The presence of chlorine in the plasma could facillitate plasma assisted etching, which would reduce film growth rate. The effect of this etching on film chlorine content, or dislocation density is difficult to predict.

If dislocation glide is important, grain size should also have some influence on hardness as well as bulk dislocation density, since the grain boundaries would impede dislocation motion. Classically in metals, hardness increases inversely with grain size, in a Hall-Petch type relationship

$$H = H_o + k\, d^{-0.5}$$

where H is the hardness, H_o the intrinsic hardnesss for a single crystal, d the grain size, and k is a materials constant. However results in the literature, reviewed by Sundgren, indicate that TiN films do not follow a Hall-Petch relationship. Over a range of grain sizes, from 500 to 6000 Å, hardness increases with grain size. For a Hall-Petch relationship to be valid, the grain boundary structure and composition should remain constant as grain size changes. However, observed changes in film grain size are often only one of several changes that occur as deposition conditions are changed. Film morphology, composition, and structure can radically change, as the present study has shown for example with changes in deposition temperature. Although low temperatures promote small grain size, they also promote poor crystallinity and high defect contents. Studies by Hibbs et.al. (Hib:84) and Jocobsson (Jac:79) indicate that film hardness decreases with the increasing presence of voids at grain boundaries. The presence of such voids

or of weak defect-dense grain boundaries should promote deformation by grain boundary sliding.

If grain boundary sliding or microcracking is an operative deformation mechanism, then grain boundary composition is also of importance. As stated earlier, grain boundaries can often have different compositions than that of the bulk material. This author knows of no study of the grain boundary composition of thin films. The films synthesized in the present study tend to fracture at the grain boundaries. With a high spatial resolution scanning Auger microscope, the scratch removal technique developed in this study could be used to investigate grain boundary composition, by analysis of grain boundaries exposed by fracture. Caution must be exercized to prevent Auger signal originating from the original film surface or the exposed interface surface. In particular, the region of electron scattering in the solid under the electron beam (the 'tear-drop' region) must be kept within the film bulk. This situation requires a small beam size, a large film thickness, and a grain boundary fracture surface orientation near-normal to the incident electron beam. It is important to realize that the high chlorine contents reported for the scratch track in figure 3.19 may stem in part from exposed grain boundaries. If chlorine content is higher at the grain boundaries, this might contribute to lower film hardness. Thus, the scratch removal technique, while clearly important for issues of adhesion, may also be an important tool in investigating the influence of grain boundary composition on film hardness.

In addition to SRT studies, TEM and Scanning Transmission Electron Microscopy (STEM) investigation of dislocation density and structure, and grain boundary structure of PACVD-produced TiN films should be performed. Improvement of hardness in PACVD-produced films requires further study of the relationship between microstructure and deformation mechanisms. Such fundamental investigations are necessary to systematically elucidate the deposition conditions that promote high film hardness.

The role of the plasma in film formation by PACVD is only partially understood at present, though some summary observations can be made. The formation of

TiN from $TiCl_4$ and NH_3 is a case of plasma-*enhanced* CVD while formation from $TiCl_4$, H_2 and N_2, or the formation of TiC from $TiCl_4$ and CH_4, are cases of plasma-*assisted* CVD since the latter two reactions are not thermodynamically favored (using standard state Gibb's free energy values) between 400 and 500°C. Using the terminology of Veprek literally, the plasma exhibits a "kinetic effect" in the NH_3-based reactions, while a "thermodynamic effect" is observed in the other reactions. However, in all cases, crystalline material is formed which could be formed by conventional CVD at higher temperatures. Unique metastable materials were not synthesized.

The actual reaction mechanisms that occur are not known at all. Only inferences can be suggested at present, based on the observed effect of deposition conditions on film properties. As stated earlier, deposition temperature strongly influences film composition–primarily the degree of chlorine retention. If chlorine contents are low, a consistent Ti:N ratio is observed. The primary effect of the other deposition conditions is to alter film growth rates. For the formation of TiN at a given surface temperature, the general hypothesis can be proposed which states that the film growth rates will be strongly influenced by the population of *excited*-state species generated in the plasma.

The effect of varying r.f. power, that growth rates can show optimum values, is qualitatively easy to explain. Increasing r.f. power increases the sheath field strength, which in turn increases the kinetic energy of electrons entering the plasma. The electron energy distribution in the plasma is changed, which in turn affects the population of excited-state species. Since each excited state has a cross-section for formation, there will be optimum sheath field strengths that promote a particular excited state. If these excited states are rate-limiting, higher powers could lead to lower growth rates, until power is sufficient to create newer excited states which promote film formation reaction kinetics. Gas composition also affects the population of excited state species. The NH_3 partial pressure kinetic results in figure 3.12 would suggest a simple relationship, that is that an increase in ground state feedstack rates is accompanied by a direct increase in growth rate,

albeit enhanced by plasma excitation. The argon-ammonia experiment clearly shows that the relationship between ground state and excited state populations need not be direct. In fact, a nearly inverse relationship was observed. There is clearly an interaction between the argon and the ammonia in the gas phase which promotes TiN formation. The argument could be made that argon bombardment of the surface somehow promotes growth. However, one would suspect that a bombardment effect should also work with H_2-N_2 plasmas. No enhancement of growth was seen with argon in such plasmas. Rather a decrease in growth rate was seen–argon behaved as an inert gas diluting the reactive species. Increasing the H_2/N_2 ratio also decreased growth rates, suggesting that excited state nitrogen was becoming rate limiting. However, this idea is pure speculation. Spectroscopic studies of the plasma are needed to elucidate volume chemical reactions.

Even without further study, the argon results could be utilized in industrial applications. Ammonia-based films can be grown quickly, but suffer from poor adhesion to steel. Hydrogen-nitrogen films adhere well to steel but tend to have lower growth rates. A sequential deposition could optimize good adhesion and high growth. The deposition could start with $TiCl_4$, H_2 and N_2 until the steel surface is well covered. The thin film studies reported in section 3.3.5 indicate that this occurs within five minutes. Once the steel is protected by an TiN layer, NH_3 could be substituted for H_2 and N_2 to increase growth rate. However, an argon-ammonia mixture would be even better, promoting an even higher growth rate while minimizing the presence of corrosive and salt-forming NH_3.

As opposed to altering only the plasma volume chemistry, the application of a substrate bias affects the plasma-surface interaction. Increasing the substrate bias increases the kinetic energy of bombarding ionic species. Such bombardment can desorb bound surfaces, change defect (including dislocation) density, alter crystalline and morphological structure, implant gas atoms into the substrate, and/or promote sputter spectrum of substrate atoms (Tho:83). In the PACVD films, the major effect of biasing has has been to decrease film growth rates. Grain morphology does not change, though there appears to be some grain size refinement.

Composition does not change. Film hardness does not improve, suggesting that biasing (up to -100V) does not affect the microstructural factors influencing hardness. This author is of the opinion that a substrate bias in the present context promotes a plasma assisted etching of TiN by Cl species from the discharge. Sputter ejection by momentum transfer is suspected to be a minimal cause of lower growth rates at -50 and -100V since studies of biasing with PVD (where Cl is not present) indicate that reductions in growth rates do not occur until magnitudes of -200V or more are applied (Sun:833). This plasma assisted etching in the present case appears to the dominant effect of the application of a substrate bias, negating any positive influences that may be occuring.

For the formation of TiC or Ti(CN), both the plasma chemistry and the surface reactions can be more complicated. In the plasma volume, carbon can form extensive bonds with itself or chlorine to make extended molecules (small polymers) which probably do not have an analog in nitrogen chemistry. On the surface, excess carbon can easily exist without titanium, whereas nitrogen would be expelled. However, in the films synthesized, all carbon in the films appeared to be carbidic as opposed to graphitic. The large degree of scatter in film chlorine content with increasing P_{CH_4} suggests that some type of complex and variable gas phase chlorine-carbon interaction was occuring. Spectroscopic studies of the plasma volume would be particularly useful in resolving the reactions which favor chlorine retention.

In summary, the present work has advanced the state of the knowledge regarding the importance of surface temperature and chlorine expulsion in controlling the morphology, composition and adhesive properties of TiN films synthesized by PACVD. Future improvements require a fundamental study of the deformation mechanisms that operate in these films and the role of microstructure in influencing hardness. Surface science studies of the relationship between grain boundary composition and mechanical properties are needed. Spectroscopic studies of the plasma are necessary to understand how to systematically improve TiN film formation rates and to control the formation of the more complicated carbonitrides

and carbides of titanium.

Chapter 5

Conclusions

This investigation has focused on determining the physical and mechanical properties of titanium nitride films synthesized by r.f. plasma assisted chemical vapor deposition. From this study, the following conclusions can be stated:

1)Chlorine removal at the surface-gas interface strongly influences the structural, chemical, and mechanical properties of TiN films formed by PACVD from $TiCl_4$. In particular, substrate temperature dictates the chlorine by-product of the $TiCl_4$ reactions. Increasing deposition temperature promotes reduced chlorine content in the films. Concommitant with this temperature increase, a transition from an amorphous zone 1 morphology, to fine-grained zone T morphology (clearly observed in the H_2-N_2 films), to a highly crystalline zone 2 morphology is observed. The films show a nearly exclusive (200) preferred orientation, though small (111) components were sometimes observed in the zone T films. The low temperature zone 1 material has extremely poor mechanical properties and disintegrates easily after formation. The temperature at which the transition to higher quality TiN film formation occurs correlates with the temperature at which gaseous HCl becomes the thermodynamically favorable byproduct over solid NH_4Cl.

2)Film adhesion is dependent on initial deposition conditions. The 'surface' during the initial stages of deposition includes the substrate, which can affect the

retention of chlorine at the resultant interface. Early film growth is characterized by the nucleation and coalesence of TiN islands. Films synthesized with $TiCl_4$ and NH_3 were found to have high interfacial chlorine contents, which is believed to be detrimental to adhesion and to have promoted low-SAT critical loads and massive spallation failure (Rickerby type A). Films synthesized with H_2 and N_2 instead of NH_3 were found to have better adhesive properties, exhibiting higher critical loads and cohesive failure modes predominantly in the coatings. Chlorine accumulation at the interface was not observed. The L_C values of the H_2-N_2 based PACVD-produced TiN films are comparable to values reported for PVD-produced TiN on M2 steel. However, high-bias substrate precleaning bombardment was not utilized in the present study, which suggests that the hydrogen discharge cleans the surface by chemical means, ie. plasma etching. This chemical pretreatment could be an alternative approach in situations where defects induced by bombardment are undesirable.

3)A new procedure, the scratch removal technique, was developed and utilized to determine the composition of weak interfaces, by combining in-situ scratching with scanning Auger microscopy of resultant fracture surfaces. SRT can quickly analyze interfacial failures and resolve sharp concentration gradients. With high spatial SAM systems, the technique could be utilized to analyze coating grain boundary composition, which would be of relevance to hardness studies if grain boundary sliding or microcracking is an operating deformation mechanism.

4)The microhardness of the PACVD-produced TiN films (9-10μm thick) on M2 steel was Hv_{100}-Hv_{200} $\sim$1500 kg/mm_2. Negative substrate biasing of magnitudes up to 100V did not improve hardness. These values are lower than bulk TiN (2000 kg/mm_2) or reported values of sputtered TiN ($\sim$2400 kg/mm^2).

5)The coreactants to $TiCl_4$ respond differently in the glow discharge. The plasma *enhances* TiN film formation in the NH_3 case, where TiN synthesis is ther-

modynamically favored down to temperatures of 180°C. The plasma *assists* and is required for TiN synthesis at temperatures below 590°C, because film formation by thermal CVD is not thermodynamically favored.

6)At a fixed deposition temperature, the plasma conditions primarily influenced growth rates. Above 400°C, a stoichiometric, within the scatter of AES (~5%) material was obtained. Power and gas composition showed optimal behaviors, suggesting that variations in these parameters affect the population distribution of excited-state species which are deposition rate-limiting. The presence of argon with ammonia enhanced film formation rates. In contrast a dilution effect was observed for argon with hydrogen and nitrogen. Negative bias inhibited film growth. Film morphology did not change though a reduction in grain size occured. The severe retardation of film growth at low voltages (-100V or less) and high pressures (0.1-1 Torr) suggests that the biasing is promoting a plasma-assisted etching of TiN with chlorine from the plasma because significant sputter desorption is not expected until higher voltages are applied.

7)Carbonitrides formed from $TiCl_4$, H_2, N_2 and CH_4 showed greater variation in composition, particularly chlorine content, at fixed temperatures. The ability of carbon to form chloro-polymers in the gas phase and to exist as excess carbon in the solid phase make the carbonitride synthesis more complex than pure nitride synthesis.

8)Titanium dimethylamide decomposition, without a plasma, produced carbonitride powders. These formed because of the fact that the heating necessary for vapor transport induced gas phase nucleation.

Chapter 6

Bibliography

The reference code used in this dissertation consists of the first three letters of the first author's surname followed by the last two digits of the year of the communication. In cases where more than one reference exists with the same code, an additional ordering digit follows the year.

References

[1] AM Staff. *American Machinist* (1979) 75.

[2] R. Anderson. 1985. Courtesy of Prof. R. Andersen and N. Rutherford, UC Berkeley Chemistry Dept.

[3] N.J. Archer. *Thin Solid Films* **80** (1981) 221.

[4] R. Avni, U. Carmi, A. Inspektor, and I. Rosenthal. *Thin Solid Films* **118** (1984) 231.

[5] R. Avni, U. Carmi, A. Inspektor, and I. Rosenthal. *J. Vac. Sci. and Technol. A.* **3(4)** (1985) 1813.

[6] P. Benjamin and C. Weaver. *Proc. Roy. Soc.* **254 A** (1960) 163.

[7] P. Benjamin and C. Weaver. *Proc. Roy. Soc.* **254 A** (1960) 177.

[8] P. Benjamin and C. Weaver. *Proc. Roy. Soc.* **261 A** (1961) 516.

[9] F.P. Bowden and D. Tabor. *Friction and Lubrication.* New York, 1960.

[10] C.L. Briant and R.P. Messner. *Phil. Mag. B* **42** (1980) 569.

[11] C.L. Briant and R.P. Messner. *Acta Metall.* **30** (1982) 457.

[12] D. Briggs and M.P. Seah. *Practical Surface Analysis.* John Wiley and Sons, Chichester, U.K., 1983.

[13] D.H. Buckley. *Int.J. Nondest. Testing* **2** (1970) 171.

[14] D.H. Buckley. *ASLE Transactions* **17** (1972) 206.

[15] R.F. Bunshah. *Thin Solid Films* **107** (1983) 21.

[16] P.J. Burnett and D.S. Rickerby. *Wear* **in press** (1987) .

[17] J.O. Carlsson. *Thin Solid Films* **130** (1985) 261.

[18] D.J. Cheng, W.P. Sun, and M.H. Hon. *Thin Solid Films* **146** (1987) 45.

[19] B.D. Cullity. *Elements of X-ray Diffraction.* Addison-Wesley, Reading, MA, 1978.

[20] L.E. Davis, N.C. MacDonald, P.W. Palmberg, G. E. Riach, and R.E. Weber. *Handbook of Auger Electron Spectroscopy.* Perkin-Elmer Corp., Eden Prarie, MN, 1976.

[21] P.T. Dawson and M.M. Tzatzov. *Surf. Sci.* **149** (1985) 105.

[22] M.F. Doerner and W.D. Nix. *J. Mater. Res.* **1(4)** (1986) 601.

[23] M.F. Doerner, D.S. Gardner, and W.D. Nix. *J. Mater. Res.* **1(6)** (1986) 811.

[24] A. Doi, N. Fujimora, T. Yoshioka, and Y. Doi. In *Proc. of the Int. Ion Engineering Conf.*, page 1137, Kyoto, Japan, Sept. 1983.

[25] M.E. Eberhart, R.M. Latanision, and K.H. Johnson. *Acta. Metall.* **33** (1985) 1769.

[26] C. Ernsberger, J. Nickerson, A.E. Miller, and J. Moulder. *J. Vac. Sci. Technol. A.* **3(6)** (1985) 2415.

[27] G. Ertl and J. Kuppers. *Low Energy Electrons and Surface Chemistry.* Verlag Chemie, Weinheim, 1974.

[28] A.G. Evans and J.W. Hutchinson. *Int. J. Solids Structures* **20** (1984) 455.

[29] J.I. Goldstein and H. Yakowitz. *Practical Scanning Electron Microscopy.* Plenum, New York, 1975.

[30] J.E. Greene, J. Woodhouse, and M. Pestes. *Rev. Sci. Instrum* **45** (1974) 747.

[31] J.E. Greene and M. Pestes. *Thin Solid Films* **37** (1976) 373.

[32] J.E. Greene and J.L. Zilko. *Surf. Sci.* **72** (1978) 109.

[33] T.W. Haas, J.T. Grant, and G.D. Dooley III. *J. Appl. Phys.* **43** (1972) 1853.

[34] G. Hakansson and J.E. Sundgren. *Thin Solid Films* **in press** (1987) .

[35] J. Halling. *Thin Solid Films* **108** (1983) 1.

[36] W. Hartweck and H.J. Grabke. *Surface Science* **89** (1979) 174.

[37] R.L. Hatshek. *American Machinist* **Spec. Rep. 752** (1983) 129.

[38] U. Helmersson, B.O. Johansson, J.-E. Sundgren, and P.Billgren. *J. Vac. Sci. Technol. A* **3** (1985) 308.

[39] U. Helmersson and J.-E. Sundgren. *Thin Solid Films* **1987** (1987) .

[40] G.E. Henein and J.E. Hilliard **54** (1983) 728.

[41] D.W. Hess. *J. Vac. Sci. Technol. A* **2** (1984) 244.

[42] M.K. Hibbs, J.-E. Sundgren, B.E. Jacobsen, and B. O. Johansson. *Thin Solid Films* **107** (1983) 149.

[43] M.K. Hibbs, B.O. Johansson, J.-E. Sundgren, and U. Helmersson. *Thin Solid Films* **122** (1984) 115.

[44] M.K. Hibbs, B.O. Johansson, J.-E. Sundgren, and U. Helmersson. *Thin Solid Films* **122** (1984) 313.

[45] M.K. Hibbs, J.-E. Sundgren, B.O. Johansson, and B. E. Jacobson. *Acta metall.* **33** (1985) 797.

[46] M.R. Hilton, L.R. Narasimhan, S. Nakamura, M. Salmeron, and G.A. Somorjai. *Thin Solid Films* **139** (1986) 247.

[47] M.R. Hilton, A.M. Middlebrook, G. Rodrigues, M. Salmeron, and G.A. Somorjai. *J. Vac. Sci. Technol. A.* **4** (1986) 2797.

[48] M.R. Hilton, G.J. Vandentop, M. Salmeron, and G.A. Somorjai. *Thin Solid Films* **154** (1987) 377.

[49] H.E. Hintermann. *Wear* **100** (1984) 381.

[50] Y. Homma. Hitachi Ltd (Tokyo), January 1987. Private communication.

[51] M.P. Hooker and J.T. Grant. *Surf. Sci.* **62** (1977) 21.

[52] L. Hultman, H.T.G. Hentzell, J.-E. Sundgren, B.-O. Johansson, and U. Helmersson. *Thin Solid Films* **124** (1985) 163.

[53] E. Humner and A.J. Perry. *Thin Solid Films* **101** (1983) 243.

[54] S.K. Hwang and Jr. J.W. Morris. *Met. Trans. A* **11** (1980) 1197.

[55] *IBM Journal of Res. and Dev.* **30** (1986) No. 4 and 5.

[56] A. Inspektor, Y. Hornik, U. Carmi, R. Avni, E. Wallura, H. Hovec, K. Koizlik, and H. Nickel. *Thin Solid Films* **72** (1980) 195.

[57] A. Inspektor. Nuclear Research Centre, Negev Israel, March 1987. Private communication.

[58] B.E. Jacobsson, R. Nimmagadda, and R.F. Bunshah. *Thin Solid Films* **63** (1979) 333.

[59] *JANAF Thermochemical Tables, 2nd Ed.* National Bureau of Standards, Washington, D.C., June 1971.

[60] J.H. Je, E. Gyarmani, and A. Naoumidis. *Thin Solid Films* **136** (1986) 57.

[61] H.A. Jehn, S. Hofmann, V.-E. Ruckborn, and W.-D. Munz. *J. Vac. Sci. and Technol. A* **6** (1986) 2701.

[62] P.C. Jindal, D.T. Quinto, and G.J. Wolfe. *Thin Solid Films* **in press** (1987) .

[63] B.O. Johansson, J.-E. Sundgren, H.T.G. Hentzell, and S.-E. Karlson. *Thin Solid Films* **111** (1984) 313.

[64] B.O. Johansson, J.-E. Sundgren, J.E. Greene, D.A. Rockett, and S.A. Barnett. *J. Vac. Sci. Technol. A* **3** (1985) 303.

[65] B. Jonsson and S. Hogmark. *Thin Solid Films* **114** (1984) 257.

[66] N. Kikuchi, Y. Oosawa, and A. Nishiyama. In *Proc. 165th Meet. of the Electrochemical Society, May 6-11, 1985*, The Electrochemical Society, Pennington, NJ, 1984. Abstract 194.

[67] B.M. Kramer. *Thin Solid Films* **108** (1983) 117.

[68] S.R. Kurtz and R.G. Gordon. *Thin Solid Films* **140** (1986) 277.

[69] P. Laeng and P.A. Steinmann. *Electrochem. Soc.* **81** (1981) 723.

[70] M.T. Laaugier. *Thin Solid Films* **117** (1984) 243.

[71] M.T. Laugier. *J. Mater. Sci.* **21** (1986) 2269.

[72] M.E. Levin. PhD thesis, University of California, Berkeley, 1987. Dept. of Chemical Engineering.

[73] R.F. Lin, G.S. Blackmann, M.A. Van Hove, and G.A. Somorjai. *Acta Cryst. B* **43** (1987) 368.

[74] C.T. Liu, C.L. White, and J.A. Horton. *Acta metall.* **33** (1985) 213.

[75] R.R. Manory, R. Avni, and A. Grill. *NASA Tech. Mem. 87219* (1985) .

[76] H.L. Marcus and P.W. Palmberg. *Trans. Met. Soc. AIME* **245** (1969) 1664.

[77] H.L. Marcus and M.E. Fine. *J.Am. Cer. Soc.* **55** (1972) 568.

[78] H.L. Marcus, H.L. Hackett, and P.W. Palmberg. *ASTM* **STP 499** (1972) 90.

[79] S. Matsumoto, Y. Sato, M. Kamo, and N. Setaka. *Jap. Jour. Appl. Phys.* **21** (1982) L183.

[80] P. Mayr and H.R. Stock. *J. Vac. Sci. and Technol. A* **4 (6)** (1986) 2726.

[81] K. Miyoshi and D.H. Buckley. *ASLE Transactions* **27** (1982) 15.

[82] K. Miyoshi, D.H. Buckley, and N. Srinivasan. *Am. Ceramic Soc. Bull.* **62** (1983) 494.

[83] F. Mohs. *Grundries der Mineralogie.* Dresden, 1822.

[84] J. L. Mukherjee, L. C. Wu, J. E. Greene, and H. E. Cook. *J. Vac. Sci. and Technol.* **12** (1975) 850.

[85] W.-D. Munz. *J. Vac. Sci. and Technol. A* **6** (1986) 2717.

[86] A. Neckel, P. Rastl, R. Eibler, P. Weinberger, and K. Schwarz. *J. Phys. C* **9** (1976) 579.

[87] D. Newey, M.A. Wilkins, and H.M. Pollock. *J. Phys. E.Sci. Instrum.* **12** (1982) 119.

[88] L.M. Niebylski. Ethyl ,Corporation Technical Center, Baton Rouge, LA., 1986. Private communication.

[89] A.J. Ninham. PhD thesis, University of Cambridge (England), 1986. Department of Metallurgy.

[90] A.J. Ninham. Lawrence Berkeley Laboratory, July 1986. Private Communication.

[91] J.J. Oakes. *Thin Solid Films* **108** (1983) 1.

[92] P.W. Palmberg and H.L. Marcus. *Trans. ASM* **62** (1969) 1016.

[93] A. Pan and J.E. Greene. *Thin Solid Films* **97** (1982) 79.

[94] A.J. Perry. *Thin Solid Films* **107** (1983) 167.

[95] A.J. Perry. *J. Vac. Sci. Technol. A* **6** (1986) 2801.

[96] A.J. Perry. *Thin Solid Films* **146** (1987) 165.

[97] R.L. Peters. Fansteel VR Wesson Corp., Lake Bluff IL, November 1983. Private communication.

[98] A. Raveh, A. Inspektor, U. Carmi, and R. Avni. *Thin Solid Films* **105** (1983) 39.

[99] A. Raveh, A. Inspektor, U. Carmi, and R. Avni. *Thin Solid Films* **108** (1983) 39.

[100] J.R. Rice and R. Thompson. *Phil. Mag* **29** (1974) 73.

[101] Y. Ron, A. Raveh, U. Carmi, A. Inspektor, and R. Avni. *Thin Solid Films* **107** (1983) 181.

[102] M. Salmeron, D.S. Kaufman, B. Marchon, and S. Ferrar. *Applied Surface Science* **28** (1987) 279.

[103] A.A. Savelev, A.A. Pukhov, B.A. Vishnyakov, A.D. Sulimen, and A.P. Ishchenko. *Fiz. Khim. Obrab. Mater.* **2** (1981) 85.

[104] L.H. Schwartz and J.B. Cohen. *Diffraction From Materials.* Academic Press, New York, 1977.

[105] H. Schneider and E. Nold. In *Proc. Int. Conf. on Analysis of Non-Metals, 1980*, page 413, de Gruyter, Berlin, 1981.

[106] W. Schintlmeister, W. Wallgram, and J. Kanz. *Thin Solid Films* **108** (1983) 1.

[107] A. Sherman. *Thin Solid Films* **113** (1984) 135.

[108] Y.R. Shen. *Ann. Rev. Mater. Sci.* **16** (1986) 69.

[109] L. Shizhi, H. Wu, Y. Hongshun, and W. Zhongshu. *Plasma Chemistry and Plasma Processing* **4, No. 5** (1984) 147.

[110] L. Shizhi and Y. Hongshun. In *Proc. of the 7th Int. Symp. on Plasma Chemistry*, page 68, ISPC-7, Eindhoven, July 1985. Paper A-1-8.

[111] L. Shizhi, Z. Cheng, S. Yulong, X. Xiang, H. Wu, X. Yan, and Y. Hongshun. In *Proc. of the 10th CVD Conf.*, page 500, The Electrochemical Society, Honolulu, Oct. 1987.

[112] H.D. Shih, F. Jona, D.W. Jepsen, and P.W. Marcus. *Surface Science* **60** (1976) 445.

[113] H.D. Shih, K.O. Legg, and F. Jona. *Surface Science* **54** (1976) 355.

[114] Gabor A. Somorjai. *Chemistry in Two Dimensions.* Cornell University Press, Ithaca, New York 14850, 1981.

[115] W.D. Sproul. *Thin Solid Films* **107** (1983) 141.

[116] P.A. Steinmann and H.E. Hintermann. *J. Vac. Sci. Technol. A.* **3** (1985) 2394.

[117] K. Sugiyama, S. Pac, Y. Takahashi, and S. Motojima. *J. Electrochem. Soc.* **122** (1975) 1545.

[118] J.-Sundgren, B.O. Johansson, and S.-E. Karlson. *Thin Solid Films* **105** (1983) 353.

[119] J.-E. Sundgren, B.O. Johansson, S.-E. Karlson, and H. T.G. Hentzell. *Thin Solid Films* **105** (1983) 367.

[120] J.-E. Sundgren, B.O. Johansson, H.T.G. Hentzell, and S.-Karlson. *Thin Solid Films* **107** (1983) 385.

[121] J.E. Sundgren and H.T.G. Hentzell. *J. Vac. Sci. and Technol. A* **4(5)** (1986) 2259.

[122] A.K. Surl, R. Nimmagadda, and R.F. Bunshah. *Thin Solid Films* **72** (1980) 529.

[123] I. Swider. Future Products Tool Corporation, Clawson MI, January 1986. Private communication.

[124] D. Tabor. *The Hardness of Metals.* Clarendon Press, Oxford, 1951.

[125] J.A. Thornton. *Ann. Rev. Mater. Sci.* **7** (1977) 239.

[126] J.A. Thornton. *Thin Solid Films* **107** (1983) 3.

[127] J.A. Thornton. *J. Vac. Sci. and Technol. A* **6** (1986) 3059.

[128] L.E. Toth. *Transistion Metal Carbides and Nitrides.* Academic Press, New York, 1970.

[129] Y.S. Touloukian, R.K. Kirby, R.E. Taylor, and T. Y.R. Lee. Thermal expansion: non-metallic solids. In *Thermophysical Properties of Matter, TRPC Data Series*, IFI-Plenum, New York, 1977.

[130] H.-C. Tsai, D.B. Bogy, M.K. Kundman, D.K. Veirs, M.R. Hilton, and S. Mayer. *J. Vac. Sci. and Technol. A* **in press** (1987-1988) .

[131] S. van-der-Zwaag and J.E. Field. *Philisophical Magazine A* **46, No. 1** (1982) 133.

[132] S. van-der-Zwaag and J.E. Field. *Philisophical Magazine A* **48, No. 5** (1983) 767.

[133] S. Veprek. *Thin Solid Films* **130** (1985) 135.

[134] C. Weaver. *J. Vac. Sci. Technol.* **12** (1975) 18.

[135] P.E. Wieranga and J.J. Franklin. *J. Appl. Phys.* **55** (1984) 4244.

[136] R. Wilson. *Metallurgy and Heat Treatment of Tool Steels.* McGraw-Hill, London, 1975.

[137] L.M. Williams. PhD thesis, University of California, Berkeley, 1982. Dept. of Chemical Engineering.

[138] L.M. Williams and D.W. Hess. *J. Vac. Sci. Technol. A* **1** (1983) 1810.

[139] R.T. Wimber. Deere and Company Technical Center, Moline, IL, April 1985. Private communication.

[140] X. Xiang and L. Shizhi. In *Proc. of the 1986 China-Japan Symposium on Thin Films*, page 18, Beijing, China, Sept. 22-24 1986.

LAWRENCE BERKELEY LABORATORY
TECHNICAL INFORMATION DEPARTMENT
UNIVERSITY OF CALIFORNIA
BERKELEY, CALIFORNIA 94720